NAS 8-20396
GEORGE C. MARSHALL
SPACE FLIGHT CENTER

STUDY OF CRACK INITIATION PHENOMENA ASSOCIATED WITH STRESS CORROSION OF ALUMINUM ALLOYS

SECOND ANNUAL REPORT

ALCOA RESEARCH LABORATORIES
NEW KENSINGTON, PA.

ALUMINUM COMPANY OF AMERICA
Alcoa Research Laboratories
Physical Metallurgy Division
New Kensington, Pennsylvania

STUDY OF CRACK-INITIATION PHENOMENA ASSOCIATED WITH STRESS CORROSION OF ALUMINUM ALLOYS

Contract Number - NAS8-20396

Control Number - DCN 1-7-54-20093 (1F)

July 15, 1968

Second Annual Report
(June 6, 1967 to June 6, 1968)

Authors

M. S. Hunter
W. G. Fricke, Jr.

Contributors

D. L. McLaughlin
J. J. Ptasienski
D. L. Robinson
D. O. Sprowls
J. D. Walsh

FOREWORD

This report was prepared by Aluminum Company of America under contract NAS8-20396 entitled "Study of Crack Initiation Phenomena Associated with Stress Corrosion of Aluminum Alloys" for the George C. Marshall Space Flight Center of the National Aeronautics and Space Administration. The work was administered under the technical direction of the Propulsion and Vehicle Engineering Laboratory, Materials Division of the George C. Marshall Space Flight Center with Mr. J. G. Williamson acting as contracting officer's representative.

A number of Alcoa Research Laboratories personnel made significant contributions to this work. Mr. D. L. McLaughlin and Mr. J. J. Ptasienski conducted the light microscope investigations. Mr. D. L. Robinson contributed the thin-foil transmission micrographs showing alloy structure. Mr. D. O. Sprowls and Mr. J. D. Walsh supervised and conducted the environmental screening tests and contributed the section of this report dealing with this work.

This report has been reviewed and approved by Mr. H. Y. Hunsicker, Chief of Physical Metallurgy Division, Alcoa Research Laboratories. The section on Effect of Environment has also been reviewed and approved by Dr. J. L. Brandt, Chief of Chemical Metallurgy Division, Alcoa Research Laboratories.

TABLE OF CONTENTS

ABSTRACT OF TECHNICAL CONTENT

During the second year of the contract, microscope observations were made of crack initiation and development in thick plate of 2219-T37, 7075-T6, 7079-T6 and 7039-T6 alloys. Procedures were those used during the first contract year with additional emphasis on electron microscopy, electron fractography and the electron microprobe.

Structures of the added alloys, 7079-T6 and 7039-T6 were similar to that of 7075-T6 plate, both having unrecrystallized structures, uneven distribution of dispersoids, two sizes of boundary precipitates and a few dislocations. Unstressed corrosion of 7079-T6 was of the intergranular type, developing on both "former" grain boundaries and fragment boundaries, whereas unstressed corrosion of 7039-T6 was of the pitting type. Stress-corrosion cracks in 7075-T6, 7079-T6 and 7039-T6 always initiated on "former" boundaries perpendicular to the stress, in many cases apparently preferring boundaries between "grains" having considerably different orientation. Cracks propagated along these same paths, selecting the straightest possible path perpendicular to the stress.

No indication was found that dislocations, constituent particles, dispersoid particles or precipitate particles had any direct effect on initiation. The uneven dispersoid distribution in the three 7XXX alloys produced substantially dispersoid-free regions which may coincide with the "former" boundaries which are the crack initiation sites. Pits representing dissolved-out constituents or matrix pitting were not related to crack initiation in 2219-T37, 7075-T6 or 7079-T6, but may be so related with 7039-T6.

Microprobe analyses of surfaces containing stress-corrosion cracks revealed an oxide type of reaction product containing chloride. Similar analyses of stress-corrosion-crack surfaces in 7075-T6 revealed lower Zn and Mg than in the matrix, a situation which could not be reconciled with observed stress-corrosion behavior. Similar microprobe fracture surface analysis with 2219-T37 revealed a definite association of microconstituent particles with mechanical fracture but not stress-corrosion cracking.

New electron fractographic methods were developed for differentiating between the stress-corrosion and mechanical portions of fractures. This procedure showed that in 7075-T6, stress-corrosion cracks have relatively flat surfaces with small facets or veins which represent the junctions of fine polygonal structures. With 2219-T37 the facets were much larger and represented the faces of the recrystallized grains.

Investigations of the effect of surface roughness showed that intergranular pre-corrosion in 7075-T6 leads to rapid crack initiation. It was impossible to distinguish between these cracks and a corrosion crevice widened by stress, however, indicating that the latter could easily be mistaken for stress-corrosion cracks. Roughness in the form of fine surface abrasion masked crack initiation and altered crack initiation but did not change the cracking mechanism below a very shallow surface layer.

Anodic and chemical surface films delayed but did not prevent crack initiation in 2219-T37 and 7075-T6. In these same alloys, a semi-logarithmic relationship was observed between stress level and crack initiation time. At high stress levels, cracks were few, and both initiation and propagation were quite rapid. At low stress levels, cracks were also few because only the most susceptible and most favorably oriented boundaries developed cracks. Initiation times were still quite short but propagation rates were extremely slow. At all stress levels, the initiation sites and propagation paths were the same in 2219-T37, 7075-T6 and 7079-T6.

In environmental screening tests in additional electrolytes, stress-corrosion cracking occurred in cation electrolytes and hydroxide solutions with alloys subject to failure in chloride solutions. Failures in 2219-T87 and 7075-T73 in several solutions were the result of excessive general corrosion and not stress-corrosion cracking. Microscope observation of stressed specimens exposed to selected environments confirmed the results of screening tests in all but one case which has yet to be rechecked. With 2219-T87 and 7075-T73, only general corrosion and no cracking was observed. With 2219-T37 and 7075-T6 in environments inducing stress-corrosion failure, crack initiation sites and propagation paths were the same as in the $NaCl-AlCl_3$ solution at pH1.

INTRODUCTION

The problem of the stress-corrosion cracking of high strength aluminum alloys continues to impose limitations in the design and use of certain alloys and tempers in components and structures that must be subjected to stress under corrosive conditions. Much effort has been expended in analyzing the stress corrosion process, and a number of very ingeneous and well-documented mechanisms have been proposed to explain this phenomenon. These proposed mechanisms have been so many and varied, however, that one can only conclude that it is improbable that all can be operative at the same time and, therefore, that each may apply only with certain rather specific combinations of material, stress and environment.

In analyzing the stress-corrosion mechanism in high strength aluminum alloys, the majority of the work has been devoted to the general behavior of the various alloys in various environments, and to the times required for failure. Under the present contract, however, a somewhat different approach is being taken by focusing attention on the initiation of stress-corrosion cracks. Crack initiation is indeed of the utmost importance because if failure is to occur, a crack must first initiate, and if a crack does initiate, failure almost certainly will occur.

SCOPE OF INVESTIGATION

The broad objective of this investigation has been to develop a better understanding of the mechanisms of stress

corrosion of commercial high-strength aluminum alloys by a comprehensive analysis of factors which might affect crack initiation. In the first year of the contract, the principal emphasis was on the relation of crack initiation sites to the metallurgical structure of the aluminum alloy, using the alloys 2219, 7075 and X7375. In addition, investigations were started to establish the effects of surface irregularities, surface film, stress and environment on crack initiation in these same alloys. The technical abstract from the report of the first year's work is included in this report as Appendix I.

During the second year of the contract, which is the portion covered by this report, the work was continued along the lines established during the first year using the same alloys, 2219 and 7075, as well as two additional alloys, 7079 and 7039. Greater emphasis was placed on electron microscopy in relating crack initiation to microstructure and, in addition, electron fractography and the electron microprobe were applied to analyses of structure and the stress-corrosion mechanism. During the second year, planned work on the effects of surface roughness and surface film was completed and the effects of environment with both crack-prone and crack-resistant tempers of 2219 and 7075 were investigated extensively. Evaluation of the effect of stress was completed with 2219 and 7075 alloys, and was started with 7079 and 7039 alloys.

MATERIALS

During the second year of the contract, work continued with the same lots of 4" thick 2219 alloy plate and 3" thick 7075 alloy plate that had been used in the first year. No further work

was conducted on X7375 alloy. With 2219 and 7075 alloys, the stress-corrosion-prone tempers 2219-T37 and 7075-T6, as well as the stress-corrosion resistant tempers 2219-T87 and 7075-T73, were used. The composition, mechanical properties and corrosion characteristics of these materials were given in the First Annual Report.

In addition to these alloys, two others were added during the second contract year. One was 7079-T651 alloy, which was obtained in the form of 6" thick commercially fabricated plate. This alloy is another material of the Al-Zn-Mg-Cu type.

The other alloy used was 7039-T6, which is representative of the Cu-free Al-Zn-Mg type of alloy. This type of alloy is subject to a pitting type of attack in the unstressed condition but, in certain tempers, is susceptible to stress-corrosion cracking. The first lot of 7039 alloy obtained was 2" thick plate in the F temper. This plate was heat treated, quenched, and aged to the T6 temper in the laboratory. The resistance to stress corrosion of this plate was quite good, however, and the plate was judged to be unsatisfactory for crack initiation investigations. Another lot of commercially fabricated 7039-T6 alloy plate was then selected from a group undergoing stress-corrosion testing. This lot was 3" thick plate and was chosen because it showed the poorest resistance to stress corrosion of the group. Poor stress-corrosion resistance was essential if crack initiation was to be analyzed.

The composition and mechanical properties of the new plate are listed in Table I. Both alloys were susceptible to

stress corrosion cracking, as shown by the data in Table I, and the usual difference related to stressing direction was noted in the 7079-T6 alloy plate where results in two directions were available.

As a further evaluation of corrosion behavior, standard type-of-attack tests as per MIL-H-6088D were made on both new alloys. The attack of the 7079-T6 alloy was a combination of pitting and intergranular, and that of the 7039-T6 plate was pitting. Thus, in 7039-T6, there was a susceptibility to pitting attack unstressed combined with a susceptibility to stress-corrosion cracking. This combination was desired to permit investigation of the effect of stress in changing corrosive attack from pitting to intergranular cracking.

During the first year of the contract, and extending into the second year, attempts were made to produce in 2219 and 7075 alloys the combination of pitting attack unstressed and a susceptibility to stress-corrosion cracking. These attempts were not particularly successful and further attempts were abandoned because the combination desired was obtained in the 7039-T6 plate.

As was done during the first contract year, specimens for all tests and examinations were taken at a location 1" below the surface. This was done to be in the region of comparatively slow cooling during quenching.

PROCEDURE AND RESULTS

Effect of Metallurgical Structure

In evaluating the relationship between crack initiation and metallurgical structure, both old and new procedures were used. The older methods, applied primarily to the new alloys, consisted of describing microstructures thoroughly, observing the initiation and development of corrosion in the absence of stress, and then making similar observations on stressed specimens. New methods included the use of the microprobe to explore corrosion films and the electron microscope and microprobe to investigate fracture surfaces. Also, methods for the observation of crack initiation by transmission electron microscopy were explored and an investigation of the evolution of the stress-corrosion-susceptible paths in 7075-T6 was started.

Characterization of 7079-T6 and 7039-T6 Plate

Light Microstructure

The light microstructures, of the new alloys, 7079-T6 and 7039-T6, were analyzed and recorded in the manner used with 2219 and 7075 alloys previously. Samples were taken 1" below the plate surface, and the longitudinal (YX) and transverse (XZ) planes were polished and examined by conventional metallographic procedures.

The 7079-T6 plate was substantially unrecrystallized and the structure consisted of clusters of grain fragments, each cluster representing a "former" grain (Fig. 1). The structure was elongated somewhat in the rolling direction, which oriented the "former" boundaries parallel to the surface of the plate. The structural elongation was not particularly great, however,

because the plate was six inches thick and had received a relatively low reduction in thickness from the ingot. The 7039-T6 plate also had a substantially unrecrystallized structure with "former" grains highly elongated in the rolling direction (Fig. 2). The structural elongation was greater than in the 7079-T6 plate because the plate was thinner and had received more reduction from the ingot.

The distribution of microconstituents in the alloys was also related to plate thickness. In the 6" thick 7079 alloy plate (Fig. 3), constituents showed little alignment in the rolling direction, whereas with the 3" thick 7039 alloy plate (Fig. 4), constituents were frequently located in stringers parallel to the rolling direction. Both alloys had considerable boundary precipitate, both on "former" boundaries and on fragment boundaries, as shown by Figs. 5 and 6.

Electron Microstructure

The electron microstructure of the 7079-T6 plate was similar to that of the 7075-T6 alloy plate described in the First Annual Report. Numerous E-phase ($Cr_2Mg_3Al_{18}$) dispersoid particles were scattered throughout the structure, with certain areas having a high concentration of particles, and others being almost dispersoid-free. Numerous precipitate particles were present on boundaries, including large particles developed during quenching and much finer particles formed during artificial aging. Within the matrix, there was a moderate number of dislocations, a large percentage of which were pinned by the E-phase dispersoid particles. Also present in the

matrix was a multitude of fine zone-type precipitates. These were randomly distributed except at some boundaries where narrow (200-300 A) precipitate-free regions were apparent. Transmission structures of the 7079-T6 plate are shown by Figures 7-8.

The structure of the 7039-T6 plate was also similar to that of 7075-T6 alloy. E-phase dispersoids were fairly numerous and unevenly distributed, two distinct sizes of boundary precipitates were apparent, and some dislocations were present in the matrix. Precipitate-free regions were similar to those in 7079-T6, although possibly somewhat wider (250-400 A). Transmission structures of the 7039-T6 plate at two magnifications are shown by Figures 9-10.

In view of the marked difference in stress-corrosion behavior between the two lots of 7039-T6 plate, the first of which was discarded because its resistance to stress-corrosion was too good, the electron microstructures of the two lots were compared. Surprisingly, no differences in structure were evident. It can only be concluded that differences in stress-corrosion behavior are not always reflected in differences in microstructure and, conversely, that features seen in the transmission microstructures are not necessarily significant in terms of stress-corrosion behavior. This casts doubt on claims that certain microstructural features are responsible for differences in stress-corrosion behavior. Instead, it appears that particular thermal treatments change both structure and stress-corrosion behavior, that the changes in the solid solution brought about by the thermal treatment are important, and that the microstructural changes may be only incidental.

In connection with the precipitate-free boundary regions observed in the electron microstructures of the various 7XXX series alloys, it was noted that some had very pronounced regions of this type, whereas others did not. This has led to considerable speculation as to why the various boundaries differ and whether this is pertinent to the initiation of stress-corrosion cracks. One hypothesis is that the boundaries which develop the precipitate-free regions are those between grains having a relatively large difference in orientation, which would generally be the "former" grain boundaries. Conversely, the hypothesis proposes that the boundaries having no precipitate-free regions are those between grains having only a small orientation difference. These would include the grain fragments in unrecrystallized material such as the commercial 7XXX alloys of this contract. This hypothesis, combined with the observation that cracks have always initiated on "former" boundaries, would lead to the deduction that the precipitate-free regions are the selective, susceptible paths involved in stress-corrosion cracking.

Considering the possible metallurgical nature of these particular boundary regions, they can be free of precipitate for either of two reasons. These regions may be depleted in solute by diffusion to the boundary and the formation of the fairly extensive grain boundary precipitate. On the other hand, these regions may be free of precipitate because they are depleted in vacancies which assist the development of zone-type precipitate. In any case, the region would be different from

the matrix, both mechanically and electrochemically. The region could be weaker mechanically, and thus selectively susceptible to mechanical rupture, either because it contained less solute or because it did not have the strengthening effect of the zone-type precipitation. From the electrochemical standpoint, the region could be a selective anodic path either because it was depleted in copper by diffusion or because it was not depleted in zinc because precipitation did not occur. It is planned to evaluate this hypothesis in some detail.

Phase Identification

In addition to characterization on the basis of microstructure, the new alloys were also characterized by diffraction analyses to establish the phases present and the degree of recrystallization. In addition to the solid solution matrix, both alloys contained Mg_2Si, (Fe, Mn, Cu) Al_6, Al_{12} (Fe, Mn)$_3$Si, and E-phase ($Al_{12}Mg_2Cr$ or $Cr_2Mg_3Al_{18}$). The amounts of Mg_2Si and E-phase were similar in the two alloys. The Al_{12} (Fe Mn)$_3$Si phase was present in slightly greater amount in 7079 than 7039 alloy. There was slightly more (Fe, Mn, Cu) Al_6 in 7039 than in 7079 alloy. Both alloys were substantially unrecrystallized with only the start of recrystallization apparent. Comparing these analyses with the light and electron microstructures, the phases detected can be matched to particles seen in the microstructure. The Mg_2Si represents undissolved Mg combined with Si, and the Fe-bearing constituents are the combination products with this insoluble impurity element. Both of these are apparent in light microstructures. The E-phase particles

are the relatively fine dispersoid particles resolved only in the electron microstructure, and represent high temperature precipitation of this phase during preheating. The non-uniform distribution of E-phase particles results from peritectic segregation of Cr within dendrite cells during solidification.

Corrosion of Unstressed Specimens - 7079-T6 and 7039-T6

The initiation and progress of corrosion of the new alloys 7079-T6 and 7039-T6 was observed in the manner used previously with 2219 and 7075 alloys. Specimens taken 1" below the surface of the plate were metallographically polished and the sequence of corrosion events in the pH1 $NaCl-AlCl_3$ solution was observed with the light microscope. The corrosion of 7079-T6 was a combination of fine intergranular attack, a wide intergranular attack, and matrix pitting. The intergranular attack developed initially along "former" boundaries in the unrecrystallized structure and later along grain fragment boundaries (Fig. 11). The matrix pitting developed adjacent to microconstituent particles but not exclusively at such sites. Cross sections showed particularly well the initial development of fine intergranular attack and the subsequent widening of this attack by the development of interfragmentary attack along the sides of the intergranular fissures. The corrosion of 7039-T6 in the pH1 $NaCl-AlCl_3$ solution was of the pitting type and frequently initiated in the vicinity of constituent particles or clusters, although not exclusively at such sites (Fig. 12). As corrosion progressed,

it spread out from initial sites, started at new random sites and was generally not related to any particular microstructural feature. In cross section, some of the pitting was aligned on boundaries, but the corrosion paths were quite wide.

The initiation and progress of corrosion of 7039-T6 were also observed in a solution of 0.5N NaCl + 0.5N Na_2CrO_4 adjusted to pH2 with HCl. This solution was used in observations of crack initiation when cracking did not occur in the pH1 NaCl-$AlCl_3$ solution, as will be described in a later section of this report. In the NaCl-Na_2CrO_4 solution <u>without</u> stress, only very little corrosion of 7039-T6 occurred even in relatively long exposure times. The majority of the corrosion that did develop was in the form of pits associated with particles or clusters of microconstituents (Fig. 13). In cross section, the corrosion tended to be very shallow and did not follow a selective path.

<u>Stressed Specimen</u>

In the First Annual Report, it was mentioned that there had been a slight error in the stressing of the tuning-fork specimens because of the biaxial stress condition in this type of specimen. New calibration curves were developed at that time and have been used with all stressed specimens during the second year of the contract. The curves generated for the new alloys 7079-T6 and 7039-T6 were developed initially on the basis of biaxial stress. Figure 14 shows the calibration for all alloys used during the second contract year.

Corrosion of Stressed Specimens

Light Microscopy

Certain variations in crack initiation times for stressed tuning-fork specimens exposed to the pH1 $NaCl$-$AlCl_3$ solution indicated that crack initiation time may be affected by minute amounts of metal dissolved from test specimens. To evaluate this effect, samples of 7075-T6 were exposed to (1) a fresh solution and (2) a solution in which two stressed tuning-fork specimens of 7075-T6 had been exposed for one hour. The corrosion mechanism unstressed was the same for both solutions but the amount of attack in a 30-minute period appeared to be less with the "used" solution. Similar tests of tuning-fork specimens stressed short transversely to 75% YS showed that crack initiation and early propagation were retarded slightly in the "used" solution, but the mechanism appeared to be the same in both solutions. To avoid any effect of this type, all specimens thereafter were exposed separately, each in a fresh solution.

During the first year of the contract, crack initiation and development were observed on polished surfaces of tuning-fork specimens, and penetration into the specimen was determined by sectioning the specimen at the end of the test. During the second year of the contract, the tuning-fork specimens were used in a somewhat different manner to permit simultaneous observation of crack initiation on both the longitudinal (YZ) and transverse (XZ) planes. In preparing the specimens for this type of exposure, both the end face and one side face were metallographically

polished in the usual manner. Next, both surfaces were masked off except for a narrow band adjacent to their mutual edge. Exposure was then conducted in the usual manner.

For evaluating this procedure, tuning fork specimens from 7075-T6 plate were stressed short transversely to 75% YS and were exposed to the pH1 NaCl-$AlCl_3$ solution. Cracks initiated primarily at the exposed edge and progressed both along the most highly stressed end face (Fig. 15) and along the side surface (Fig. 16) where stress would decrease as the crack became deeper. Cracks initiated on "former" boundaries and progressed along such boundaries in the manner noted in observations of the end face only. In many instances, cracks seemed to form preferentially on boundaries between "former" grains which developed different shades on etching (Fig. 16). This indicates that orientation between adjoining grains or former grains may influence crack initiation.

Occasionally, cracks would form on portions of a boundary on the two exposed faces very close to their mutual edge and would progress away from the edge. This developed very high stress on the unfractured metal at the edge, and mechanical fracture would occur. This mechanical fracture did not follow the boundary on which the stress-corrosion cracks had initiated. Thus, examinations of the surface of such a fracture might indicate that the crack had started transgranularly and had then sought an intergranular path. Actually, the sequence of events was reversed and the transgranular portion of the fracture did not occur first and was produced by a mechanical rather than a stress-corrosion mechanism. It is believed that

this was the case in the region shown in Figs. 15 and 16. While the majority of the cracking is definitely intergranular, the fracture appears to be transgranular (or perhaps interfram-mentary) at the corner.

This type of examination also provided additional evidence of the necessity of favorably oriented, susceptible paths for stress-corrosion crack propagation. In the area shown in Figs. 15 and 16, the crack initiated and developed rapidly during the first ten minutes of exposure. In the next ten minutes, however, very little propagation was noted, even though there were no major neighboring cracks, the development of which would relieve the stress. Metallographic etching disclosed that the crack had developed along a favorably oriented boundary between "grains" having different orientation. The crack had stalled when it reached the end of one of these "grains," even though favorably oriented paths along "grain" and fragment boundaries were still available. Thus, relative orientation on the two sides of a boundary may influence crack initiation, either as a separate factor or as it influences the corrosion susceptibility of the boundary path.

Crack initiation in 7079-T6 plate was observed in the usual manner, employing tuning-fork specimens, the end faces of which were metallographically polished and masked before exposure. A short transverse stress of 75% YS was used and exposure was in the pH1 NaCl-$AlCl_3$ solution. With these specimens, cracks developed in comparatively short times (20-30 min.), the cracks initiating on "former" boundaries. Some cracks initiated

near or at constituent particles (Fig. 17) but others originated elsewhere (Fig. 18). Cracks formed and propagated perpendicular to the stress and along relatively straight paths (Fig. 17). In some cases, cracks ceased growing because other larger cracks in the vicinity had relieved the stress locally. In such regions, interfragmentary attack, typical of unstressed corrosion, tended to develop beside the crack and adjacent to "former" boundaries (Fig. 18). Cracking in cross section was similar to that observed on the polished surface. Cracks penetrated almost exclusively along "former" grain boundaries perpendicular to the stress (Fig. 19).

The stress-corrosion behavior of the 7039-T6 plate was observed by stressing tuning-fork specimens short transversely to 75% YS and exposing them to the pH1 NaCl-$AlCl_3$ solution. During the first few minutes of exposure, attack of the surface developed readily, and at the end of ten minutes numerous cubic pits and a general very fine matrix corrosion were apparent (Fig. 20). As the exposure continued, the attack continued in a cubic fashion but no cracking was evident. After an exposure of 12.5 hours, most of the polished surface had been corroded away and, since it would not have been possible to discern cracks if they did initiate, the test was stopped and the specimen was sectioned. Examination of the cross sections revealed very clearly the cubic nature of the attack and showed that there was a tendency for the corrosion to penetrate along "former boundaries" in the structure. Such corrosion was widespread but the penetration was along relatively wide paths, giving a serrated appearance to the edge of the cross section at the corroded surface. No

true cracks had initiated (Fig. 20).

The test was then repeated using a stress of 90 %YS. Again, fairly general corrosion took place but no cracks initiated. After 14 hours of exposure, during which time almost the entire specimen surface was corroded away, the test was stopped and the surface was repolished lightly to see whether any cracks had initiated at the base of the corrosion crevices. No cracks had developed. Cross sectioning the specimen revealed the same cubic pitting with a tendency to penetrate more rapidly along "former boundaries." This type of penetration produced a saw-tooth edge on the cross section but the selectivity of attack was quite minor and it appeared doubtful that true stress-corrosion cracks ever would initiate. This seemed illogical in view of the rapid failure of this material in the 3.5% NaCl alternate immersion test under a stress of 65% YS. On the other hand, it has often been observed that stress-corrosion cracks are less likely to develop when considerable general corrosion occurs. From this it was concluded that the pH1 NaCl-$AlCl_3$ solution was unsatisfactory for the studies of crack initiation in 7039-T6 because it developed too much general corrosion.

A solution of 0.5N NaCl + 0.5N Na_2CrO_4 adjusted to pH2 with HCl was then tried with 7039-T6 specimens stressed short transversely to 75%. This environment had developed cracks in 7039-T6 in other tests at these laboratories. In this solution, cracks developed quite readily in the tuning-fork specimens. Cracks tended to initiate at constituents which were attacked or

at pits where particles had been dissolved (Fig. 21). Cracks developed only along "form- " :.ndaries perpendicular to the stress, and associated themselves with constituent particles only when such particles were on boundaries (Fig. 22). At the exposed surface in Figure 21, there is some indication that a pit formed initially and that when this pit reached a boundary, an intergranular crack developed. Not enough examinations have been made, however, to establish whether this crack initiation mechanism is typical of 7039-T6 or whether the particular micrograph is merely a coincidence.

Electron Microscopy

The electron microscope investigation of embryonic stress-corrosion cracks used oxide replica techniques, as had been done during the first contract year. As explained in the First Annual Report, the oxide replica is capable of revealing structure within a minute crack or crevice as well as on the surface of a specimen.

Examinations were made of crack initiation in tuning-fork specimens of 7075-T6 and 2219-T37 stressed to 75% YS in the longitudinal direction. This was a follow-up of the light microscope work on the effect of stressing direction carried out during the first year. With the longitudinal stress, crack initiation and boundary penetration were the same as with short transverse stress, cracks initiating at random sites on boundaries and propagating along a ragged intergranular front between grains (Fig. 23). With the longitudinally stressed specimens, however, a number of cracks initiated on boundaries parallel to, or at a low angle to the stressing direction (Fig. 24). As explained in previous reports, this was associated with the biaxial stress

condition in the specimen and the ease of crack initiation under the much lower short-transverse direction stress.

In the 7075-T6 specimens, possible crack development was noted at the junction of dispersoid-lean regions and those having average dispersoid population (Fig. 25), although it cannot yet be said whether such junctions are prime targets for crack initiation. In 2219-T37 specimens, a number of cracks were noted in regions near constituent particles. Cracks were invariably associated with the boundaries rather than the constituent particles, however, confirming earlier light microscope examinations.

Tuning-fork specimens of 7079-T6, stressed short transversely to 75% YS and exposed to the pH1 NaCl-$AlCl_3$-HCl solution, were also examined with the electron microscope. Cracks initiated as fine-scale attack of the boundary (Fig. 26) possibly by dissolving the Mg-Zn precipitates formed during quenching. Frequently, initiation occurred on polygon boundaries representing the junction of dispersoid-free regions with regions of average structure (Fig. 26). Cracking proceeded downward along the boundary, often along a very irregular front (Fig. 27). In this deepening process, the dissolution tended to be exaggerated where the polygons making up the grain boundary come together, giving the surface of the crack a veined appearance (Fig. 28). Even when the crack was comparatively deep, the base of the crack was very irregular since it propagated by dissolving new metal along narrow tendrils (Fig. 29). These often suggested cubic attack,

indicating that a crystallographic factor is involved. Although an unusually large number of constituent particles were associated with the stress-corrosion cracks in this alloy, they did not seem to contribute to crack initiation or propagation.

Microprobe Investigations

Corrosion Films

In an attempt to relate crack initiation to the surface films or reaction products developed, electron microprobe analyses were made on a 7075-T6 specimen exposed to the pH1 NaCl-$AlCl_3$ solution just long enough to initiate cracks at 75% YS. The surface appeared relatively clean under the microscope, with only occasional speckled patches of surface film.

Electron beam scanning pictures showed an uneven distribution of oxygen and chlorine on the surface. Both elements were concentrated within the stress-corrosion cracks and in the speckled patches. Five step-scans were made across short cracks to obtain quantitative data. The results fell between the two examples illustrated in Figures 30 and 31.

In the first example, a comparatively narrow crack, up to 4.5% O and 1.17% Cl were detected in the crack, but the actual levels may have been considerably higher since the electron beam could not be confined wholly to the crack. Some oxygen and a little Cl could be found for a distance of about 15 microns to one side of the crack but a much shorter distance to the other. In the other example, a wider crack, the oxygen and

Cl did not reach as high levels in the crack, but the Al concentration dropped closer to that of Al_2O_3.

The portions of the specimen surface which appeared clean showed no oxygen or Cl. The areas with the speckled films showed an average of 0.9% O and 0.14% Cl, but again this is probably lower than the true value.

There is thus evidence that stress-corrosion cracks in 7075-T6 contain an oxide-type corrosion product involving Cl. The microprobe cannot determine the state of chemical combination of the elements, but it is likely the Cl is present as an adsorbed chloride.

Fracture Surfaces

As described in the First Annual Report, microprobe scans across grain boundaries were made in the search for solute-depleted regions thought to be present at grain boundaries in stress-corrosion susceptible material. Even though scans were made at a low angle to the boundaries to increase the effective breadth of any such regions, only slight evidence of any composition variation was found.

During the second year of the contract, the microprobe was again used to analyze boundary regions, but in a different way. The new approach was to reduce the depth from which the analysis was obtained by reducing the accelerating potential, and then scanning the fractured surfaces of stress-corrosion cracks. It was reasoned that if stress-corrosion cracking proceeds through a grain boundary zone depleted in alloying elements, and the zone is not completely consumed by corrosion,

remnants of the zone will be found on the faces of the fracture. Microprobe analysis of the fracture faces would then show the composition of the zone if the depth of analysis was confined to small enough dimensions.

This technique was applied to a 7075-T6 specimen which had been broken open to expose the surface of a relatively large stress-corrosion crack. After mechanically flattening the fracture surface to minimize roughness effects, comparative analyses were made of the stress-corrosion and tensile portions of the fracture. First, analyses were made with a wide analytical spot to obtain an overall analysis. Results were:

	Cr	Cu	Zn	Mg
Stress-Corrosion Fracture	0.169	1.42	5.60	2.36
Tensile Fracture	0.172	1.52	5.79	2.52

The differences in Mg and Zn appear significant; those in Cu and Cr are questionable.

To obtain more statistically significant data, a total of 40 separate analyses were made on each of the two types of fracture with the beam focused to a fine analytical spot. Histograms showing the distribution of the various analyses are shown in Fig. 32. Since the distributions of the tensile and stress-corrosion areas overlap, Weibull analyses of the data were made. It was found that the data for Cu and Cr came from the same population. Values for Zn and Mg, however, were from different populations and therefore were significantly different. Numerically, the stress-corrosion fracture showed 0.26% less Zn and 0.03% less Mg than the tensile fracture.

A boundary region depleted in Zn and Mg is not unexpected because of the relatively high diffusion rates of these elements and the fact that precipitation on grain boundaries had occurred. Such a situation however, would not support an electrochemical thoery of stress-corrosion cracking because a region depleted in zinc would be cathodic to the matrix and would not be corroded preferentially. On the other hand, it must be remembered that (1) any anodic region might have been completely corroded away during the cracking process and (2) the penetration of the microprobe beam may have been much greater than the depth of the region involved in stress-corrosion cracking.

Differences in composition between fracture surfaces produced by stress-corrosion and by meahanical means were also found with 2219-T37 alloy, but for a different reason. With the microprobe spot defocused to cover a relatively large area, a stress-corrosion fracture analyzed 6.91% Cu and 0.25% Mn, as compared to 9.98% Cu and 0.42% Mn for a tensile fracture. The fact that the copper contents are much higher than the amount present in the alloy indicates that constituent particles are involved.

When the rough fractures were flattened in a hydraulic press, the stress-corrosion fracture showed 6.56% Cu and 0.27% Mn while the tensile fracture showed 7.51% Cu and 0.33% Mn. The reduction in the Cu values for both surfaces, and of the Mn value on the mechanical fracture, is believed to result from pressing the constituents into the matrix and therefore having a smaller constituent volume in the material analyzed.

The reason for the lower values on the stress-corrosion region was evident when many analyses were made on the two types of fracture using a finely focused beam. When the beam happened to fall on a constituent particle, the analysis was high in the element contained in the particle. When the beam fell between particles, the analysis reflected the solid solution level of the matrix.

With forty analyses on each type of fracture, the stress-corrosion region showed an average analysis of 6.33% Cu and 0.27% Mn, while the tensile region showed 6.37% Cu and 0.26% Mn. When analyses which had obviously hit particles were eliminated from the averages, however, both types analyzed about 5.87% Cu and 0.23% Mn, which is approximately the composition of the alloy and close to the solubility limits for these elements.

This work points out that the difference in overall analysis in the two regions is due not to a difference in matrix composition but to a difference in the number of constituent particles on the fracture surface. This is in keeping with previous electron microscope observations which had indicated that tensile fracture in 2219-T37 occurs preferentially through constituent particle clusters while stress-corrosion fractures show no such inclination and include very few particles.

Electron Fractography

Methods

In the search for the best methods for investigating crack initiation by electron fractography, a new and improved method was developed. This method overcame certain of the

complexities of the oxide-replica method for examining embryonic cracks and permitted instant differentiation of stress corrosion and mechanically fractured regions on fracture surfaces of tuning-fork test specimens. This method consisted of first applying a relatively thick (22 volt) oxide replica to test specimen that had previously developed a stress-corrosion crack. The specimen was then broken open by squeezing the legs in a vise, localizing the fracture to the desired area by appropriate saw cuts. At this point, the fracture surface contained oxide-covered stress-corrosion cracks and an as-yet-unreplicated tensile-fracture surface.

A second oxide replica was then formed on the fracture surface at 15 volts. Because the second forming voltage was lower than the first, no additional oxide was produced on the areas representing stress-corrosion cracks. Oxide was formed on the mechanically fractured area, however. This oxide appeared lighter in the electron microscope because it was thinner. The second forming, moreover, repaired damage to the original oxide film and permitted differentiation of topographical features developed during the stress-corrosion test from those developed mechanically during final fracturing of the specimen. An example of the use of this technique is shown by Fig. 33.

This method is also quite effective if a carbon film is substituted for the second oxide film. Application of the carbon at an angle, or using chromium shadowing, also shows whether the various features are above or below the general fracture surface. An illustration of the combination oxide-

carbon replica technique is shown by Fig. 34.

The oxide-carbon replica method was also useful for visual examination of fracture surfaces. Because of the aluminum oxide layer on the stress-corrosion portion of the fracture, the color of the carbon in this region was different than that on the rest of the surface which had no oxide. The stress-corrosion fracture was a bluish-grey color which contrasted strongly with the brown color of the remaining fracture. At a glance one could tell the relative depth and number of stress-corrosion cracks present. At the same time, the surface films were so thin that the fractures could be examined in detail in the light or electron microscopes, the difference in color showing unequivocally which type of fracture was being examined.

Fracture Surfaces

Electron microscope examinations of oxide replicas of the surfaces of stress-corrosion cracks in tuning-fork specimens of 7075-T6 were used to gain additional information regarding crack initiation. The most characteristic feature was a network of furrows which appeared to represent either (1) the boundaries of the polygonal grain fragments observed at high magnification in the light microscope of (2) the boundaries of the relatively equiaxed polygons observed in the electron microscope in dispersoid-lean regions. Thus, while the "former" boundary path of the cracks was quite straight at light microscope magnifications, it actually consisted of tiny facets which were polygon boundaries.

As the cracks developed, they contined to follow polygon boundaries, frequently giving the fracture a faceted

appearance (Fig. 35). When the facets were not well-defined, the fracture surfaces usually had a network of shallow furrows defining the edges of the polygons. When these furrows extended to the surface, it was usually possible to see that they matched exactly with the polygon boundaries on the surface (Fig. 36). There was surprisingly little secondary cracking or tendency of branch cracks to follow polygon boundaries into the metal behind the fracture face. Instead, a crack confined itself to as planar an interface as the polygon boundaries would allow. This is analogous to crack initiation in 2219-T37 seen under the light microscope where cracks selected the straightest possible path along grain boundaries perpendicular to the stress.

Stress-corrosion crack surfaces frequently had constituent or dispersoid particles projecting above the general surface but there was no indication that either interacted with the crack.

There were some areas within the stress-corrosion fracture which showed characteristics of tensile rather than of stress-corrosion fracture. These were generally quite small and represented portions of the grain boundary which had not cracked during the corrosion test. There was absolutely no indication of plastic deformation on the stress-corrosion fracture itself, indicating either that stresses were entirely in the elastic range or that any plastically deformed metal was completely consumed by corrosion.

The tip of the stress-corrosion crack had fine-scale irregularities, sometimes cubic, but more generally rounded (Fig. 37). This and other freatures of the crack front were the same as those seen in examinations of surface oxide replicas. Beyond the stress-corrosion crack front there was usually a flat, rather featureless area representing the initial rapid tensile or "pop-in" failure produced when the specimen was being broken open. Beyond this region was the dimpled fracture appearance characteristic of tensile failure (Fig. 38). Each dimple was associated with a tiny dispersoid particle, indicating the strong interaction of this type of particle with tensile fracture, but not with stress-corrosion fracture.

Similar examinations were also made of tuning-fork specimens of 2219-T37 exposed to the pH1 NaCl-$AlCl_3$ solution. Unlike the 7075-T6 failures, where the deepening stress-corrosion crack followed a network of polygonal fragments between unrecrystallized grains, cracks in 2219-T37 followed relatively planar boundaries between recrystallized grains. There was, therefore, no distinctive grooving of the fracture surface in this alloy. The fracture appeared relatively smooth at low magnifications, but at high magnifications proved to be finely etched by corrosion. The boundaries between the smoother and the more deeply etched areas were scalloped or stepped, the latter suggesting solution was by a crystallographic mechanism. In a few areas, the micro-roughness of the fracture surface was in the form of fine parallel lines (Fig. 39). This is

perhaps an etching effect, but might be the remnants of slip steps and, hence, evidence for plastic deformation occurring in the stress-corrosion zone. Small rectangular constituent particles were commonly found lying on the stress-corrosion face of 2219 fractures, but there was no evidence that they contributed to the fracture.

There was ample evidence that the stress-corrsion cracks in 2219-T37 proceed in a very irregular manner rather than on a broad front. There were many islands within the stress-corrosion area that failed in a tensile manner, and at the ends of cracks, there were often spade-like tendrils advancing in front of the main crack beneath the surface. Examples of the irregular crack development in 2219-T37 are shown at a crack front in Fig. 40, and near a surface in Fig. 41.

Grain Boundary Evolution

Contract work to date has shown consistently that "former" grain boundaries in 7075-T6 plate are the crack initiation sites and propagation paths. Toward the end of the second year of the contract, an investigation was started to follow the evolution of these boundaries from ingot to plate in an attempt to explain why they are particularly susceptible to crack initiation. For this work a 12 in. x 30 in. DC ingot of 7075 alloy was obtained and, after removal of 2" from each surface by machining, the 8" thick center section was hot rolled into plate. At various thicknesses, slices were removed for subsequent examination, some being retained

in the as-fabricated condition and others being heat treated to the T6 temper. The strength of the material increased slightly as the material was rolled (Table II). In the as-rolled plate, this is probably the result of increased residual cold work. In the T6 plate, increased elements in solid solution prior to the precipitation treatment and the development of a wrought structure are probably responsible for the higher strength of the thinner plate.

The electron microprobe was used to study progressive changes in microsegregation as the ingot was rolled to plate of decreasing thickness. In the ingot, the elements Zn, Mg, and Cu were found to be more concentrated at the edges of dendrite cells than in the center of the cells. As the ingot was preheated and the individual dendrites began losing their identity during rolling, these compositional variations were reduced.

The ranges of analyses observed are indicated in Figs. 42-44. The lower portion of each figure shows the actual range for each element together with a point indicating a typical or average composition for the solid solution of each sample. These analyses purposely do not include the portion of an element that is combined in constituent particles. The upper graph of each figure shows the observed range of analysis compared to the average bulk analysis. The closer the index approaches zero, the more nearly homogeneous the sample has become.

Preheating and a small amount of rolling were sufficient to distribute Cu fairly uniformly in the unheat-treated plate. The

approach to uniformity in the elements Zn and Mg, however, was more gradual, increasing as rolling progressed. Heat treating to the T6 temper produced additional homogenization. In the T6 temper the degree of microsegregation was essentially independent of plate thickness. Zinc analyses of the matrix leveled off at the overall Zn content of the alloy. Mangesium and Cu, however, leveled off at somewhat lower amounts than were actually present, indicating a portion of both of these elements was confined in intermetallics.

A special effort was made to detect compositional differences in the vicinity of grain boundaries of the various thicknesses of plate. No such differences were detected, even when the microprobe trace was made at a low angle to the grain boundary.

Solution potentials of the various products reflected the compositional differences (Table II). The as-rolled samples became more anodic as the matrix Zn content increased during rolling. All T6 samples were identical with a solution potential typical of 7075-T6.

Stress corrosion tests of the slices are essentially complete (Table II). Unfortunately for the purposes of the investigation, stress corrosion behavior was unexpectedly good. The reason for this is not clear but may be related to the fact that the plate was cooled and reheated a number of times as samples were taken at various thicknesses during fabrication. A somewhat different procedure will be used on other ingots to duplicate production procedures more closely.

Metallographic examinations of all samples will be made to observe the development of "former" boundaries.

Corrosion of Thin Metal Films

One proposed phase of the contract work was to observe crack initiation by transmission electron microscopy. It was planned to thin samples to 1000A or less so that their structure could be examined with the electron microscope. These thin metal films were first to be corroded in the absence of stress to observe the relationship between corrosion sites and features of electron microstructure. They were then to be exposed in the stressed condition to observe crack initiation at electron microscope magnifications. The most critical factor in this approach to the analysis of corrosion and stress corrosion is in the thin specimen preparation. Either there must be no selective attack during thinning, or the features of any selective attack must be readily distinguishable from those developed during corrosion and stress corrosion.

Considerable work was done in evaluating specimen preparation techniques but, to date, no sure way of differentiating between thinning effects and corrosion features was found. Rather than risk uncertain or erroneous conclusions, this approach to crack initiation analysis was delayed until the coming year.

Effect of Surface Roughness

During the first year of the contract, the effect of mechanically- and chemically-produced surface irregularities on crack initiation was investigated. During the second year of the

contract, the effects of surface roughness in the forms of pre-corrosion and mechanical abrasion were evaluated.

Pre-Corrosion

In evaluating the effects of pre-corrosion on crack initiation, tuning-fork specimens of the stress-corrosion-susceptible alloys 2219-T37 and 7075-T6 were exposed unstressed in the pH1 $NaCl-AlCl_3$ solution until well-defined intergranular fissures developed. The specimens were then stressed to 75% YS short transversely. In the initial experiments, it was thought that cracks extended after application of stress and before exposure, possibly as a result of corroding solution left in the corrosion crevices. Experiments showed that with relatively deep corrosion crevices, extension by stress-corrosion cracking under the influence of residual solution could indeed occur (Fig. 45). With smaller crevices, however, it was relatively easy to flush out the solution, and crack extension did not occur unless further exposure to the corroding solution was made.

The next step in the investigation of the effects of pre-corrosion was to examine specimens corroded and then stressed, but before corrosion in the stressed condition. This was necessary because difficulty was foreseen in differentiating between intergranular corrosion crevices widened by corrosion and true stress-corrosion cracks. In one series of experiments, tuning-fork specimens of 7075-T6 and 2219-T37 were corroded in the unstressed condition and were then stressed short transversely to 90% YS. As shown by Figs. 46 and 47, stressing widened the corrosion crevices perpendicular to the stress and only perpendicular to the stress. The resulting crevices looked exactly like the stress-corrosion

cracks developed in the same alloys in the same environment. This was a very important observation because it points out quite strikingly that intergranular corrosion crevices later widened by stress could be mistaken for stress-corrosion cracks.

The final step in the investigation was to re-expose samples that had been first corroded and then stressed. This was done with 7075-T6 samples stressed short transversely to 75% YS. Comparing the same areas before and after the stress-corrosion exposure, it was obvious that the cracks extended quite rapidly by a stress-corrosion mechanism. It was impossible, however, to distinguish between the widened-corrosion-crevice and stress-corrosion portions of the final crack. Two areas, before and after the stress-corrosion exposure are shown in Fig. 48.

Mechanical Roughness

In evaluating the effect of fine, mechanically-produced surface roughness, specimens of 2219-T37 and 7075-T6 were taken through the 3-0 metallographic paper grinding operation, some with the grinding marks parallel to the longitudinal direction, and others with the marks parallel to the short-transverse direction of the structure. With unstressed specimens exposed to the pH1 test solution it was very difficult to observe the corrosion paths (Fig. 49) because (1) the grinding marks were the most prominent features at the high light-microscope magnifications used, and (2) because the plastic deformation associated with the grinding apparently altered the microstructure. With tuning-fork specimens stressed short transversely to 75% YS, cracking was not observed

until a period well beyond that required for obvious cracking in polished specimens (Figs. 50 and 51). When cracks did become visible, it was impossible to establish their paths because of the gross roughness of the ground surface. The delay in apparent cracking was undoubtedly caused to some degree by the masking effect of the roughness. Almost certainly, however, cracks were actually present before they were apparent under the microscope.

This was verified by examining cross sections of 7075-T6 specimens stressed to 75% YS and exposed to the pH1 solution until cracks were just visible under the light microscope. At this stage, fairly deep cracks were present (Fig. 52), indicating that crack initiation had actually occurred at a much earlier time. The cracks at the ground surface were not of the fine intergranular type, however, but consisted of wide crevices, generally intergranular, from which fine intergranular stress-corrosion cracks emanated. Thus, fine mechanical surface roughening had an affect on crack initiation, although it neither promoted or prevented cracking. Instead, it altered crack development in a narrow layer at the surface. Once this region was breached, however, cracking proceeded in a normal manner.

Effect of Surface Film

During the first year of the contract, it was noted that natural oxide film formed between final polishing and exposure of a tuning-fork specimen had a pronounced effect on crack initiation time but not on the initiation sites or mechanism of cracking. During the second year of the contract,

the effects of a group of artificially produced surface films were evaluated.

In the first phase of this work, films about 85, 250 and 750 angstroms in thickness were applied to 7075-T6 and 2219-T37 specimens by anodizing at 6, 18 and 54 volts in a 3% tartaric acid solution adjusted to a pH of 5.5 with ammonium hydroxide. During the anodizing operation, the micro-constituents and boundary precipitate particles were generally dissolved out, leaving pits of a corresponding size both within the matrix and at boundaries (Figs. 53 and 54).

Tuning-fork specimens of each alloy with each of the three barrier-type coatings were stressed short transversely to 75% YS and were exposed to the pH1 solution. The films had an effect on the time to crack initiation, the thicker films preventing cracking for longer times, although not for times proportional to film thickness. Cracking times were:

Film Thickness - A	Crack Initiation Time - Min. 7075-T6	2219-T37
85	5	5
250	8	10
750	18	18.5

The crack initiation mechanism was the same as with as-polished specimens, cracks starting either at random sites or at pits on boundaries and progressing along boundaries perpendicular to the stress (Figs. 53-54). Since it would be expected that the time to cracking is the time required for the environment to breach the films, the fact that cracking time was not proportional to film thickness suggests that the film is thinner or weaker than normal at the boundaries. This

was confirmed by electron microscope examinations which showed film weakness at boundaries where the precipitate particles had been dissolved out or converted to a porous type of oxide (Fig. 55). Similar behavior was noted with the constituent particles and dispersoids but this was not significant because cracks did not initiate at these locations.

Additional electron microscope examinations were made to study the effect of barrier oxide films on crack initiation and the propagation of cracks formed before application of the oxide film. Tuning-fork specimens of 2219-T37 and 7075-T6 were stressed short transversely to 75% YS and were exposed to the pH1 NaCl-$AlCl_3$ solution until small stress-corrosion cracks formed. A 22-volt barrier oxide film was applied to the specimen and the specimen was re-exposed to induce propagation of existing cracks and the development of new ones. Finally, a 15-volt anodizing treatment was applied. In areas unaffected by the re-exposure, features would be replicated in 22-volt oxide. New features developed during the re-exposure would be replicated in 15-volt oxide. Features developed during the first exposure, and growing during the second exposure would be reproduced in two different thicknesses of oxide. This is the dual-oxide procedure described earlier in this report.

These examinations confirmed the findings from light microscope work described previously. There appeared to be a delay in crack development which presumably represented the time required for the environment to breach the barrier oxide film. Oxide breakdown occurred more readily at boundaries and at constituents but only the boundary breakdown

led to crack initiation. Boundary pitting through the oxide was associated with crack development but did not appear to be an essential condition for crack initiation.

With cracks existing before application of the first barrier films, mixed effects were noted. Some cracks did not propagate at all during the second exposure. It could not be established, however, whether the oxide had exerted a protective effect or whether these cracks were ones which do not propagate because of stress redistribution. Other cracks propagated by breaching the oxide and proceeding along the same paths they had followed before the oxide film was applied. With some of these, the breach was small and the crack developed from this location as a focal point, but the majority developed along a fairly broad front. Examples of cracks which propagated during the second exposure are shown by Fig. 56 and 57.

The effects of three other films on crack initiation in 2219-T37 and 7075-T6 were also evaluated. One was a chemically formed phosphate film applied by boiling for two minutes in a 2% NaH_2PO_4 solution at pH7. Other work at these laboratories has shown that a film of this type can delay or prevent attack of aluminum surfaces. The other two films were of the anodic barrier type and were formed to a thickness of about 250 A by forming at 18 volts. One was formed in the 2% NaH_2PO_4 solution at pH7, the other in a 3% CrO_3 solution adjusted to pH7 with NH_4OH.

During formation of the films, occasional pits developed in the boiling phosphate solution, apparently where certain

constituent particles were dissolved out. Anodic film formation in the phosphate electrolyte had no noticeable effect on the polished surfaces. Anodic barrier formation in the chromate electrolyte developed a certain amount of constituent dissolution, as well as some general pitting within grains. In addition, considerable fine pitting developed on the grain boundaries, presumably where precipitate particles were dissolved.

The effect of these films on stress-corrosion crack initiation was determined by applying the films to tuning-fork specimens stressed short transversely to 75% YS and exposing to the pH1 NaCl-$AlCl_3$-HCl solution. With the chemically formed phosphate film, crack initiation was delayed with 2219-T37 but no effect was noted with 7075-T6, cracks developimg very rapidly. With the film formed anodically in the phosphate electrolyte, cracking of 2219-T37 was again delayed appreciably, but crack initiation in 7075-T6 was about as rapid as without the film. With the anodic film formed in the chromate solution, crack initiation was considerably delayed with both alloys, possibly as a result of inhibition by the chromate ion. With all films, the crack initiation sites and the cracking mechanism appeared to be the same as with samples without the films.

This work led to three conclusions:

1. The presence of the films had no effect on crack initiation sites or the cracking mechanism.

2. The films themselves could delay but could not prevent crack initiation. The delays presumably represented the time required for the corroding environment to breach the surface film.

3. The pits developed during film formation had no noticeable effect on crack initiation sites or the cracking mechanism.

Effect of Stress

During the first year of the contract, preliminary evaluations of the effect of stress showed that there was a relationship between stress level and crack initiation time. During the second year, this relationship was evaluated quantitatively using tuning-fork specimens stressed short transversely and exposed to the pH1 NaCl-$AlCl_3$ solution. It was found that crack initiation time increased as stress level decreased, and in a semi-logarithmic manner as shown by Fig. 58.

During the second contract year, the effect of stress near the threshold level was investigated. Tuning-fork specimens of 7075-T6 stressed short transversely to 20%, 15% and 10% YS and exposed to the pH1 NaCl-$AlCl_3$ solution were used. In the 3.5% NaCl alternate immersion test, this alloy had shown failures down to 15% YS with 1/8" diameter tensile specimens.

At the 20 and 15% stress levels, cracks initiated in fairly short periods, with prominent cracks being visible on the polished surfaces after a 15-minute exposure (Figs. 59 and 60). With the 10% YS stress level, a few cracks formed but it would have been very difficult to distinguish between these cracks and crevices of intergranular corrosion except for the fact that they were exclusively oriented perpendicular to the stressing direction (Fig. 61). Cracks were much fewer at these lower levels than at the 75% stress level, presumably

because cracks developed on only the most susceptible and most favorably oriented boundaries. The crack initiation sites and path and mode of propagation were the same as at the much higher stress levels, except that no plastic deformation at crack tips was noted. Crack propagation at these very low levels was very slow and cracks were not very large even after relatively long periods of exposure.

Fairly prominent cracks were present in cross sections of samples corroded at all three low stress levels. As has been the case with 7075-T6 alloy throughout the contract work, cracks developed on "former" grain boundaries oriented perpendicular to the stress and followed such boundaries as they penetrated below the polished surface. At 20% YS (Fig. 62), cracks progressed to a considerable depth at the light microscope magnifications used. At 15% YS, cracks were shorter in similar exposure times, but still extended well below the level of general surface corrosion (Fig. 63). At 10% YS, cracks were still shallower, and in some instances were difficult to distinguish from the general intergranular corrosion. There were, however, very definite but shallow cracks at this stress level (Fig. 64).

Comparing behavior at the various stress levels evaluated during the contract, large differences in the rates of crack initiation and propagation have been noted. At all stress levels, however, the crack initiation sites and the paths followed by the cracks have been the same. Thus, stress level had a large effect on the rate but no noticeable effect on the mode of stress-corrosion cracking.

In initial evaluations of the effect of stress with the alloys added for the second year of the contract, crack initiation in 7079-T6 at 90% YS was investigated. Tuning-fork specimens stressed short transversely and exposed to the pH1 $NaCl-AlCl_3$ solution were used. No particular effect of stress level was noted, crack initiation and propagation being the same as at 75% YS. Cracks initiated and propagated on "former" boundaries perpendicular to the stress. Also, occasional areas of interfragmentary attack developed, apparently after the stress was relieved locally by crack development nearby. Crack initiation and development in 7079-T6 at 90% YS is shown by Figs. 65 and 66.

Effect of Environment

Screening Tests

During the contract period covered by this report, environmental tests were continued to: (1) determine the effect of specific anions on the stress-corrosion behavior of 2219 / and 7075-T7351 plate; (2) perform supplemental tests to resolve uncertainties over interpretation of test data in very corrosive solutions with pH 2; and (3) investigate stress-corrosion behavior of 2219 and 7075 alloy specimens in electrolytes of certain cations and in alkaline solutions at pH 11-11.5.

The testing was conducted with the commercially fabricated 4" thick 2219-T37 and 2" thick 7075-T651 alloy plate described in the First Annual Report. The 2219-T87 and 7075-T7351 tempers were obtained by artificially aging

portions of the plate in the laboratory. Limited testing was also conducted with T651 and T7351 temper specimens from a second lot of commercially fabricated 2.5" thick 7075 alloy plate.

Test procedures were the same as those employed in screening tests described in the First Annual Report. Short transverse specimens, 0.125" in diameter, were stressed to 75% YS in a "constant-strain" fixture and exposed to the various environments at 80-85F. Tensile tests were made of unstressed specimens at periods corresponding to stressed specimen failures, and of all specimens remaining at the end of the 60 day exposure when all tests were terminated.

Specific Anions - 2219-T87 and 7075-T7351

Thirty-three electrolytes, including both neutral and acidic solutions of various halides and complex anions were tested.

The test results are summarized in Table III for 2219-T87 in all electrolytes and in Table IV for 7075-T7351 in all electrolytes. The performance of the alloys in representative electrolytes is illustrated in Figures 67 and 68.

No evidence of stress-corrosion cracking was detected in specimens of 2219-T87 or 7075-T7351 alloys in any solution. A few failures occurred in solutions that are highly corrosive. Metallographic examination of the failed specimens showed that the attack of 7075-T7351 specimens was exclusively pitting while that of 2219-T87 specimens was predominantly pitting with a

slight amount of intergranular corrosion. This intergranular corrosion was generally very broad and was accompanied by the dissolution of a portion of the grain body.

The most corrosive solutions were those containing sodium chloride either alone or in combination with other sodium salts and acidified to a pH 2. Severe corrosion with some failures, principally in 2219-T87 specimens, also occurred in the acidic solutions of bromide and iodide anions. Acidic solutions of sulfate anions caused severe corrosion of the 7075-T7351 specimens but only mild corrosion of the 2219-T87 specimens. Acidified solutions of other sodium salts (fluorides, nitrates, chromates and phosphates) caused only mild corrosion of either alloy. Neutral solutions of the various sodium salts were not highly corrosive and caused no failures. However, the addition of H_2O_2 stimulated corrosion and induced failure of both alloys in a neutral NaCl solution, and 7075-T7351 in a neutral sulfate solution. The only other failures in neutral solutions occurred after 44-60 days exposure, with 7075-T7351 specimens in NH_4Cl and with both alloys in NaCl plus Na_2SO_4.

Because corrosion patterns in the acidified chloride solutions are varied, visual ratings shown in Figure 69 are unreliable to estimate corrosion damage. The misleading conclusions that might be drawn from use of visual ratings only are illustrated by examination of Figs. 70, 71, 72 and 73.

Metallographic examinations indicated that all of the 2219-T87 and 7075-T7351 test failures were the result of severe localized corrosion and not stress-corrosion cracking.

Because a comparison of tensile losses for stressed and unstressed specimens suggest an apparent acceleration of corrosion because of stress in several of the acidic solutions in which no failures occurred, crack initiation studies with tuning fork specimens were conducted in a limited number of solutions to investigate possible minor stress corrosion effects. These results are described in the "Selected Environments" section.

Supplemental Testing in pH 2 Solutions

Tests of 2219-T37, 7075-T651, 2219-T87 and 7075-T7351 specimens were made to establish whether certain failures in highly acid media were actually stress-corrosion failures. Both unstressed and stressed specimens were removed at several intervals for tensile tests and metallographic examinations to determine: (a) the initial type of attack, (b) the effect of prolonged exposure upon the pattern of attack, and (c) whether the corrosion was accelerated by applied stress. The results of these tests are listed in Tables V and VI, with portions of the previous results listed for comparison.

2219-T37 and 7075-T651 Specimens

Metallographic examination showed that corrosion of both items in sodium chloride solutions was initiated as fine intergranular attack which, with longer exposure, was broadened by dissolution of the surrounding grain bodies, resulting in an apparent combination of pitting plus intergranular attack. Figure 74 illustrates the initial intergranular attack and a fissure that appears to be the beginning of a stress-corrosion crack in one of the 7075-T651 specimens. Similar attack was noted with the 2219-T37 specimens, but the attack sites were

much more numerous. The losses in strength of stressed specimens of either alloy were significantly higher than the losses of corresponding unstressed specimens (Figures 75, top and 76, top) thereby indicating a marked accelerating effect of stress which is a prime criterion for stress corrosion.

The occurrence of intergranular fissures, and the accelerating effect of stress confirmed that failures of 2219-T37 and 7075-T651 alloy specimens in the acidified chloride solutions were the result of stress-corrosion cracking. The longer times to failure with the 2219-T37 specimens were related to the uniform pattern of intergranular attack, and the low level of elastic strain energy developed in the stressing frame by the specimens of this relatively low yield strength alloy. With a uniform pattern of attack, high reductions in cross-section area can be endured (see Figure 77), and fracture would not be expected unless at least one corrosion fissure had developed into a stress-corrosion crack.

Corrosion of 7075-T651 specimens exposed in a sodium sulfate solution initiated as surface pitting which tended to become directional with prolonged exposure (Figure 78), and there was no evidence of intergranular corrosion such as had been detected in the earlier screening test results. The results of initial screening tests and these supplemental tests of 7075-T651 specimens in acidified sulfate solutions have shown only a slight tendency for intergranular corrosion to occur, with directional pitting being the predominant type of attack. However, the observance of some intergranular attack, and the

definite acceleration of corrosion by high sustained stress (Figure 79), strongly suggests that failures were the result of stress-corrosion cracking. Because this could not be definitely ascertained by light microscopy, fractrographic examination of failed specimens will be undertaken in an attempt to clarify the cause of failure.

2219-T87 and 7075-T7351 Specimens

Microscopic examination revealed only pitting attack in 2219-T87 (Figure 80) and 7075-T7351 (Figure 81) specimens exposed in acidified chloride solutions. Attack in 7075-T7351 specimens exposed in an acidified bromide solution was also exclusively pitting, while specimens of both alloys exhibited only mild surface pitting after exposure in the acidified fluoride solution. The character of the attack did not change significantly with prolonged exposure in any of the electrolytes.

The application of stress did not significantly affect the rate of corrosion in 2219-T87 specimens exposed in acidified chloride solutions (Fig. 76 - bottom). Stress did result in slightly higher rates of corrosion of 7075-T7351 specimens in this environment, however, and plots of corrosion losses for stressed and unstressed specimens tended to diverge with increased exposure time (Fig. 75 - bottom).

The results of these tests substantiated prior test indications that failures of 2219-T87 and 7075-T7351 specimens in very corrosive acidic solutions were the result of severe

localized corrosion rather than stress-corrosion cracking, despite a slight acceleration of corrosion due to stress in the 7075-T7351 specimens.

Electrolytes Containing Certain Cations and Alkaline Solutions at pH 11-11.5

Eight electrolytes were selected for this phase of the screening tests. The solutions involved are listed in Table VII, together with the results of stress-corrosion tests.

Stress-corrosion cracking of 2219-T37 and 7075-T651 alloy specimens occurred in [illegible] (pH 2) and neutral (pH 7) solutions of calcium chloride. Failures were also encountered with 2219-T87 and 7075-T7351 specimens, but metallographic examination revealed no evidence of stress-corrosion cracking. The corrosive attack in $CaCl_2$ solutions was very similar to that in NaCl solutions.

Both tempers of each alloy corroded very rapidly in ferric chloride (pH 1.5), cupric chloride (pH 2) and sodium hydroxide (pH 11.5) electrolytes. In the ferric chloride and sodium hydroxide solutions, the specimens suffered either complete dissolution or extreme reduction in cross section after only a 24-hour exposure (Figure 82). Even with such extremely severe uniform corrosion, the stressed specimens did not fail, thus indicating that stress-corrosion cracks either did not occur, or if cracks did develop, they were too numerous and too close together to permit a sufficient concentration of stress to result in fracture.

In the cupric chloride solution, there was an immediate deposition of copper over the entire specimen surface with

subsequent rapid attack that necessitated removal of the test specimens after 10-30 minutes exposure (Figure 83).

Severe corrosion also occurred in the cupric sulfate solution (pH 2.0-2.5), and was associated with the random deposition of fine copper particles; however, in contrast to the $CuCl_2$ solution, the attack was relatively slow, and the specimens were exposed until failure. The 2219-T37 specimen failures appeared to be due to stress-corrosion cracking (Figure 84). No evidence of intergranular corrosion or stress cracking was detected in the 7075 alloy specimens (Figures 85 and 86); however, the low tensile losses of the unstressed specimens of 7075-T651 suggest that the T651 failures probably were the result of stress-corrosion cracking similar to the performance of 7075-T651 in acidified Na_2SO_4 (pH 2).

In the ammonium hydroxide electrolyte (pH 11) stress-corrosion cracking occurred only with the 7075-T651 specimens.

In sodium chloride solutions of similar alkalinity (pH 11), stress-corrosion cracking occurred with both the 2219-T37 and 7075-T651 specimens. Failures also occurred with 2219-T87 and 7075-T7351 specimens, but these failures were the result of severe local pitting (Figure 87).

The results of these environmental tests have amply demonstrated that the susceptibility of aluminum alloys to stress-corrosion cracking depends not only upon the alloy and temper, but also to a high degree upon the environment. This behavior is by no means peculiar to aluminum alloys, for a

similar environmental dependency is well illustrated in the literature for other alloy systems.

Selected Environments

From the many solutions evaluated in the environmental screening tests, two groups were selected for crack initiation studies with the light microscope. Each group consisted of five solutions, one group to be used with 7075-T6 and 2219-T37, and the other to be used with 7075-T73 and 2219-T87. The procedures used were the same as those used throughout the contract work and involved microscope observation of the progress of corrosion in unstressed specimens and observation of stressed tuning-fork specimens for crack initiation and development. With the stressed specimens, a short transverse stress of 75% YS was used. As of the end of the second contract year, most of the tests on 7075-T6 and 2219-T37, and preliminary tests on 7075-T73 and 2219-T87 were complete.

7075-T6 and 2219-T37

The solutions involved and the failure times in the previously described screening tests of 7075-T651 and 2219-T37 were:

Solution		Adjusted With	Failure Times - Days 7075-T6	2219-T37
1N NaAc	4	HAc	4,6,13	---
1N Na_2SO_4	2	H_2SO_4	39,40,47	OK-60
0.5N NaCl + 0.5N Na_2CrO_4	2	HCl	8,10,19	1,1,OK-60
4N NaCl + 0.5N KNO_3	0.4	HNO_3	1,1,1	1,1,1
0.5N NaCl + 0.5N Na_2SO_4	2	H_2SO_4	2,2,3	No Test

In the 1N NaAc solution at pH4, only slight pitting of 7075-T6, with some interfragmentary corrosion, occurred in an unstressed specimen (Fig. 88). Observation of the polished surface

of a tuning-fork specimen for a period of 59 hours (2-1/2 days) revealed only a mild general etching and no cracks whatsoever. Cross sections verified these observations by showing only a shallow pitting type of attack and no cracking (Fig. 88). Further tests are planned to resolve the anomaly of relatively rapid failure in the screening test and no crack development in tuning-fork specimens.

In the 1N Na_2SO_4 solution at pH2, unstressed 7075-T6 sustained only slight pitting and intergranular attack, and 2219-T37 showed negligible attack after a three hour exposure (Fig. 89). With stressed tuning-fork specimens, 7075-T6 was attacked generally during the initial portion of the exposure, with occasional selective pitting, as shown by Fig. 90. As the exposure continued, the pitting became more severe and, in addition, a few directional crevices developed perpendicular to the stress. After 67 hours exposure, these crevices were quite noticeable on the surface and, in cross section, were seen to follow a relatively wide intergranular path along "former" boundaries (Fig. 90).

With 2219-T37 in the 1N Na_2SO_4 solution at pH2, general corrosion developed quite rapidly as was the case with 7075-T6. As the exposure continued. an occasional crevice developed, but these crevices did not grow. Sectioning after a 65-hour exposure showed that the crevices were along boundaries, but they were wide, blunt and shallow, and appeared to be selective attack rather than stress-corrosion cracking (Fig. 91). This is in agreement with the screening tests which yielded no failures.

In the 0.5N NaCl + 0.5N Na_2CrO_4 solution at pH2, unstressed specimens of 7075-T6 developed only a very slight pitting attack in a 3-hour exposure (Fig. 92), whereas 2219-T37 developed a network of intergranular attack in a matter of minutes (Fig. 92). Under stress, no cracks initiated in 7075-T6 during a 4-hour exposure, but much longer exposures are planned because of the relatively long failure times in the screening tests. With 2219-T37 under stress in this environment, cracks initiated and propagated very rapidly (Fig. 93 and Fig. 94-top). The crack initiation sites and propagation paths in this environment were the same as those in the NaCl-$AlCl_3$ solution at pH1.

The 4N NaCl + 0.5N KNO_3 solution at pH 0.4 developed intergranular and interfragmentary attack in unstressed specimens of 7075-T6 and intergranular attack of similar specimens of 2219-T37 in very short periods (Fig. 95). In the stressed condition, cracks initiated and developed with extreme rapidity in 7075-T6 alloy. After 30 seconds exposure, relatively large cracks had formed and, after a total exposure of two minutes, these cracks had lengthened and deepened until they had the appearance of gaping crevasses at the magnifications being used (Fig. 96). In cross section, these cracks were seen as deep fissures (Fig. 97), the particular crack shown having deepened at a rate of seven mils per minute. Cracking was also quite rapid with 2219-T37 alloy as shown by Figs. 98 and 99. With both alloys, crack initiation sites and propagation paths were the same as in the pH1 NaCl-$AlCl_3$ solution used throughout the contract.

In the 0.5N NaCl + 0.5N Na_2SO_4 solution at pH2, unstressed 7075-T6 developed a pitting and interfragmentary attack rather slowly, whereas unstressed 2219-T37 developed an intergranular network of attack quite rapidly (Fig. 100). With stressed tuning-fork specimens of 7075-T6, cracks initiated on "former" boundaries and propagated rapidly along such boundaries as shown by Fig. 101. This figure provides another excellent example of crack initiation and development on boundaries between grains showing greatly different contrast on etching. Seen in cross section, the cracks generally selected "former" boundaries for propagation as shown by Fig. 102. When cracks penetrated regions where "former" boundaries were not well defined, however, such as at the bottom of Fig. 102, the cracks selected segments of "former" boundaries wherever possible and followed an interfragmentary path elsewhere. This situation has been observed with all environments, but is particularly well illustrated by this micrograph.

Stressed specimens of 2219-T37 exposed to the pH2 NaCl-Na_2SO_4 solution developed cracks very rapidly. These cracks initiated and propagated on grain boundaries perpendicular to the stress as shown by Fig. 103 and the bottom micrograph in Fig. 94. In the cross section, the cracks are very shallow because the exposure had been of only five minutes duration.

At this point in the microscope observation of the effect of environment on crack initiation, correlation with screening tests has been good with the exception of 7075-T6 in the NaAc solution at pH4. At an earlier stage in this

investigation, there were indications that, with alloy-environment combinations having long failure times, the times for crack initiation were disproportionately long. As these tests near completion, however, crack initiation times correlate reasonably well with failure times in the screening tests. This points out that the environment probably affects initiation time and propagation rate to about the same degree.

7075-T73 and 2219-T87

The alloy-environment combinations used in the microscope work with 7075-T73 and 2219-T87, and the results of screening tests were:

Solution	pH	Adjusted With	Failure Times - Days 7075-T73	2219-T87
1N NaCl	2	HCl	18,18,22	54,54,54
1N NaCl	2	H_2SO_4	2,2,4	8,9,9
1N KHF_2	1.5-2.0	--	OK 60	OK 60
1N NaBr	2	HBr	OK 60	--
1N NaCl	2	CrO_3	--	16,21,OK 60

Preliminary work on the above combinations at the end of the second year of the contract has involved only relatively short time tests of tuning-fork specimens stressed short transversely to 75% YS. In the 1N NaCl solution adjusted to pH2 with HCl, 7075-T73 developed random, cubic-type pits but no cracks (Fig. 104). Specimens of 2219-T87 developed a somewhat directional pitting perpendicular to the stress (Fig. 105). Some of the attack was concentrated around constituent clusters which were oriented perpendicular to the stress.

With the 1N NaCl solution adjusted to pH2 with H_2SO_4, 7075-T73 developed large, cubic-type pits quite rapidly, but no cracks were apparent either on the polished surface or in cross section (Fig. 106). Specimens of 2219-T87 in the same environment also developed matrix pitting quite rapidly, some of it around constituent clusters, but again no cracking was observed (Fig. 107).

In the 1N KHF_2 solution at approximately pH2, considerable general pitting developed. In 7075-T73, some of the larger pits were associated with constituent clusters, but other pits developed in profusion at apparently random sites (Fig. 108). In 2219-T87, pits also developed at constituent clusters, but in this alloy is appeared that the particles, as well as the surrounding solid solution, were being corroded away (Fig. 109).

With 7075-T73 in the 1N NaBr solution adjusted to pH2 with HBr, there was considerable general corrosion of the surface, with some selective attack at constituent clusters (Fig. 110). At the end of the one-hour exposure used with the initial specimen, the attack had revealed details of the microstructure, indicating that it had darkened or dissolved out the fine precipitates on grain and fragment boundaries and also the fine dispersoids.

With 2219-T87 in the 1N NaCl solution adjusted to pH2 with CrO_3, attack was much slower than in other environments of the selected group, and only slight pitting in the vicinity of constituent clusters developed in a 260-minute exposure (Fig. 111).

The tuning-fork specimen tests of 2219-T87 and 7075-T73 have given no indication that the screening test failures were anything but failures from excessive corrosion. Longer exposures will be required, however, to fully resolve this question.

CONCLUSION

The most important observations during the second year of the contract were:

1. Stress-corrosion cracks in 7075-T6, 7079-T6 and 7039-T6 initiated on "former" grain boundaries perpendicular to the stress. In preliminary work with 7039-T6 some tendency was noted for crack initiation at pits on or immediately adjacent to these boundaries. Propagation in all alloys was along the "former" boundaries and followed the straightest possible boundary paths perpendicular to the stress.

2. Cracks appeared to initiate more readily on "former" boundaries between "grains" developing different colors on etching, which suggests considerably different orientation.

3. In 7XXX alloys, some tendency was noted for crack initiation at the junctions of regions having different dispersoid population. These junctions may be the "former" boundaries, since fracture surfaces had polygonal facets resembling the structure in relatively dispersoid-free regions.

4. No direct relationship was found between crack initiation and dislocations, dispersoids, constituents or precipitates.

5. Intergranular pre-corrosion in 7075-T6 induced rapid crack initiation, but corrosion crevices widened by stress could not be distinguished from, and could be mistaken for, stress-corrosion cracks.

6. Surface abrasion altered crack initiation but only until corrosion or cracking had breached a very shallow surface layer.

7. Anodic and chemical films delayed but did not prevent crack initiation.

8. Crack initiation time showed a semi-logarithmic relation to stress level.

9. Stress level affected crack number and propagation rate but had no effect on crack initiation sites or propagation paths.

10. With 2219-T37 and 7075-T6, environment had no effect on crack initiation sites or propagation paths but determined whether cracks developed and altered crack initiation time and propagation rate.

11. Preliminary investigations indicated that failures in 2219-T87 and 7075-T73 in certain environments were the result of excessive corrosion and not stress-corrosion cracking.

APPENDIX I

ABSTRACT OF FIRST ANNUAL REPORT

The initiation and development of stress-corrosion cracks in heavy plate of 2219 and 7075 alloys was investigated. Heavy plate of X7375 (7075 without Cr) was also used for specific structural comparisons. Corrosion and stress-corrosion tests in a pH 1 $NaCl$-$AlCl_3$-HCl solution were made using metallographically polished unstressed specimens, and special tuning-fork specimens, the most highly stressed region of which was metallographically polished and masked just prior to exposure.

The majority of the work was concerned with the effect of metallurgical structure. In all crack-susceptible materials, intergranular corrosion and stress-corrosion cracking started and progressed in boundary regions. With 2219 alloy, this path was the boundaries of the recrystallized grains, whereas in 7075 alloy, it was the boundaries of fragment clusters, which were the boundaries of "former" grains. Cracks formed on boundaries oriented perpendicularly to the stressing direction, with the result that boundary orientation and directionality of structure were of the utmost importance. In 7075 alloy, which had an unrecrystallized structure, cracks developed and propagated rapidly under short-transverse stress because the structure was highly elongated in the rolling direction, which oriented the boundaries perpendicular to the stress. A similar situation prevailed in 2219 alloy because of the directionality of the recrystallized structure and the presence of series of favorably oriented boundaries perpendicular to the short-transverse stress.

This investigation revealed no other microstructural feature that influenced crack initiation or propagation. The constituent particles, zones and precipitates within grains had no direct effect because they were not located where cracking occurred. Boundary precipitate particles also had no direct effect and no evidence was found that dislocations were associated with cracking. Microstructural features, such as zones and precipitate particles, may have an indirect effect on crack initiation because their formation and development will influence the localized electrochemical relationships at boundaries.

In a brief investigation, it was shown that the pronounced effect of stressing direction is related to grain shape and structural orientation. Cracks formed with equal ease under short-transverse and longitudinal stresses in both 2219 and 7075 alloys, but propagation was blocked with longitudinal stresses because favorably oriented boundaries were not available. Even where favorable boundary segments were present on an exposed surface, subsurface propagation was prevented because boundary orientations were unfavorable.

Surface irregularities in the form of pits developed by dissolution of microconstituents, artificially induced cubic pits, and fine scratches, also had no effect on crack initiation or propagation. If such features were present at a boundary, a crack would be associated with them, but the controlling feature was the boundary and not the irregularity.

Increasing the stress increased the rate of crack formation and decreased the number of major cracks, but did not alter the mechanism of crack initiation in the particular materials used.

Surface films formed in air delayed crack initiation with a relationship similar to that typical of natural film formation. This indicated that the time required for crack initiation may represent the time required for the environment to breach the existing film. This leads to the hypothesis that the ability of environments to form or dissolve films may determine whether cracking will or will not occur.

At his point in the contract, the two most important factors in crack initiation appear to be (1) grain shape, structural directionality and recrystallization, which control the orientation of corrosion-susceptible boundary paths with respect to the stressing direction, and (2) the electrochemical relationships existing at boundaries which constitute these susceptible paths. Other factors appear to have no direct effect, although the formation of zones and precipitates accompanies the formation of the susceptible paths and probably has an indirect influence on the localized electrochemical relationships.

TABLE I

CHARACTERISTICS OF 7079-T651 AND 7039-T6 PLATE

Spec. No.	Alloy	Thickness	Composition - %							
			Si	Fe	Cu	Mn	Mg	Cr	Zn	Ti
235972	7079-T651	6"	0.10	0.20	0.73	0.18	3.71	0.19	4.49	0.05
314759	7039-T6	3"	0.13	0.19	0.03	0.26	2.88	0.20	4.02	0.03

Alloy	Direction	Location	Tensile Properties		
			T.S.-ksi	Y.S. ksi	Elongation %
7079-T651	Longitudinal	1" below surface	75.9	67.1	12.0
	Long. Trans.	1" below surface	76.5	65.1	8.0
	Short Trans.	1" below surface	74.6	65.5	6.0
7039-T6	Longitudinal	Center	63.2	53.8	16.2
	Long. Trans.	Center	64.2	54.4	12.5
	Short Trans.	Center	63.9	54.6	7.5

Stress Corrosion - Center of Plate - 3.5% NaCl Alt. Imm.

7079-T651 - 0.125" Diameter Specimens

Direction	Stress - % Y.S.	F/N (1)	Days to Fail
Longitudinal	75	2/3	14, 84, OK 84
Short Transverse	50	3/3	5, 12, 13
	25	2/3	21, 21, OK 84
	15	0/3	OK 84

7039-T6 C-Rings - 64% Y.S. Short Transverse

F/N (1)	Days to Failure
9/9	8,8,9,9,9,9,11,13,29

(1) Number failed/number exposed

TABLE II

CHARACTERISTICS OF 7075 INGOT AND PLATE USED FOR GRAIN BOUNDARY STUDIES

Thickness(3)	Tensile Properties(1) As-Fabricated T.S. Ksi	Y.S. Ksi	El. %	T6(2) T.S. Ksi	Y.S. Ksi	El %
12" ingot	28.4	14.9	4.5	68.8	63.4	4.0
5.70" plate	33.0	14.9	14.0	70.3	64.0	5.5
4.17" plate	32.3	17.4	9.0	70.1	64.5	4.0
3.00" plate	33.6	18.9	9.0	72.0	66.0	4.0
2.15" plate	34.6	19.2	12.0	72.8	66.4	3.5

(1) Short transverse specimens, 1/8" dia., centered on mid-thickness.
(2) Slices 1 1/4" thick heat treated 2 hrs. @ 870F, water quenched and aged 4 days at room temperature plus 24 hrs. at 250F.
(3) Plate samples from 12" ingot, scalped to 8", preheated and hot rolled.

SOLUTION POTENTIAL AND STRESS CORROSION RESISTANCE

Thickness(3)	Solution Potential(4) As Fab	T6	Stress Corrosion (5) As Fab F/N(6)	Days	T6 F/N(6)	Days
12" Ingot	859	808	0/3	OK 84	3/3	12,14,39
5.70" Plate	903	810	0/3	OK 84	0/3	OK 84
4.17" Plate	931	811	0/3	OK 84	2/3	42,57 (OK 84)
3.00" Plate	945	809	0/3	OK 84	3/3	54,64,67
2.15" Plate	940	809	0/3	OK 84	3/3	42,47,52

(4) In NaCl-H_2O_2 vs 0.1N calomel electrode (-mv)
(5) 1/8" dia. short transverse tensile specimens exposed to 3.5% NaCl Alt. Imm. Stressed to 75% YS; no failures at 25% YS.
(6) Number failed/number exposed

TABLE III

RESISTANCE TO STRESS-CORROSION CRACKING OF ALUMINUM ALLOYS IN VARIOUS AQUEOUS SOLUTIONS
2219-T87 ALLOY SHORT TRANSVERSE TENSILE SPECIMENS, 0.125" DIAMETER
TENSILE STRENGTH-69.5 ksi, YIELD STRENGTH-59.6 ksi, % ELONGATION-4.5

Solution	Nominal pH	Adjusted With	Actual pH Range	Stressed - 75% Y.S. F/N(1)	Days	% Loss(2) in T.S.	Type of(3) Attack	Unstressed Specimens Days	% Loss(4) in T.S.	Type of(3) Attack	Visual Examination Film(5)	Localized(6) Corrosion
Halide Anions												
1N NaCl	2	HCl	2.0 - 4.2	3/3(7)	54,54,54	--	P + SI	21,54	51,66	P + SI	Red	3b
1N NaCl	7	NaOH	4.9 - 7.0	0/3	OK-60	25	P + SI	21,60	22,33	P	Gray	2b
1N NaBr	2	HBr	2.0 - 4.0	2/3(7)	53,60(OK60)	64	P + SI	21,60	32,51	P	Light Red	2b
1N NaBr	7	NaOH	4.2 - 7.0	0/3	OK-60	16	P	21,60	14,12	P + SI	Gray	2a
1N NaI	2	HI	2.0 - 4.0	3/3(7)	29,32,34	--	P + SI	21	32	?	Dull	2b
1N NaI	7	NaOH	5.5 - 7.0	0/3	OK-60	5	P + SI	21,60	8, 9	P + SI	Dull	1
1N KHF_2	2	--	1.5 - 2.0	0/3	OK-60	7	P	21,60	11,14	P	Red	1
1N NaF	7	HF	7.0 - 7.4	0/3	OK-60	6	P	21,60	8, 9	P	None	1
Complex Anions												
1N $NaNO_3$	2	HNO_3	2.0 - 2.3	0/3	OK-60	18	P	21,60	13,22	P	Light Red	1
1N $NaNO_3$	7	NaOH	4.0 - 7.0	0/3	OK-60	11	P	21,60	9,10	P	Dull	1
1N Na_2CrO_4	2	CrO_3	2.0 - 2.3	0/3	OK-60	10	P	21,60	11, 8	P	None	1
1N Na_2CrO_4	7	CrO_3	7.0	0/3	OK-60	8	P	21,60	12,11	P	None	1
1N Na_2SO_4	2	H_2SO_4	2.0	0/3	OK-60	21	P	21,60	3,11	P	Black	1
1N Na_2SO_4	7	NaOH	4.9 - 7.0	0/2	OK-60	10	P	21,60	2, 3	P	Gray	1
0.5N Na_2SO_4 + 0.5N $NaNO_3$	2	H_2SO_4	2.0 - 2.4	0/3	OK-60	22	P	21,60	8,14	P	Dark Gray	1
0.5N Na_2SO_4 + 0.5N Na_2CrO_4	2	H_2SO_4	2.0 - 2.5	0/3	OK-60	27	P	21,60	9,23	P	Black	1
1N $NaHSO_4$	1	--	0.9 - 1.0	0/3	OK-60	21	P	21,60	20,38	P	Dark Red	2a
1N NaH_2PO_4	4	--	4.2 - 4.3	0/3	OK-60	3	P	21,60	10,11	P	Black	1
Sodium Chloride plus Oxidising Acids												
1N NaCl	2	HNO_3	2.0 - 4.3	3/3(7)	5,7,7	--	P + SI	5, 7	61,76	P + SI	Red	2b
1N NaCl	2	H_2SO_4	2.0 - 4.0	3/3(7)	8,9,9	--	P	8, 9	56,60	P + SI	Red	3b
1N NaCl	2	CrO_3	2.0	2/3(7)	16,21(OK60)	24	P + SI	16,60	8,75	P	None	1
4N NaCl + 0.5N KNO_3	0.4	HNO_3	0.4 - 3.5	3/3(7)	25,25,25	--	P + SI	21,25	61,60	P + SI	Gray Red	3a
Sodium Chloride plus Complex Anions												
0.5N NaCl + 0.5N $NaNO_3$	2	HNO_3	2.0 - 3.2	0/3	OK-60	27	P	21,60	10,26	P	Light Red	2a
0.5N NaCl + 0.5N $NaNO_3$	7	NaOH	4.5 - 7.0	0/3	OK-60	15	P	21,60	6,18	P	White	2a
0.5N NaCl + 0.5N Na_2SO_4	2	H_2SO_4	2.0 - 2.7	3/3(7)	4,5,5	--	P + SI	4, 5	54,58	P + SI	Dark Gray	2a
0.5N NaCl + 0.5N Na_2SO_4	7	NaOH	4.8 - 7.0	1/3(7)	46(2 OK 60)	17	P + SI	21,60	3,21	P + SI	Gray	1
0.5N NaCl + 0.5N Na_2CrO_4	2	HCl	2.0 - 2.4	2/3(7)	16,22(OK 60)	48	P + SI	16,60	9,28	P + SI	None	1
0.5N NaCl + 0.5N Na_2CrO_4	7	HCl	7.0	0/3	OK-60	10	P	21,60	17, 6	P + SI	None	1b
Ammonium Salts												
1N NH_4Cl	7	HCl	6.0-7.0	0/3	OK 60	8	P	21,60	12,10	P	None	2a
Miscellaneous												
1N NaCl + 3 g/l H_2O_2	5.5	--	--	3/3(7)	6,6,7	--	P + SI	6, 7	72,67	P + SI	Black	3a
1N NaCl + 1N $AlCl_3$	2	HCl	2.0 - 3.1	3/3(7)	4,4,5	--	P + SI	4, 5	70,85	P + SI	Black	2a
1N Na_2SO_4 + 3 g/l H_2O_2	5.8	--	--	0/3	OK-60	12	P	21,60	16,16	P	None	2b
1N Na_2SO_4 + 1N $Al_2(SO_4)_3$	2	H_2SO_4	2.0 - 2.3	0/3	OK-60	20	P	21,60	9,23	P	Black	1

Notes: (1) F/N denotes number of specimens failed over number exposed.
(2) Results are average of tests of those specimens which did not fail.
(3) Type of attack: P = pitting; P + SI = pitting plus slight intergranular.
(4) Results are for tests of individual specimens exposed for the specified periods.
(5) Wet surface films observed at the termination of maximum exposure in the solution.
(6) Localized corrosion: 1 = negligible, 2 = mild, 3 = severe; a = random, b = directional, 1b indicates 1 or 2 local corrosion sites. Ratings are based upon appearance after maximum exposure time in each solution.
(7) Failures associated with severe corrosion. Microscopic examination revealed no evidence of stress-corrosion cracking.

TABLE IV

RESISTANCE TO STRESS-CORROSION CRACKING OF ALUMINUM ALLOYS IN VARIOUS AQUEOUS SOLUTIONS
7075-T7351 ALLOY SHORT TRANSVERSE TENSILE SPECIMENS, 0.125" DIAMETER
TENSILE STRENGTH-67.6 KSI, YIELD STRENGTH-57.7 KSI, % ELONGATION-6.0

Solution	Nominal pH	Adjusted With	Actual pH Range	Stressed - 75% Y.S. F/N(1)	Days	% Loss(2) in T.S.	Type of(3) Attack	Unstressed Specimens Days	% Loss(4) in T.S.	Type of(3) Attack	Visual Examination Film(5)	Localized(6) Corrosion
Halide Anions												
1N NaCl	2	HCl	2.0 - 4.2	3/3(7)	18,18,22	--	P	18,22	50,60	P	Dark Red	3b
1N NaCl	7	NaOH	4.8 - 7.0	0/3	OK-60	11	P	21,60	25, 6	P	White	2b
1N NaBr	2	HBr	2.0 - 4.1	0/3	OK-60	69	P	21,60	30,41	P	Dark Red	2b
1N NaBr	7	NaOH	4.0 - 7.0	0/3	OK-60	5	P	21,60	6, 9	P	Dull	1
1N NaI	2	HI	2.0 - 3.4	0/3	OK-60	57	P	21,60	15,23	P	Dull	2b
1N NaI	7	NaOH	5.8 - 7.4	0/3	OK-60	5	P	21,60	3, 4	P	Dark Gray	1
1N KHF_2	2	--	1.5 - 2.0	0/3	OK-60	7	P	21,60	3, 4	P	Red	2a
1N NaF	7	HF	7.0 - 7.3	0/3	OK-60	0	P	21,60	0, 0	P	None	1
Complex Anions												
1N $NaNO_3$	2	HNO_3	2.0 - 2.7	0/3	OK-60	14	P	21,60	4,13	P	Gray-Red	2a
1N $NaNO_3$	7	NaOH	4.1 - 7.0	0/3	OK-60	1	P	21,60	12, 1	P	White	1
1N Na_2CrO_4	2	CrO_3	2.0	0/3	OK-60	0	P	21,60	2, 0	P	None	1
1N Na_2CrO_4	7	CrO_3	7.0	0/3	OK-60	3	P	21,60	0, 0	P	None	1
1N Na_2SO_4	2	H_2SO_4	2.0 - 2.5	0/3	OK-60	53	P(8)	21,60	17,47	P	Dark Red	2b
1N Na_2SO_4	7	NaOH	4.5 - 7.0	0/2	OK-60	1	P	21	0	P	Gray	1
0.5N Na_2SO_4 + 0.5N $NaNO_3$	2	H_2SO_4	2.0 - 3.5	0/3	OK-60	48	P	21,60	13,42	P	Black	2a
0.5N Na_2SO_4 + 0.5N Na_2CrO_4	2	H_2SO_4	2.0 - 2.4	0/3	OK-60	21	P	21,60	1,10	P	Gray	1
1N $NaHSO_4$	1	--	0.9 - 1.0	3/3(7)	33,34,35	--	P	21,35	50,72	P	Dark Red	3b
1N NaH_2PO_4	4	--	4.2 - 4.4	0/3	OK-60	0	P	21,60	2, 0	P	Black	1
Sodium Chloride Plus Oxidising Acids												
1N NaCl	2	HNO_3	2.0 - 4.3	3/3(7)	6,7,8	--	P	6, 8	46,49	P	Gray-Red	2b
1N NaCl	2	H_2SO_4	2.0	3/3(7)	2,2,4	--	P	2, 4	36,54	P	--	2b
1N NaCl	2	CrO_3	2.0	3/3(7)	39,42,42	--	P	21	21	P	None	1
4N NaCl + 0.5N KNO_3	0.4	HNO_3	0.4 - 3.5	2/2(7)	19,19	--	P	19	68	P	Gray-Red	3a
Sodium Chloride Plus Complex Anions												
0.5N NaCl + 0.5N $NaNO_3$	2	HNO_3	2.0 - 3.8	0/3	OK-60	30	P	21,60	10,29	P + SI	Red	2b
0.5N NaCl + 0.5N $NaNO_3$	7	NaOH	4.3 - 7.8	0/3	OK-60	7	P	21,60	1, 4	P	Gray-White	1
0.5N NaCl + 0.5N Na_2SO_4	2	H_2SO_4	2.0	3/3(7)	2,4,4,	--	P	2, 5	27,55	P + SI	--	1
0.5N NaCl + 0.5N Na_2SO_4	7	NaOH	4.7 - 7.0	1/3(7)	60(2 OK 60)	34	P	21,60	18,16	P	Gray-White	1b
0.5N NaCl + 0.5N Na_2CrO_4	2	HCl	2.0	3/3(7)	48,52,60	--	P	21,60	1, 5	P	None	1
0.5N NaCl + 0.5N Na_2CrO_4	7	HCl	7.0	0/3	OK-60	0	P	21,60	2,12	P	None	1
Ammonium Salts												
1N NH_4Cl	7	NH_4OH	6.2 - 7.0	2/3(7)	44,52(OK 60)	28	P	21,60	24,49	P	White	2b
Miscellaneous												
1N NaCl + 3 g/l H_2O_2	5.5	--	--	3/3(7)	18,22,23	--	P	18,23	43,61	P	Gray-White	2a
1N NaCl + 1N $AlCl_3$	2	HCl	2.0 - 2.8	3/3(7)	7,10,19	--	P	7,19	67,82	P	Red	3b
1N Na_2SO_4 + 3 g/l H_2O_2	5.8	--	--	2/3(7)	29,31(OK 60)	50	P	21,60	0,23	P	Gray	1b
1N Na_2SO_4 + 1N $Al_2(SO_4)_3$	2	H_2SO_4	2.0 - 2.4	0/3	OK-60	54	P	21,60	16,45	P	Dark Red	2b

Notes:
(1) F/N denotes number of specimens failed over number exposed.
(2) Results are average of tests of those specimens which did not fail.
(3) Type of attack: P = pitting, P + SI = pitting plus slight intergranular.
(4) Results are for tests of individual specimens exposed for the specified period.
(5) Wet surface films observed at the termination of maximum exposure in the solution.
(6) Localized corrosion: 1 = negligible; 2 = mild; 3 = severe; a = random; b = directional; 1b indicates 1 or 2 local corrosion sites. Ratings are based upon appearance after maximum exposure time in each solution.
(7) Failures associated with severe corrosion. Microscopic examination revealed no evidence of stress-corrosion cracking.
(8) Microscopic examination revealed slight evidence of transgranular cracking.

TABLE V

RESISTANCE TO STRESS-CORROSION CRACKING OF ALUMINUM ALLOYS IN ACIDIC ELECTROLYTES
2219-T37 AND 7075-T651 ALLOY SHORT TRANSVERSE TENSILE SPECIMENS, 0.125" DIAMETER

Alloy	Solution	Nominal pH	Adjusted With	Exposure Period	Unstressed Specimens % Loss(2) in T.S.	Unstressed Specimens Type of(4) Attack	F/N	Stressed 75% YS(1) % Loss(3) in T.S.	Stressed 75% YS(1) Type of(4) Attack
2219-T37	1N NaCl	2	HCl	2 days	27	I	0/2	42	I
				4 days	30	I	0/2	39	I
				8 days	50	P+I	1/2 8 da.	71	I
				16 days	66	I	2/2 16 da.	--	I
				24 days	53	P+SI	1/2 17 da.	82	P+SI
	Previous Test(6)			19 days	65	I	3/3 19 da.	--	I
	1N NaCl	2	H_2SO_4	1 day	30	I	0/2	52	I
				2 days	49	I	1/2 2 da.	69	I
				4 days	46	I	0/2	63	I+SP
				8 days	69	I	0/2	88	I
				16 days	100(5)	--	2/2 8,10 da.	--	I
	Previous Test(6)			8 days	71	I	3/3 8 da.	--	I
7075-T651	1N NaCl	2	HCl	8 hours	4	I	0/2		I
				16 hours	16	I	2/2 16 hr.		I
				32 hours	16	I	1/2 32 hr.		I
				64 hours	25	I	1/2 40 hr.		I
				96 hours	33	P	2/2 6,24 hr.		I
	Previous Test(6)			3 days	41	P+I	3/3 3 da.	--	P+I
	1N NaCl	2	H_2SO_4	1 hour	0	N.A.A.	0/2	0	N.A.A.
				2 hours	0	N.A.A.	0/2	2	N.A.A.
				3 hours	0	I	1/2 3 hr.	18	I
				4 hours	2	P+I	2/2 4 hr.	--	I
				8 hours	1	P+I	2/2 4 hr.	--	P+I
				24 hours	7	I	2/2 4 hr.	--	P+SI
	Previous Test(6)			24 hours	47	P+I	3/3 1 da.	--	P+I
	1N Na_2SO_4	2	H_2SO_4	4 days	1	P	0/2	3	P
				8 days	3	P	0/2	3	P
				16 days	7	P	0/2	31	P
				24 days	12	P	0/2	18	P
				48 days	21	DP	1/2 34 da.	38	DP
	Previous Test(6)			47 days	32	P	3/3 39-47 da.	--	P+I

Notes: (1) Tensile Properties: 2219-T37 alloy - 58 ksi tensile, 44 ksi yield, 8% elongation
7075-T651 alloy- 79 ksi tensile, 68 ksi yield, 3% elongation

(2) Results shown are for tests of individual specimens

(3) Results shown are average of tests of specimens that did not fail in previous tests; all others are for individual specimens

(4) Type of attack: N.A.A. = no appreciable attack; P = pitting; DP = directional pitting; P + SI = pitting plus slight intergranular; P + I = pitting plus intergranular; I = intergranular; I + SP = intergranular plus slip plane.

(5) Broke while being placed in testing machine.

(6) Detailed results given in First Annual Report

TABLE VI

RESISTANCE TO STRESS-CORROSION CRACKING OF ALUMINUM ALLOYS IN ACIDIC ELECTROLYTES
2219-T87 AND 7075-T7351 ALLOY SHORT TRANSVERSE TENSILE SPECIMENS, 0.125" DIAMETER

					Unstressed Specimens			Stressed 75% Y.S.(1)	
Alloy	Solution	Nominal pH	Adjusted With	Exposure Period	% Loss(2) in T.S.	Type of(4) Attack	F/N	% Loss(3) in T.S.	Type of(4) Attack
2219-T87	1N NaCl	2	HCl	3 days	28	DP	0/2	21	DP
				7 days	42	DP	0/2	43	P
				14 days	42	P	0/2	37	P
				21 days	57	P	0/2	61	DP
	Previous Test (5)			54 days	66	P+SI	3/3 54 da.	--	P+SI
	1N NaCl	2	H_2SO_4	8 hours	12	P	0/2	7	P
				16 hours	17	P	0/2	13	P
				24 hours	12	P	0/2	13	P
				48 hours	19	P	0/2	19	P
	Previous Test (5)			9 days	60	P+SI	3/3 8-9 da.	--	P
	1N NaCl	2	CrO_3	7 days	8	N.A.A.	0/2	6	N.A.A.
				14 days	22	P	1/2 10 da.	7	P
				28 days	19	DP	1/2 18 da.	43	DP
				42 days	23	N.A.A.	1/2 35 da.	3	P
	Previous Test (5)			60 days	75	P	2/3 16-21 da.	24	P+SI
	1N KHF_2	1.5	--	7 days	11	P	0/2	11	P
				28 days	2	P	0/2	13	P
				42 days	3	P	0/2	10	P
				60 days	4	P	0/2	1	P
	Previous Test (5)			60 days	4	P	0/2	1	P
7075-T7351	1N NaCl	2	HCl	7 days	8	P	0/2	10	P
				28 days	27	P	0/2	34	P
				42 days	39	P	0/2	56	P
				60 days	54	DP	1/2 60 da.	67	DP
	Previous Test (5)			22 days	60	P	3/3 18-22 da.	--	P
	1N NaCl	2	H_2SO_4	1 day	2	P	0/2	3	P
				3 days	8	P	0/2	3	P
				7 days	22	P	0/2	31	P
				10 days	26	P	1/2 10 da.	52	P
	Previous Test (5)			4 days	54	P	3/3 2-4 da.	--	P
	1N NaBr	2	HBr	6 days	2	P	0/2	6	P
				28 days	10	P	0/2	15	P
				42 days	34	P	0/2	23	P
				60 days	43	DP	1/2 50 da.	40	DP
	Previous Test (5)			60 days	41	P	0/3	69	P
	1N KHF_2	1.5	--	7 days	0	P	0/2	0	P
				28 days	1	P	0/2	2	P
				42 days	2	P	0/2	3	P
				60 days	0	P	0/2	0	P
	Previous Test (5)			60 days	4	P	0/3	7	P

Notes: (1) Tensile Properties: 2219-T87 alloy - 69 ksi tensile, 60 ksi yield, 4.5% elongation
7075-T7351 alloy- 62 ksi tensile, 55 ksi yield, 3% elongation

(2) Results shown are for tests of individual specimens

(3) Results are average of tests of specimens that did not fail in previous tests, all others are for tests of individual specimens

(4) Type of attack: N.A.A. = no appreciable attack, P = pitting, DP = directional pitting, P+SI = pitting plus slight intergranular

(5) Detailed results given in First Annual Report

TABLE VII

RESISTANCE TO STRESS-CORROSION CRACKING OF ALUMINUM ALLOYS IN VARIOUS AQUEOUS SOLUTIONS

Short Transverse Tensile Specimens, 0.125" Diameter

Alloy	Solution	Nominal pH	Adjusted With	Actual pH Range	Stressed 75% Y.S. F/N[1]	Stressed 75% Y.S. Days	Stressed 75% Y.S. %Loss in T.S.[2]	Stressed 75% Y.S. Type of Attack[3]	Unstressed Specimens Days	Unstressed Specimens %Loss in T.S.[4]	Unstressed Specimens Type of Attack[3]	Visual Examination Film[5]	Visual Examination Localized Corrosion[6]	REMARKS
2219-T37	1N $CaCl_2$	2	HCl	2.0-4.1	3/3	8,11,29	--	I + P	8, 29	52, 79	I + P	Dark Red	3b	
	1N $CaCl_2$	7	HCl	7.0-7.6	3/3	14,26,29	--	P + I	14, 29	30, 36	P + I	Gray	1b	
	1N $FeCl_3$	1.5	--	---	0/3	1	--	--	--	--	--	--	--	Removed from test[7]
	1N $CuCl_2$	2	HCl	2.0-3.4	0/3	30 min.	--	I + P	30 min.	53	I + P	Copper Deposits	3a	Removed from test[7]
	1N $CuSO_4$	2	H_2SO_4	2.0-2.8	3/3	47,55,57	--	I	21, 55	47, 71	I + P	Copper Deposits	3a	
	1N NaOH	11.5	--	---	0/3	1	--	--	--	--	--	--	--	Removed from test[7]
	1N NH_4OH	11	--	10.3-11.0	0/3	OK 60	14	N.A.A.	21, 60	16, 16	P	Dark Gray	2a	
	1N NaCl	11	NaOH	9.4-11.0	3/3	4, 4, 4	--	P	4, 21	28, 43	P + SI	Dark Gray	2a	
2219-T87	1N $CaCl_2$	2	HCl	2.0-4.2	1/3	36(20K60)	58	P	21, 60	47, 76	P	Red	3b	Stress Corrosion doubtful[8]
	1N $CaCl_2$	7	HCl	7.0-7.4	3/3	47,47,55	--	P	21, 55	34, 47	P	Gray	2b	Stress Corrosion doubtful[8]
	1N $FeCl_3$	1.5	--	---	0/3	1	--	--	--	--	--	--	--	Removed from test[7]
	1N $CuCl_2$	2	HCl	2.0-3.2	0/3	20 min.	--	P	20 min.	54	P	Copper Deposits	3a	Removed from test[7]
	1N $CuSO_4$	2	H_2SO_4	2.0-3.4	0/3[10]	40	--	--	21	33	P	Copper Deposits	3a	
	1N NaOH	11.5	--	---	0/3	1	--	--	--	--	--	--	--	Removed from test[7]
	1N NH_4OH	11	--	10.6-11.2	0/3	OK 60	21	P	21, 60	14, 20	P	Black	2a	
	1N NaCl	11	NaOH	9.0-11.0	3/3	16,20,42	--	P	16, 42	34, 47	P	Black	1	Stress Corrosion doubtful[8]
7075-T651	1N $CaCl_2$	2	HCl	2.0-4.1	3/3	1, 1, 1	--	I + P	1	32	I + P	Black	2b	
	1N $CaCl_2$	7	HCl	7.0-7.8	3/3	14,26,27	--	P	14, 27	0, 3	N.A.A.	Gray	1	
	1N $FeCl_3$	1.5	--	---	0/3	1	--	--	--	--	--	--	--	Removed from test[7]
	1N $CuCl_2$	2	HCl	2.0-3.5	0/3	10 min.	--	P + SI	10 min.	61	P + SI	Copper Depsoits	3a	Removed from test[7]
	1N $CuSO_4$	2	H_2SO_4	2.0-2.5	3/3	11,11,14	--	P	11, 14	23, 28	P	Copper Deposits	2a	Stress corrosion questionable[9]
	1N NaOH	11.5	--	---	0/3	1	--	P	1	83	P	--	3a	Removed from test[7]
	1N NH_4OH	11	--	10.7-11.3	3/3	3, 3, 4	--	P	3, 21	1, 6	P	Gray-Black	2a	
	1N NaCl	11	NaOH	9.0-11.0	3/3	4, 6, 7	--	P	4, 7	0, 0	P	Black	1	
7075-T7351	1N $CaCl_2$	2	HCl	2.0-4.1	3/3	29,38,50	--	P	21, 50	40, 71	P	Dark Red	3b	Stress corrosion doubtful[8]
	1N $CaCl_2$	7	HCl	7.0-8.0	0/3	OK 60	44	P	21, 60	26, 32	P	Gray	1b	
	1N $FeCl_3$	1.5	--	---	0/3	1	--	--	--	--	--	--	3a	Removed from test[7]
	1N $CuCl_2$	2	HCl	2.0-3.0	0/3	30 Min.	46	P	30 min.	43	P	Copper Deposits	3a	Removed from test[7]
	1N $CuSO_4$	2	H_2SO_4	2.0-2.6	3/3	28,28,31	--	P	21, 31	51, 64	P	Copper Deposits	3a	Stress corrosion doubtful[8]
	1N NaOH	11.5	--	---	0/3	1	--	--	--	--	--	--	3a	Removed from test[7]
	1N NH_4OH	11	--	11.1-11.2	0/3	OK 60	14	P	21, 60	11, 11	P	Black	2a	
	1N NaCl	11	NaOH	9.2-11.0	1/3	50(20K60)	33	P	9, 60	9, 23	P	Black	1	Stress corrosion doubtful[8]

NOTES:

(1) F/N denotes number of specimens failed over number exposed.

(2) Results are the average of tests of those specimens which did not fail in test.

(3) Type of attack: N.A.A. = No Appreciable Attack; P = Pitting;
P + SI = Pitting + Slight Intergranular;
P + I = Pitting + Intergranular;
I + P = Intergranular + Pitting.

(4) Results are for tests of individual specimens exposed for the specified periods.

(5) Wet surface film observed at the termination of maximum exposure in the solution.

(6) Localized corrosion: 1 = negligible; 2 = mild; 3 = severe;
a = random; b = directional.

(7) Removed from test due to either severe reduction in cross section or complete dissolution of specimen.

(8) Metallographic examination revealed no evidence of intergranular corrosion or secondary cracking. This and high tensile loss indicate failure was probably due to corrosion.

(8a) Failures associated with severe localized or general pitting; metallographic examination revealed no evidence of secondary cracking.

(9) Metallographic examination revealed no evidence of intergranular corrosion or secondary cracking, but tensile loss data suggest failure may have been due to stress-corrosion cracking.

(10) Specimens removed from test due to severe corrosion of the specimen and stressing frame at the edge and beneath the cellulose acetate coating used to isolate the stressing frame.

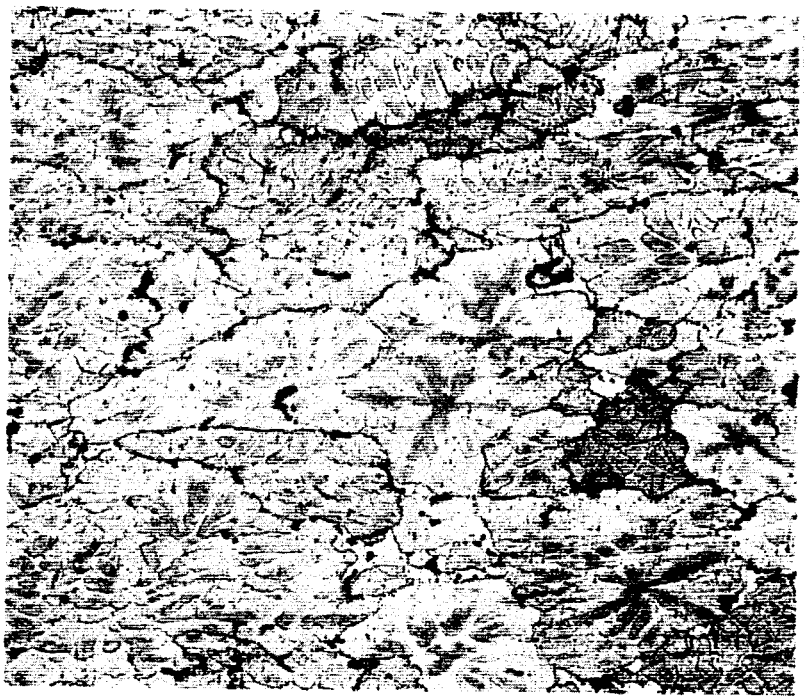

Transverse
XZ Plane

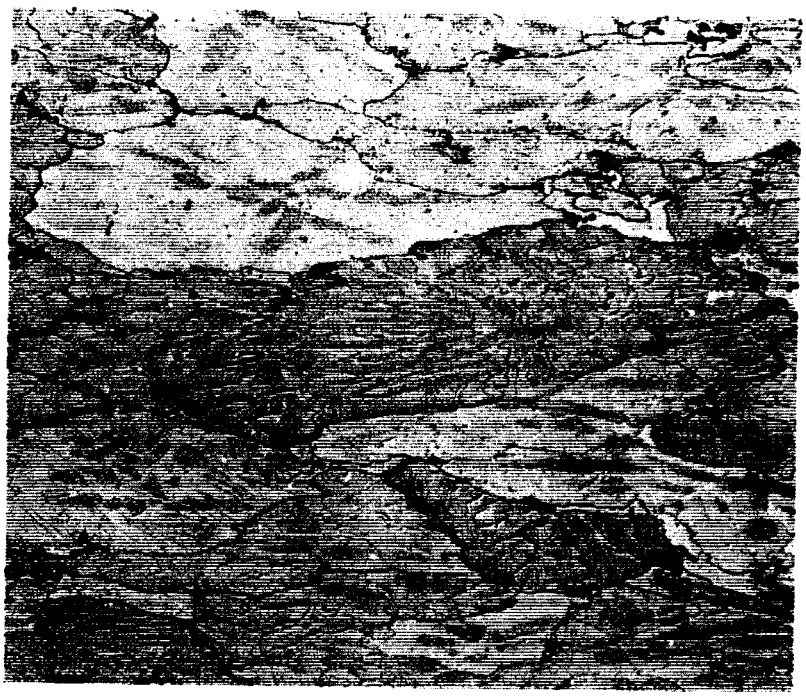

Longitudinal
YZ Plane

Keller's Etch 100X

Microstructure of 7079-T6 Plate

Figure 1

165537
165534

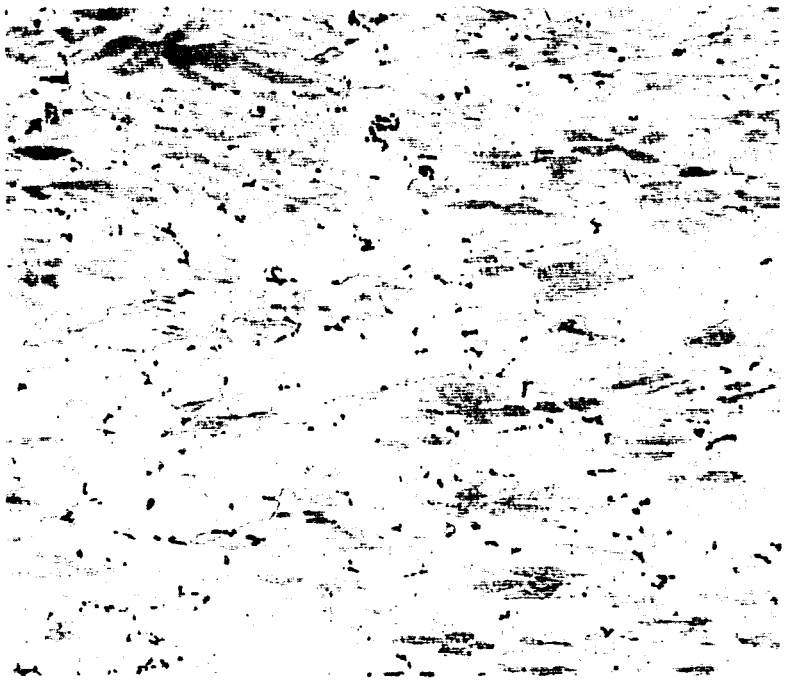

Transverse
XZ Plane

Longitudinal
YZ Plane

Keller's Etch 100X

Microstructure of 7039-T6 plate.

Figure 2

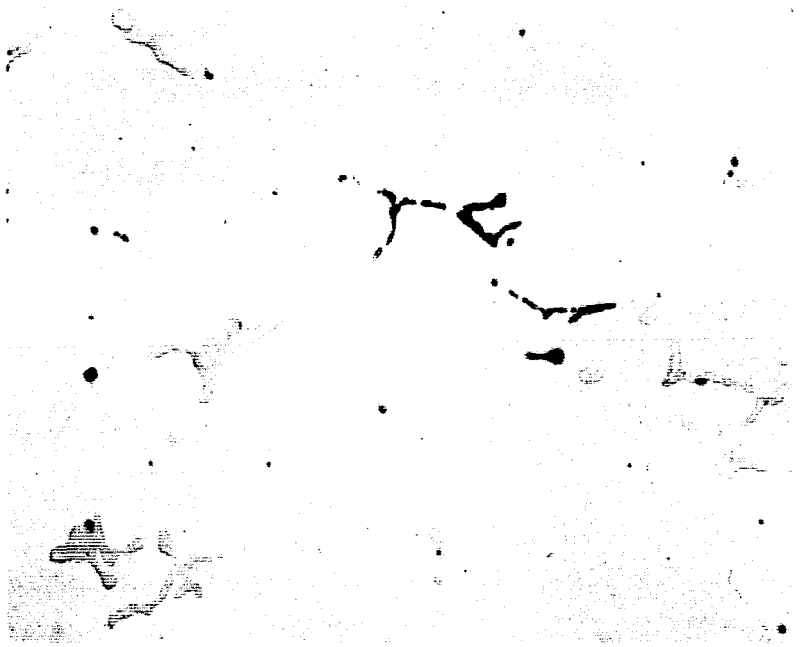

Transverse
XZ Plane

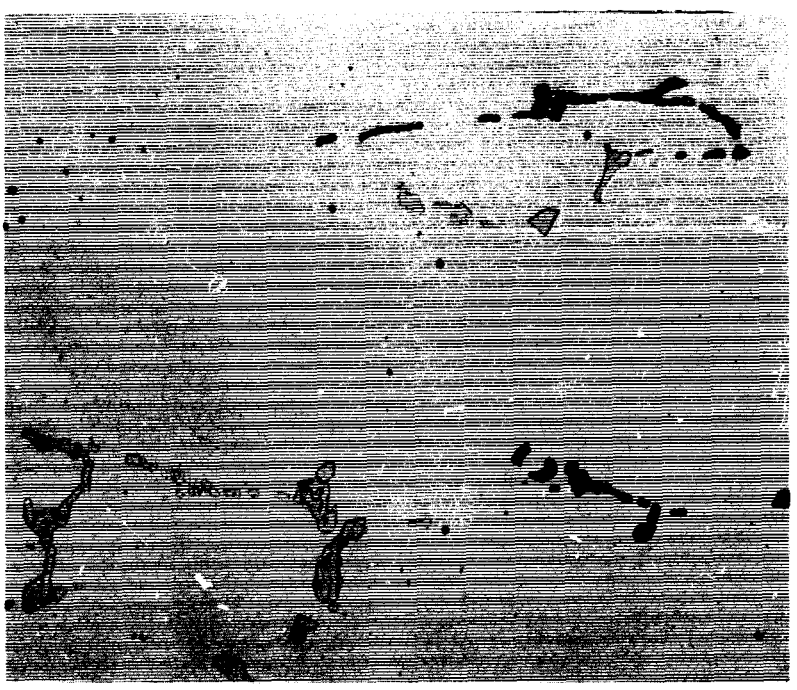

Longitudinal
YZ Plane

As Polished 500X

Distribution of Microconstituents
in 7079-T6 Plate

Figure 3

Transverse
XZ Plane

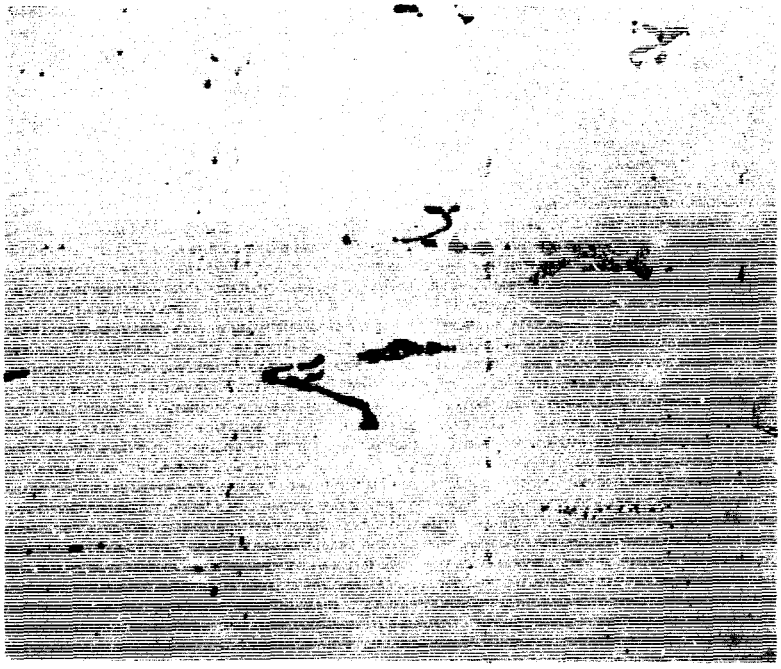

Longitudinal
YZ Plane

As Polished 500X

Distribution of microconstituents
in 7039-T6 plate.

Figure 4

Transverse
XZ Plane

Longitudinal
YZ Plane

Keller's Etch 500X

Microstructure of 7079-T6 plate
at higher magnification

Figure 5

Transverse
XZ Plane

Longitudinal
YZ Plane

Keller's Etch 500X

Microstructure of 7039-T6
plate at higher magnification.

Figure 6

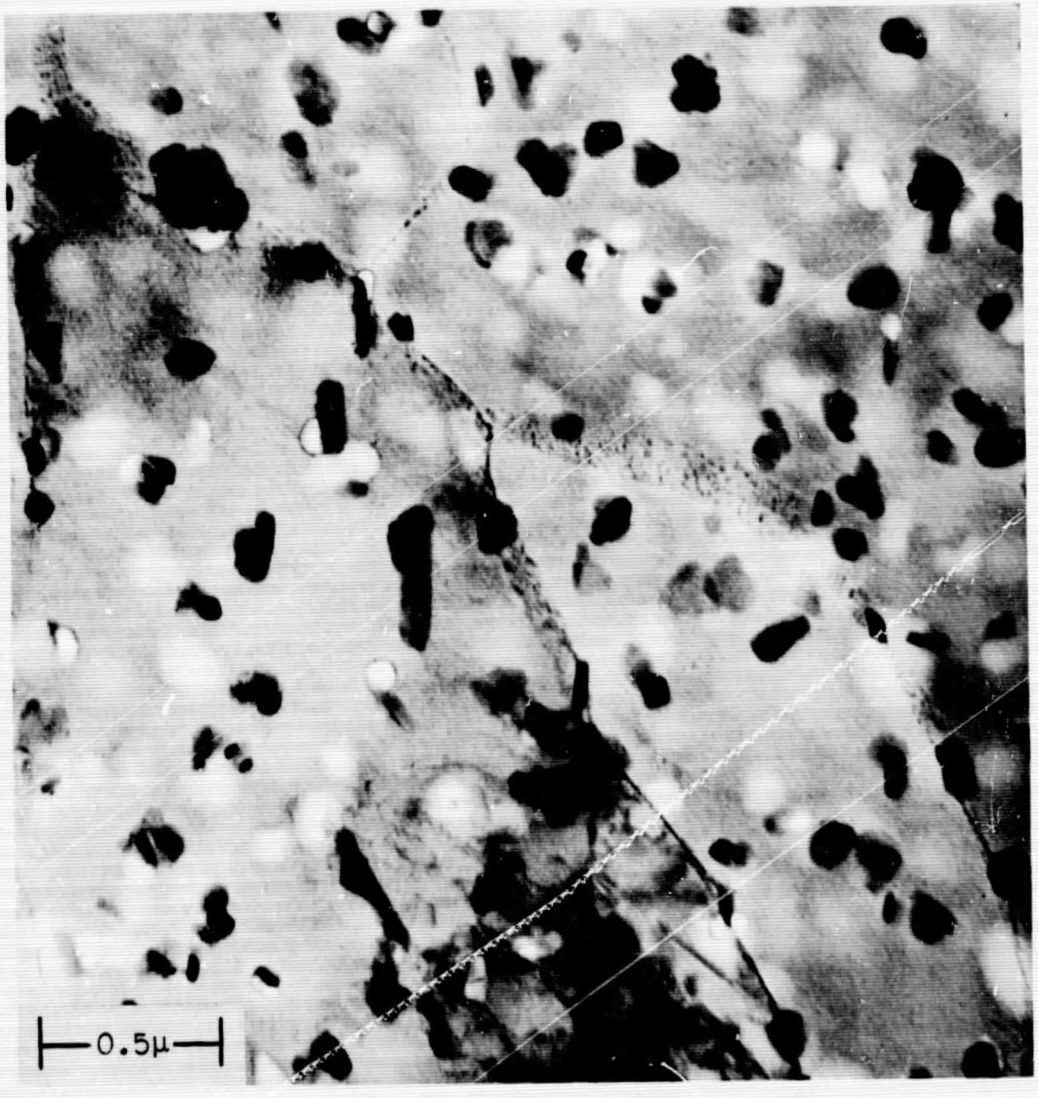

Electron transmission microstructure of 7079-T6 plate showing dispersoids, dislocations and precipitates.

Figure 7

Electron transmission microstructure of 7079-T6 plate in dispersoid-lean region. Two sizes of boundary precipitate, precipitate-free boundary region, and fine zones in matrix are apparent.

Figure 8

Electron transmission microstructure of 7039-T6 plate showing polygonized structure, dispersoid distribution and occasional dislocations.

Figure 9

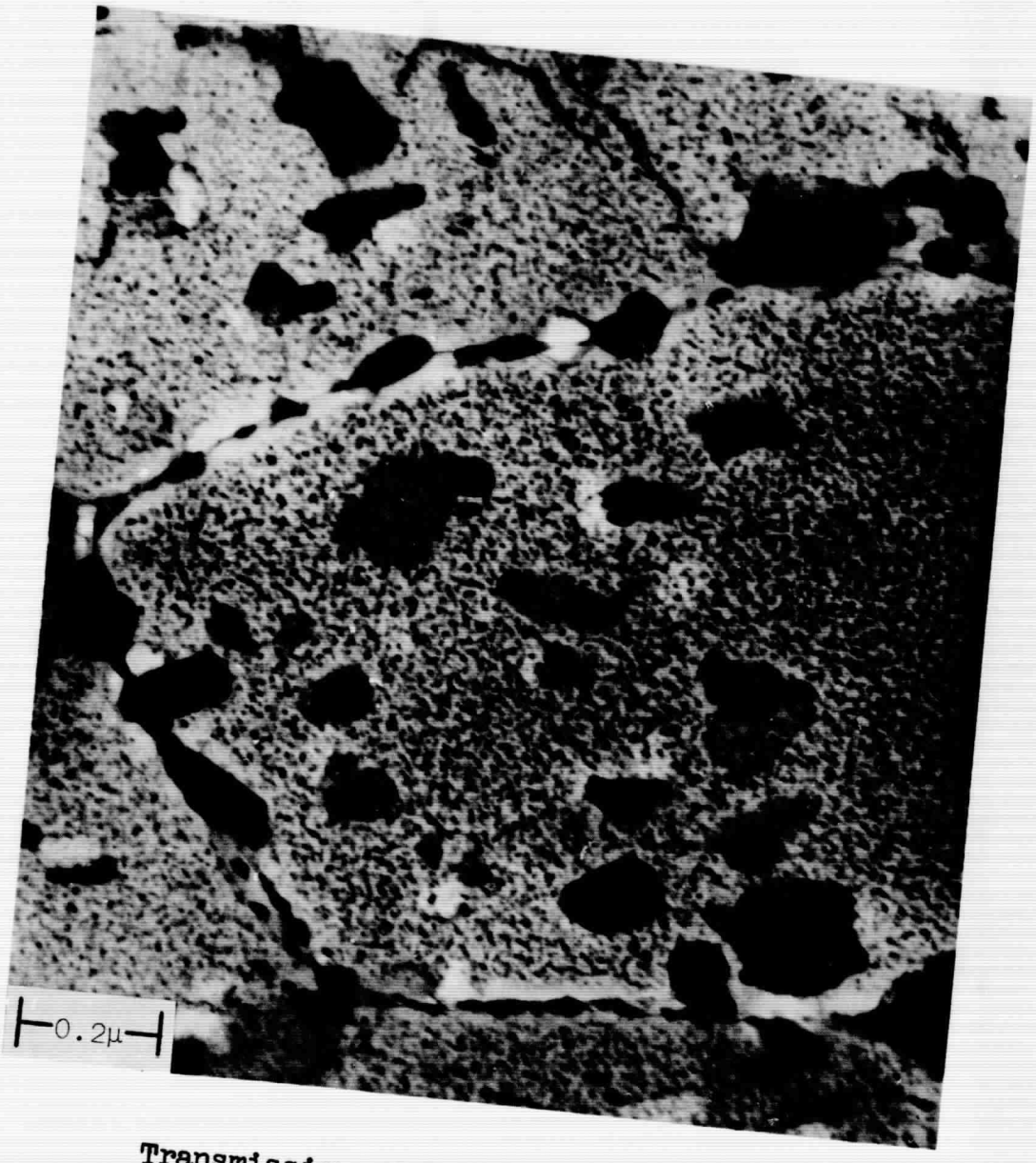

Transmission microstructure of 7039-T6 plate at higher magnification. Note two sizes of boundary precipitate, heavy zone-type precipitate, and precipitate-free boundary region.

Figure 10

165723
165725
165727
165729

60 min.

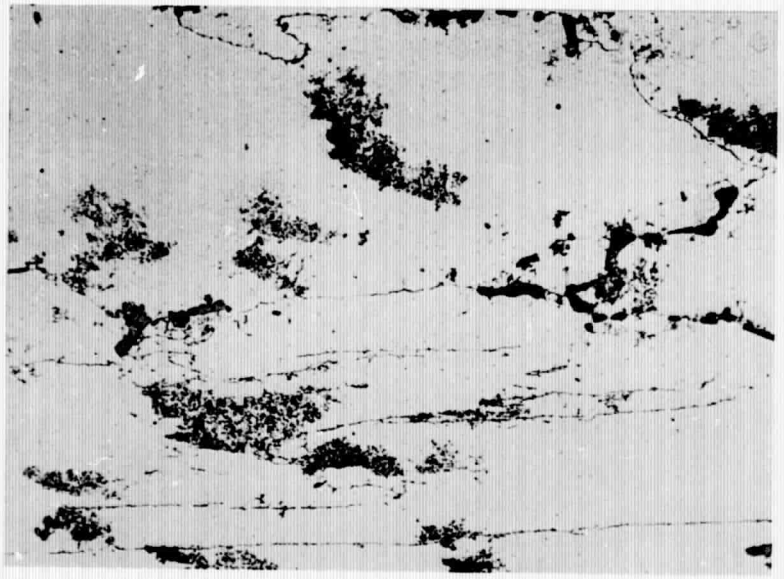

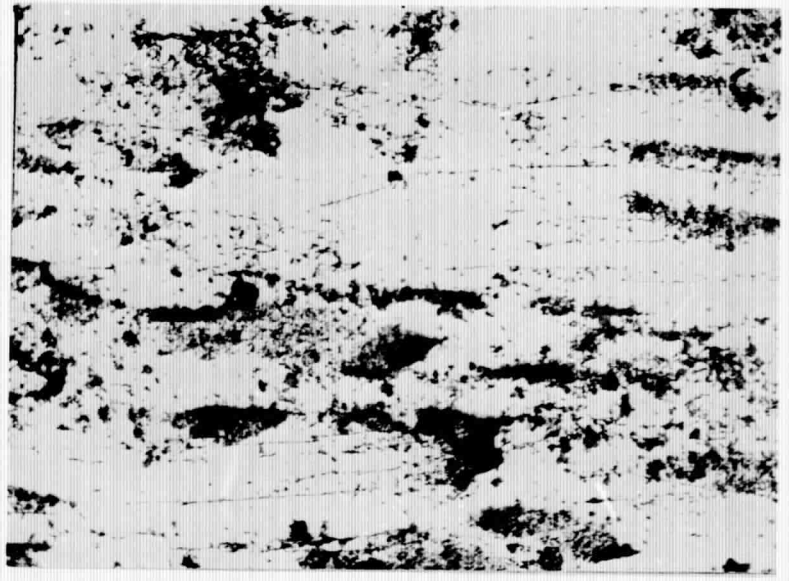

150 min.

210 min.

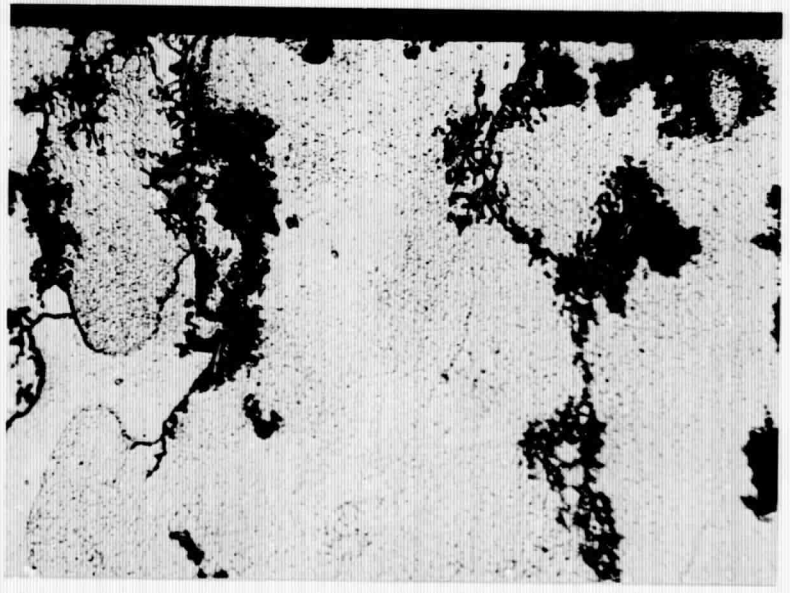

210 min.
X-Sect.
Keller's
Etch

Development of intergranular, interfragmentary and matrix pitting attack of 7079-T6 plate exposed unstressed to pH1 NaCl-$AlCl_3$ solution (X500).

Figure 11

167503
167505
167506
167507

15 min.

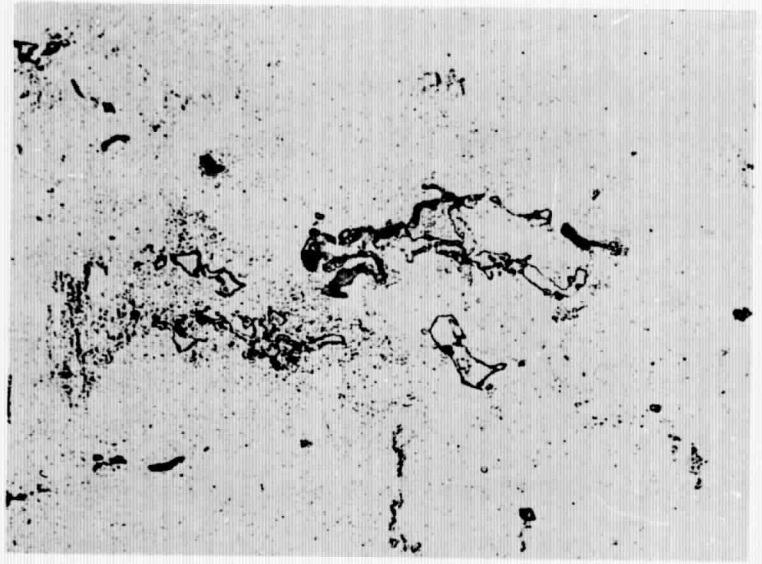

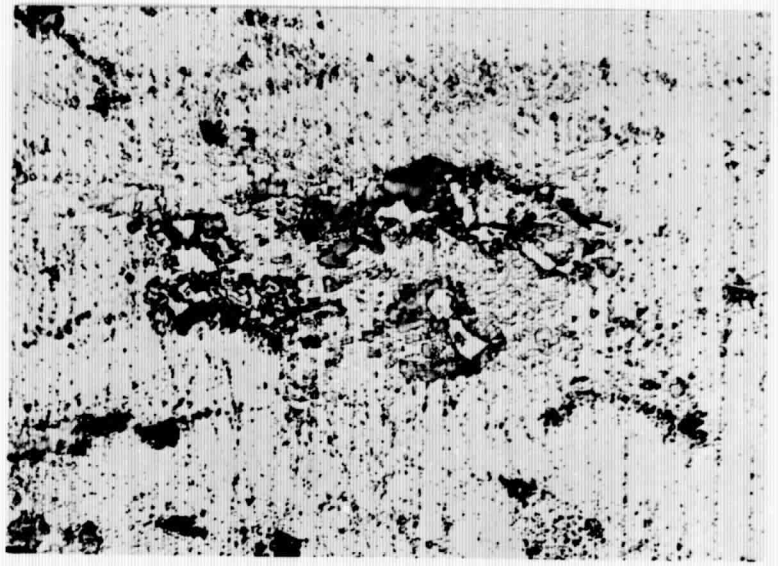

105 min.

150 min.

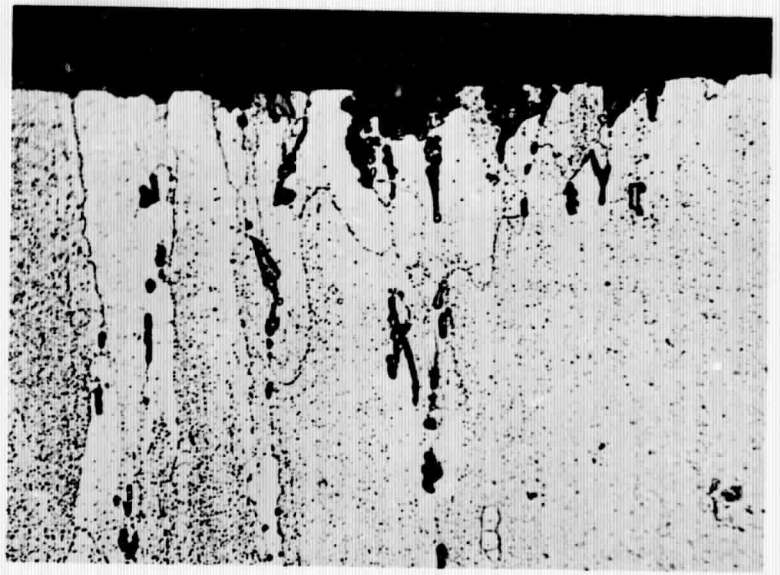

150 min.
X-Sect.
Keller's
Etch

Development of pitting attack in 7039-T6 plate exposed unstressed to pH1 NaCl-$AlCl_3$ solution (X500).

Figure 12

168270
168271
168272

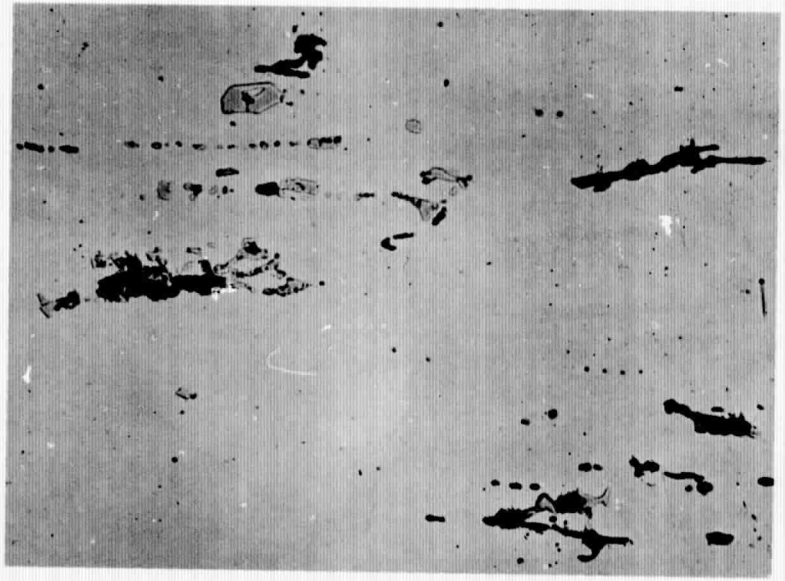

19 hrs

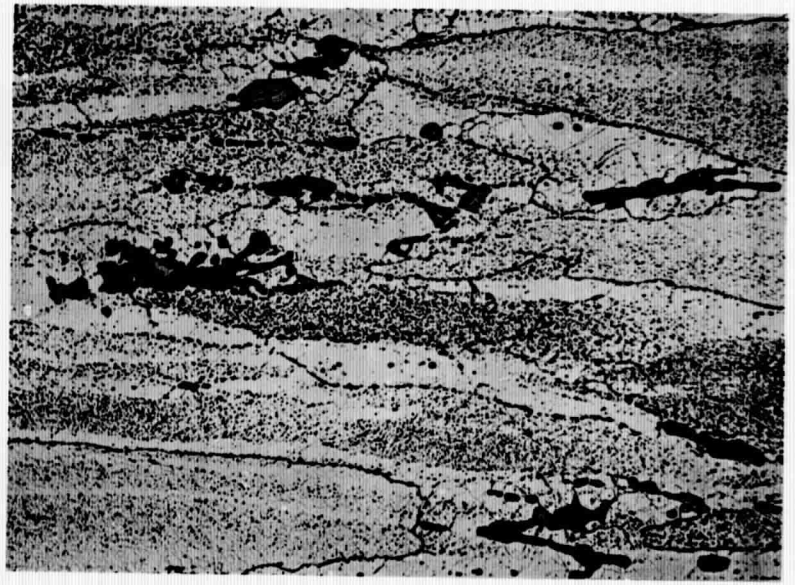

19 hrs
Keller's
Etch

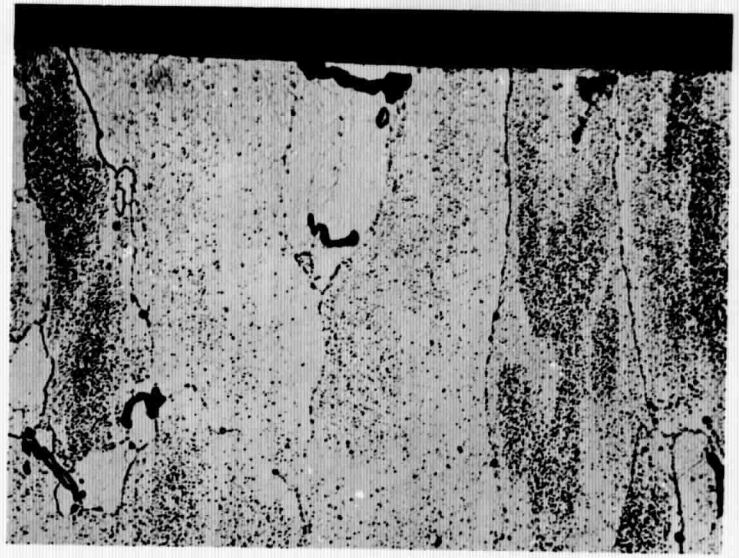

19 hrs
X-Sect.
Keller's
Etch

Development of pitting attack in 7039-T6 plate exposed unstressed to pH2 solution of 0.5N NaCl + 0.5N Na_2CrO_4 (X500).

Figure 13

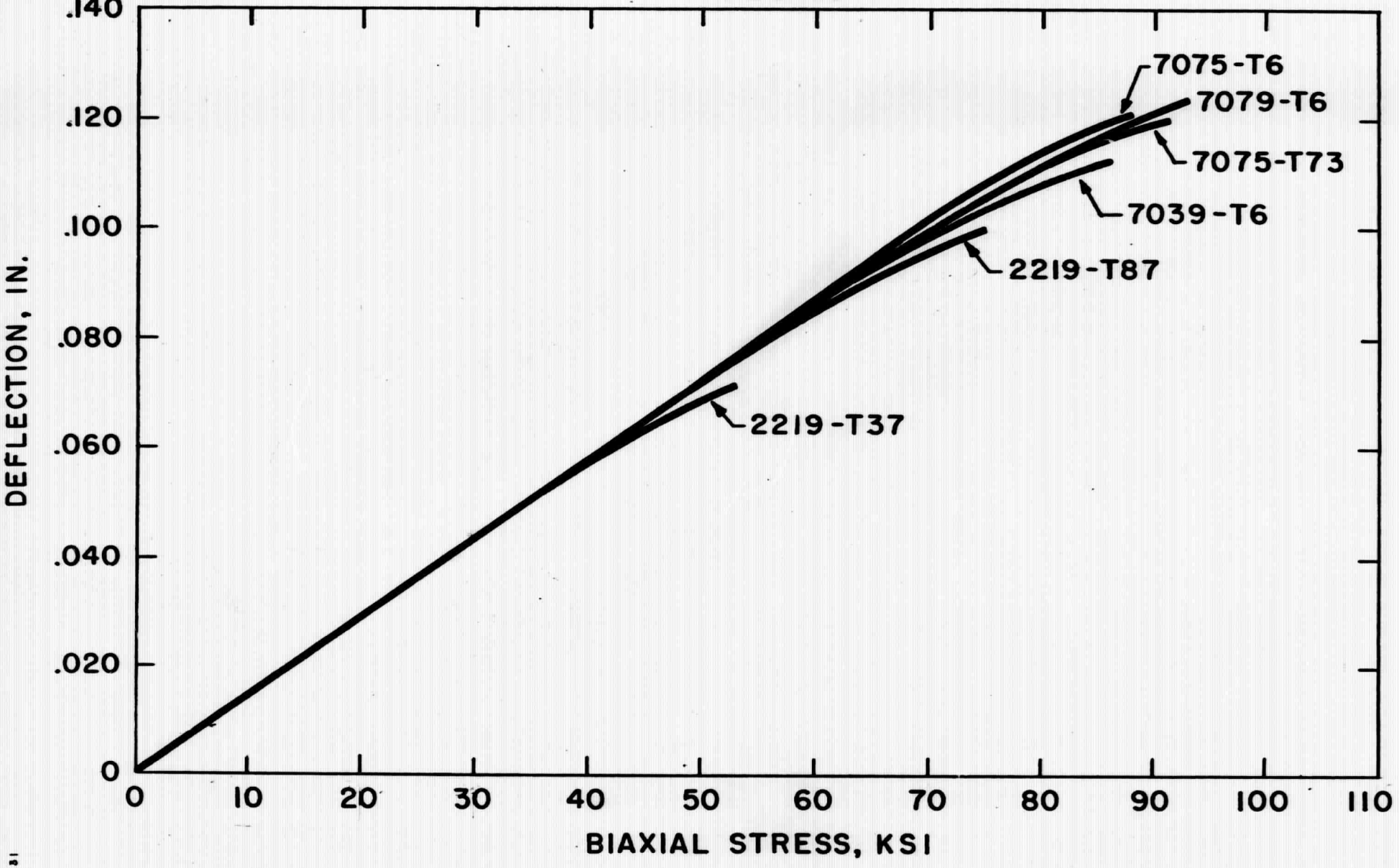

XFJ31

STRESS-DEFLECTION RELATIONSHIP OF TUNING-FORK STRESS CORROSION TEST SPECIMEN

FIGURE 14

164602
164607
164608

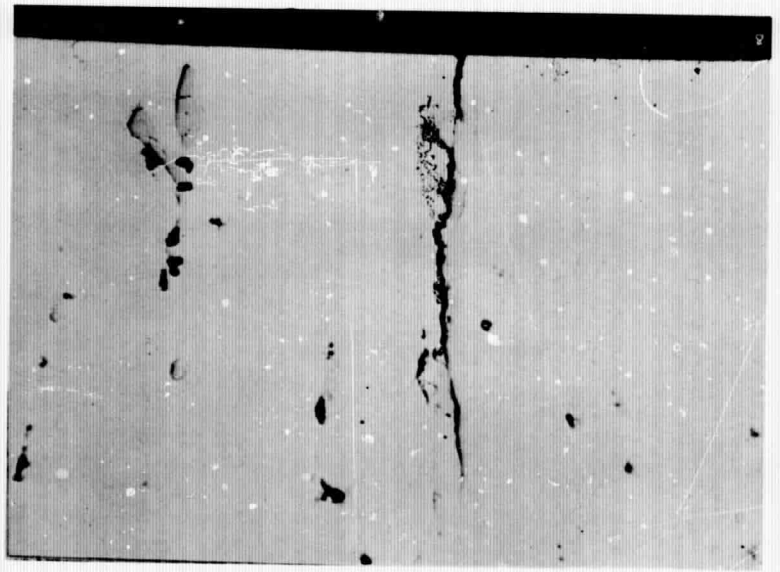

10 min.

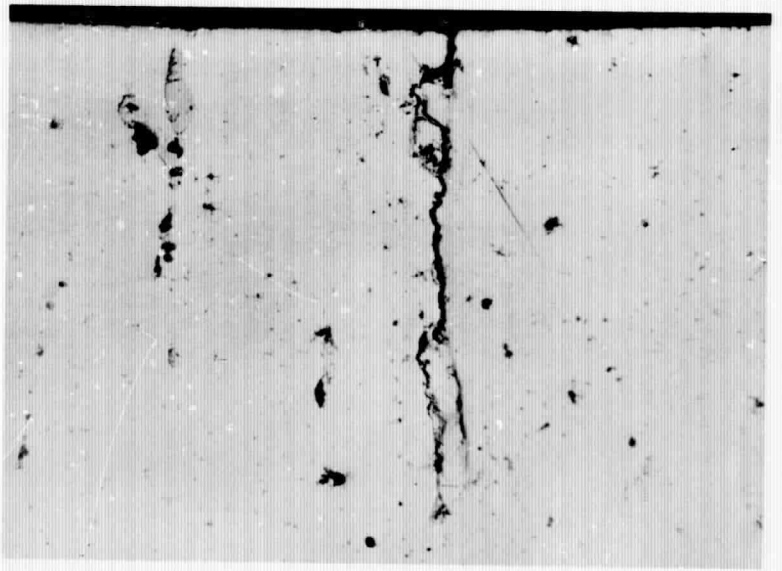

20 min.

← STRESS →

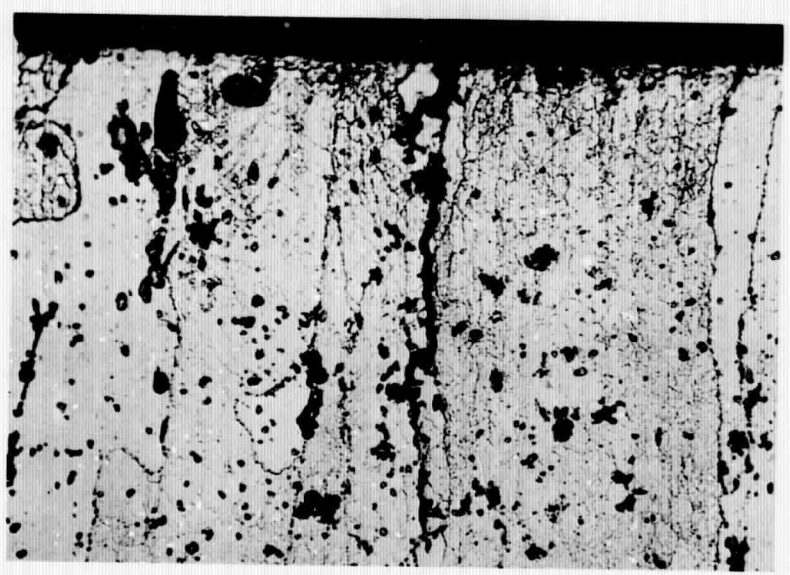

20 min. - Keller's Etch

Crack initiation on end face - 7075-T6 stressed short transversely to 75% YS (X500)
(See Figure 16 for matching side surface of same specimen)

Figure 15

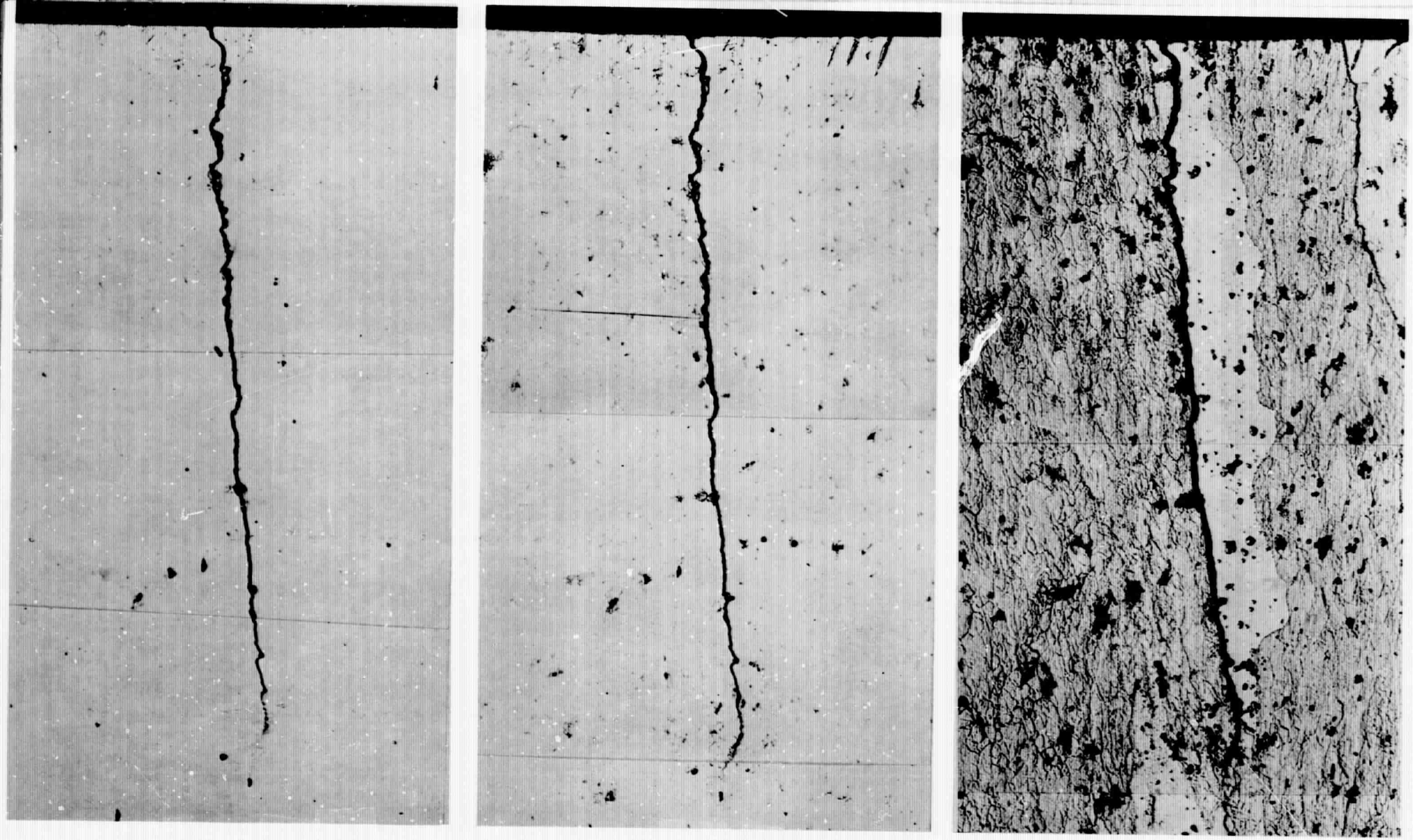

10 min.

20 min.

20 min.
Keller's Etch

164603-5
164609-14

Crack initiation on side face - 7075-T6 stressed short transversely to 75% YS (X500)

(See Figure 15 for matching end surface of same specimen)

Figure 16

166029
166031-32

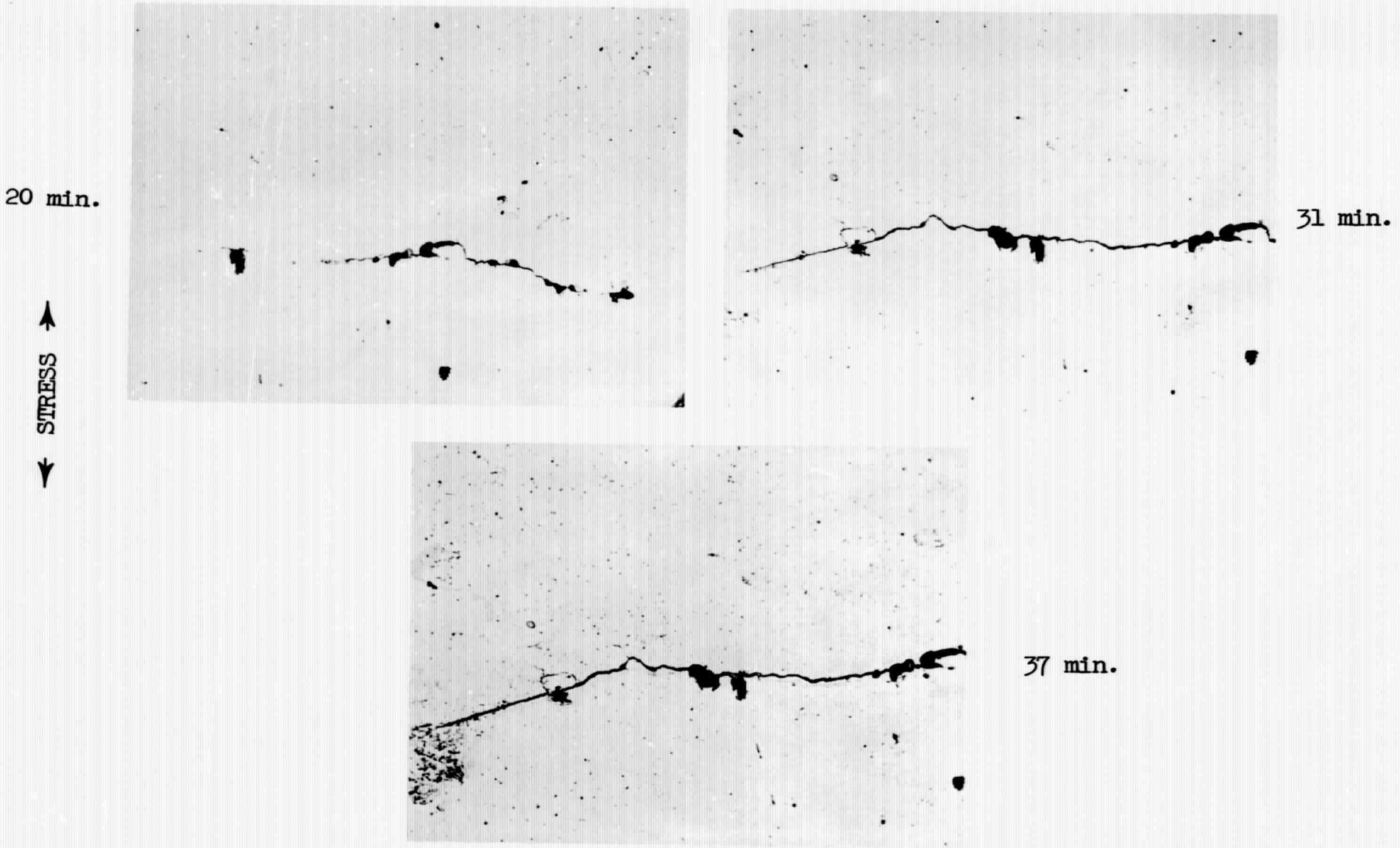

Stress corrosion crack initiation and development in 7079-T6 specimen stressed short transversely to 75% YS and exposed to the pH1 solution. (X500)

Figure 17

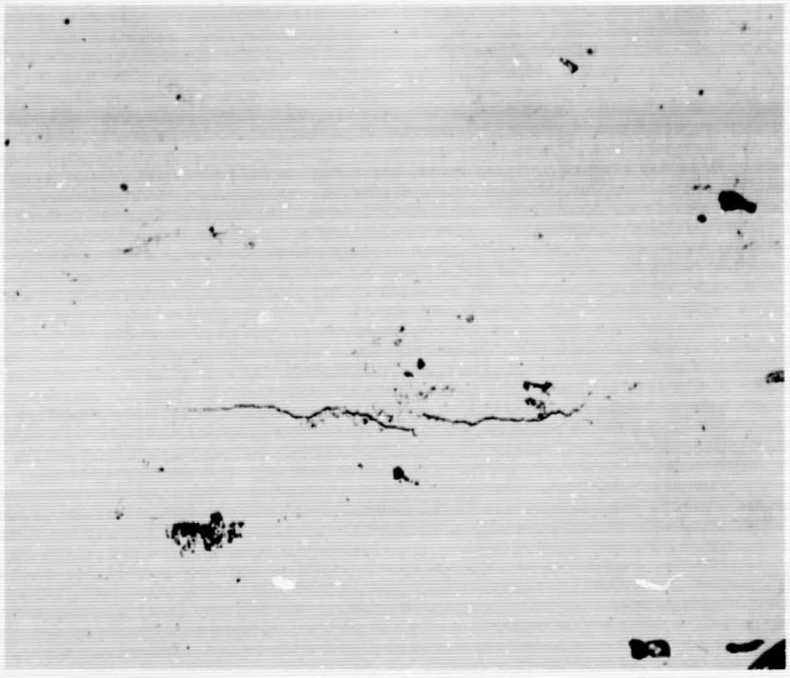

25 min.

STRESS

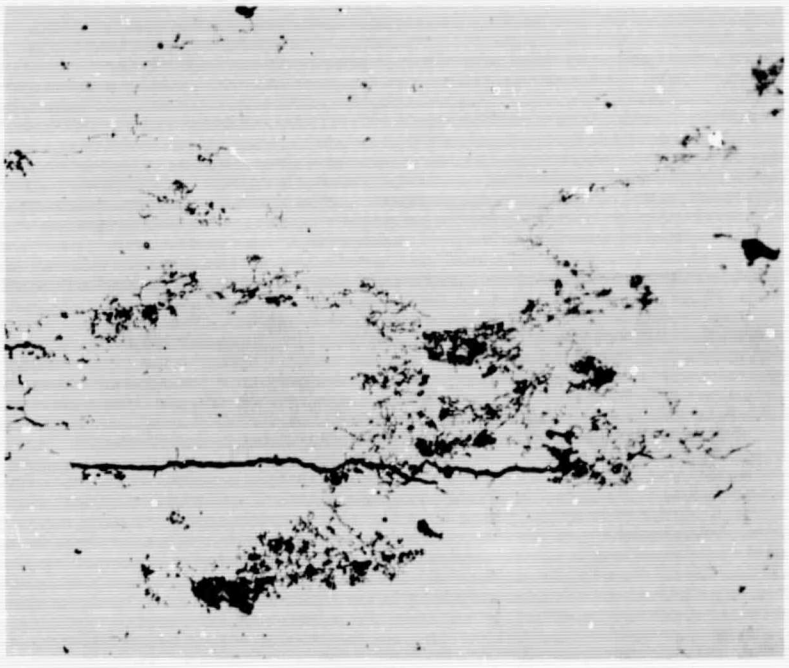

53 min.

Shows development of interfragmentary attack along sides of a stopped crack in 7079-T6 specimen. Also note interfragmentary fringes along "former" grain boundary. (X500)

166023
166026

Figure 18

166215-18

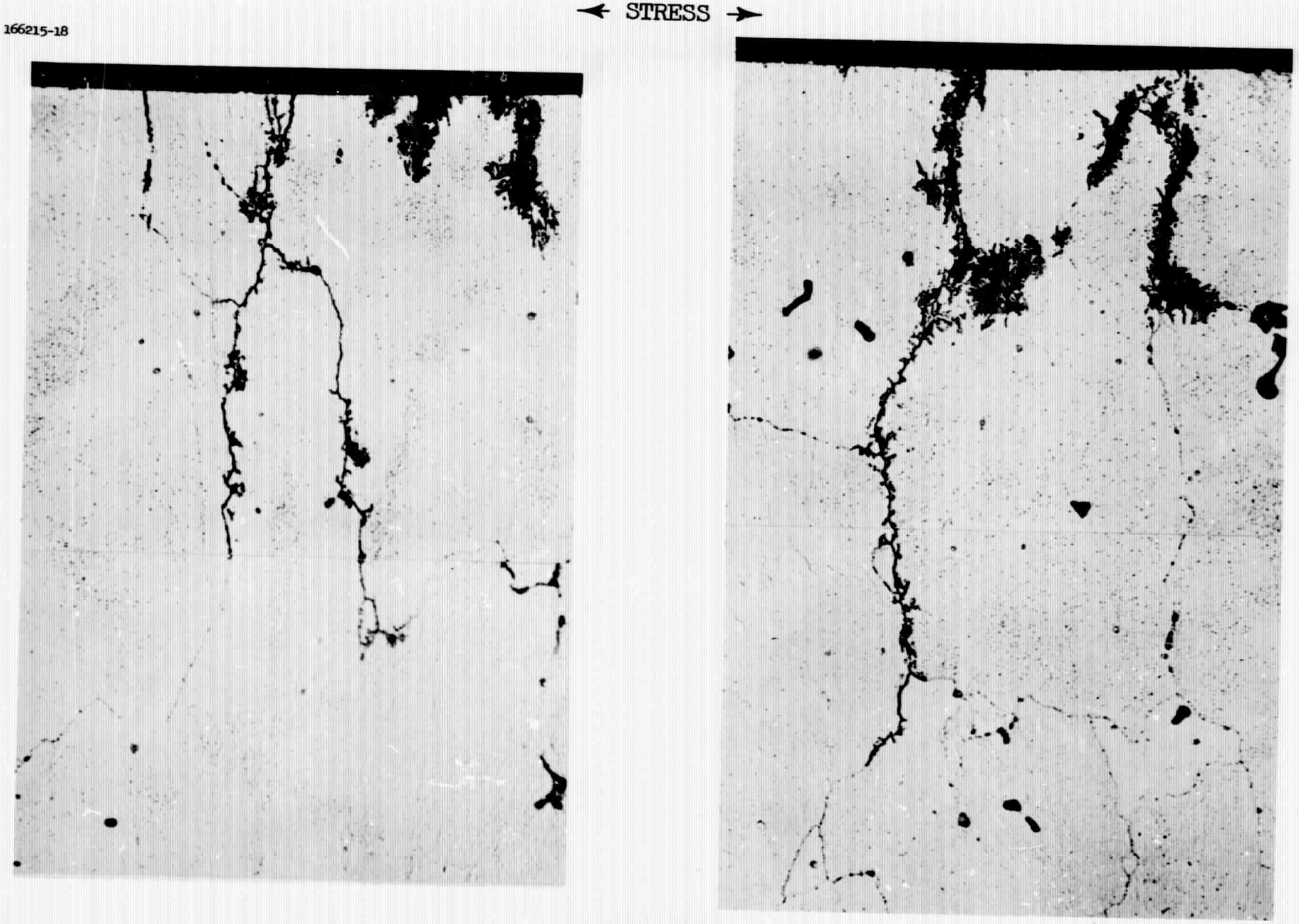

Stress corrosion cracks and interfragmentary corrosion of 7079-T6 specimen after 90 minute exposure to the pH1 solution stressed short transversely to 75% YS. (X500)

Figure 19

168073
168074
168075

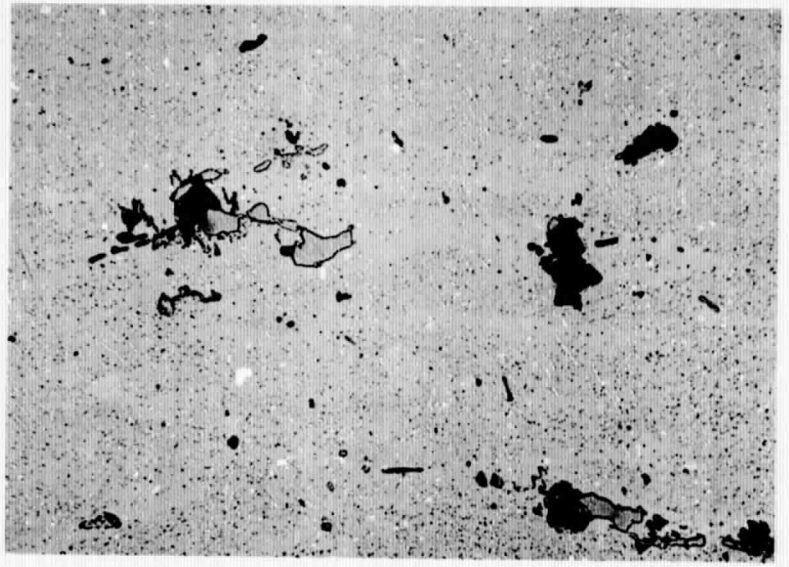

10 min.
500X

STRESS

12.5 hrs
100X

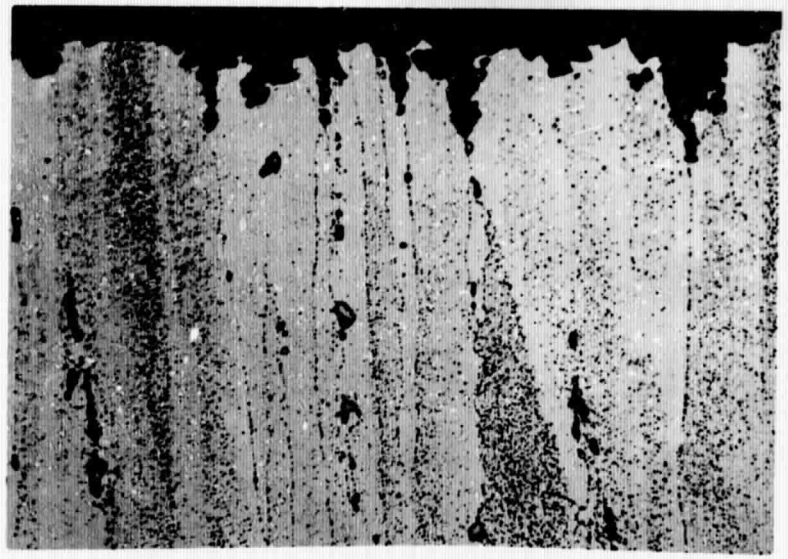

X-Sect.
12.5 hrs
Keller's
Etch
500X

Cubic pitting of 7039-T6 plate stressed short transversely to 75% YS and exposed to pH1 NaCl-$AlCl_3$ solution (X500).

Figure 20

168263
168265
168266
168267

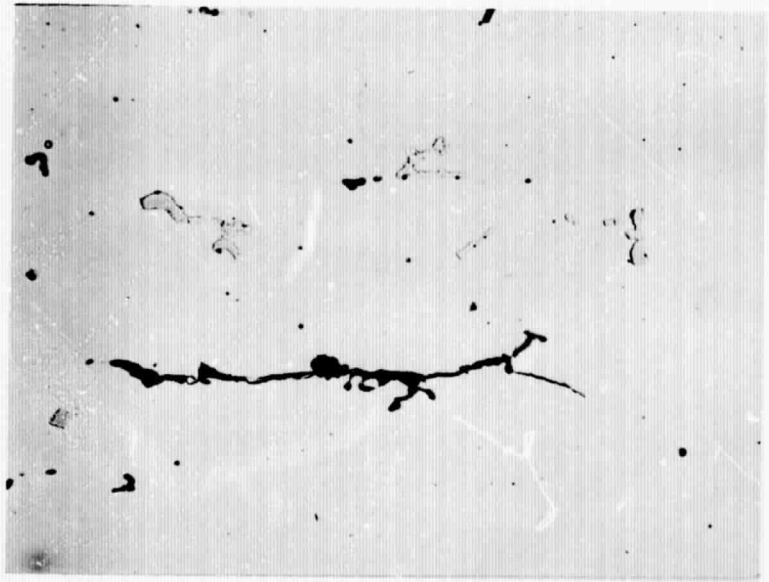

135 min.

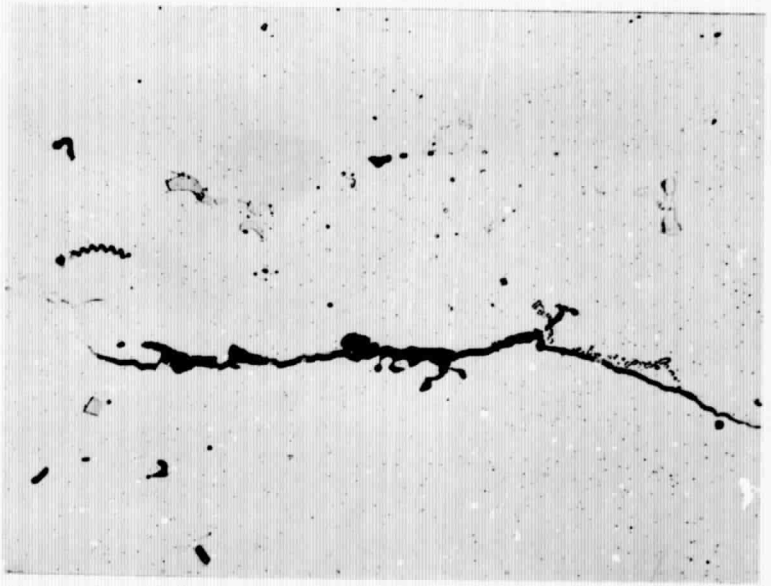

375 min.

STRESS

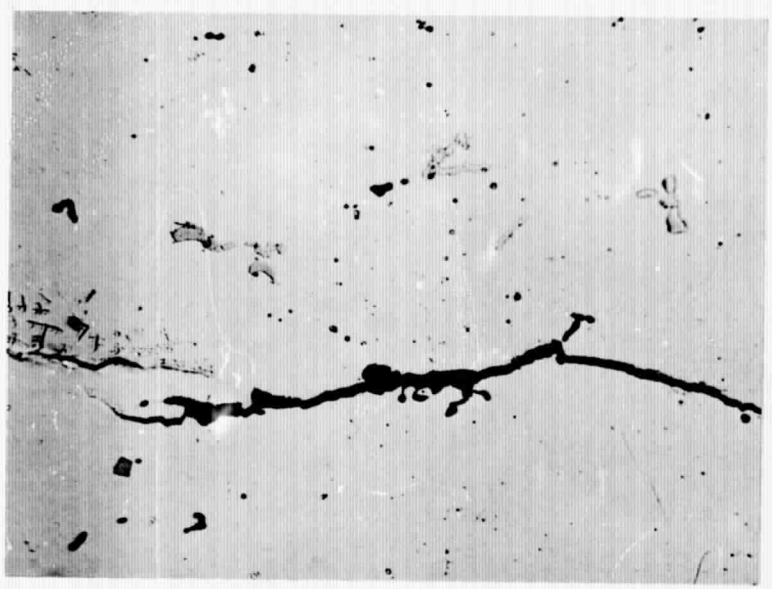

435 min.

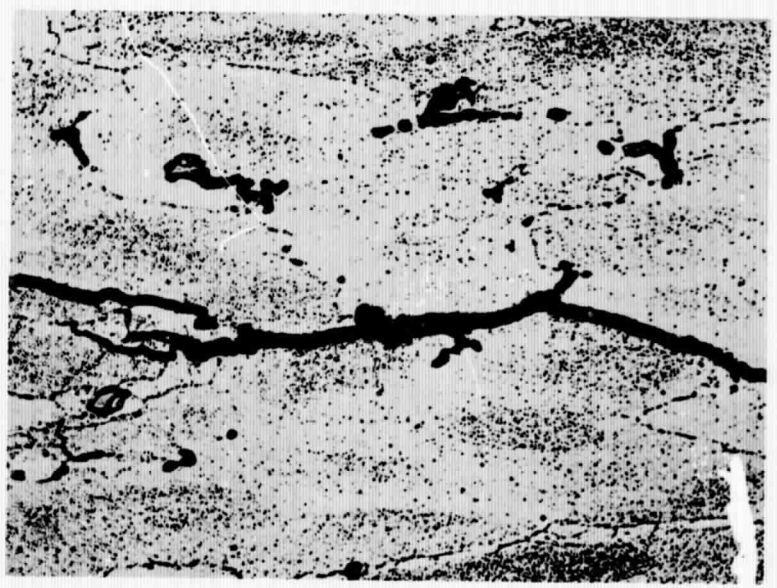

435 min.
Keller's
Etch

Crack initiation in 7039-T6 plate stressed short transversely to 75% YS and exposed to pH2 solution containing 0.5N NaCl + 0.5N Na_2CrO_4 (X500).

Figure 21

← STRESS →

Cross section of sample in Fig. 21 (X500).

Figure 22

Oxide Replica 10,000X

Embryonic crack in 7075-T6
stressed longitudinally to 75% YS.

Figure 23

Oxide Replica 20,000X

Cracks initiating at low angle to stress in 7075-T6 stressed longitudinally to 75% YS.

Figure 24

Oxide Replica 10,000X

Possible crack initiation along junction of normal and dispersoid-free region in 7075-T6 stressed to 75% YS.

Figure 25

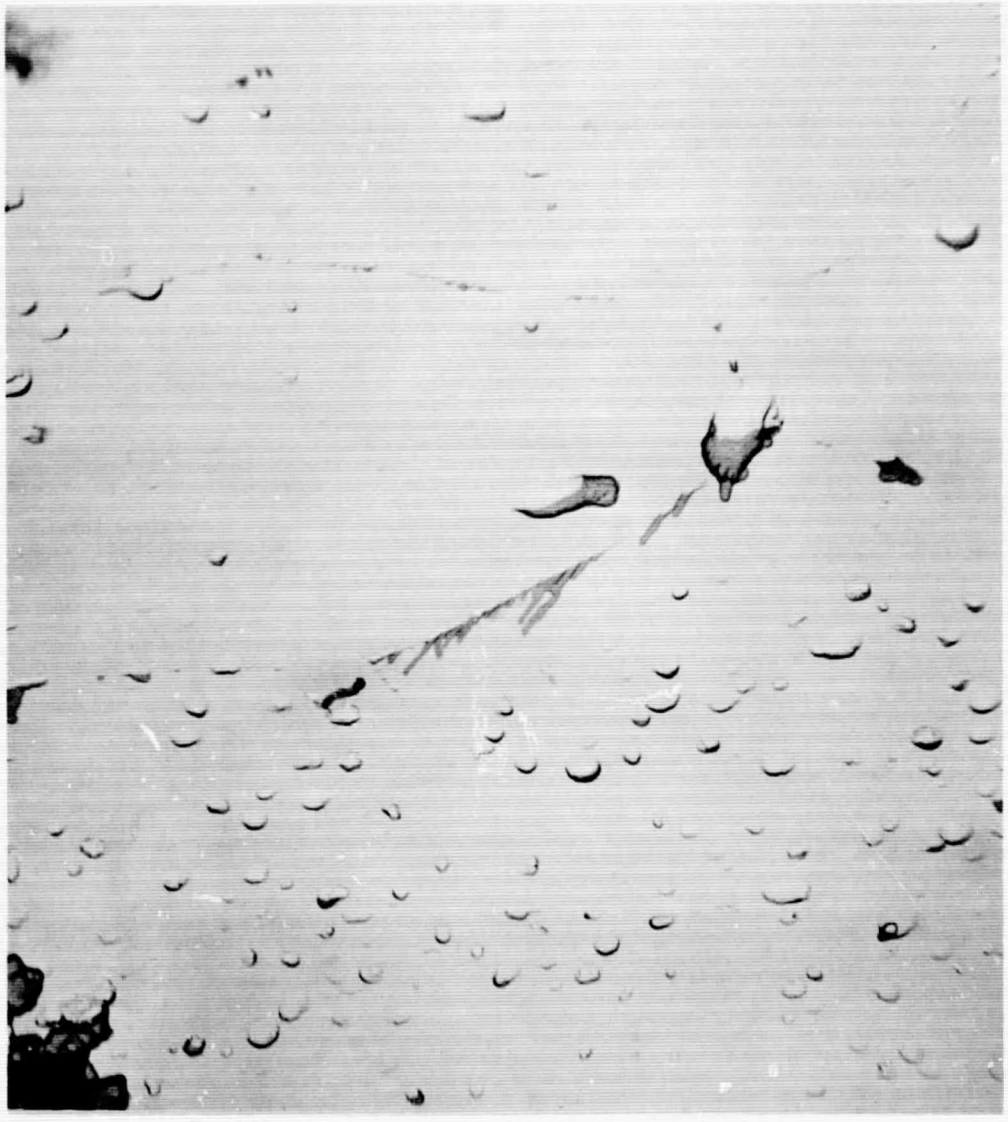

Oxide Replica 15,000X

Beginning of a stress-corrosion crack
on cellular "former" boundary in 7079-T6.

Figure 26

180/1/3

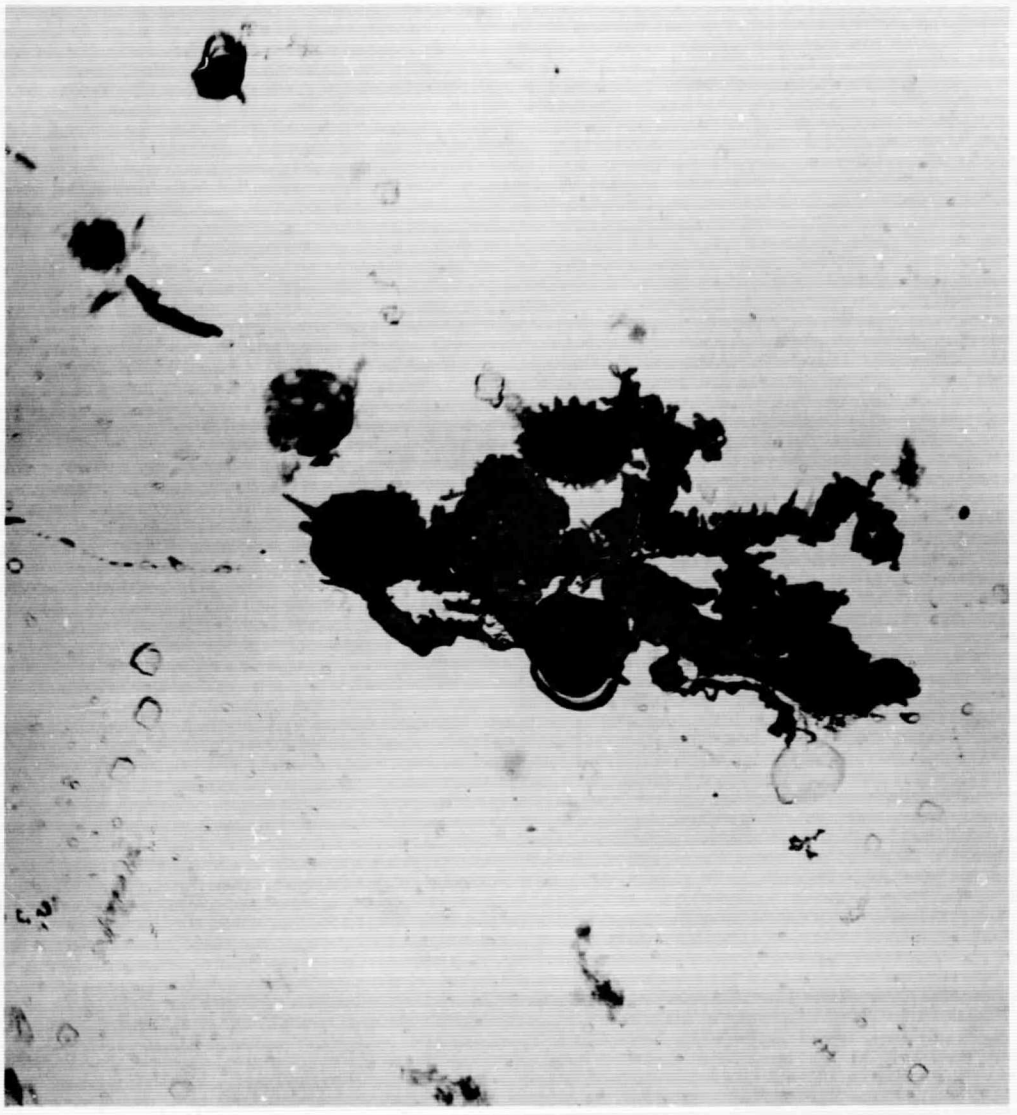

Oxide Replica 5,000X

Small stress-corrosion crack on cellular "former" boundary in 7079-T6. Rounded black objects are constituent particles.

Figure 27

180/5/1

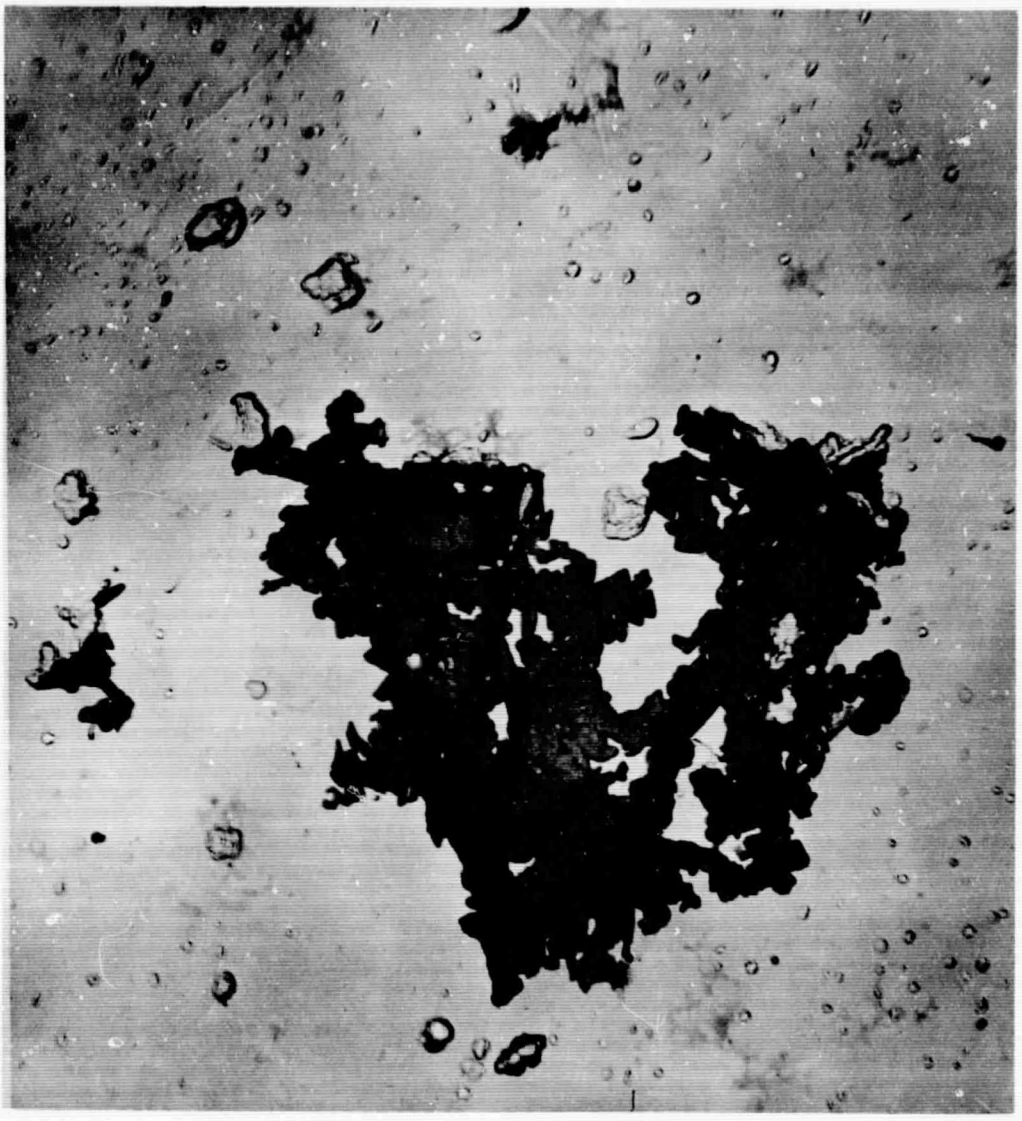

Oxide Replica 10,000X

Small stress-corrosion crack in 7079-T6 showing veining produced by attack of polygon junctions in "former" boundaries.

Figure 28

180/4/2

Oxide Replica 15,000X

End of a relatively large stress-corrosion crack in 7079-T6. The opening of the crack onto the surface can be seen at the top of the picture and deeper parts of the crack at the bottom.

Figure 29

180/5/2

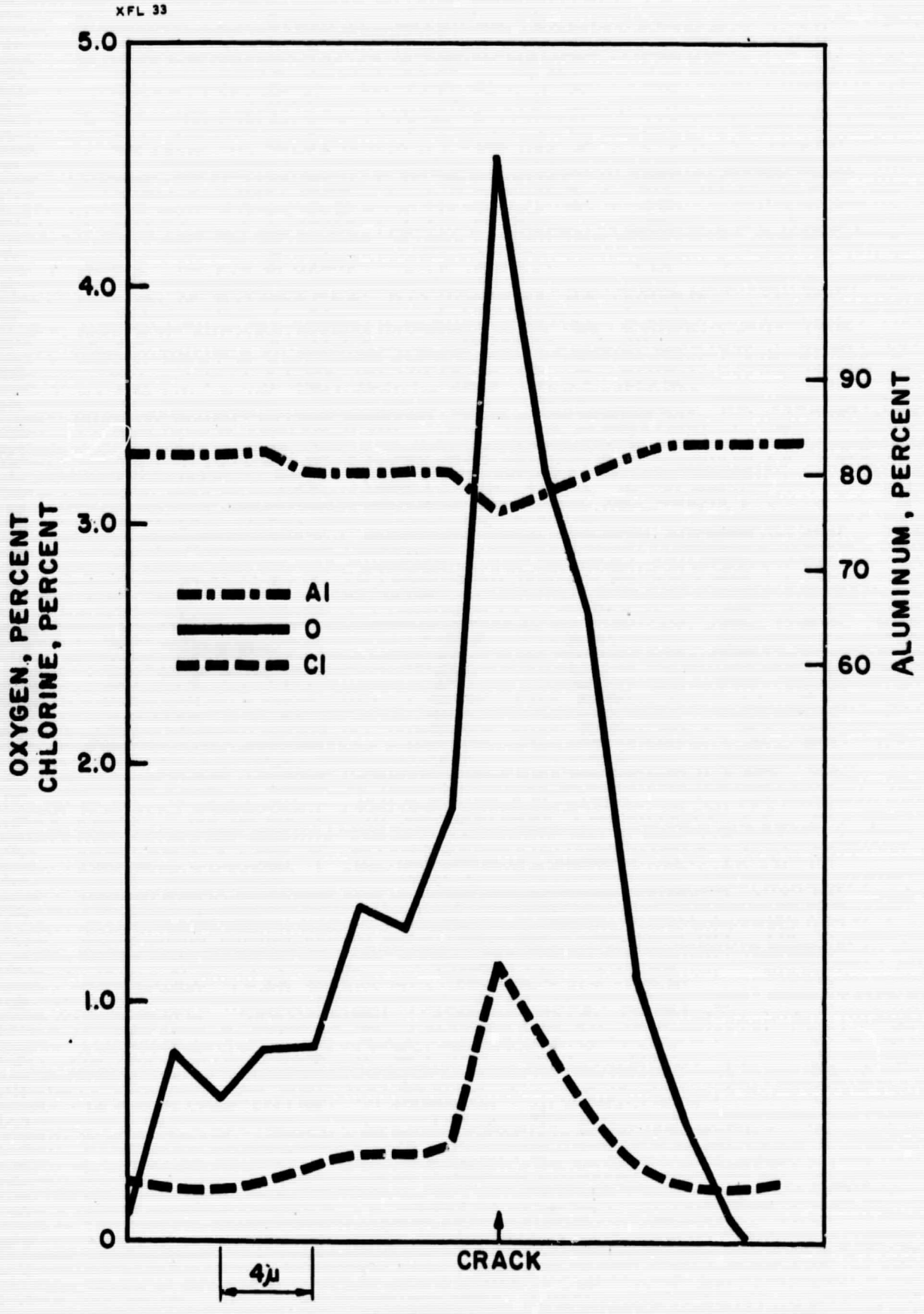

DISTRIBUTION OF Al, Cl AND O IN VICINITY OF STRESS-CORROSION CRACK

FIGURE 30

XFL34

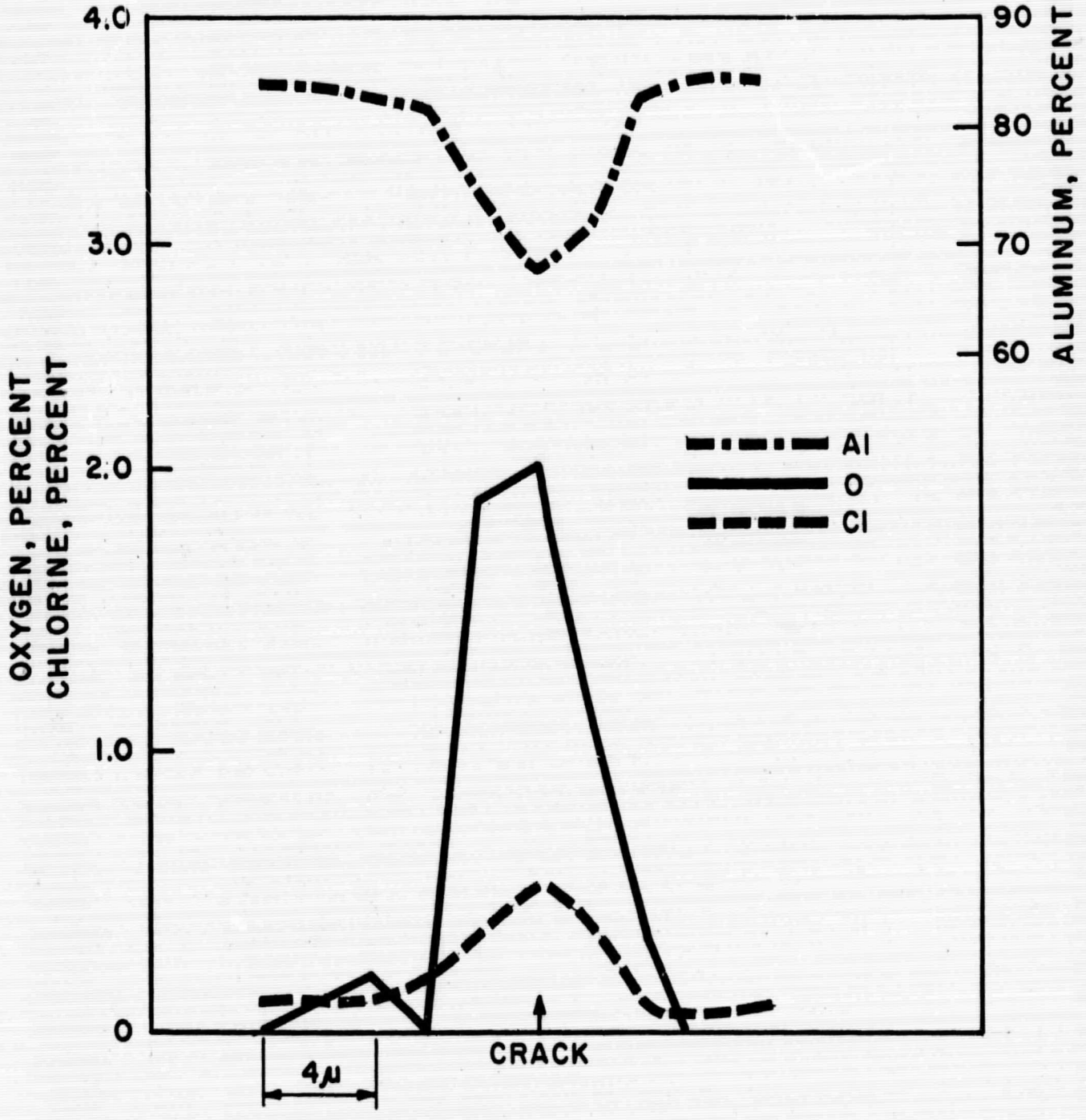

DISTRIBUTION OF Al, Cl AND O IN VICINITY OF STRESS-CORROSION CRACK

FIGURE 31

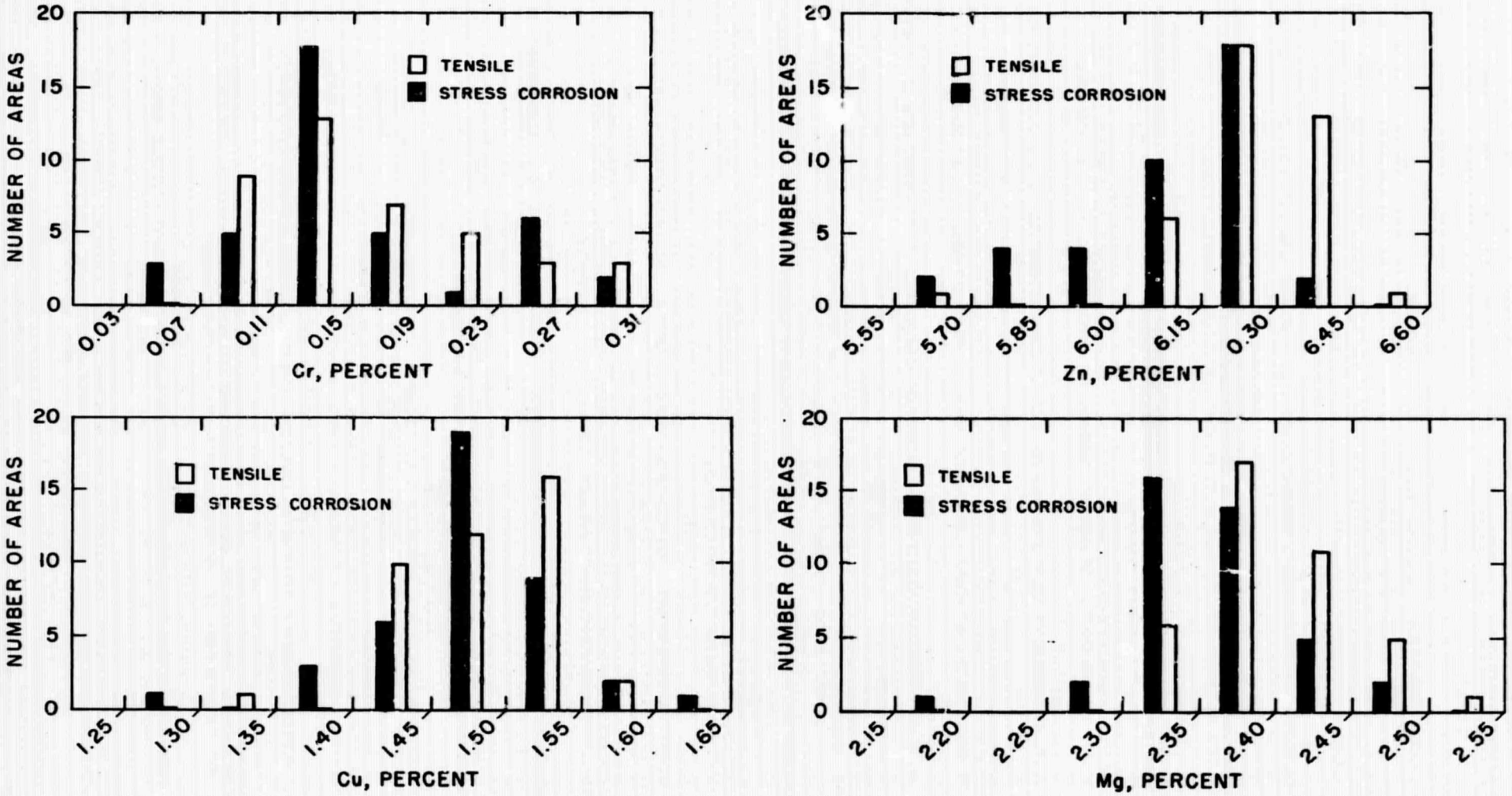

COMPOSITION OF STRESS CORROSION CRACK SURFACE OF 7075-T6

FIGURE 32

Oxide Replica 5000X

Transition from a stress corrosion fracture replicated in 22v oxide (lower half) to tensile fracture replicated in 15 v oxide. Note that thick oxide was cracked during the breaking open of the specimen and the cracks were repaired by application of the second oxide.

7075-T6 stressed 75% YS

Figure 33

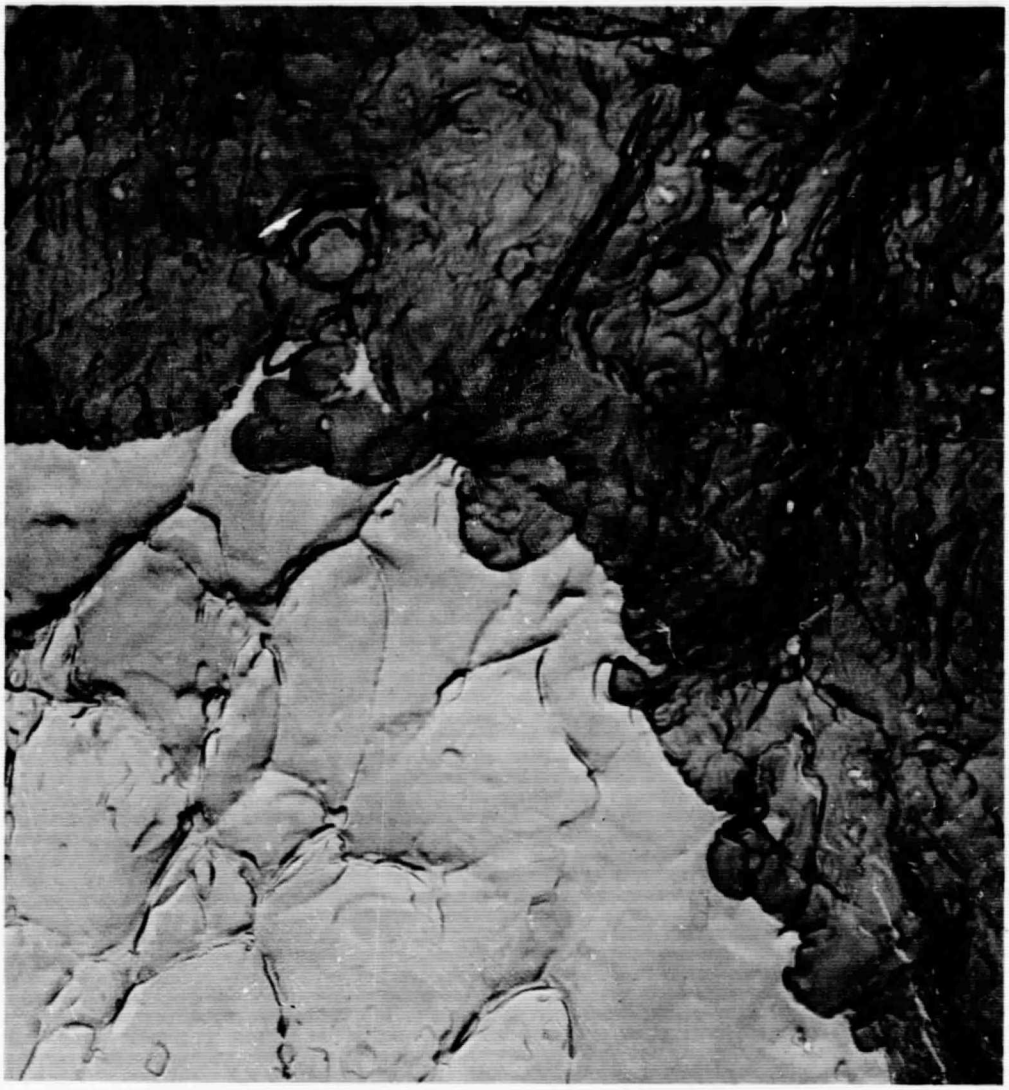

Oxide-Carbon Replica 20,000X

Transition from a stress corrosion fracture (upper portion) replicated in oxide and carbon to a tensile fracture replicated in carbon alone. 7075-T6 stressed short transversely to 75% YS.

Figure 34

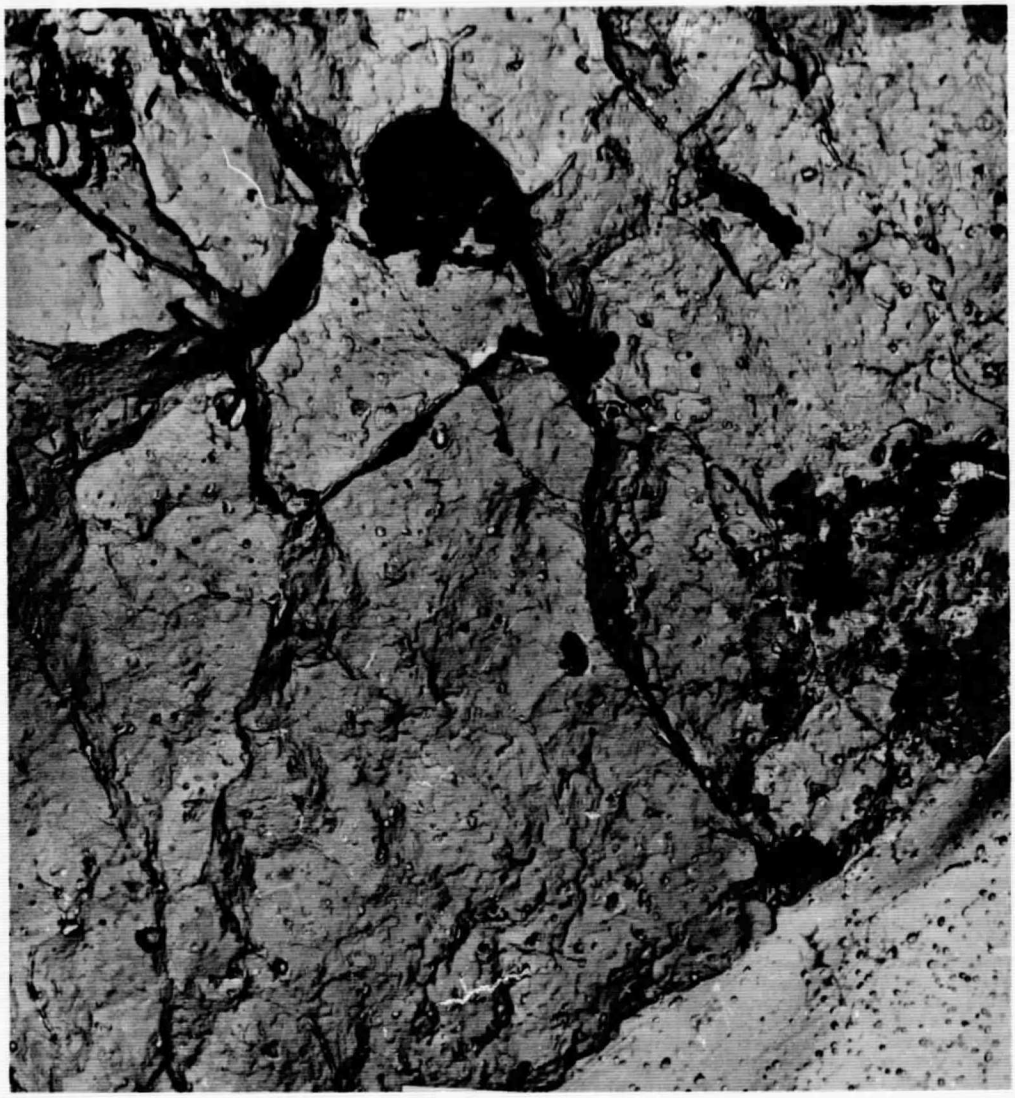

Oxide-Carbon Replica 5000X

Stress corrosion fracture in 7075-T6 stressed to 75% YS. Stress corrosion proceeded from specimen surface seen at lower right, along polygon boundaries. At the top, a small polygon is almost completely surrounded by stress corrosion cracks. Some corrosion product is seen near the surface at right.

Figure 35

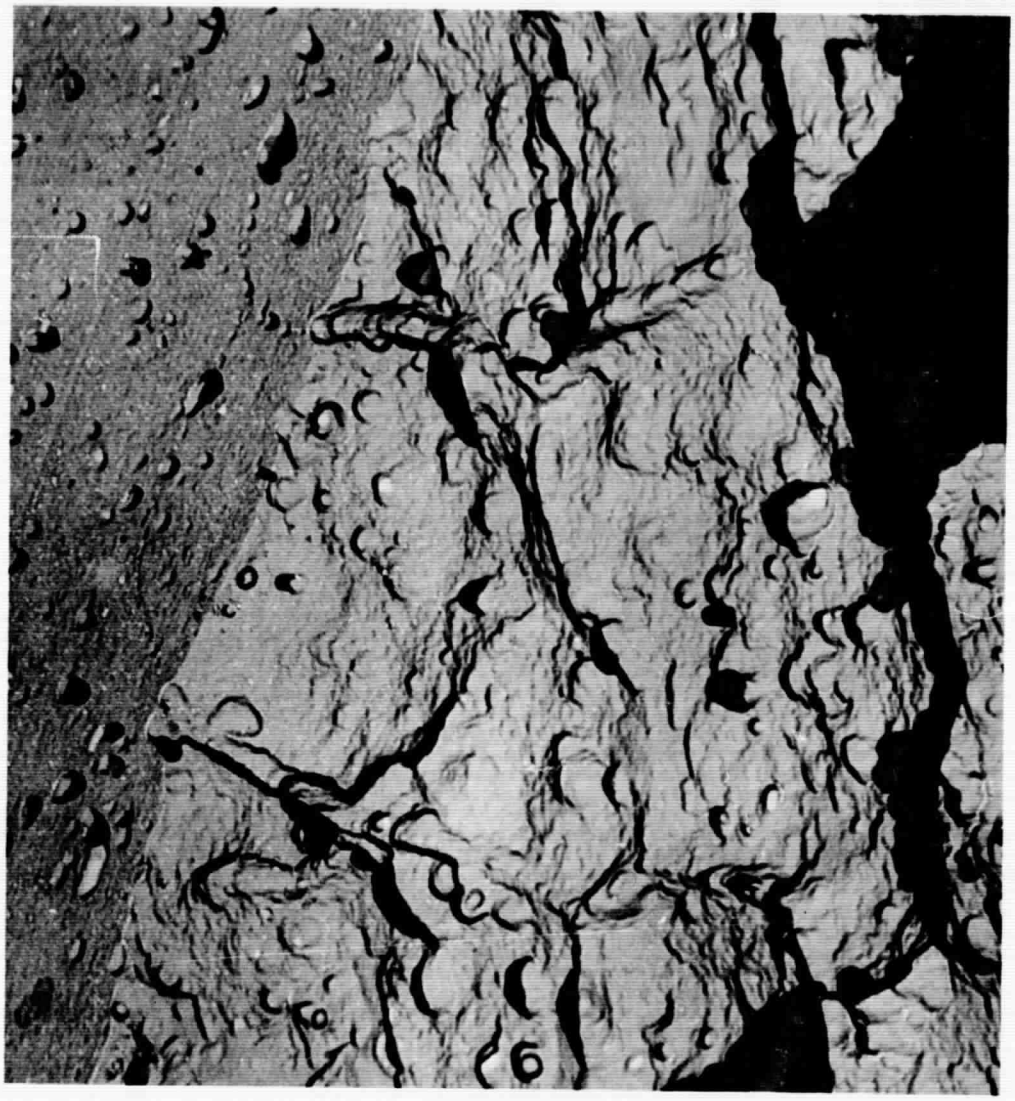

Double Oxide Replica 20,000X

Intersection of stress corrosion fracture with specimen surface. Furrows on fracture match with polygon boundaries seen on surface at left of figure. 7075-T6 stressed 75% YS.

Figure 36

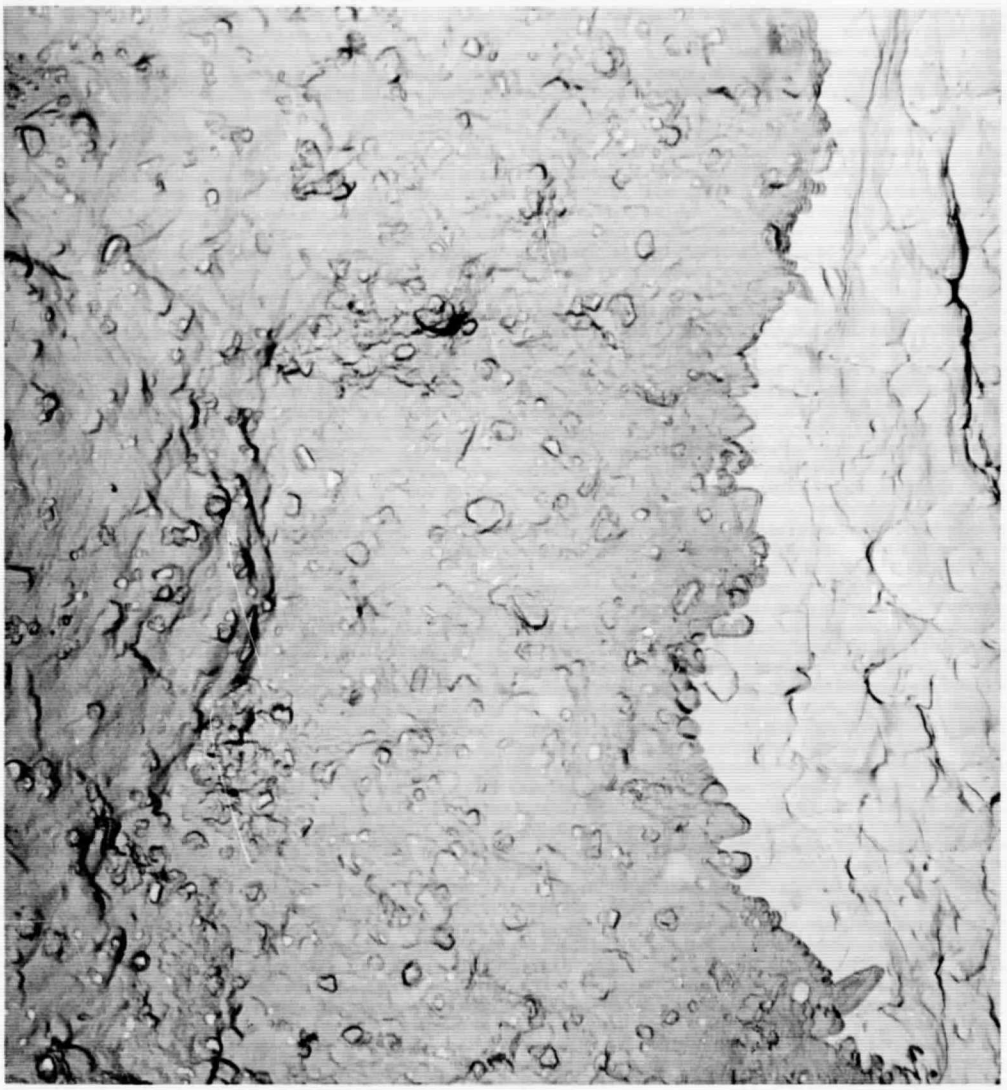

Oxide-Carbon Replica 10,000X

Transition from stress corrosion fracture (left) to tensile fracture showing that tip of stress corrosion crack is irregular. 7075-T6 stressed to 75% YS short transversely.

Figure 37

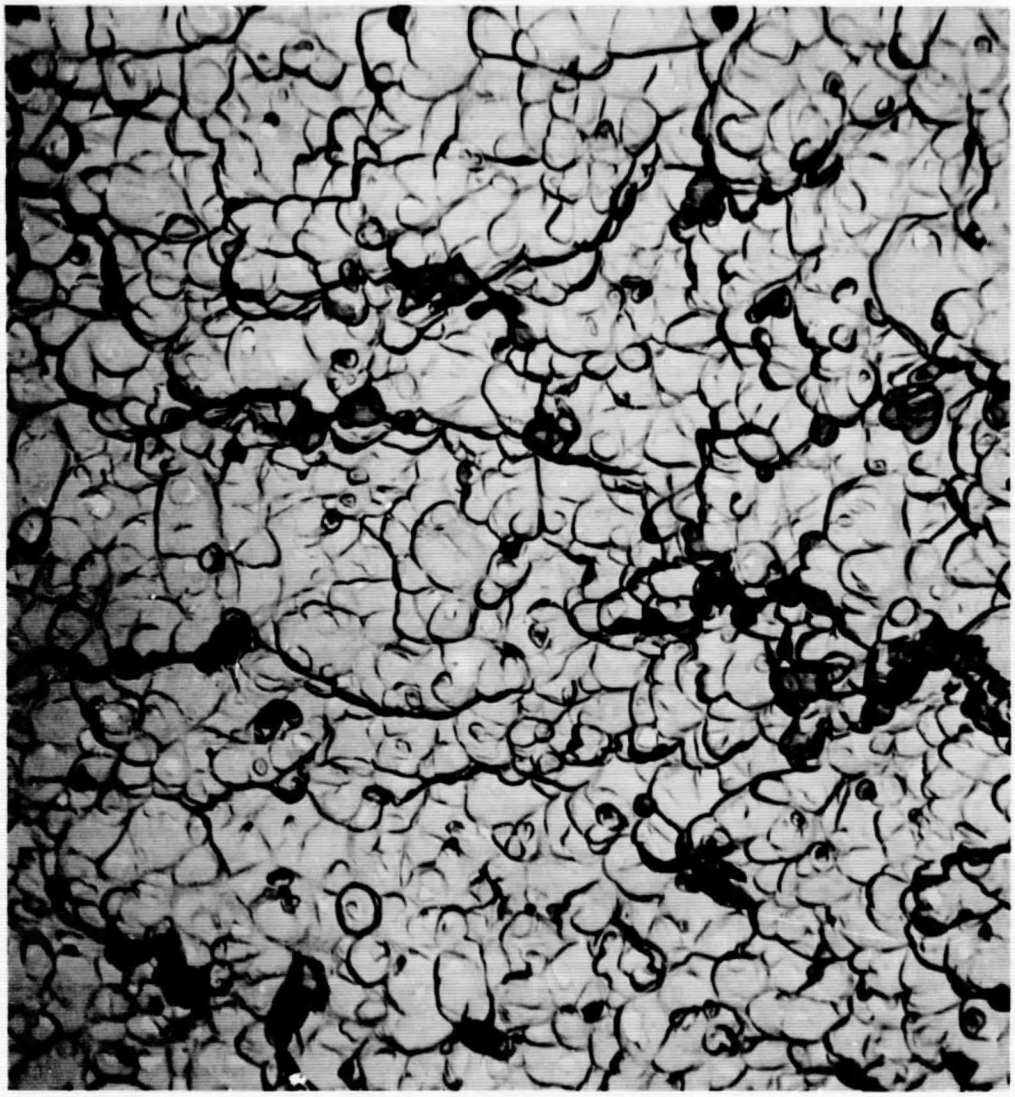

Oxide Replica 20,000X

Typical tensile fracture in 7075-T6
showing small particles associated with dimples.

Figure 38

Oxide Replica 20,000X

Parallel markings on stress corrosion fracture which might be indicative of plastic deformation. 2219-T37 with S.T. stress of 75% YS.

Figure 39

Double Oxide Replica 20,000X

Spade-like tendril of stress corrosion crack which juts out from main stress corrosion crack which is out of view to the right. Specimen surface is above this area and parallel to top edge of photograph. The tip of this stress corrosion tendril is dark because the replicating oxide broke leaving a double thickness at the tip. The stress corrosion tendril is surrounded by tensile fracture both above and below. 2219-T37 with S.T. stress of 75% YS.

Figure 40

173/5/3

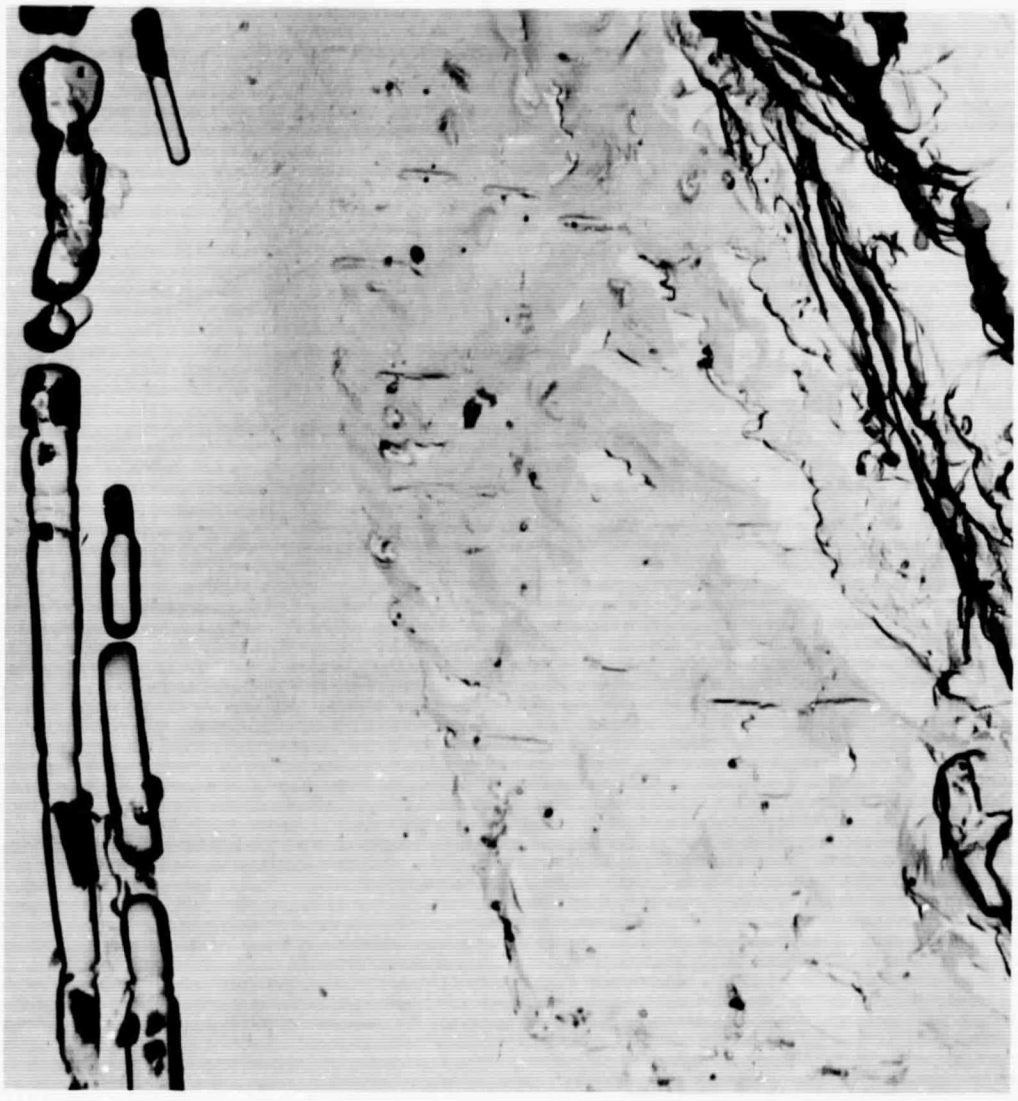

Double Oxide Replica 10,000X

A very shallow stress corrosion crack which avoided constituent stringers on surface. Uncracked islands are seen in the stress corrosion fracture and a long tendril of stress corrosion crack is seen coming from the top of photograph, paralleling the tensile fracture at right. 2219-T37 with 60% YS short transverse stress.

Figure 41

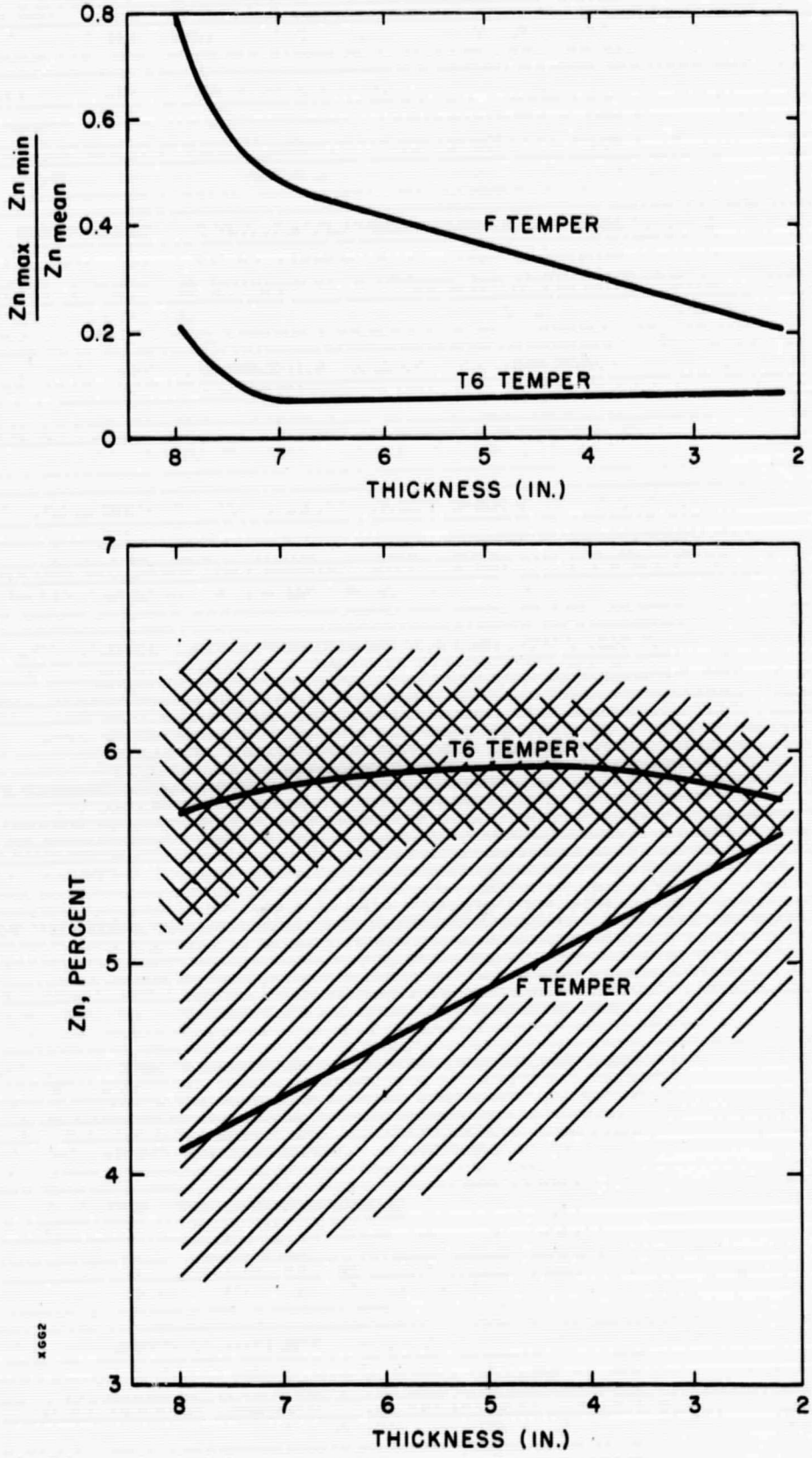

HOMOGENIZATION OF ZINC DURING ROLLING OF 7075 INGOT

FIGURE 42

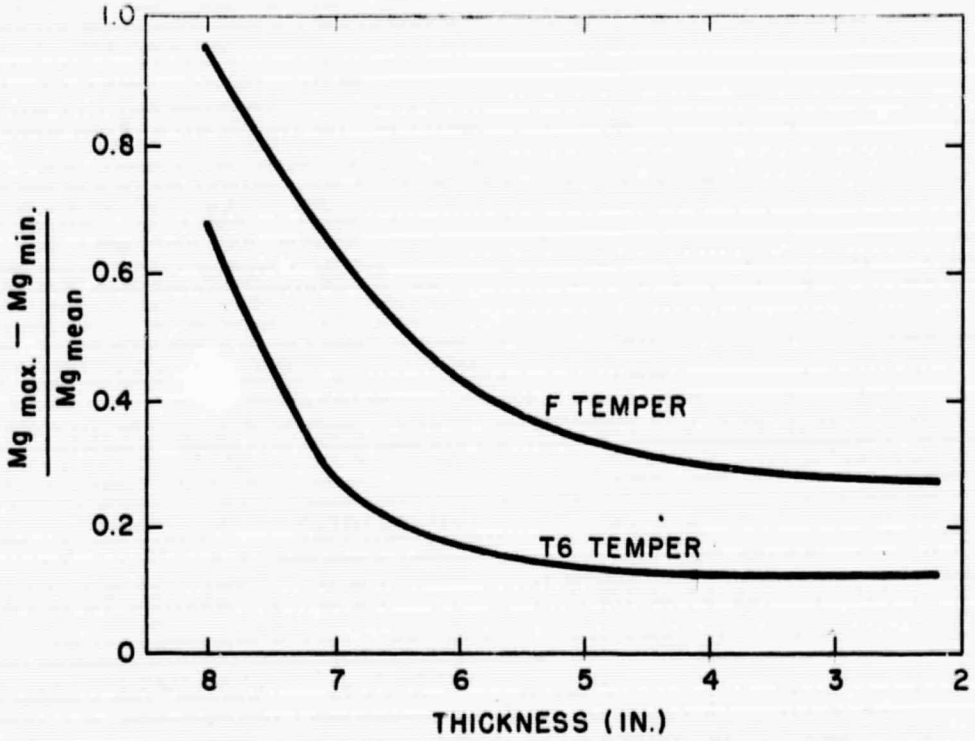

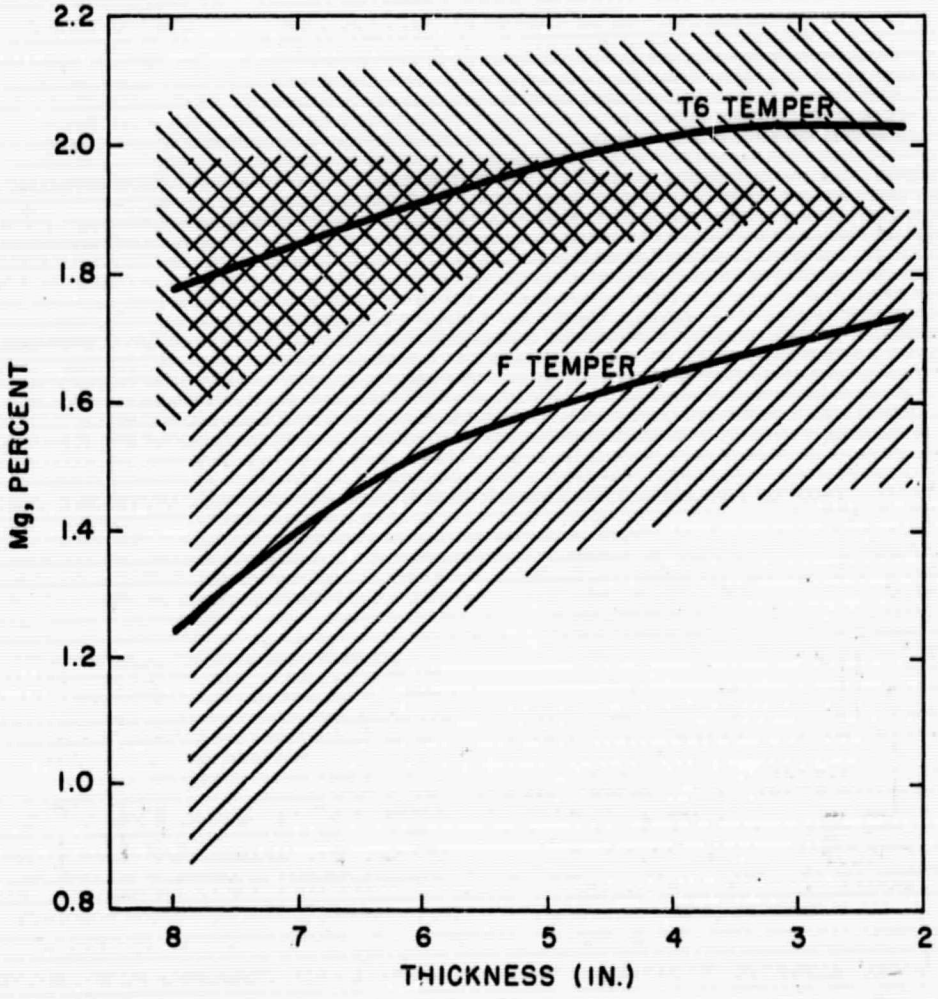

X664

HOMOGENIZATION OF MAGNESIUM DURING ROLLING OF 7075 INGOT

FIGURE 43

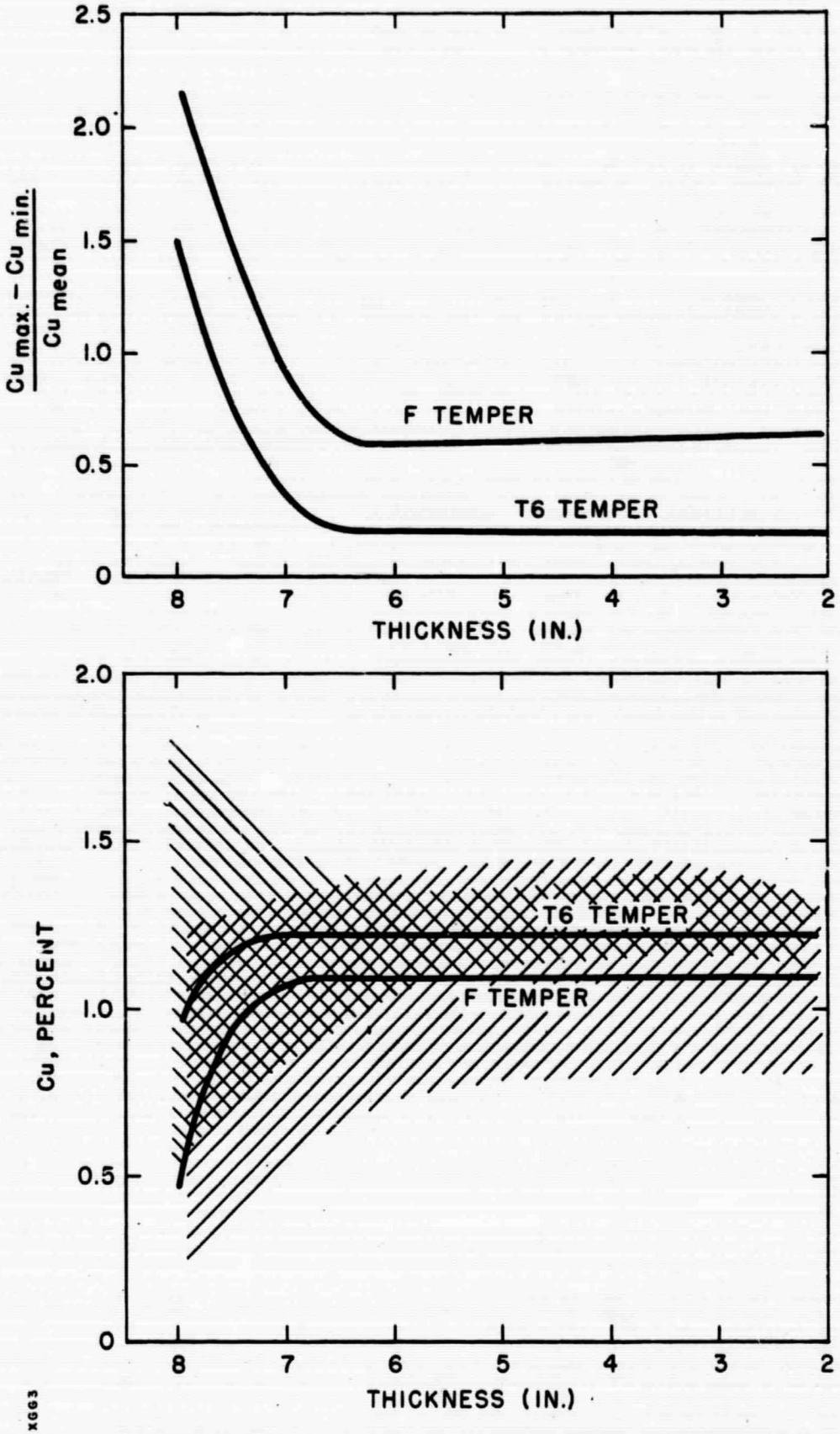

HOMOGENIZATION OF COPPER DURING ROLLING OF 7075 INGOT

FIGURE 44

163581-86

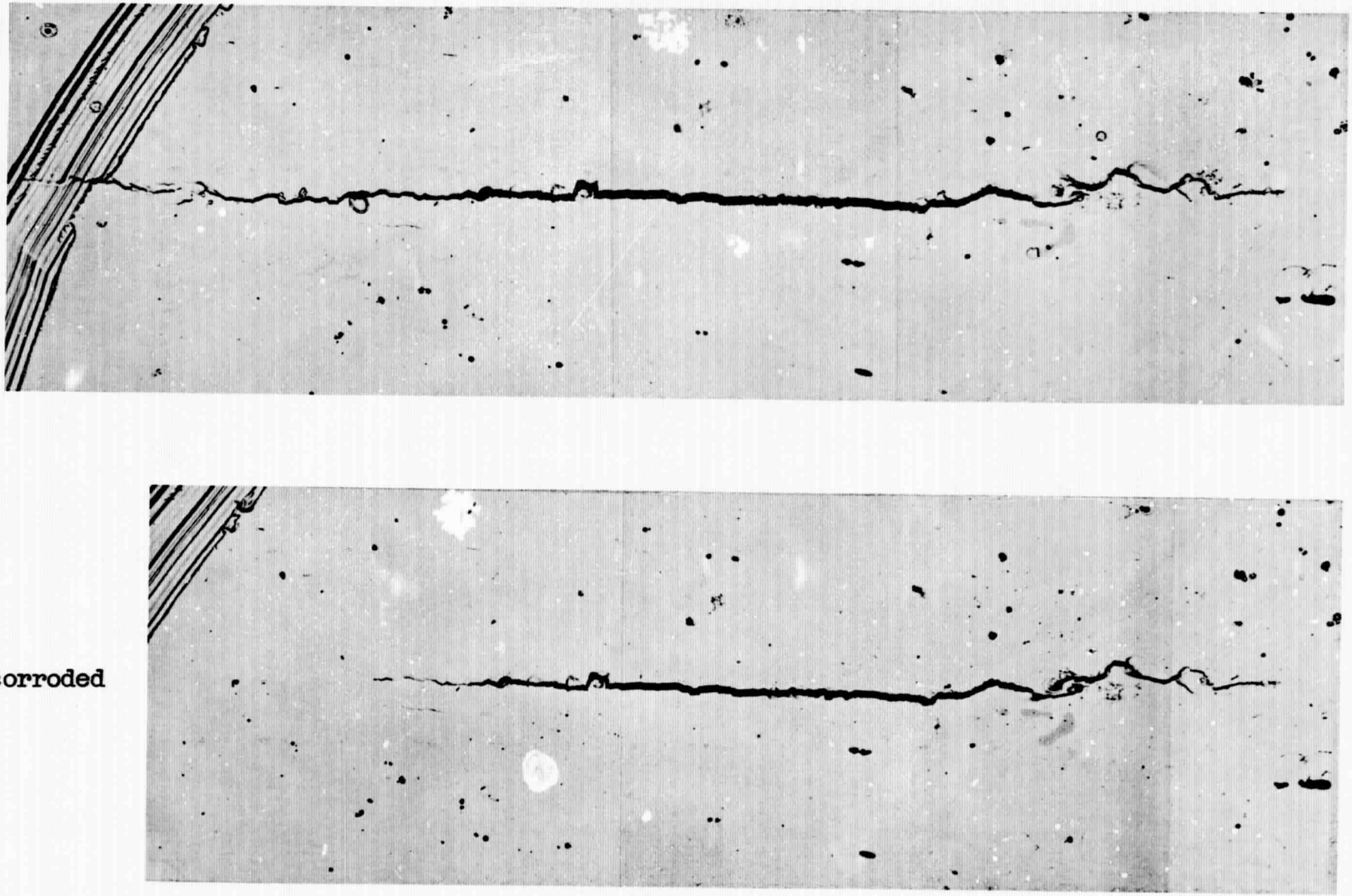

Extension of large crack after stress-corrosion exposure and rinsing. (X500)

Figure 45

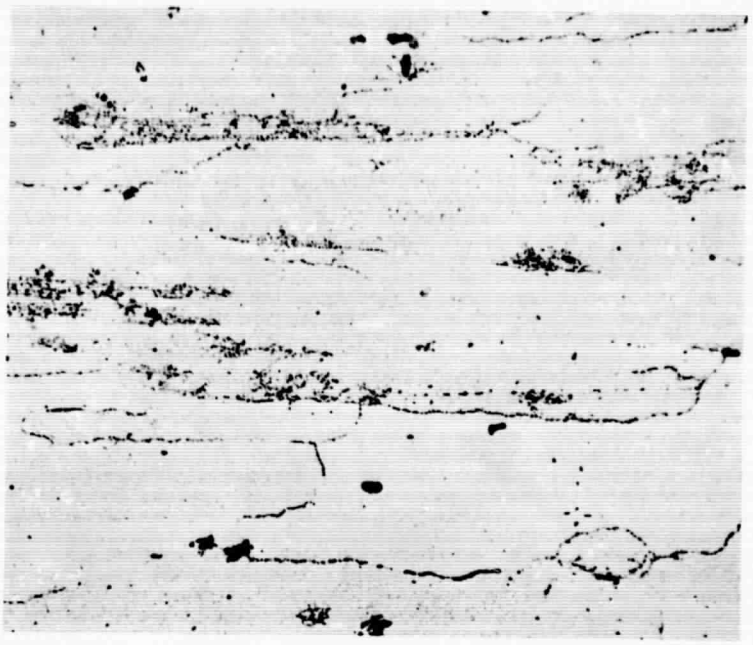

As-corroded

Stress

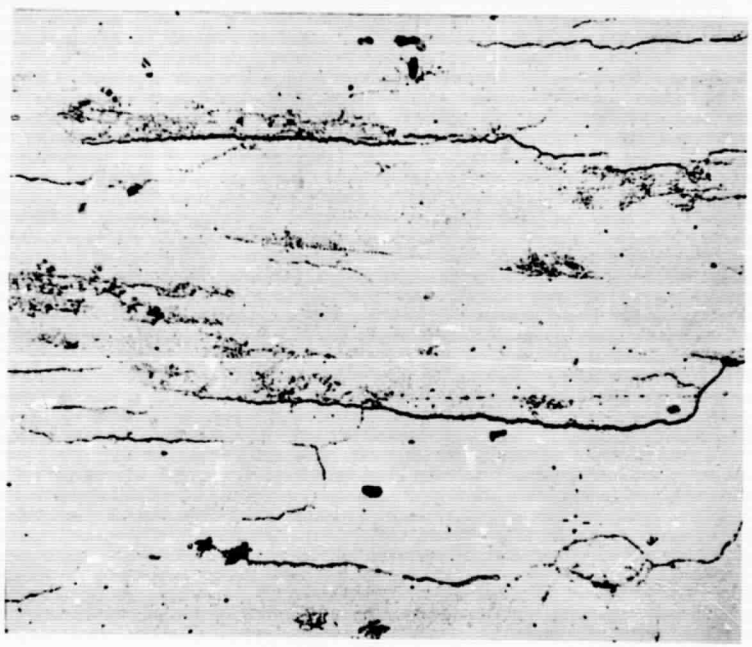

Stressed

Widening of corrosion crevices in 7075-T6 corroded and then stressed short transversely to 90% YS. (X500)

Figure 46

As-corroded

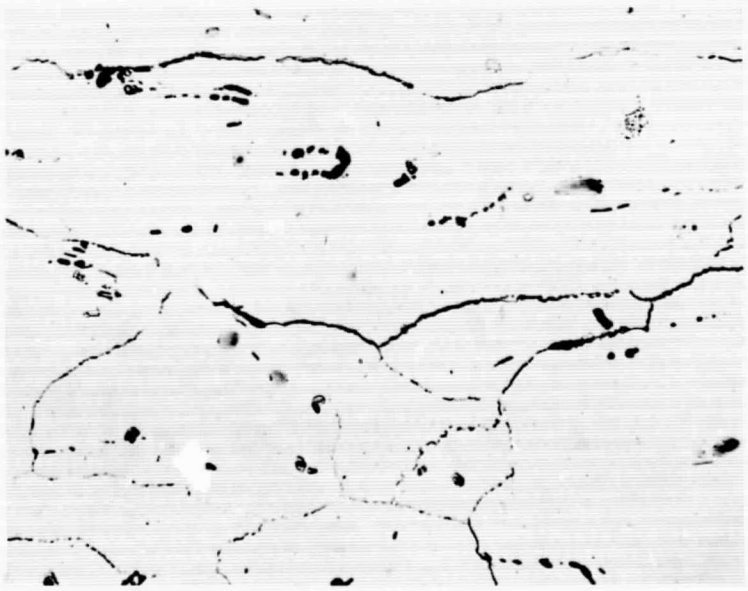

Stress

Stressed

Widening of corrosion crevices in 2219-T37 corroded and then stressed short transversely to 90% YS. (X500)

Figure 47

163577
163578

Area A

Area B

164855
164857
164859
164861

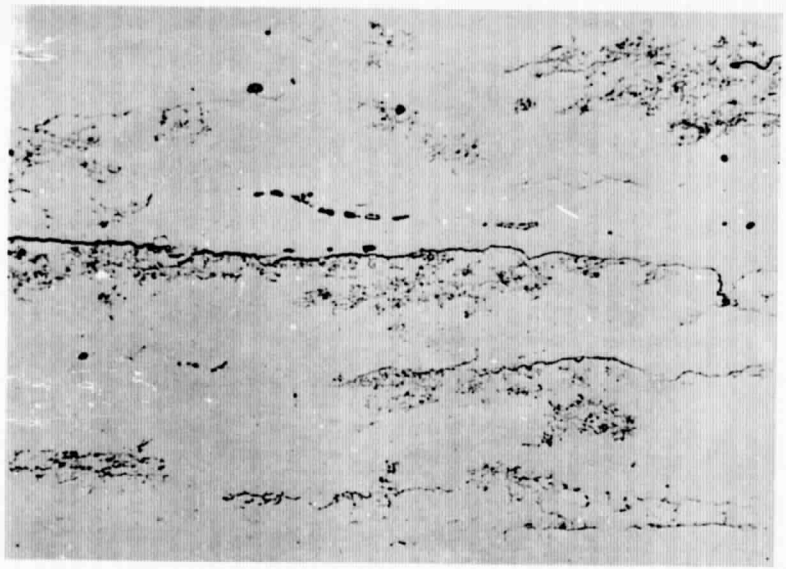

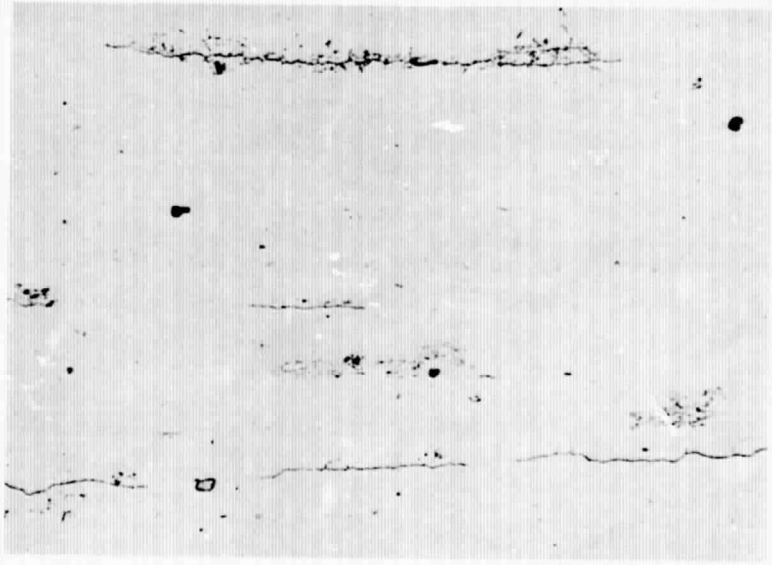

Corroded 20 min., then stress S.T. to 75%

STRESS

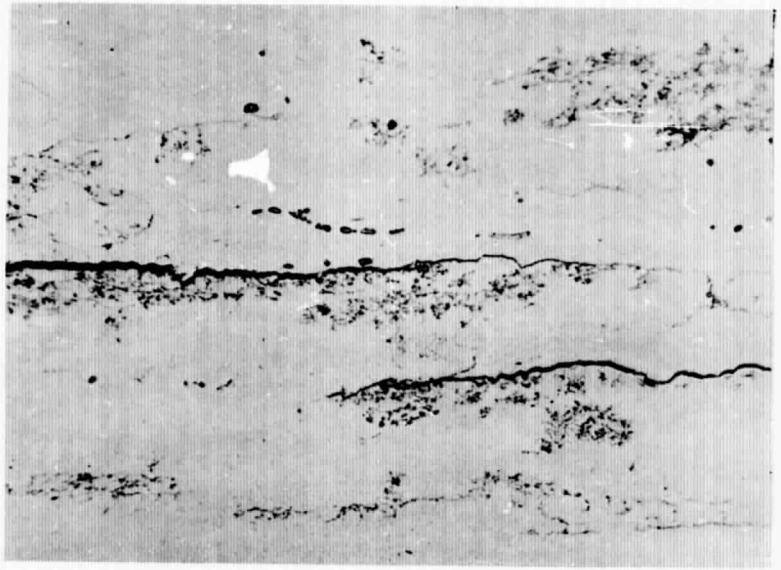

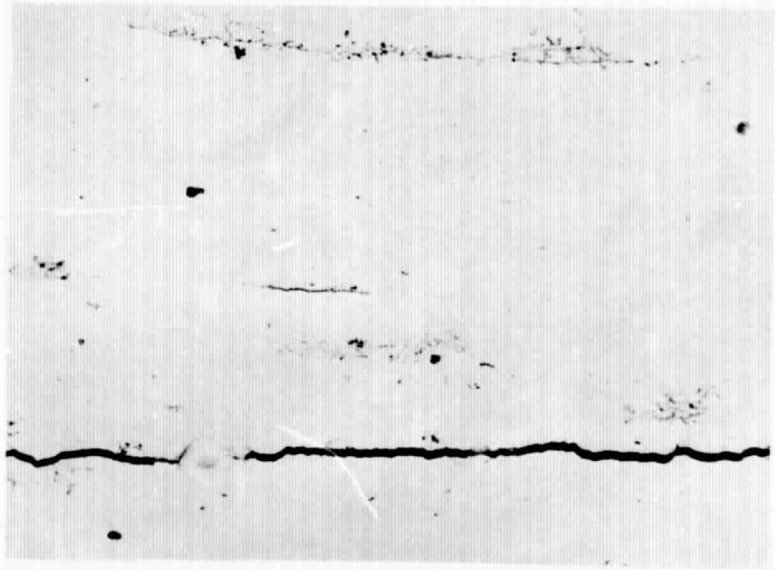

Above after additional 15 min. exposure

Stress corrosion crack initiation in pre-corroded specimen of 7075-T6. (X500)

Figure 48

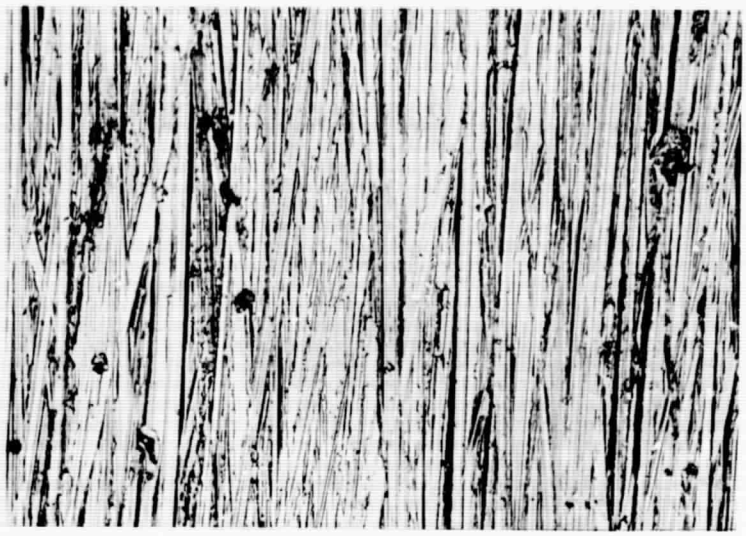

Not corroded

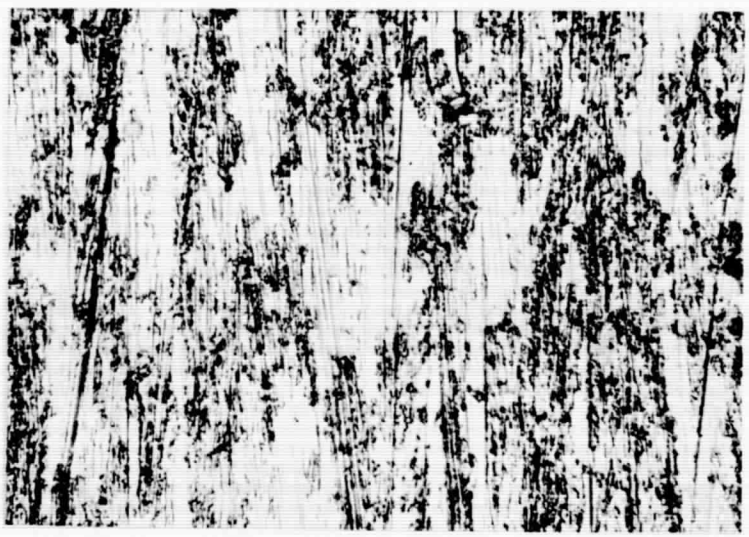

10 min.

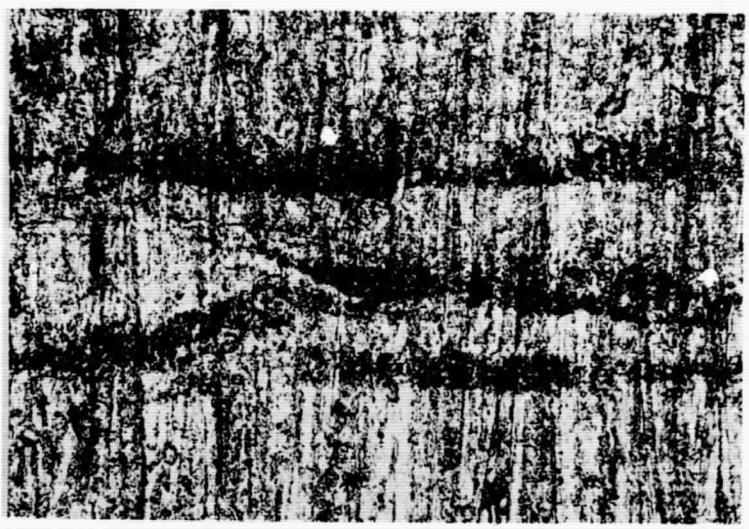

60 min.

164056-58

Progress of corrosion of unstressed 7075-T6 with 3-0 metallographic paper finish. (X500)

Figure 49

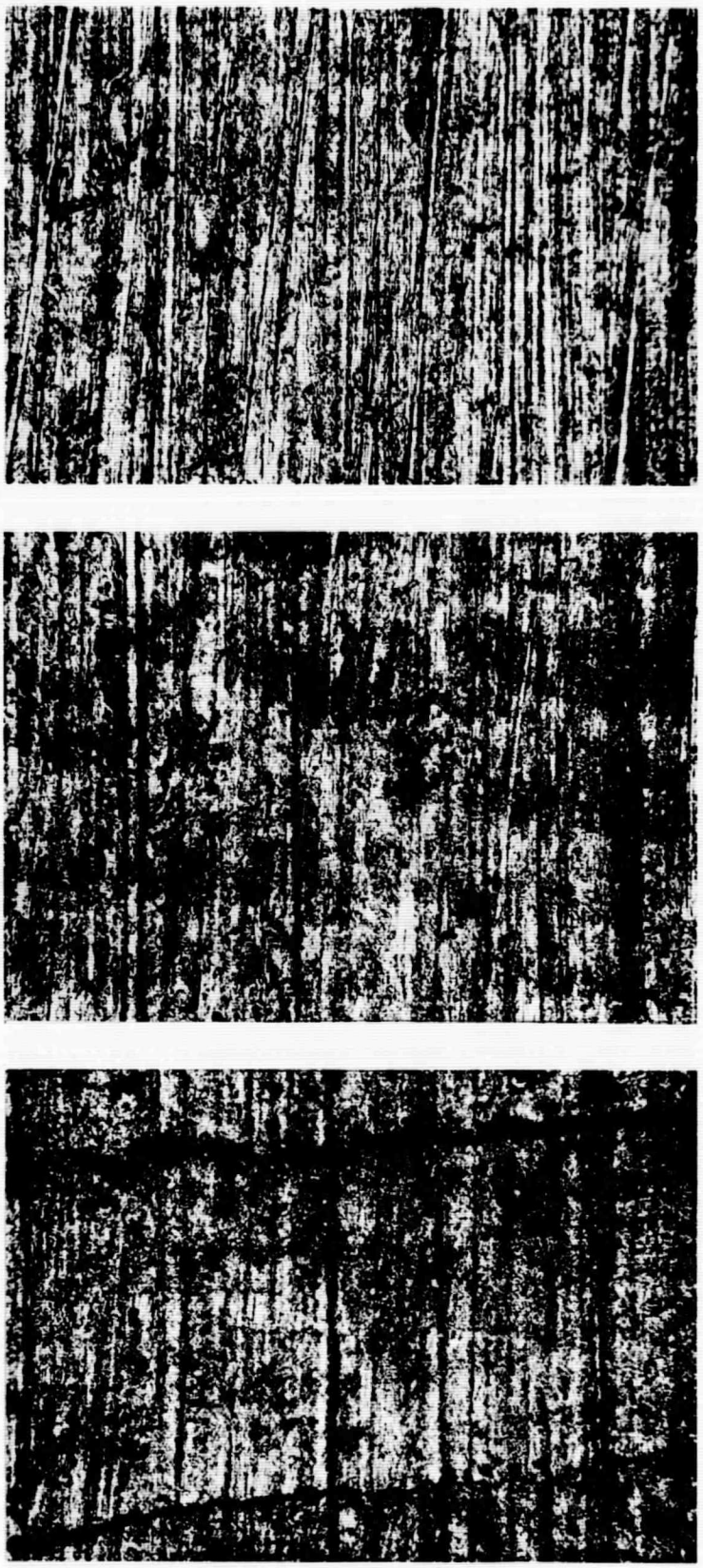

164321
164322
164361

Crack development in 7075-T6 given 3-0 metallographic paper finish, stressed to 75% YS short transversely and exposed to pH1 solution. Abrasion marks in short transverse direction.

(X500)

Figure 50

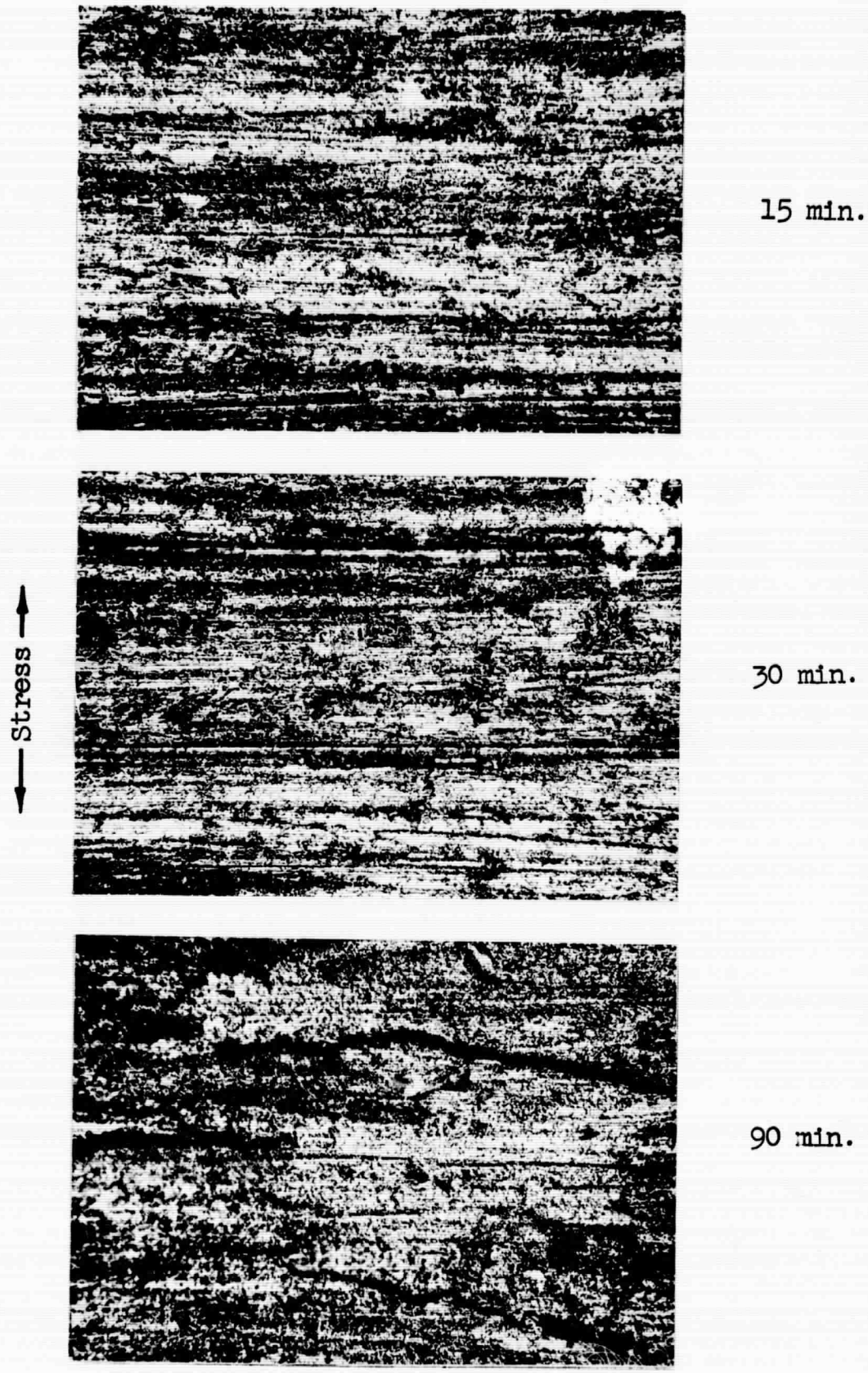

Same as Fig. 50 but abrasion marks longitudinal. (X500)

Figure 51

Cross section of crack seen in Fig. 51 (X500)

Figure 52

164075-77

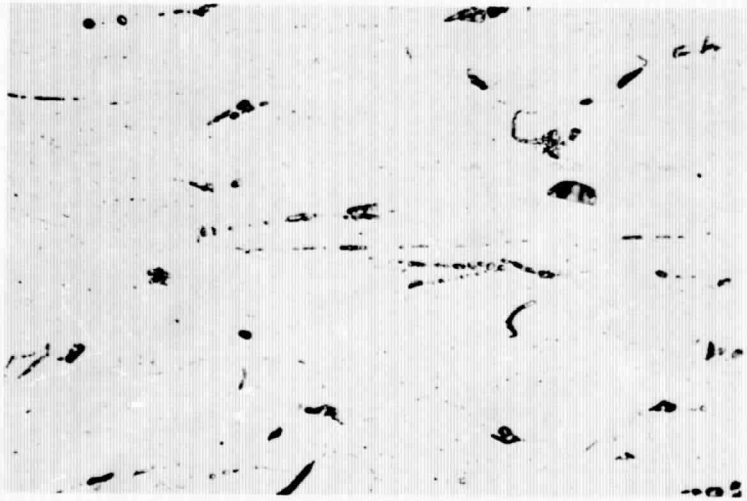

As-coated

← Stress →

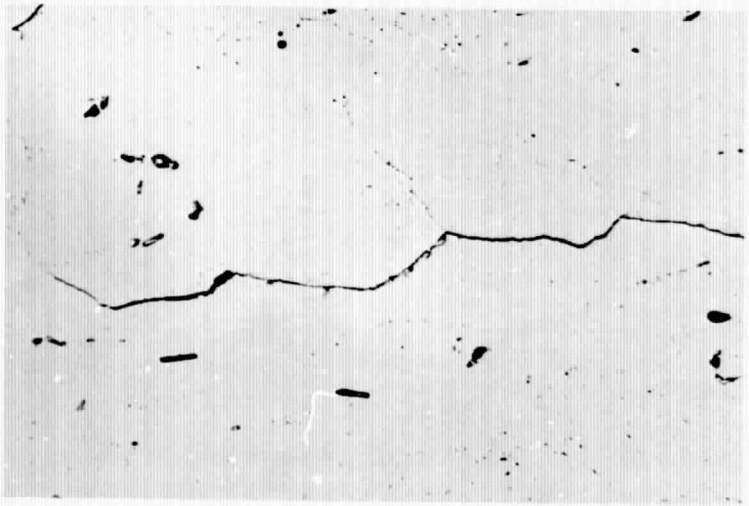

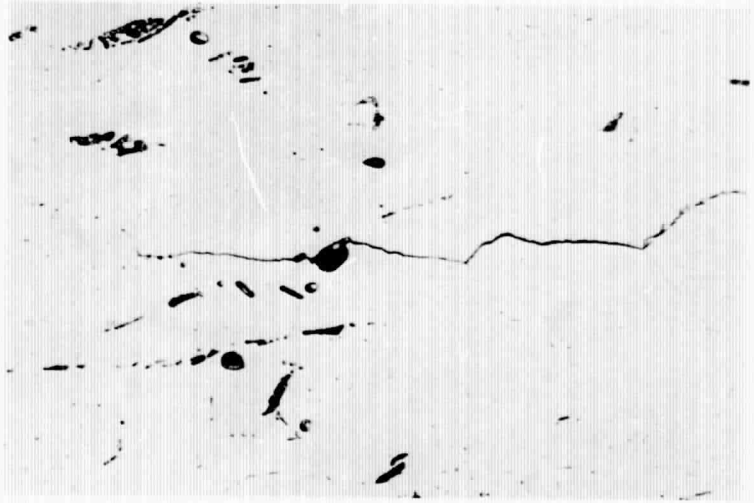

Exposed
10 minutes

Crack initiation in 2219-T37 given 18V barrier oxide coating and stressed short transversely to 75% YS. (X500)

Figure 53

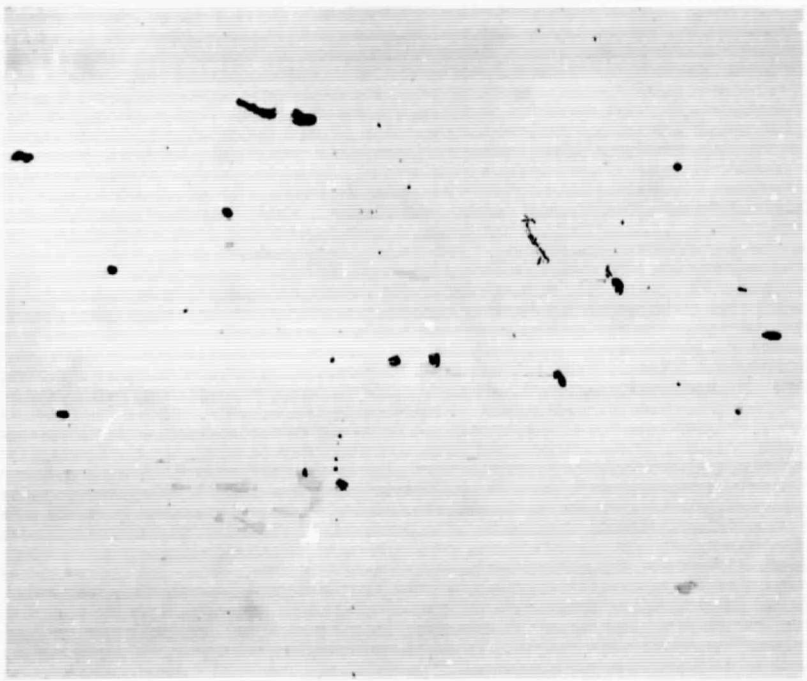

As formed

Stress

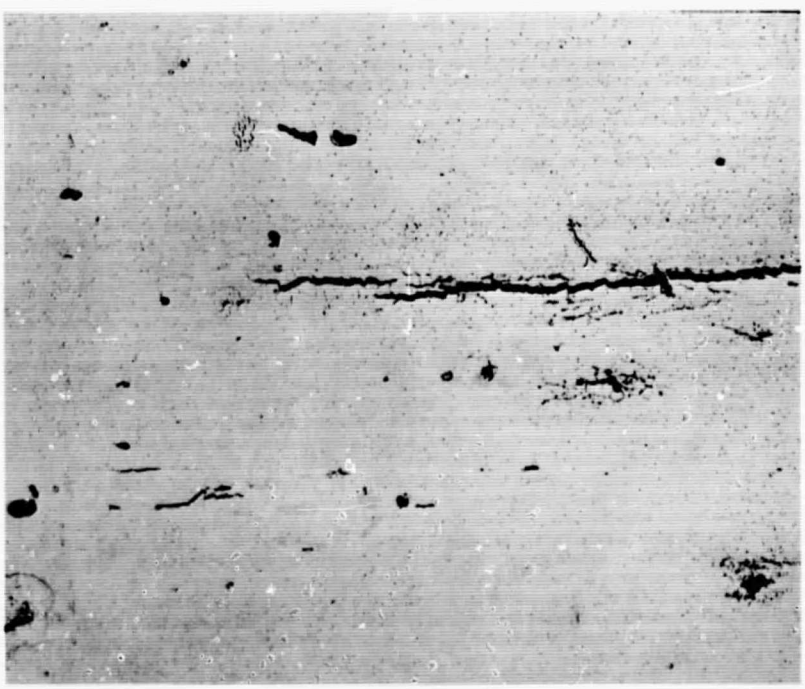

Exposed
10 minutes

Crack initiation in 7075-T6 given 6-volt barrier oxide film and stressed 75% YS short transversely. (X500)

Figure 54

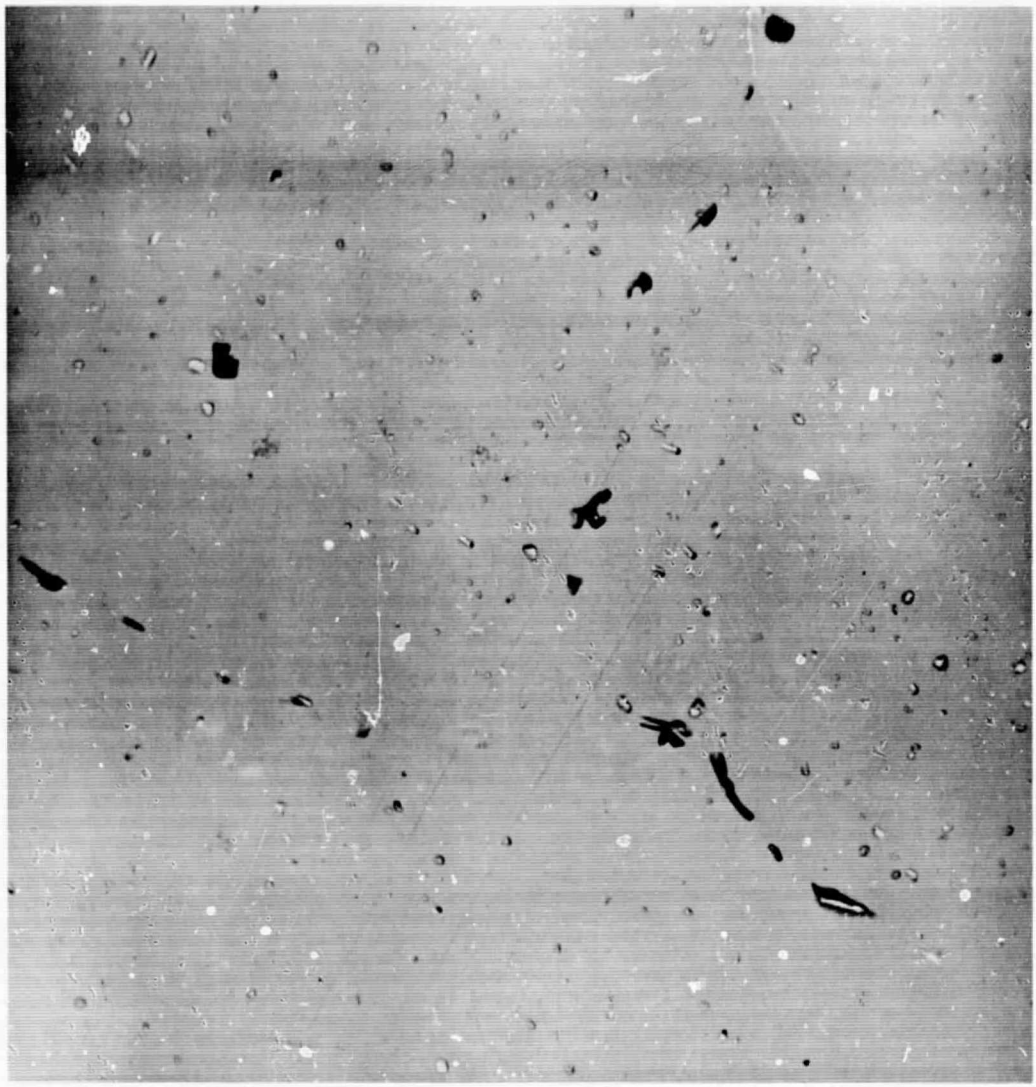

Oxide Transmission 10,000X

Oxidation of dispersoids and boundary precipitates in 7075-T6 given 18V barrier film.

Figure 55

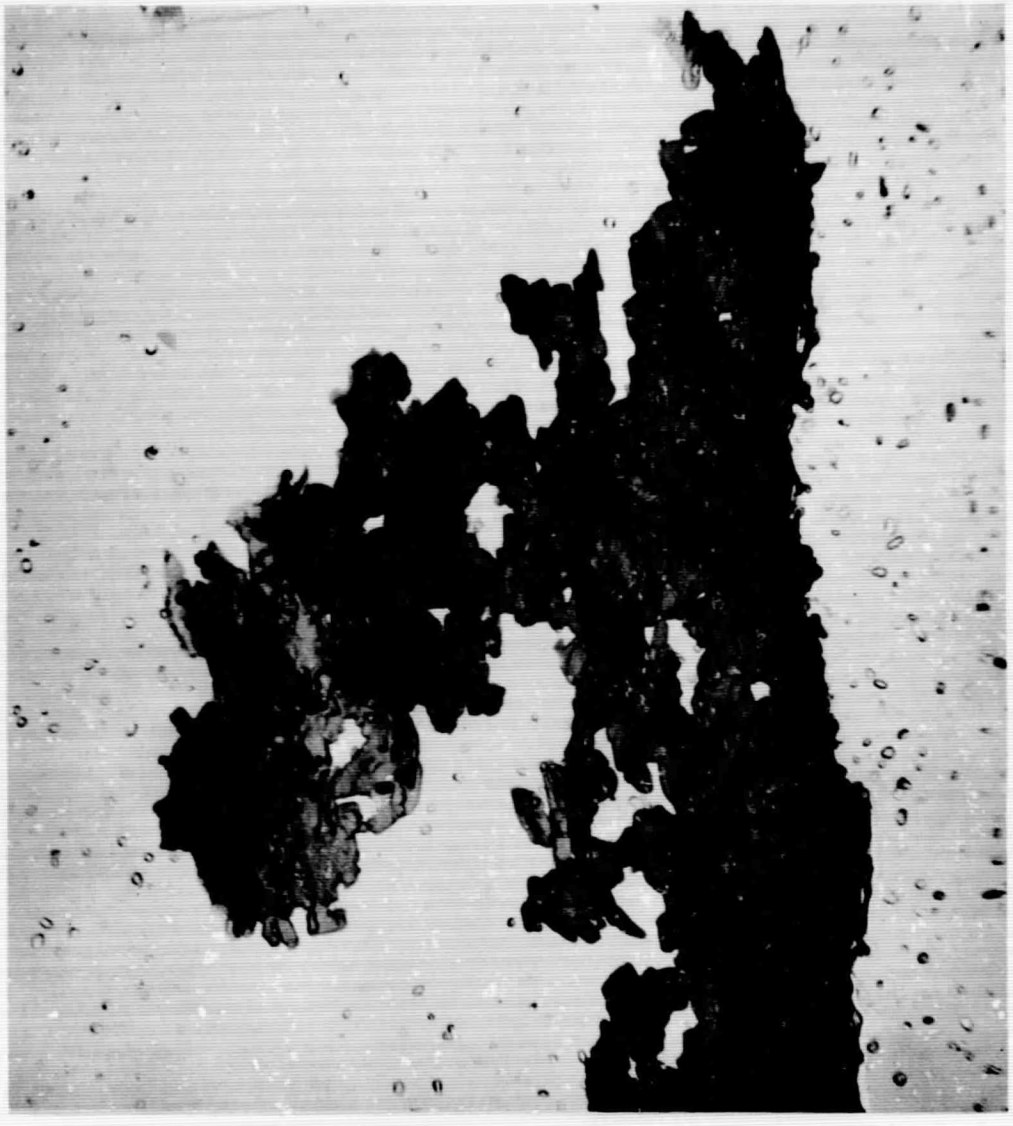

Dual-Oxide Replica 7075-T6 10,000X

Stress-corrosion crack extending from vertical boundary at right. Portions formed during the second immersion are lighter colored.

Figure 57

179/5/2

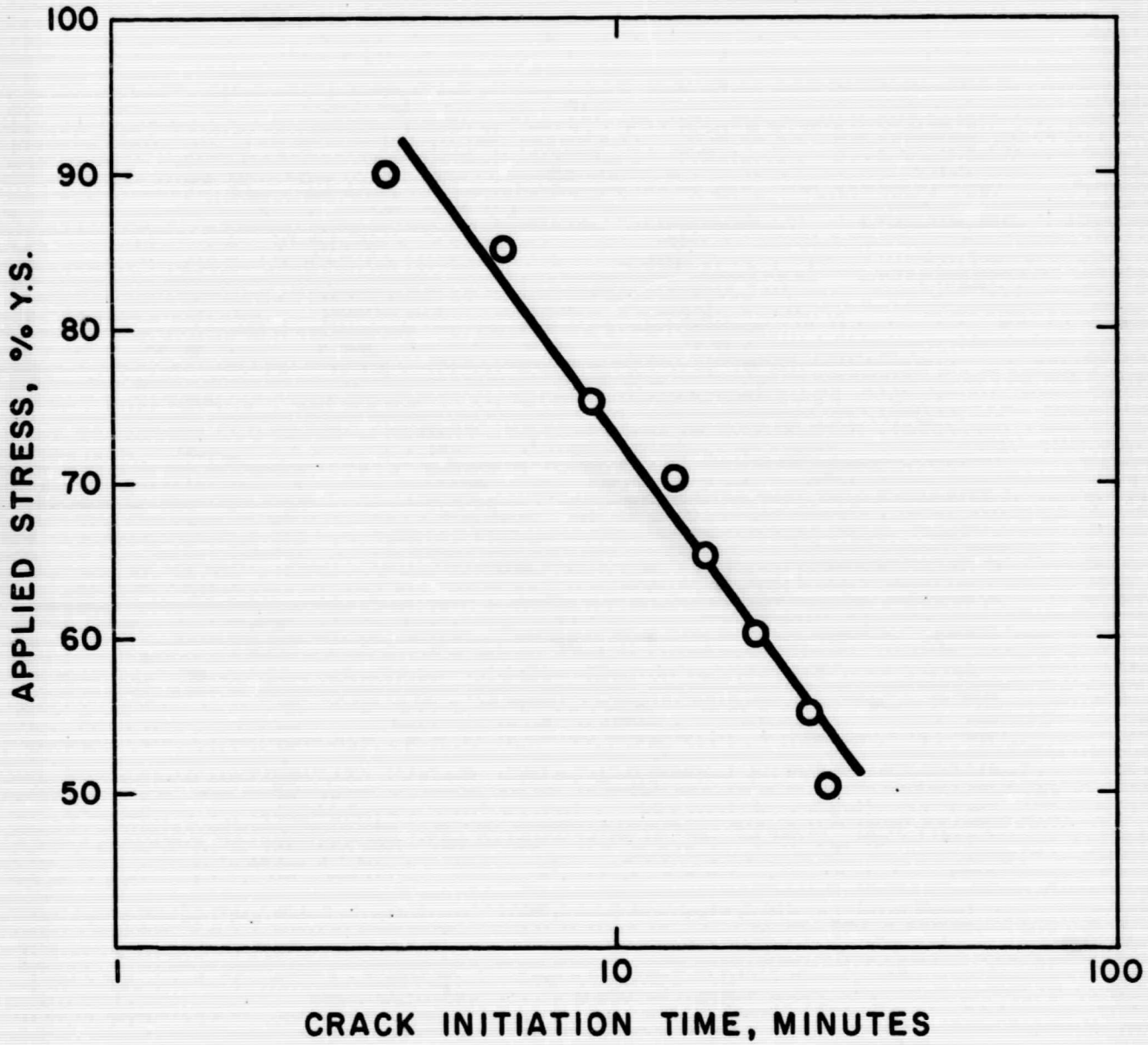

RELATION BETWEEN APPLIED STRESS AND CRACK INITIATION TIME

FIGURE 58

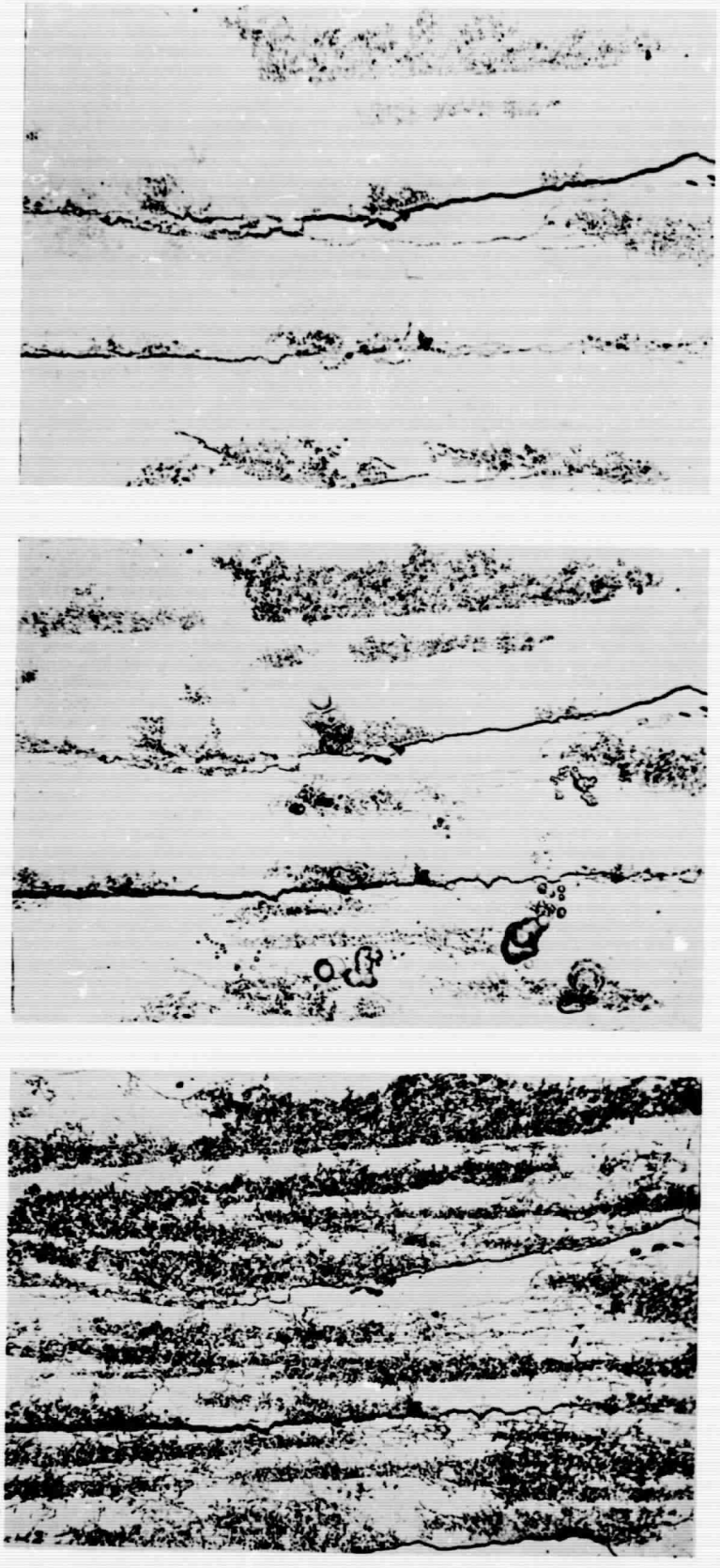

Crack development in 7075-T6 stressed short transversely to 20% YS. (X500)

164301
164307
164313

Figure 59

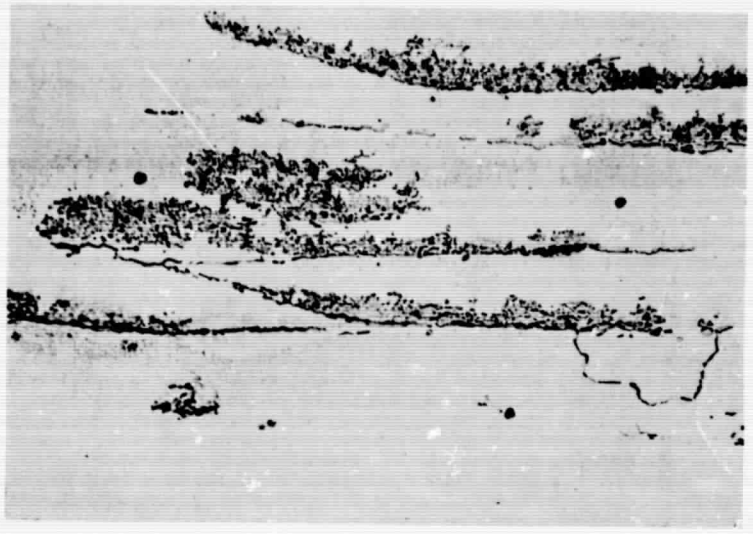

15 min.

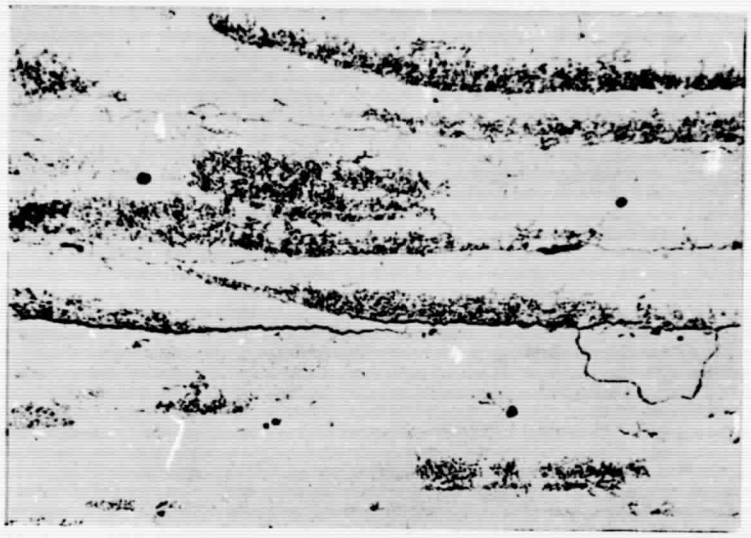

← STRESS →

60 min.

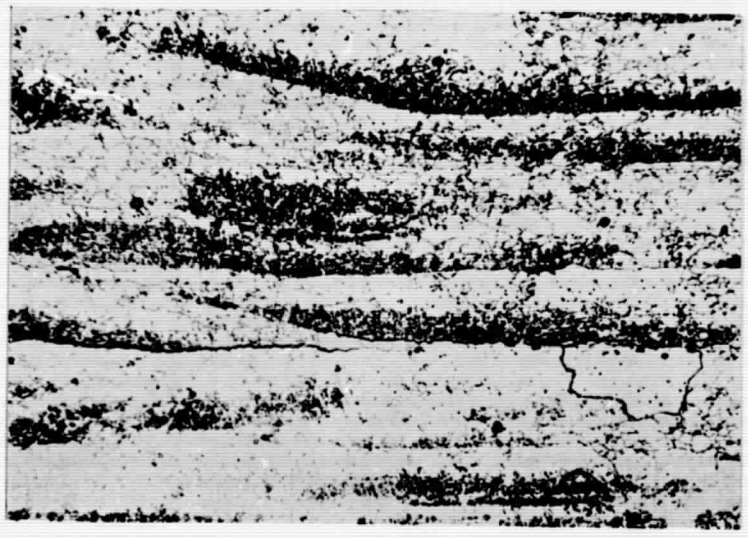

120 min.

1642B7
164291
164297

Crack development in 7075-T6 stressed short transversely to 15% YS. (X500)

Figure 60

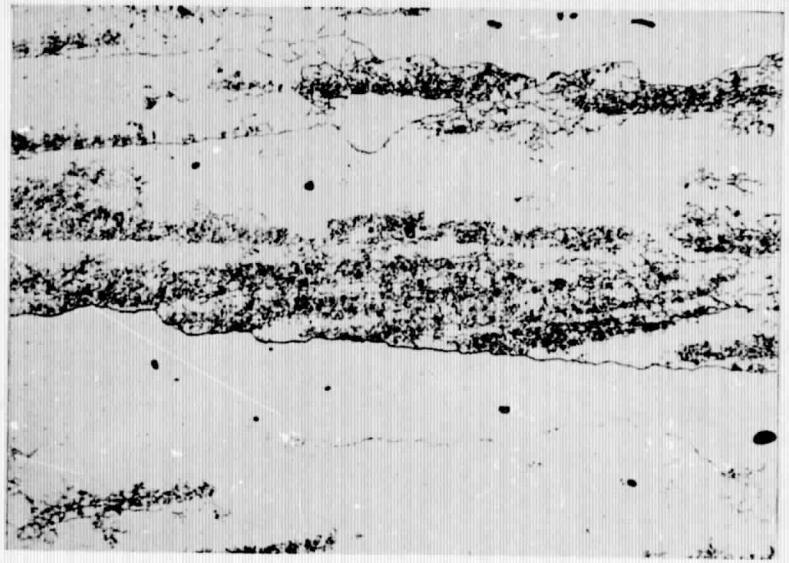

30 min.

STRESS

60 min.

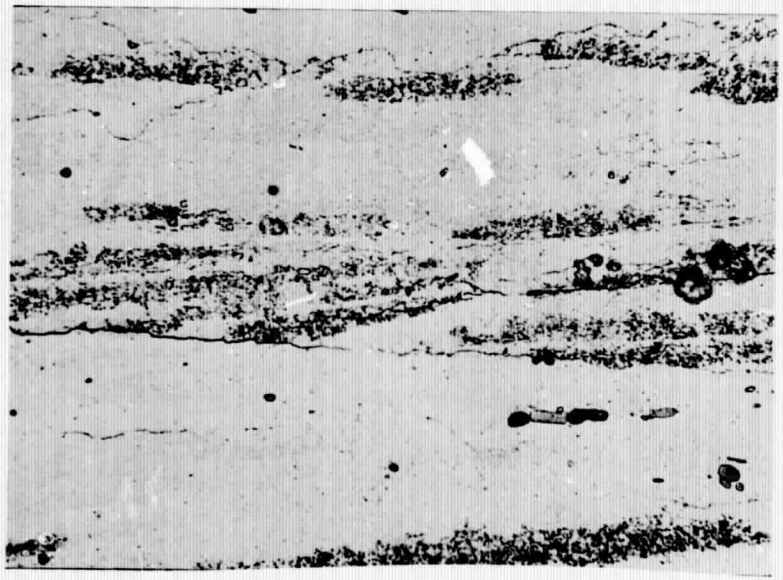

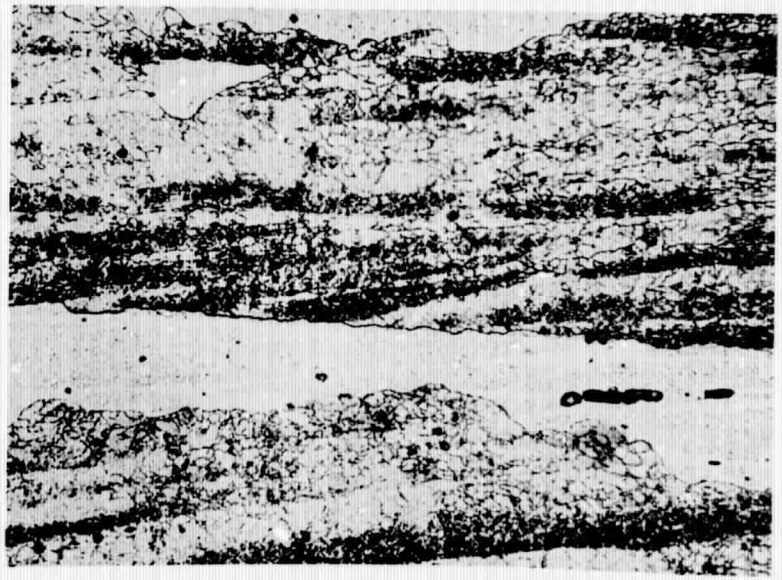

120 min.

Crack development in 7075-T6 stressed short transversely to 10% YS. (X500)

Figure 61

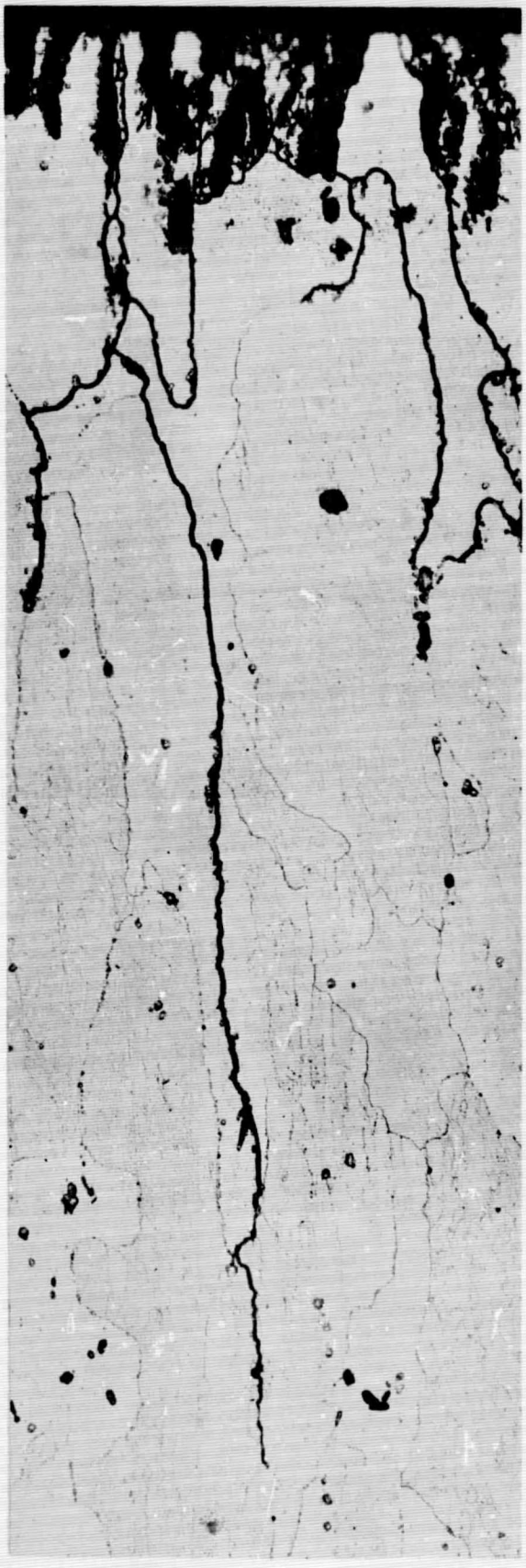

STRESS

Crack development in 7075-T6
stressed short transversely to 20% YS
(X500). Surface appearance in Fig. 59.

Figure 62

164888-92

Crack development in 7075-T6 stressed short transversely to 15% YS (X500). Surface appearance in Fig. 60.

Figure 63

16895-7

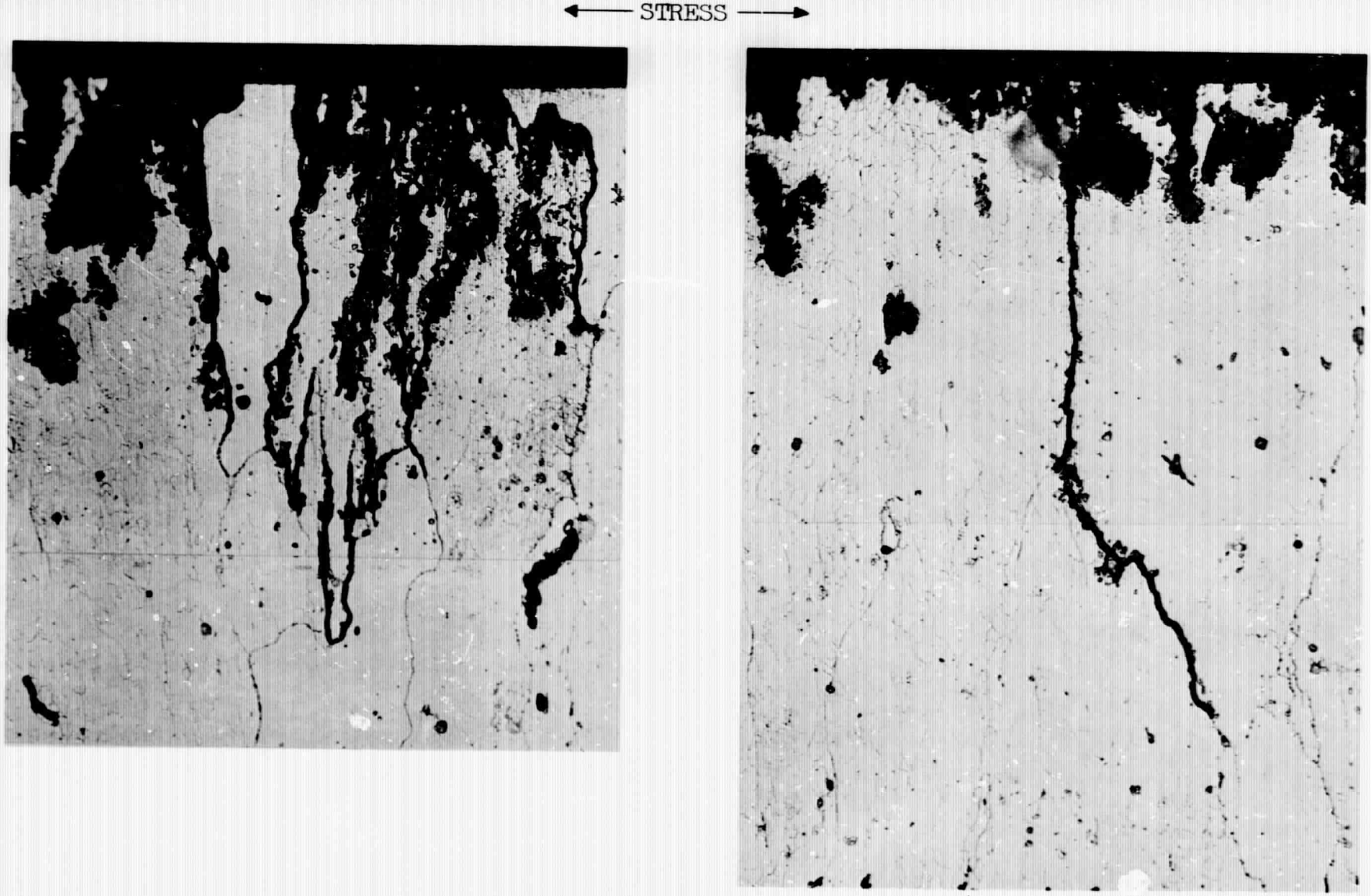

Crack development in 7075-T6 stressed short transversely to 10% YS (X500).
Surface appearance in Figure 61.

Figure 64

168273
168274
168275
168276

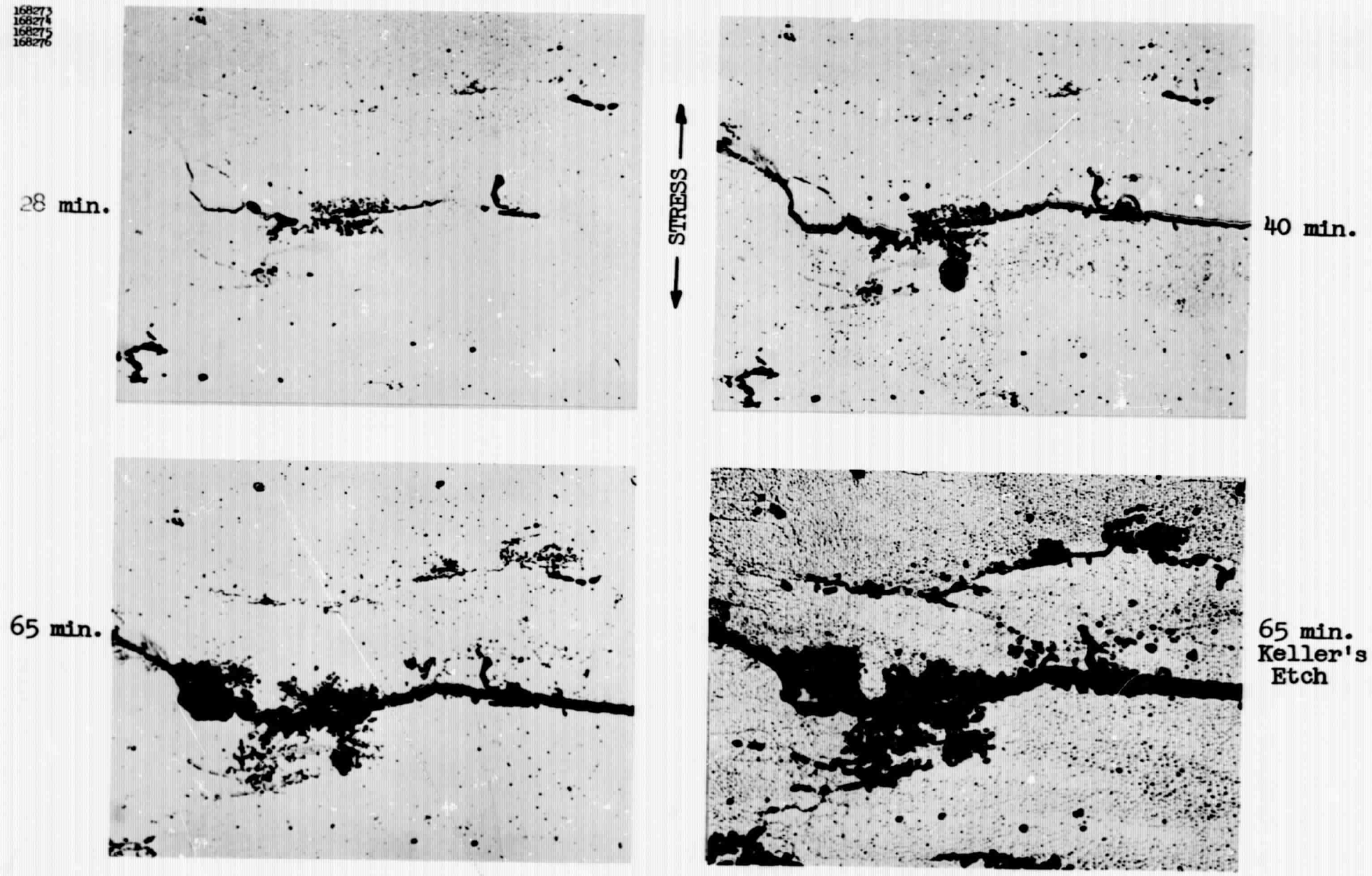

Crack initiation in 7079-T6 plate stressed short transversely to 90% YS and exposed to pH1 NaCl-$AlCl_3$ solution (X500).

Figure 65

Cross section of sample in Fig. 65 showing crack development (X500).

Figure 66

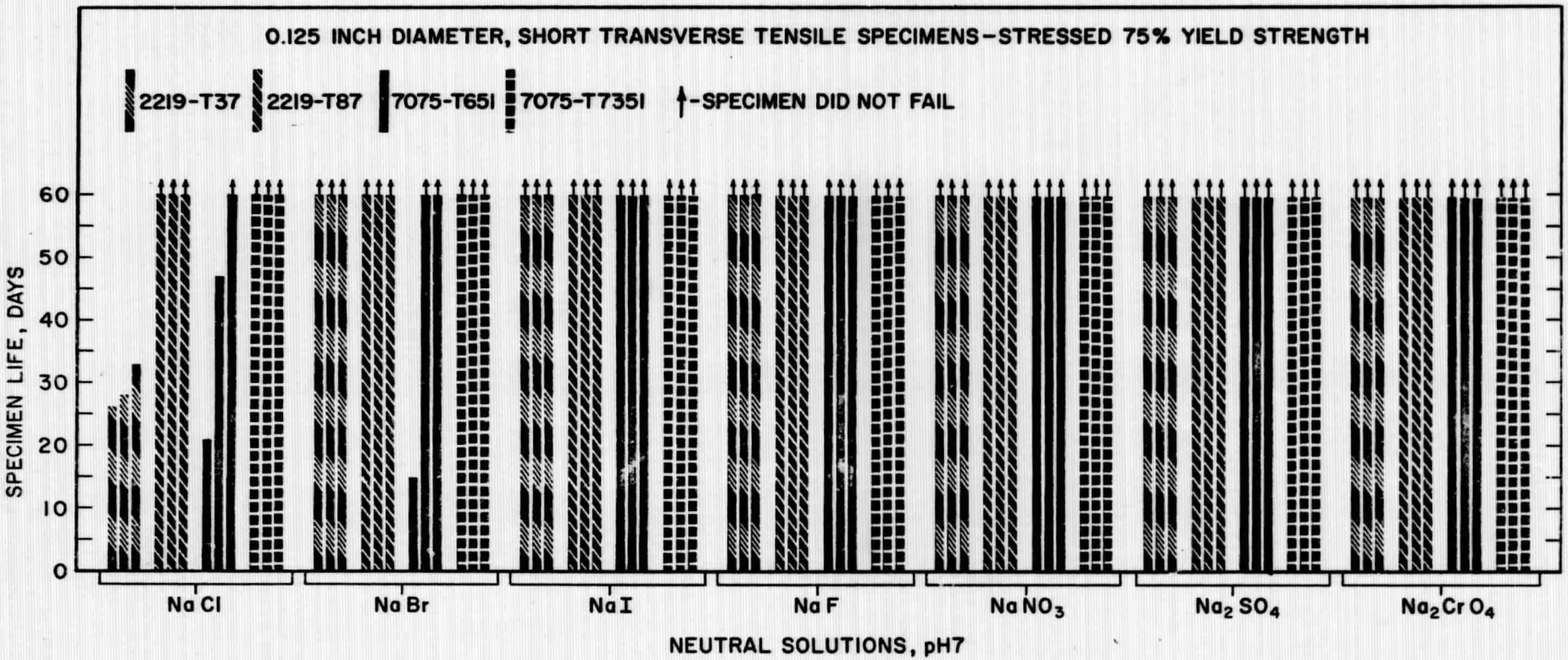

EFFECT OF ENVIRONMENT ON RESISTANCE TO STRESS–CORROSION CRACKING

FIGURE 67

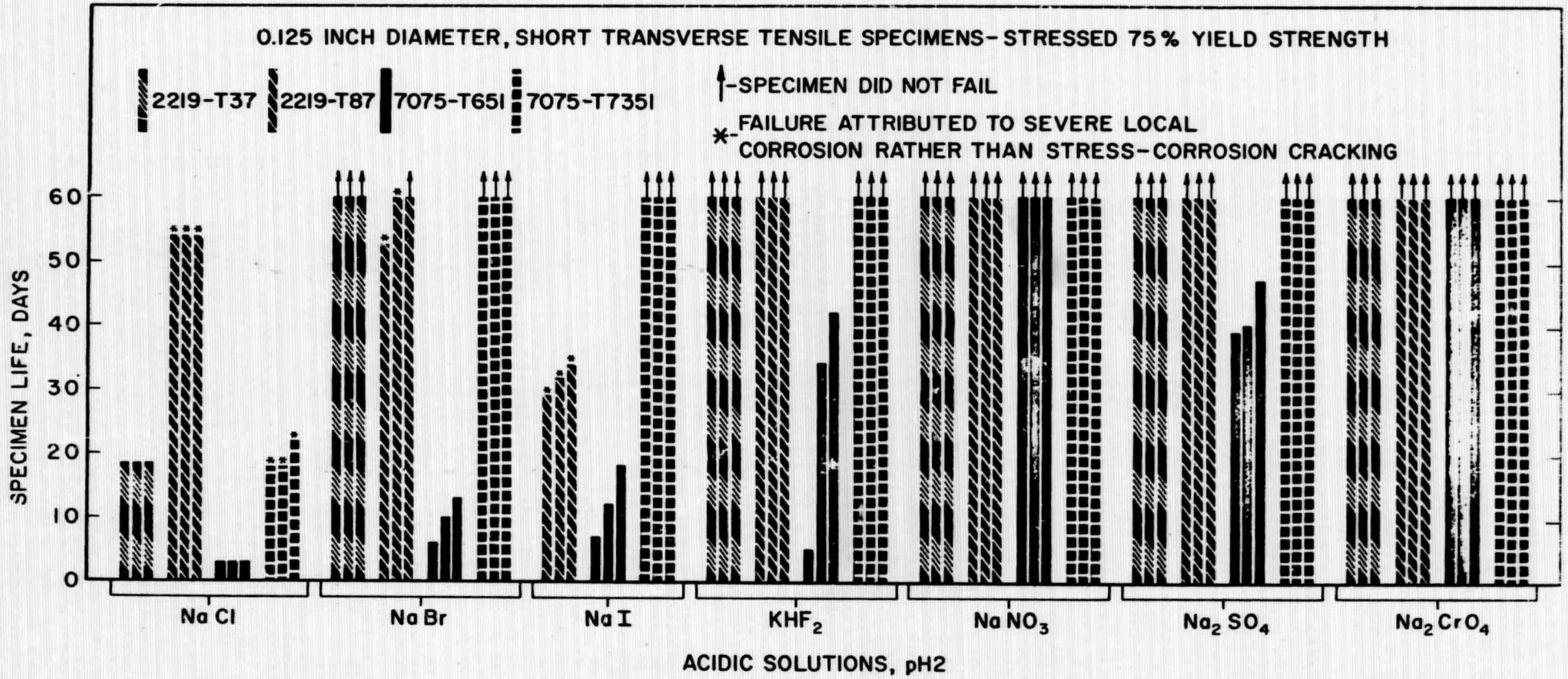

EFFECT OF ENVIRONMENT ON RESISTANCE TO STRESS-CORROSION CRACKING

FIGURE 68

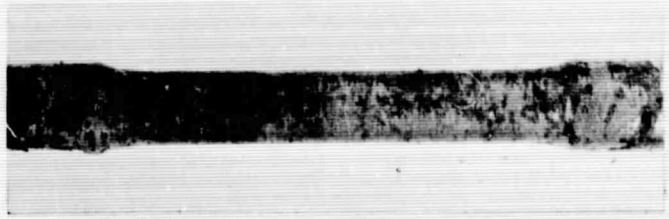

0.5N NaCl + 0.5N Na_2SO_4
(H_2SO_4)

Visual Rating - Negligible
Exposure Period - 4 days
Percent Loss in T.S. - 55

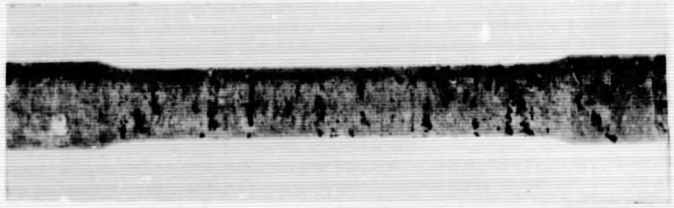

1N NaCl (HNO_3)

Visual Rating - Mild, directional
Exposure Period - 7 days
Percent Loss in T.S. - 49

1N NaCl + 1N $AlCl_3$
(HCl)

Visual Rating - Severe, directional
Exposure Period - 10 days
Percent Loss in T.S. - 82

4N NaCl + 0.5N KNO_3
(HNO_3)

Visual Rating - Severe, random
Exposure Period - 19 days
Percent Loss in T.S. - 68

Illustrates the varied corrosion patterns of 7075-T7351 alloy in acidified solutions containing sodium chloride. The specimens shown were exposed unstressed, and were removed from test at times corresponding to the failure of stressed specimens.

(Mag. 3X)

Figure 69

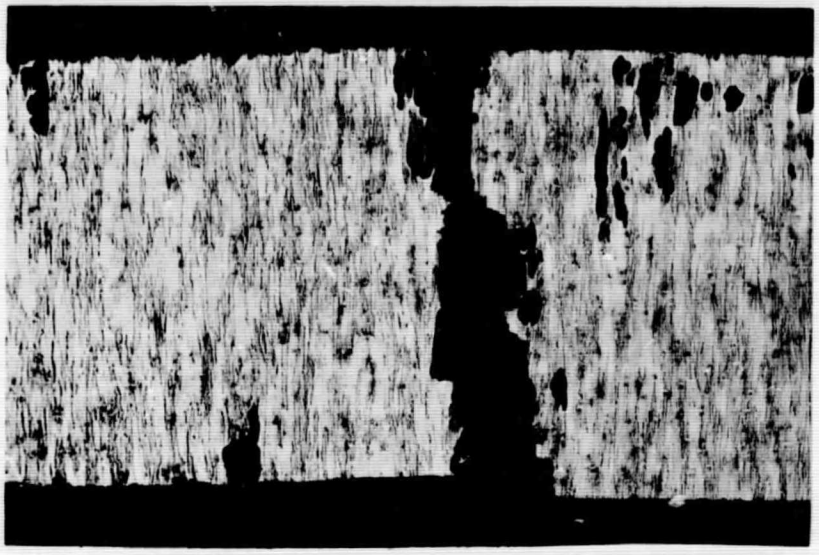

Etch: Keller's Mag. 20X

Stressed 75% Y.S. - Failed 4 days

Etch: Keller's Mag. 100X
Unstressed - 4 days

Etch: Keller's Mag. 100X
Stressed 75% Y.S. - F 4 days

7075-T7351 exposed to 0.5N NaCl + 0.5N Na_2SO_4 pH2 (H_2SO_4). Sections through corrosion pits in specimens which visually showed negligible attack.

164-580
164-581
164-594

Figure 70

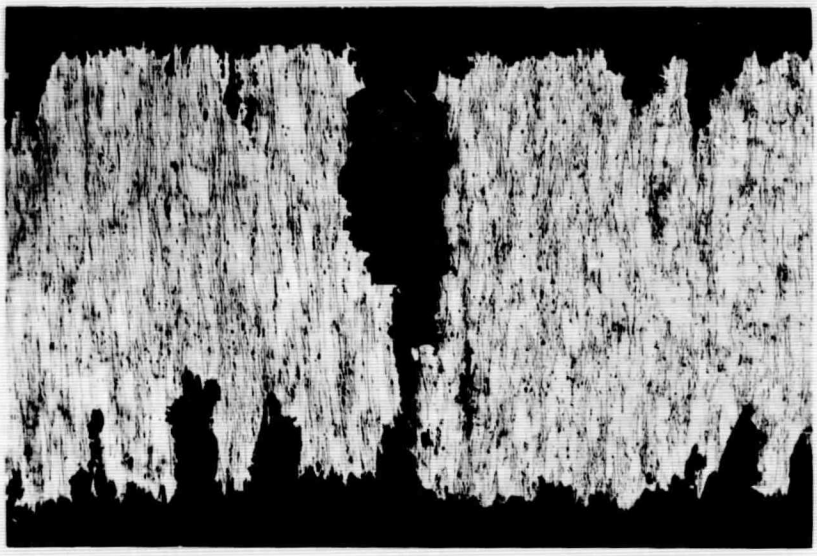

Etch: Keller's Mag. 20X

Stressed 75% Y.S. - Failed 10 days

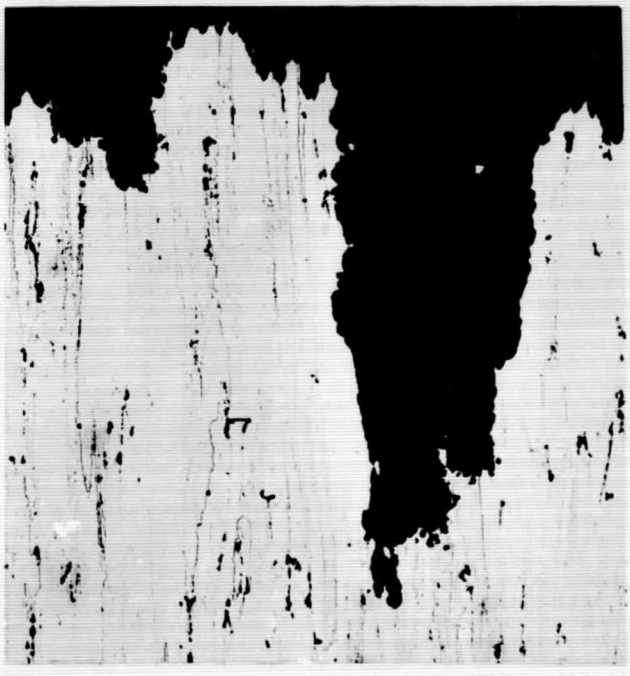

Etch: Keller's Mag. 100X

Unstressed - 10 days

Etch: Keller's Mag. 100X

Stressed 75% Y.S. - F 10 days

164582
164583
164585

Sections through corrosion pits in specimens with a visual corrosion rating of severe, directional attack.

Figure 71

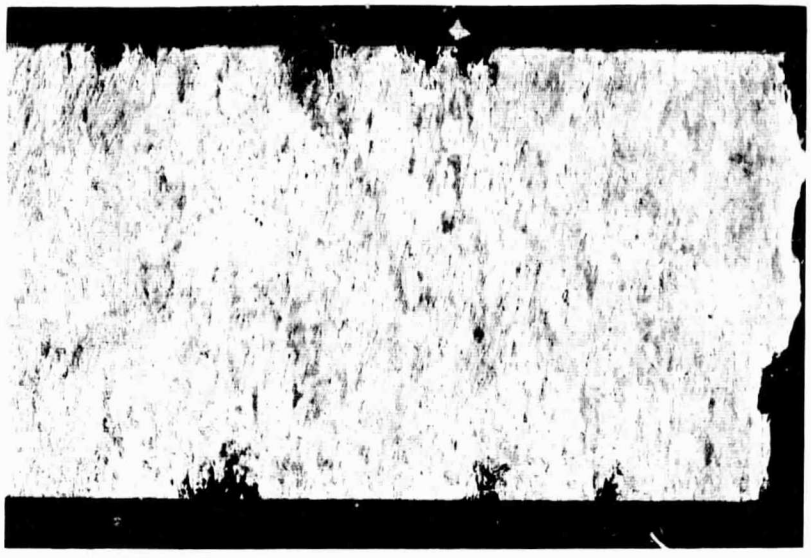

Etch: Keller's Mag. 20X

Stressed 75% Y.S. - Failed 22 days

Etch: Keller's Mag. 100X

Unstressed - 22 days

Etch: Keller's Mag. 100X

Stressed 75% Y.S. - F 22 days

Sections through corrosion pits in specimens which visually showed negligible attack.

Figure 72

164573
164574
164579

Etch: Keller's Mag. 20X

Stressed 75% YS - Exposed 8 hours

Etch: Keller's Mag. 100X

Unstressed - Exposed 8 hours

Etch: Keller's Mag. 100X

Stressed 75% YS - Exposed 8 hours

Illustrates initial intergranular attack and incipient stress-corrosion cracking (arrow).

Figure 74

Etch: Keller's Mag. 20X

Stressed 75% YS - Exposed 8 hours

Etch: Keller's Mag. 100X

Unstressed - Exposed 8 hours

Etch: Keller's Mag. 100X

Stressed 75% YS - Exposed 8 hours

Illustrates initial intergranular attack and incipient stress-corrosion cracking (arrow).

Figure 74

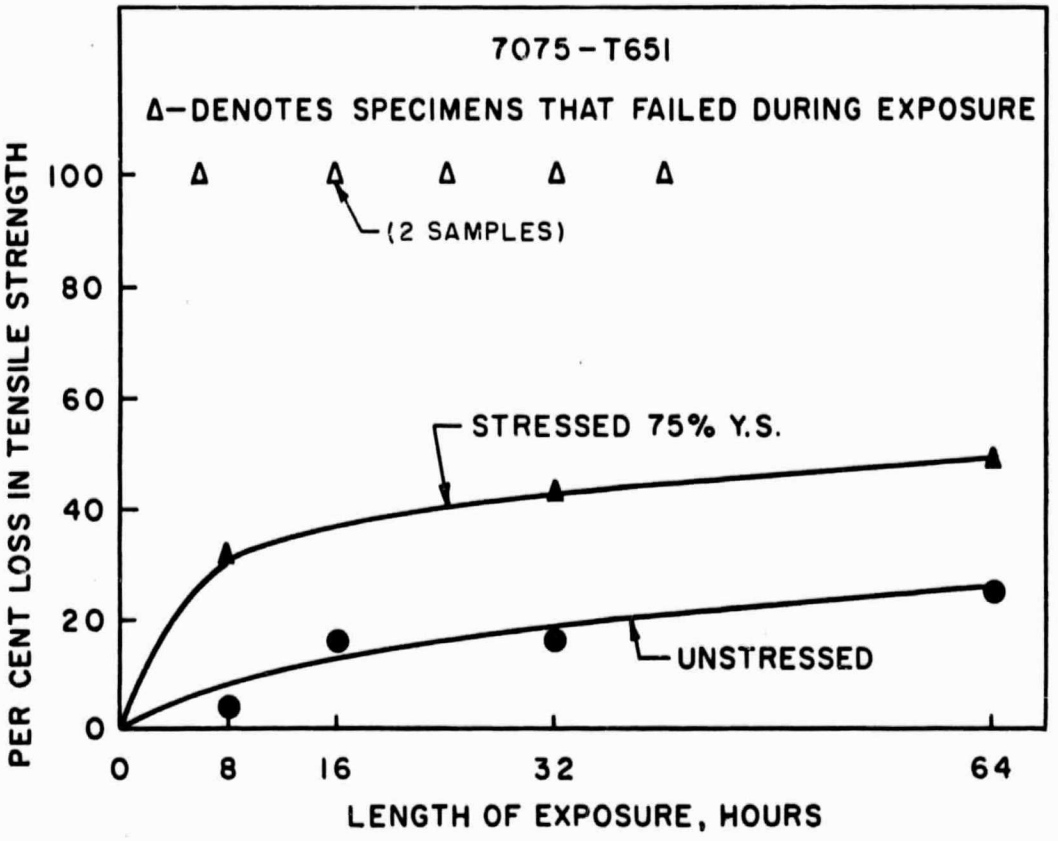

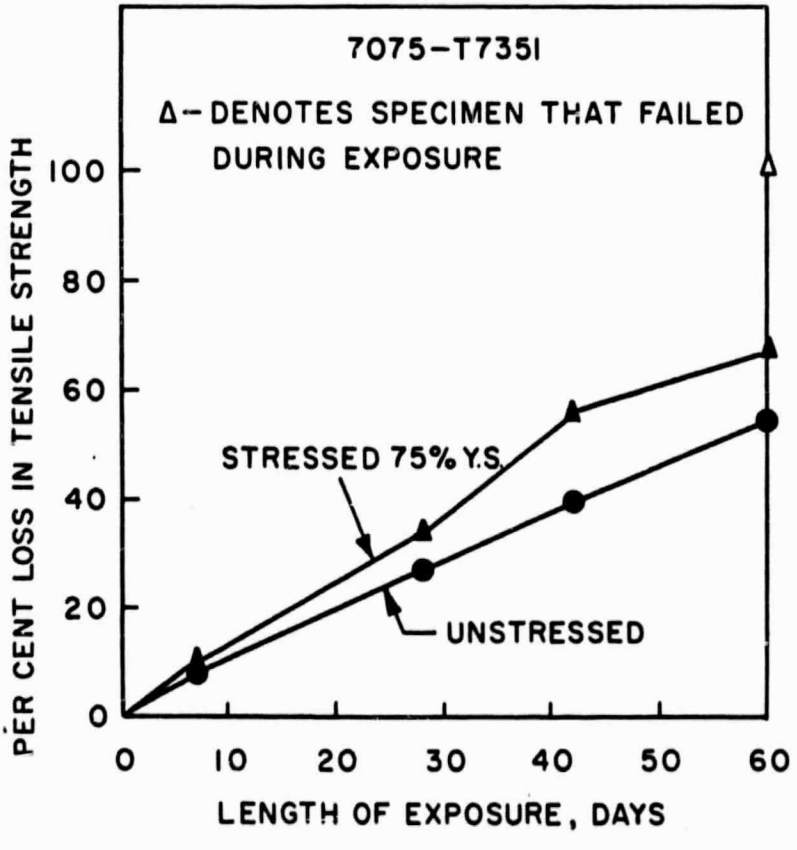

EFFECT OF STRESS ON CORROSION RATE OF 7075 ALLOY IN ACIDIFIED NaCl (pH2)

FIGURE 75

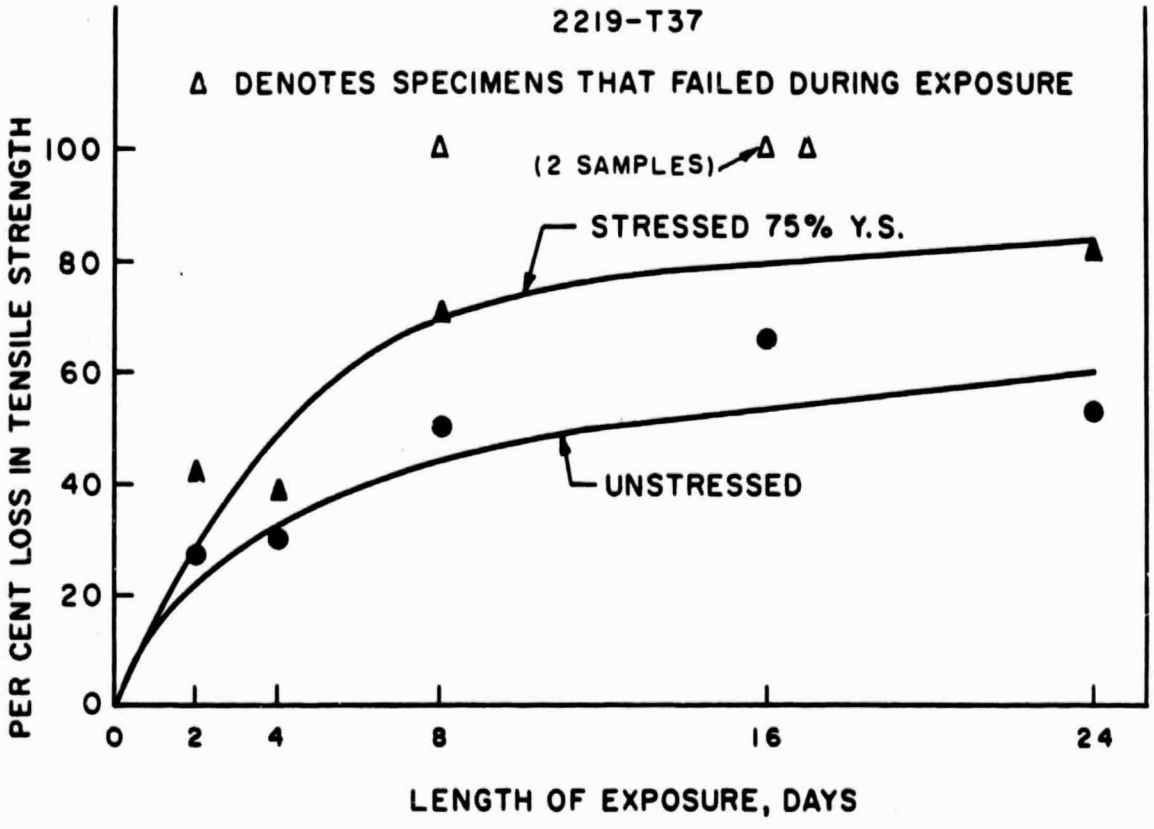

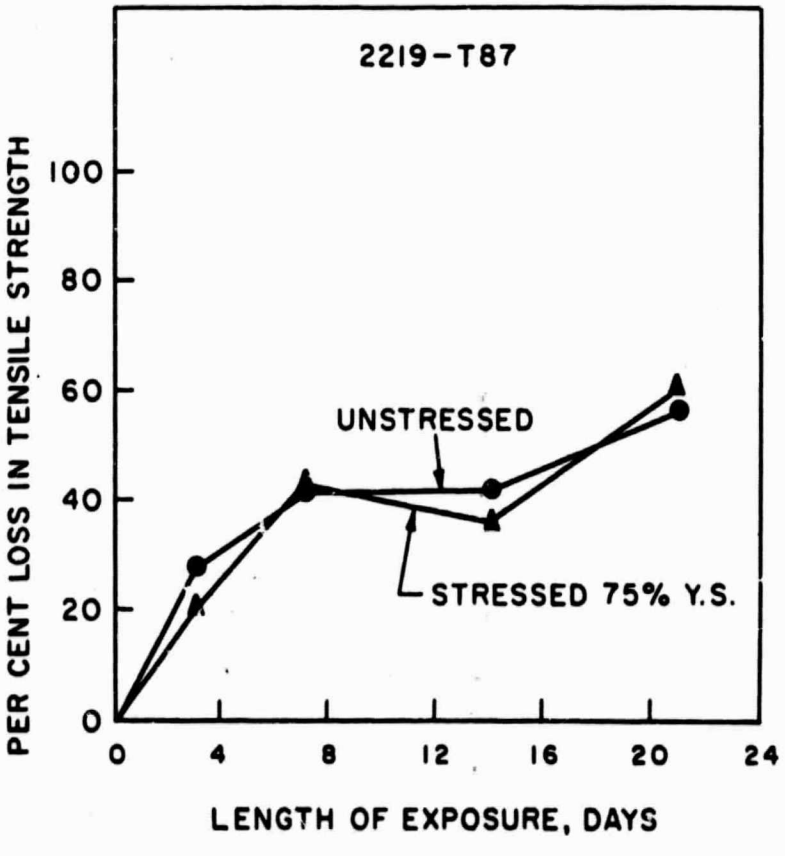

EFFECT OF STRESS ON CORROSION RATE OF 2219 ALLOY IN ACIDIFIED NaCl (pH2)

FIGURE 76

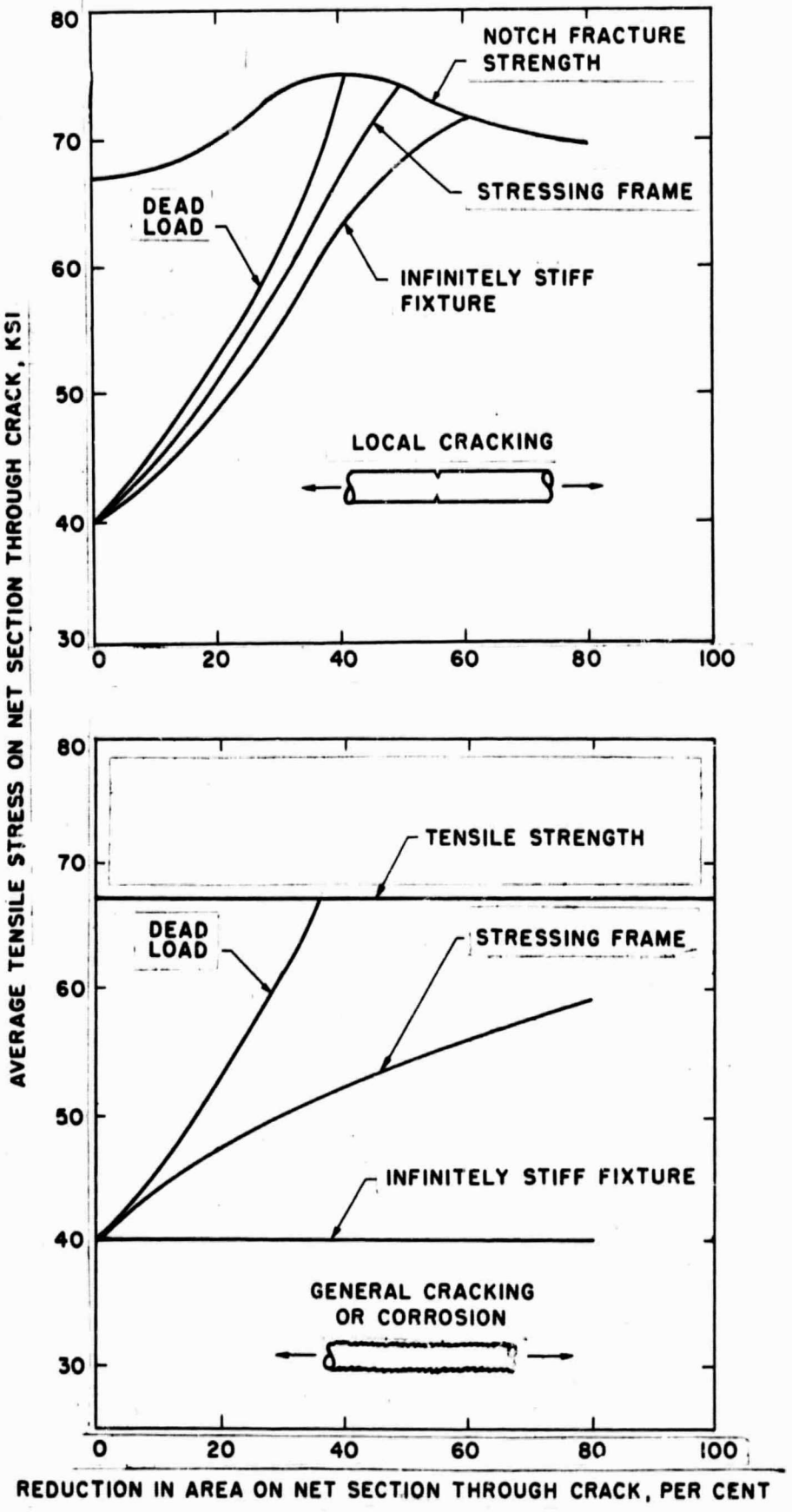

EFFECT OF LOADING METHOD AND EXTENT OF CRACKING ON AVERAGE NET SECTION STRESS.

FIGURE 77

166076-81

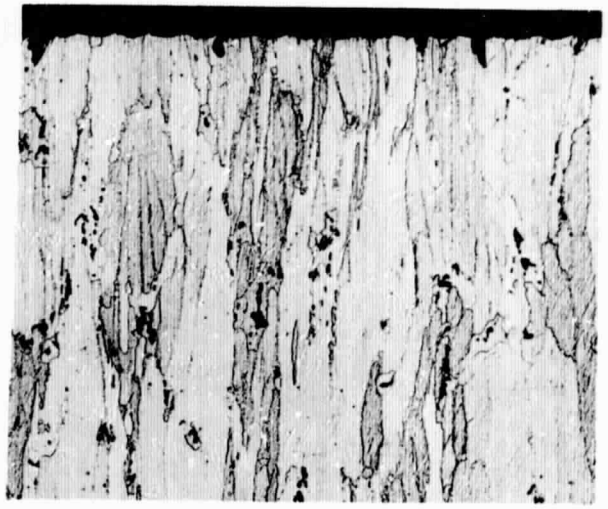

Unstressed - Exposed 4 days

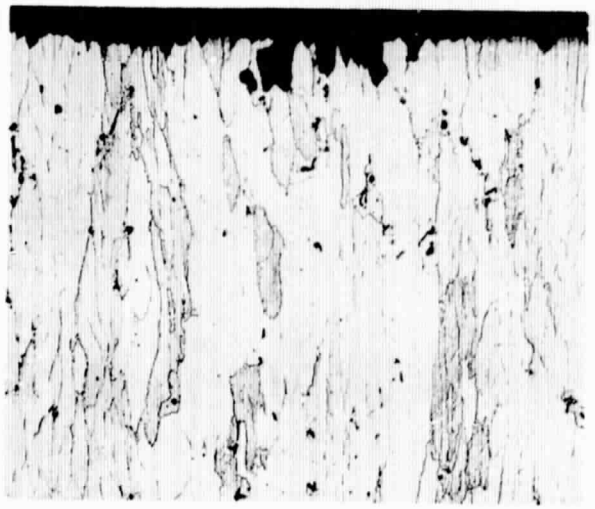

Unstressed - Exposed 16 days

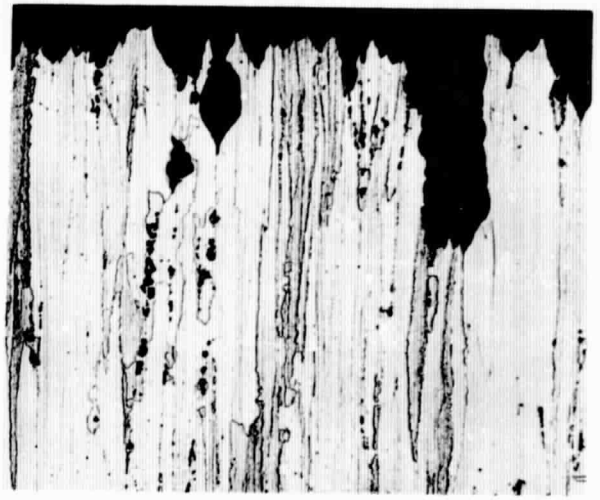

Unstressed - Exposed 48 days

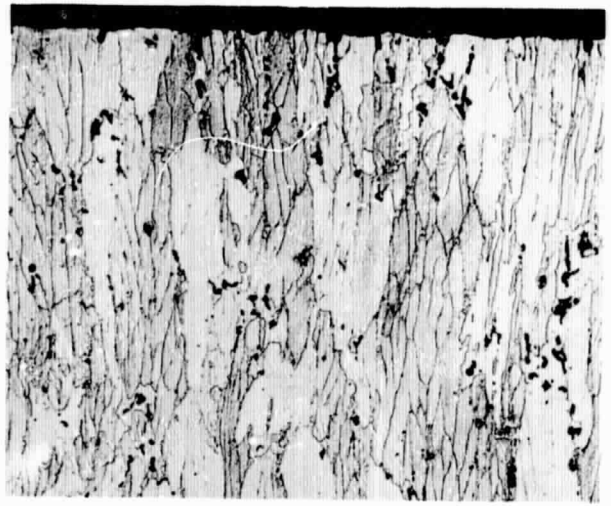

Stressed 75% YS - Exposed 4 days

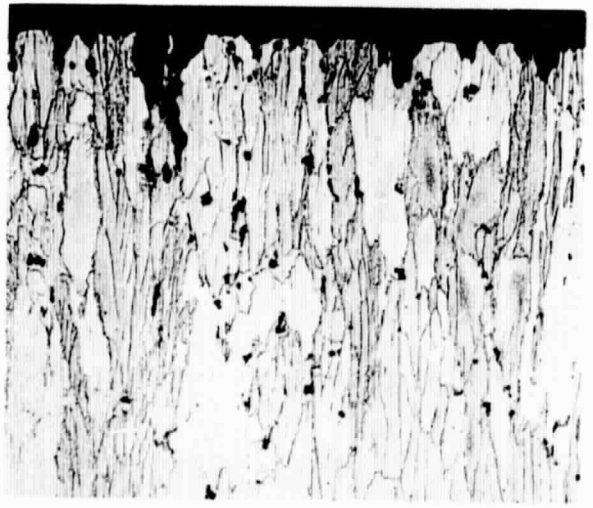

Stressed 75% YS - Exposed 16 days

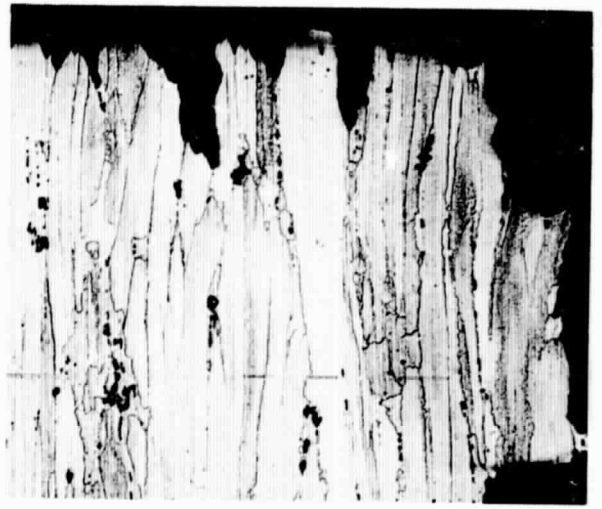

Stressed 75% YS - Failed 38 days

7075-T651 Exposed to 1N Na_2SO_4 pH2 (H_2SO_4)
(Etch: Keller's - Mag. 100X)

Illustrates the predominantly pitting type corrosion.

Figure 78

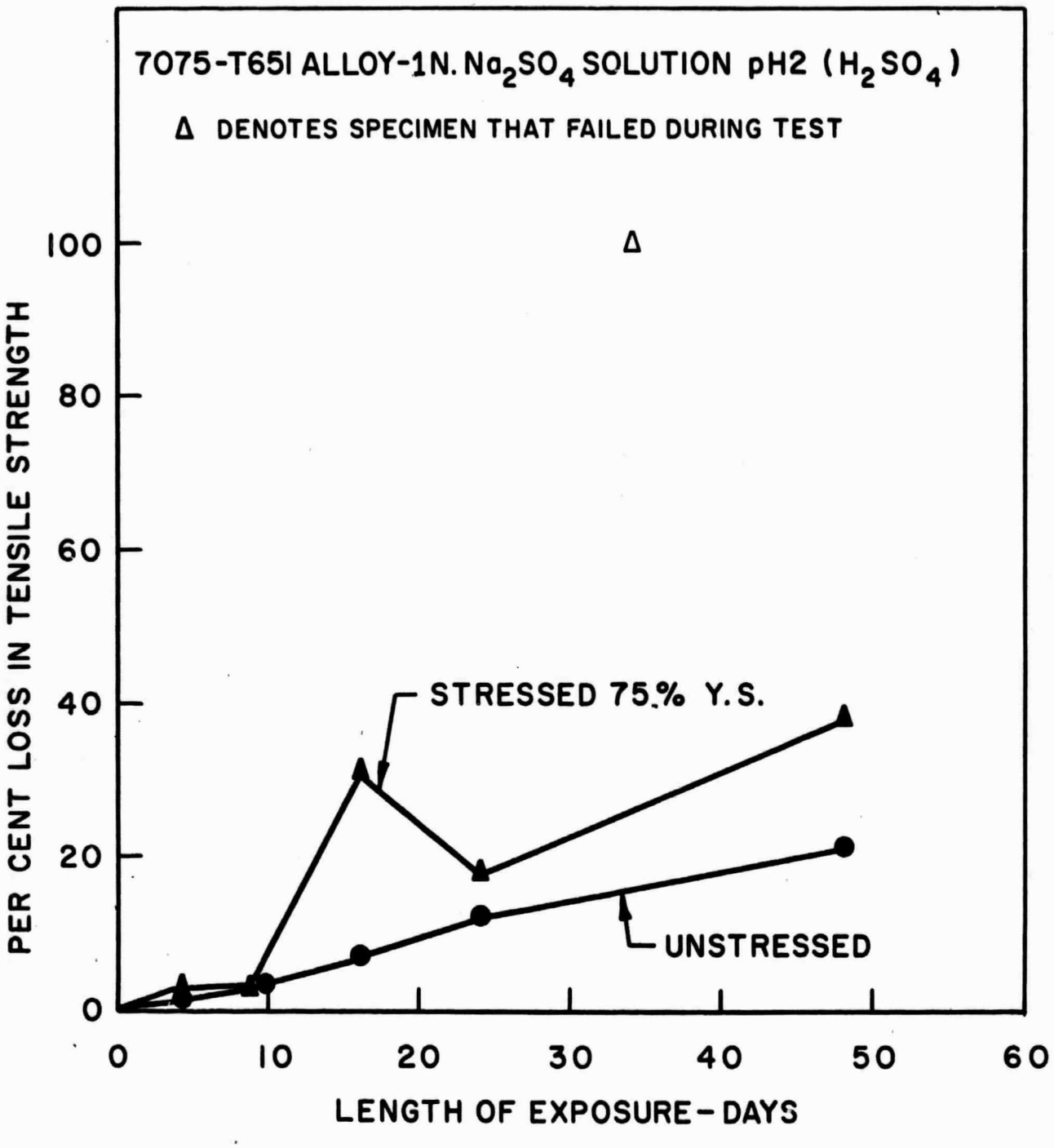

EFFECT OF STRESS ON CORROSION RATE

FIGURE 79

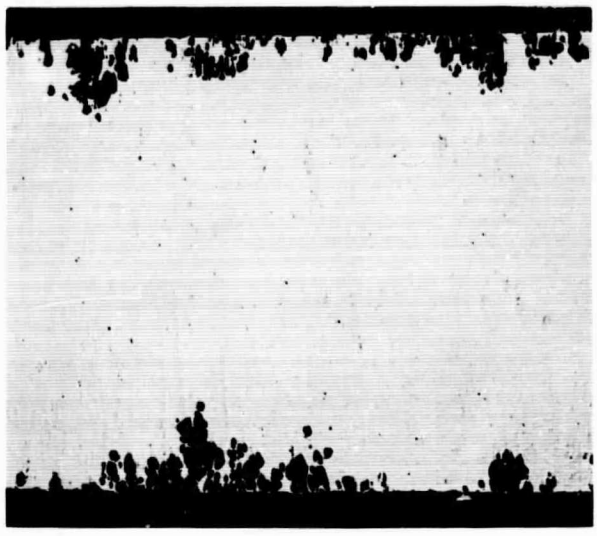

Mag. 20X

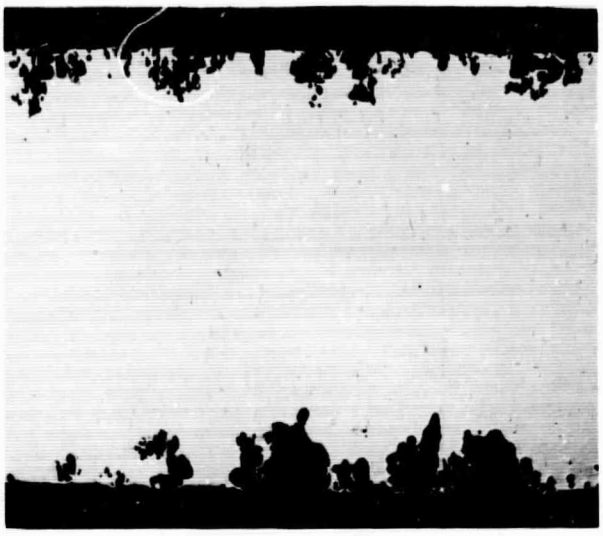

Mag. 20X

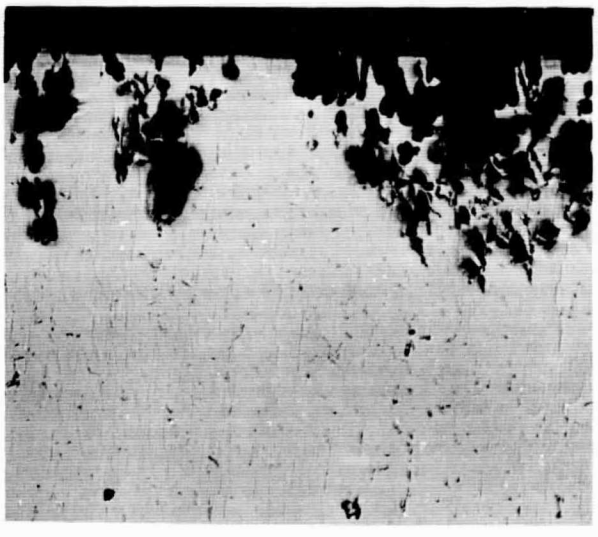

Mag. 100X
Exposed 7 days

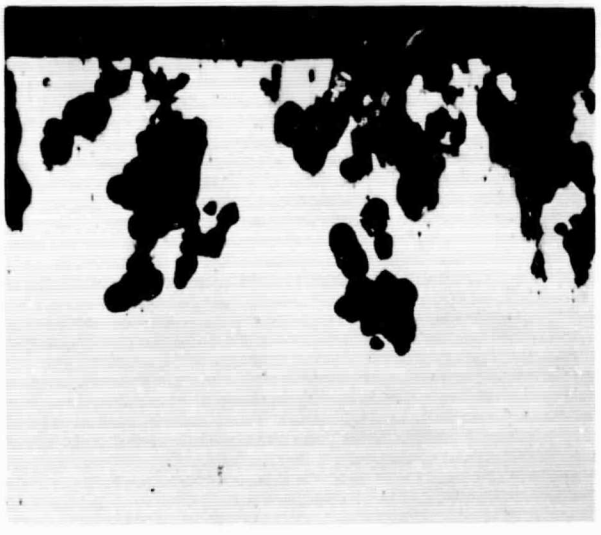

Mag. 100X
Exposed 14 days

2219-T87, Stressed 75% YS, Exposed to 1N NaCl pH2 (HCl)
(Specimens shown as-polished)

Illustrates general surface pitting.

Figure 80

166083
166892-6
166866

166870
167032-33
167222-23

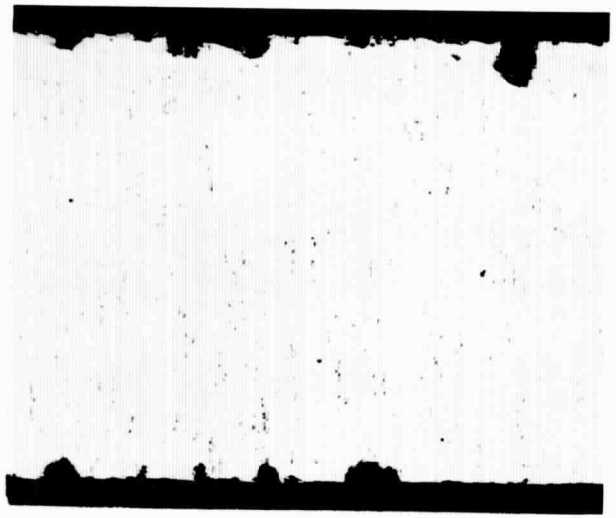

Mag. 20X

Mag. 20X

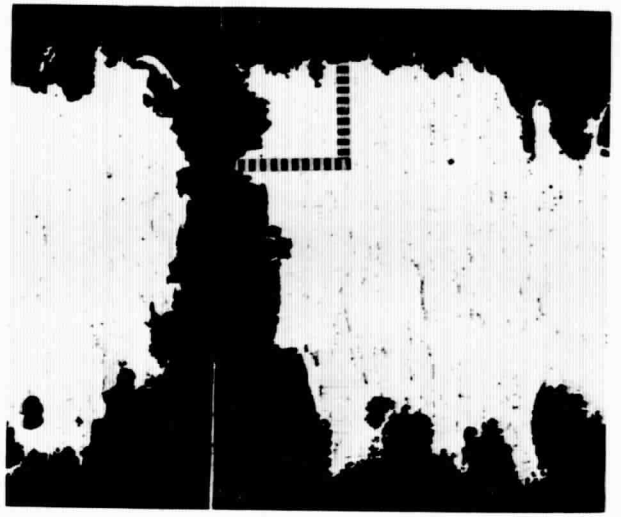

Mag. 20X

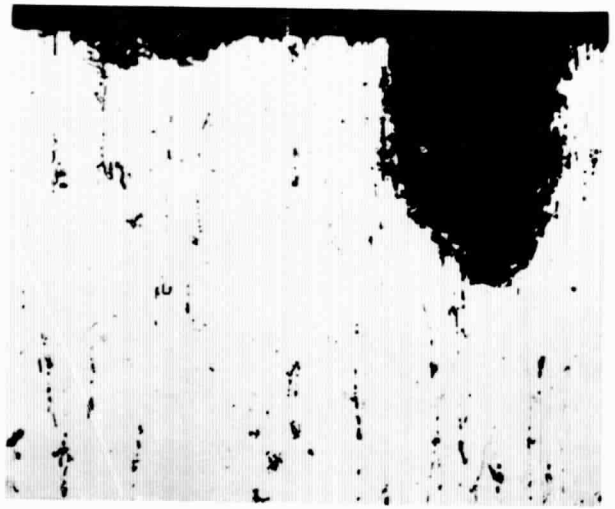

Mag. 100X
Exposed 7 days

Mag. 100X
Exposed 42 days

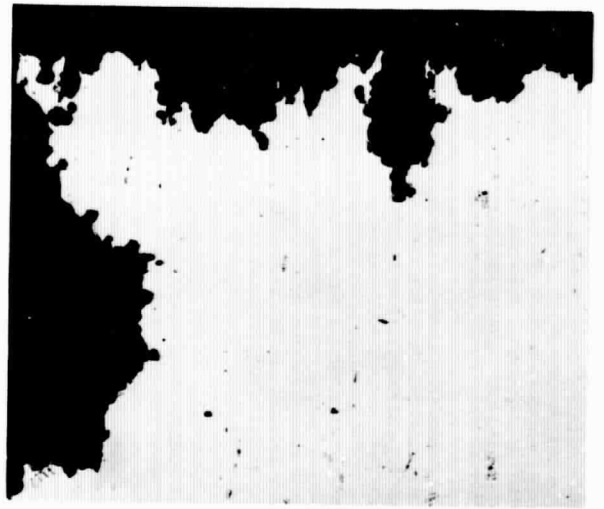

Mag. 100X
Failed 60 days

7075-T7351, Stressed 75% YS, Exposed to 1N NaCl pH2 (HCl)
(Specimens shown as-polished)

Illustrates severe general pitting attack.

Figure 81

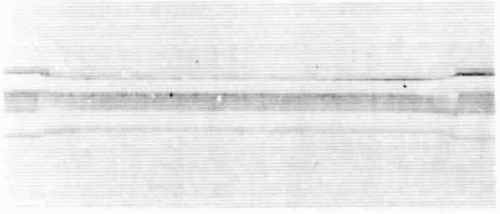

Unexposed Blank

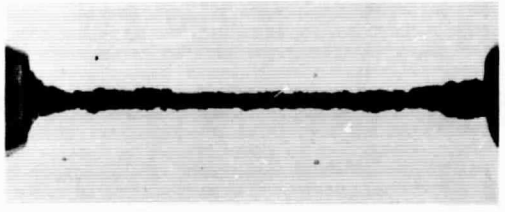

1N NaOH (pH 11.5)

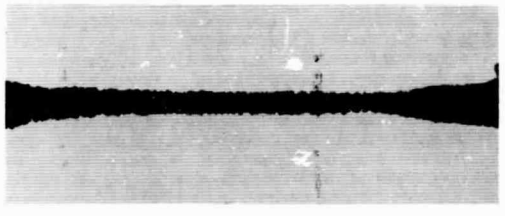

1N $FeCl_3$ (pH 1.5)

7075-T7351

Illustrates the extreme severity of the corrosive attack in the solutions noted. The specimens shown were exposed in the unstressed condition for a period of 1 day. (Mag. 2X)

Figure 82

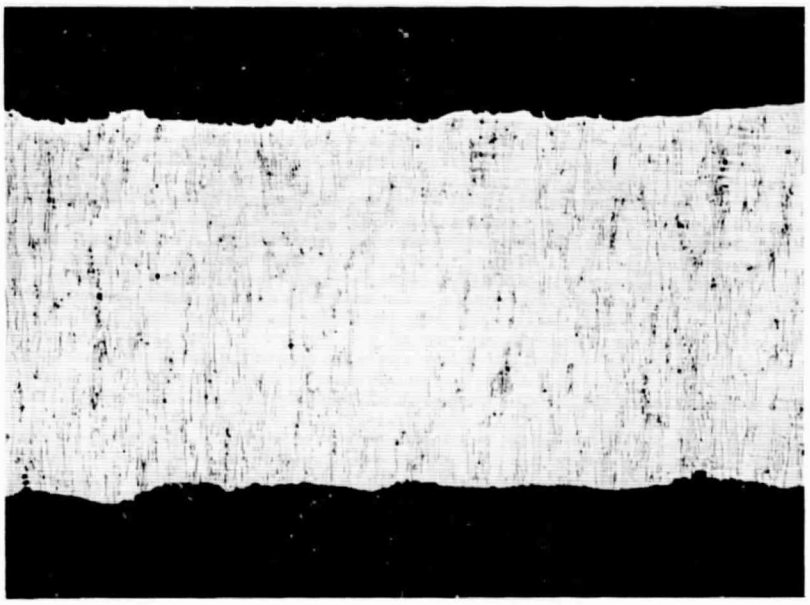

Etch: Keller's Mag. 20X

Stressed 75% YS - Exposed 30 minutes

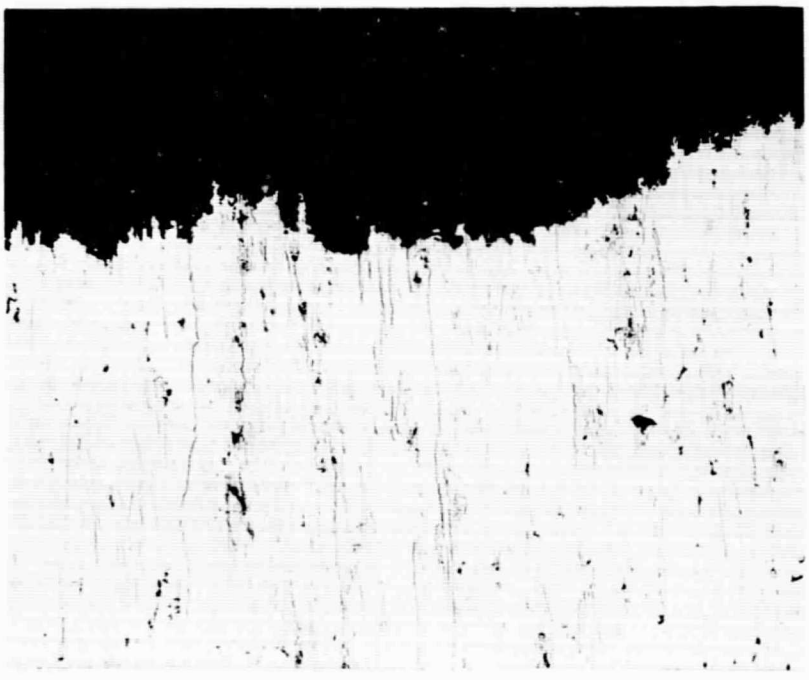

Etch: Keller's Mag. 100X

Stressed 75% YS - Exposed 30 minutes

7075-T7351 Exposed to 1N $CuCl_2$ pH 2 (HCl)

Illustrates severe reduction in cross section as a result of pitting type attack. Specimen reduction is typical of that encountered with all materials.

Figure 83

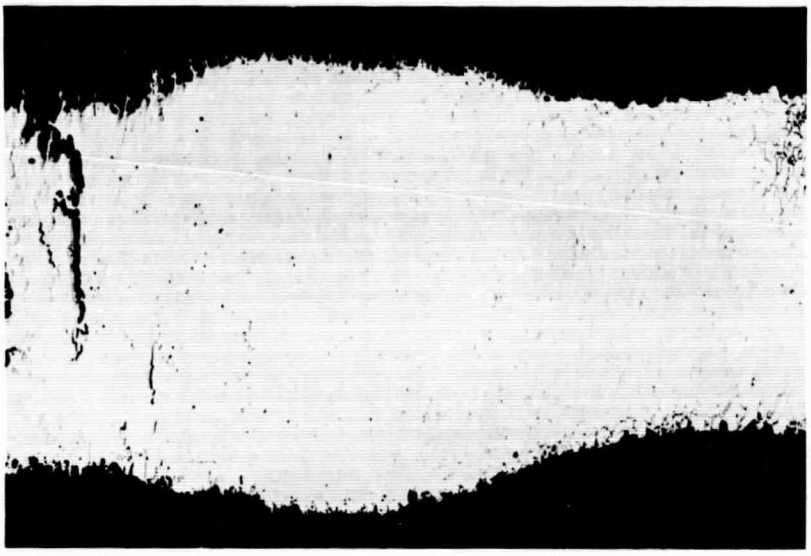

As Polished Mag. 20X

Stressed 75% YS - Failed 55 days

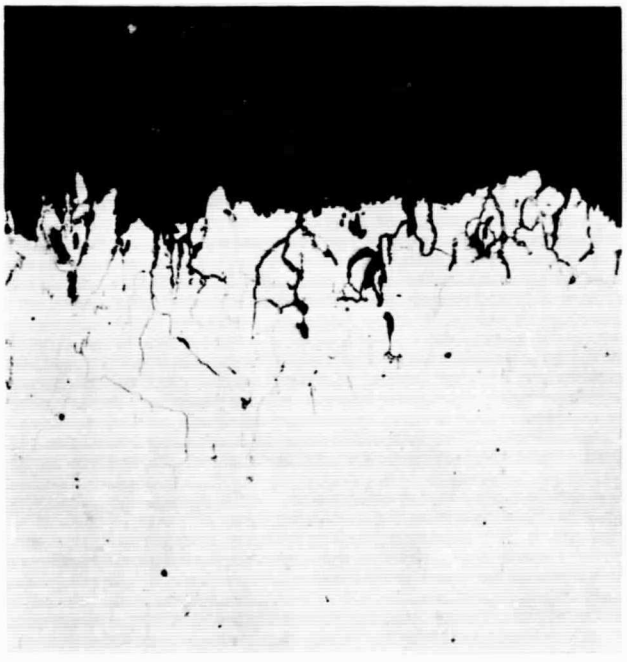

As Polished Mag. 100X

Unstressed - Exposed 31 days

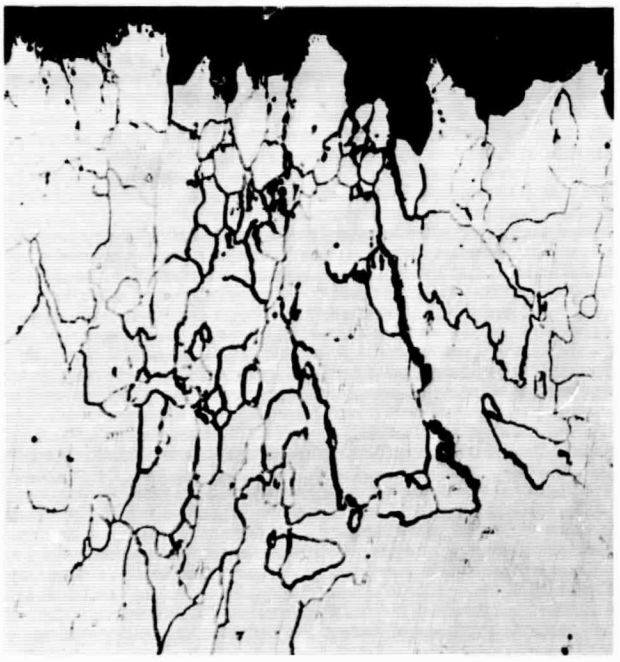

As Polished Mag. 100X

Stressed 75% YS - Failed 55 days

2219-T37 Exposed to 1N $CuSO_4$ pH2 (H_2SO_4)

Illustrates severe intergranular attack and apparent stress-corrosion crack (upper left).

165614
165690-1

Figure 84

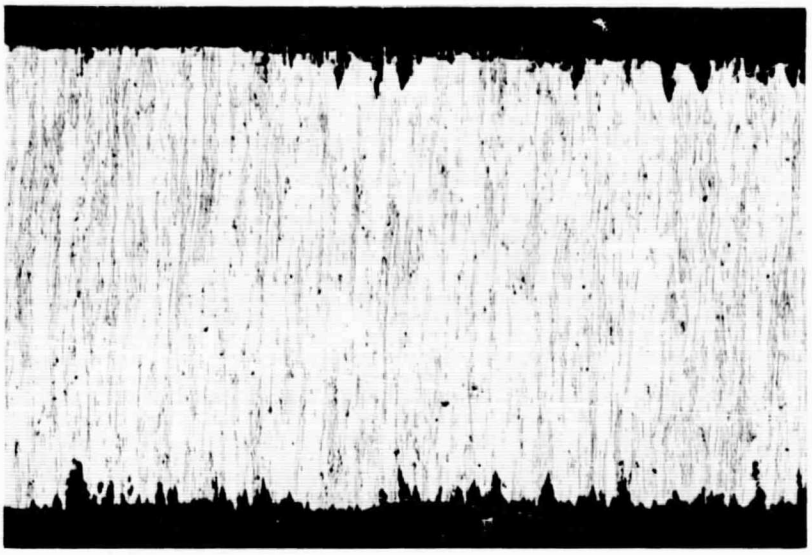

Etch: Keller's Mag. 20X

Stressed 75% YS - Failed 11 days

Etch: Keller's Mag. 100X

Unstressed - Exposed 11 days

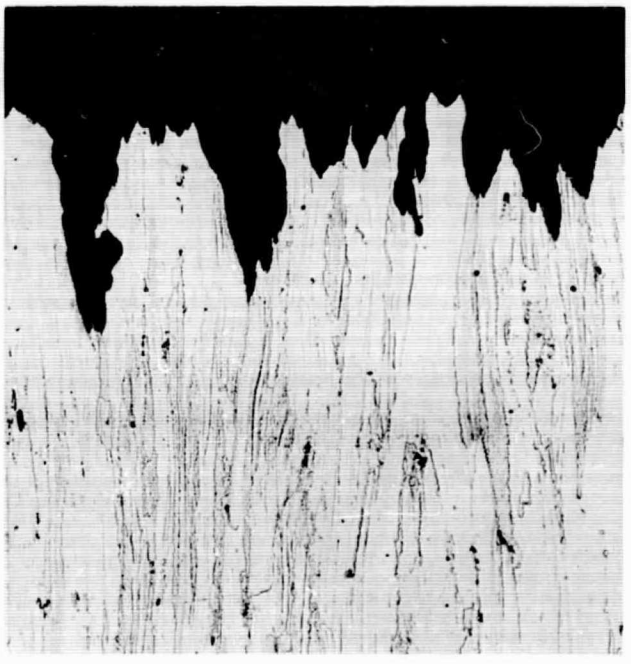

Etch: Keller's Mag. 100X

Stressed 75% YS - Failed 11 days

7075-T651 Exposed to 1N $CuSO_4$ pH2 (H_2SO_4)

Illustrates general surface pitting
and absence of any intergranular attack.

15990-30
15990

Figure 85

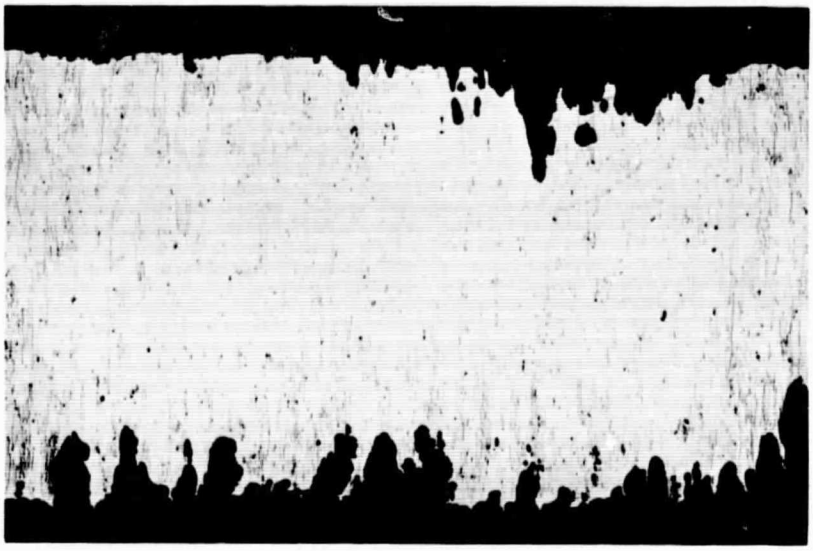

Etch: Keller's Mag. 20X

Stressed 75% YS - Failed 28 days

Etch: Keller's Mag. 100X

Unstressed - Exposed 28 days

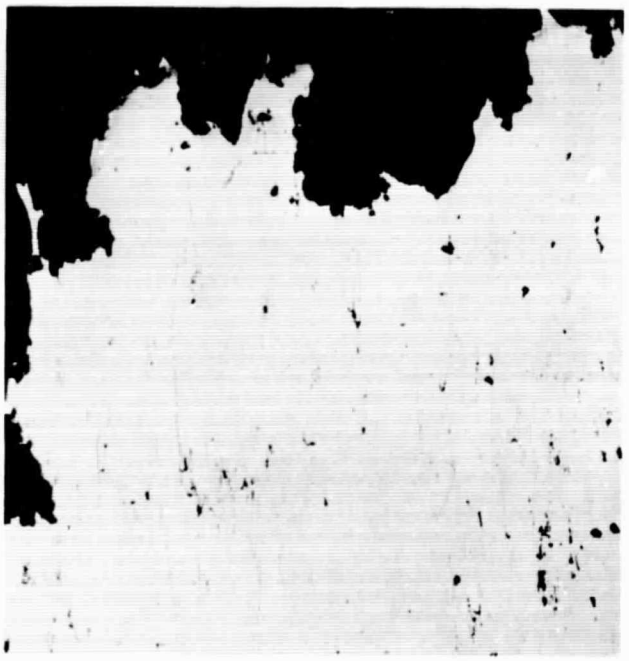

Etch: Keller's Mag. 100X

Stressed 75% YS - Failed 28 days

7075-T7351 Exposed to 1N $CuSO_4$ pH2 (H_2SO_4)

Illustrates severe general surface pitting.

156681-2
163677

Figure 86

As Polished Mag. 20X

Stressed 75% YS - Failed 20 days

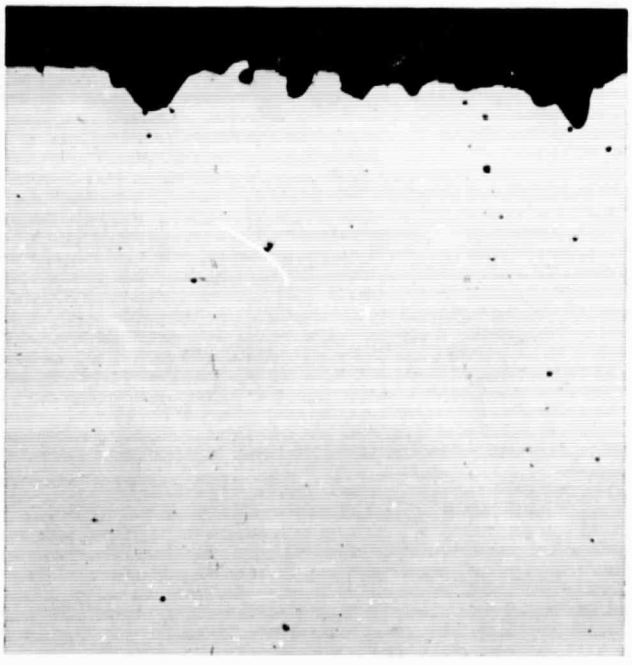

As Polished Mag. 100X

Unstressed - Exposed 20 days

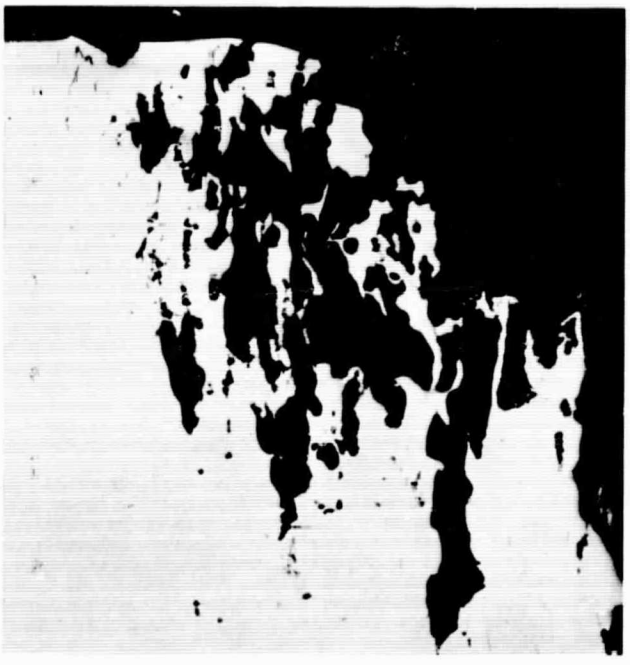

As Polished Mag. 100X

Stressed 75% YS - Failed 20 days

2219-T87 Exposed to 1N NaCl pH11 (NaOH)

Illustrates the slight overall surface attack and the severe localized pitting in the failure region.

Figure 87

164020
168090
168091

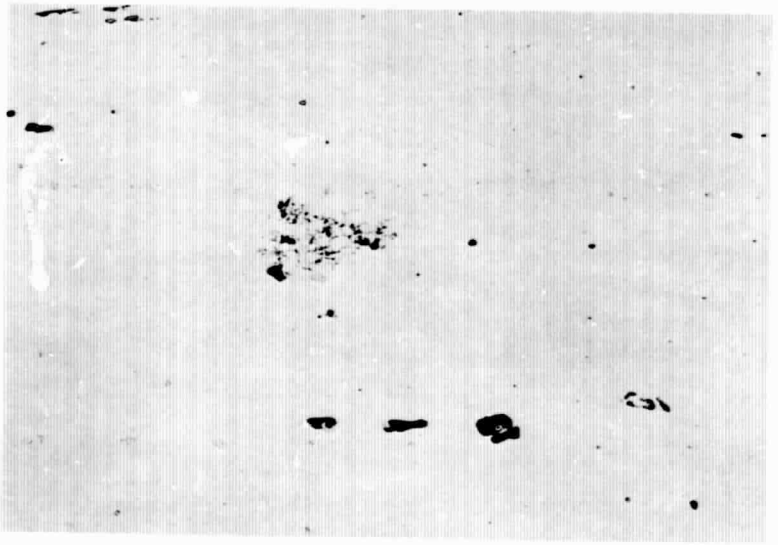

Unstressed
16 hrs

59 hrs
stressed
75% YS. S.T.
surface

59 hrs
stressed
X-Sect.
Keller'
Etch

Development of pitting attack in 7075-T6 exposed to 1N NaAc solution at pH4.
(X500)

Figure 88

7075-T6
3 hrs

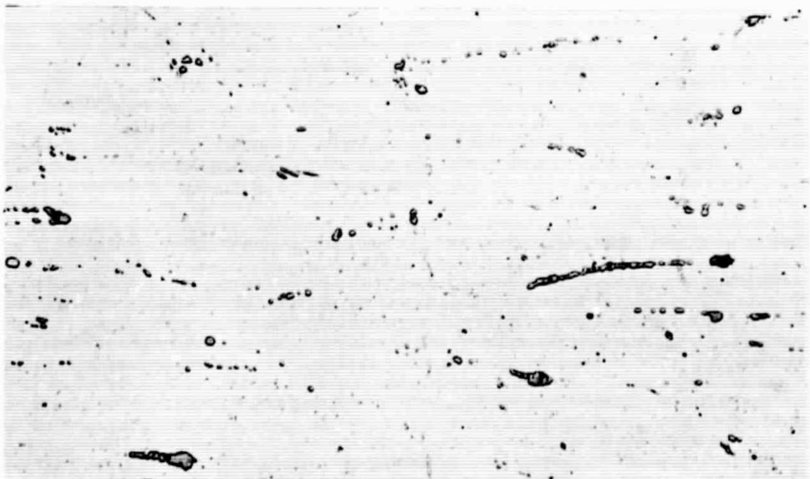

2219-T37
3 hrs

Unstressed corrosion in 1N Na_2SO_4 solution at pH2. (X500)

164022 164024

Figure 89

168076
168077
168078

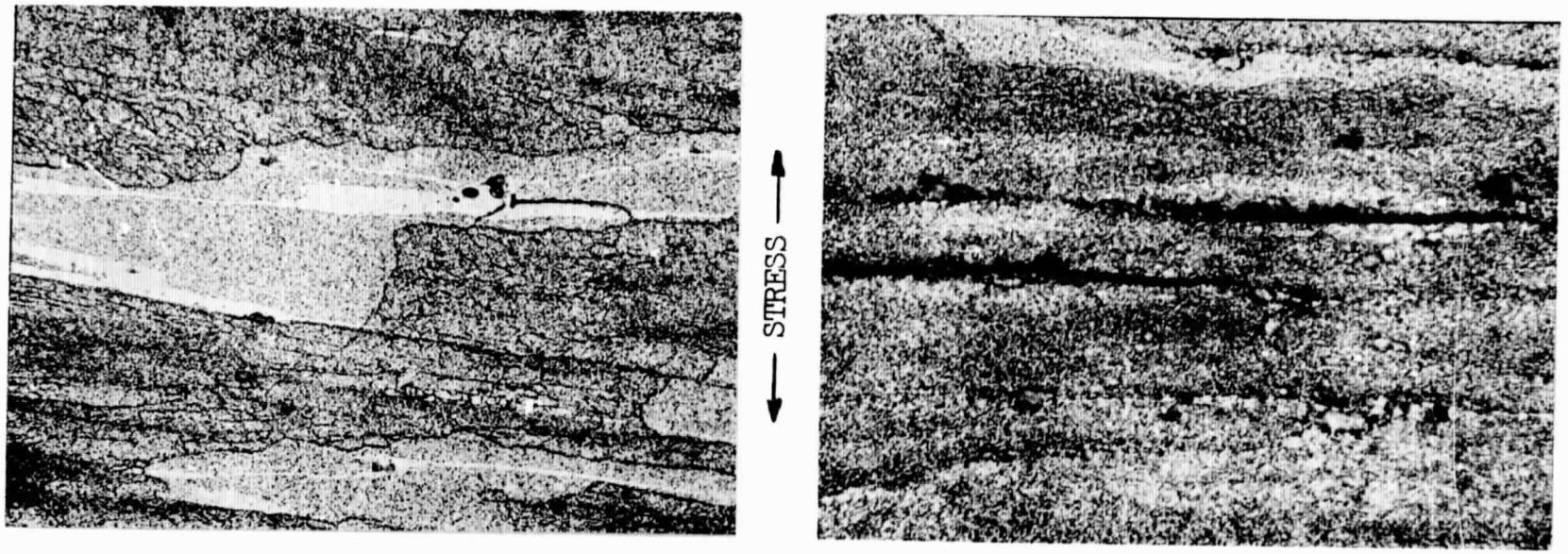

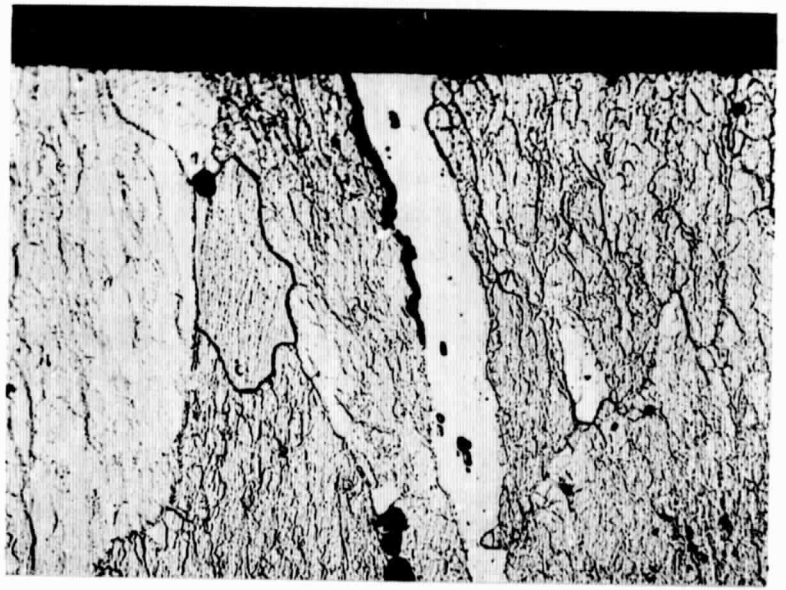

67 hrs
X-Sect.
Keller's
Etch

Crack initiation in 7075-T6 stressed to 75% YS
S.T. and exposed to 1N Na_2SO_4 solution at pH2 (X500)

Figure 90

168083
168084
168136

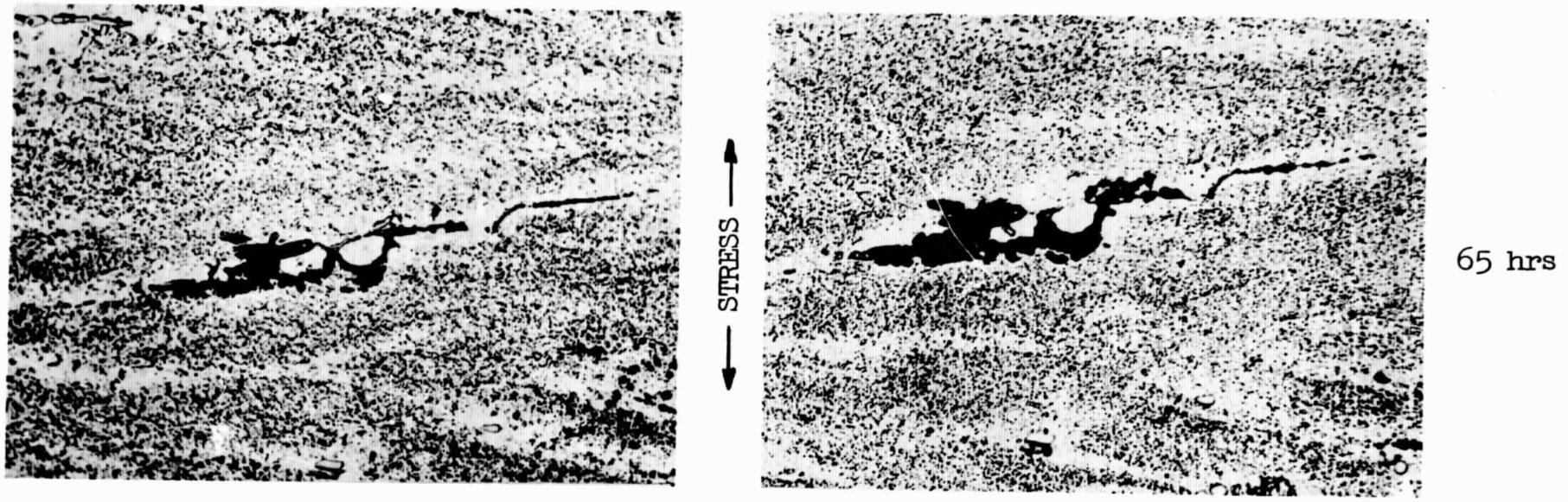

65 hrs
X-Sect.
Keller's etch

Selective attack in 2219-T37 stressed to 75% YS S.T. and exposed to 1N Na_2SO_4 solution at pH2 (X500).

Figure 91

7075-T6
3 hrs

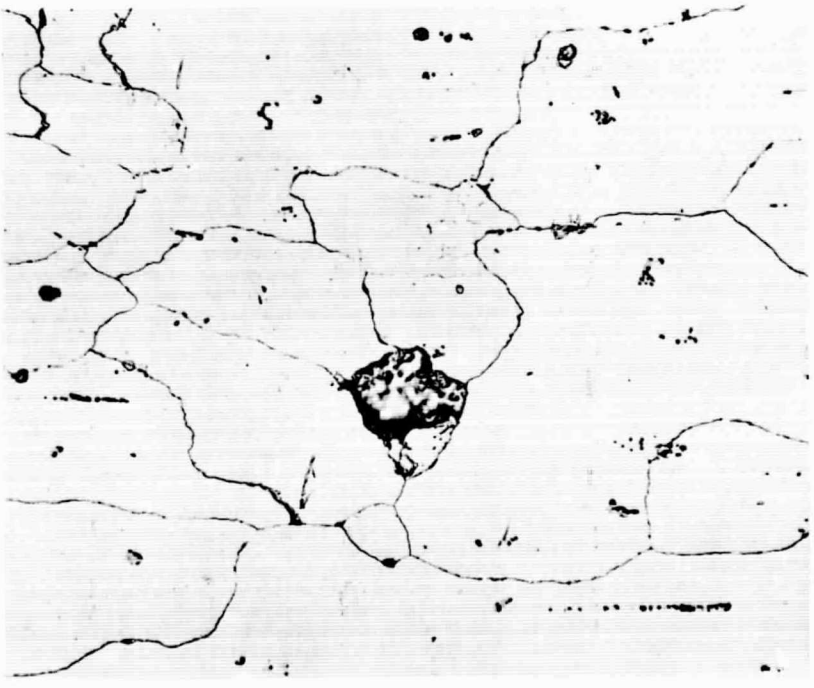

2219-T37
15 min.

Unstressed corrosion in 0.5N
NaCl + 0.5N Na_2CrO_4 solution at pH2.
(X500)

Figure 92

166605-6
166794

6 min.

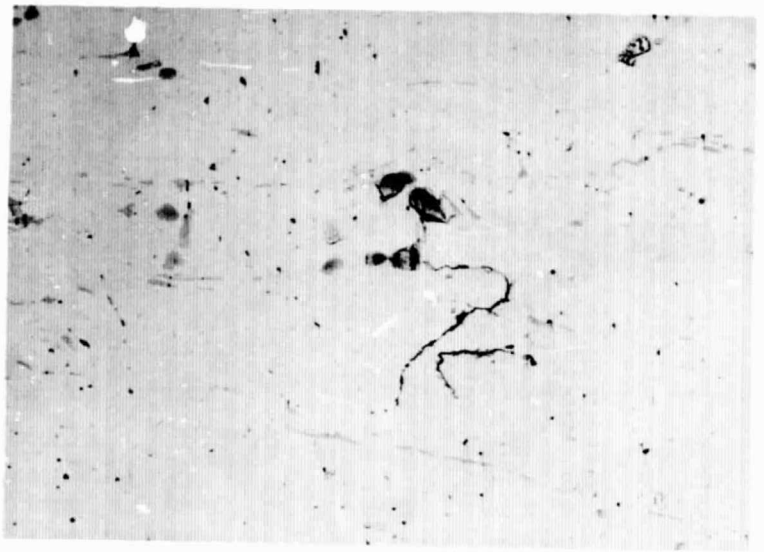

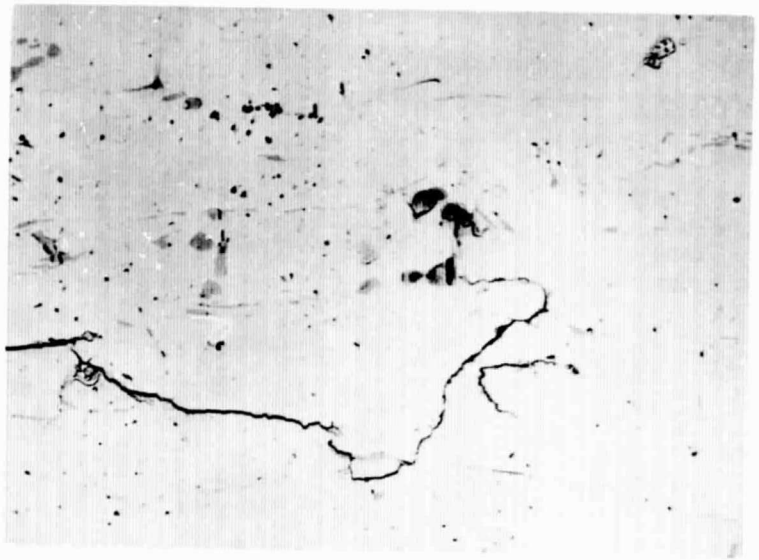

16 min.

STRESS

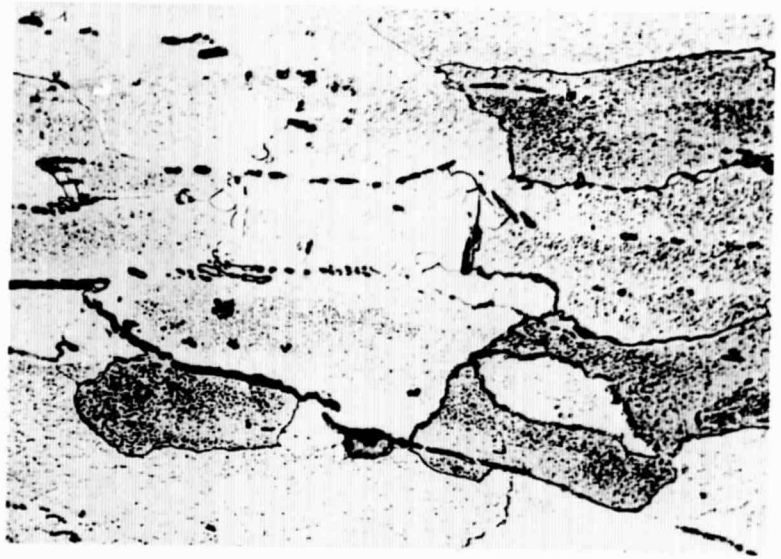

16 min.
Keller's etch

Tuning fork specimen of 2219-T37 stressed short transversely to 75% YS and exposed to 0.5N NaCl + 0.5N Na_2CrO_4 solution at pH2. (X500)

Figure 93

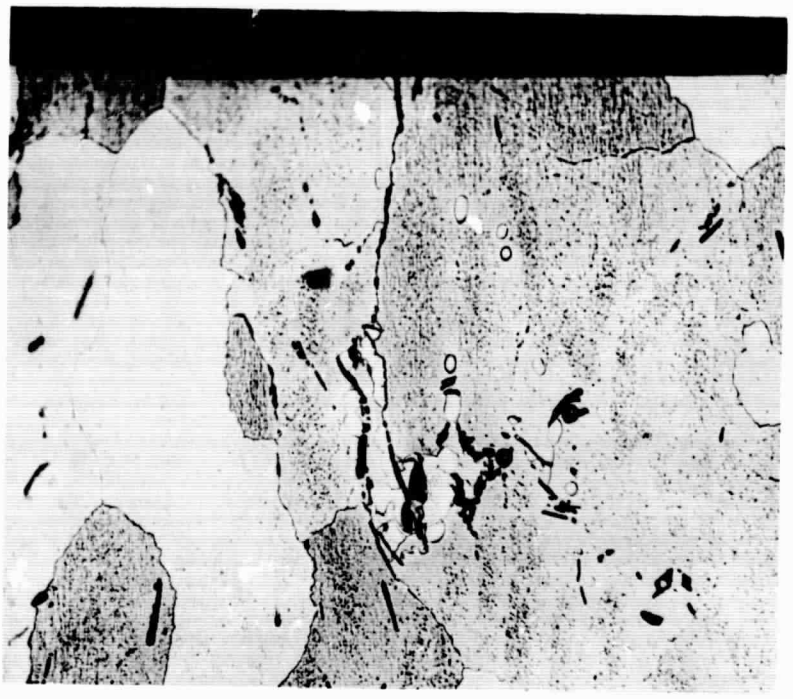

0.5N NaCl +
0.5N Na_2CrO_4

← STRESS →

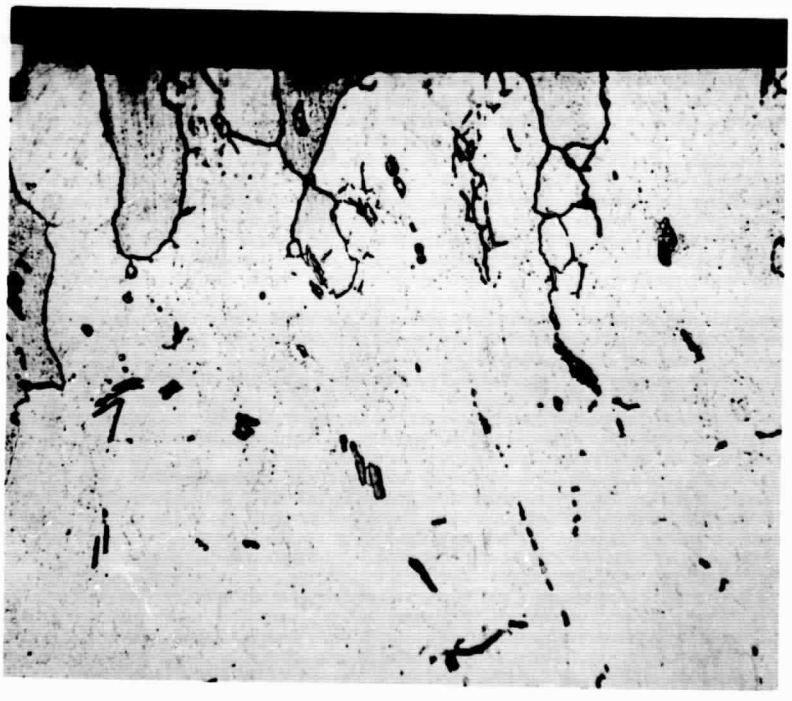

0.5N NaCl +
0.5N Na_2SO_4

Cross sections of 2219-T37 tuning fork specimens stressed short transversely to 75% YS and exposed to pH2 environments noted. (X500)

167011
167014

Figure 94

7075-T6
30 min.

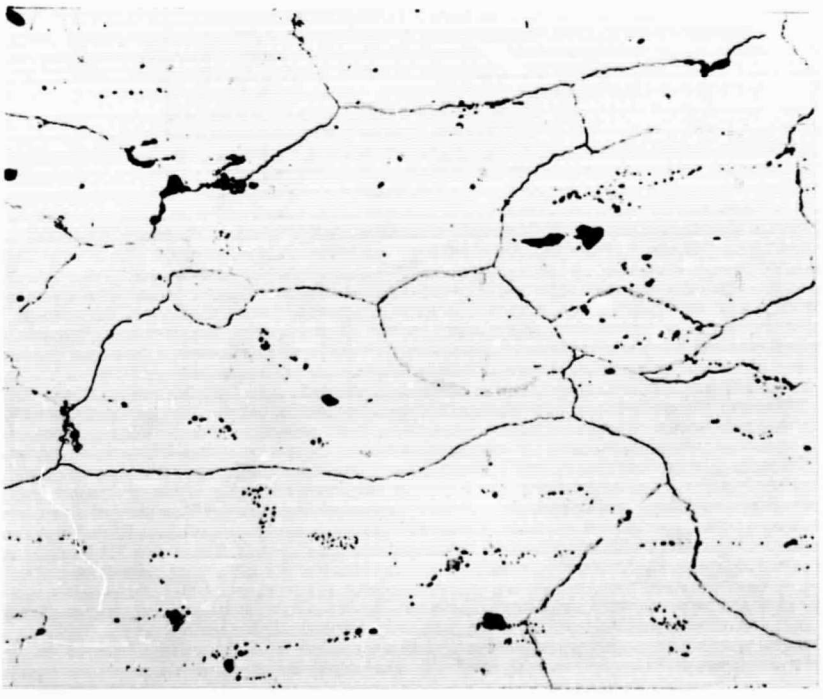

2219-T37
30 min.

Unstressed corrosion in 4N
NaCl + 0.5N KNO_3 solution at pH 0.4.
(X500)

Figure 95

165911
165913-14
166219

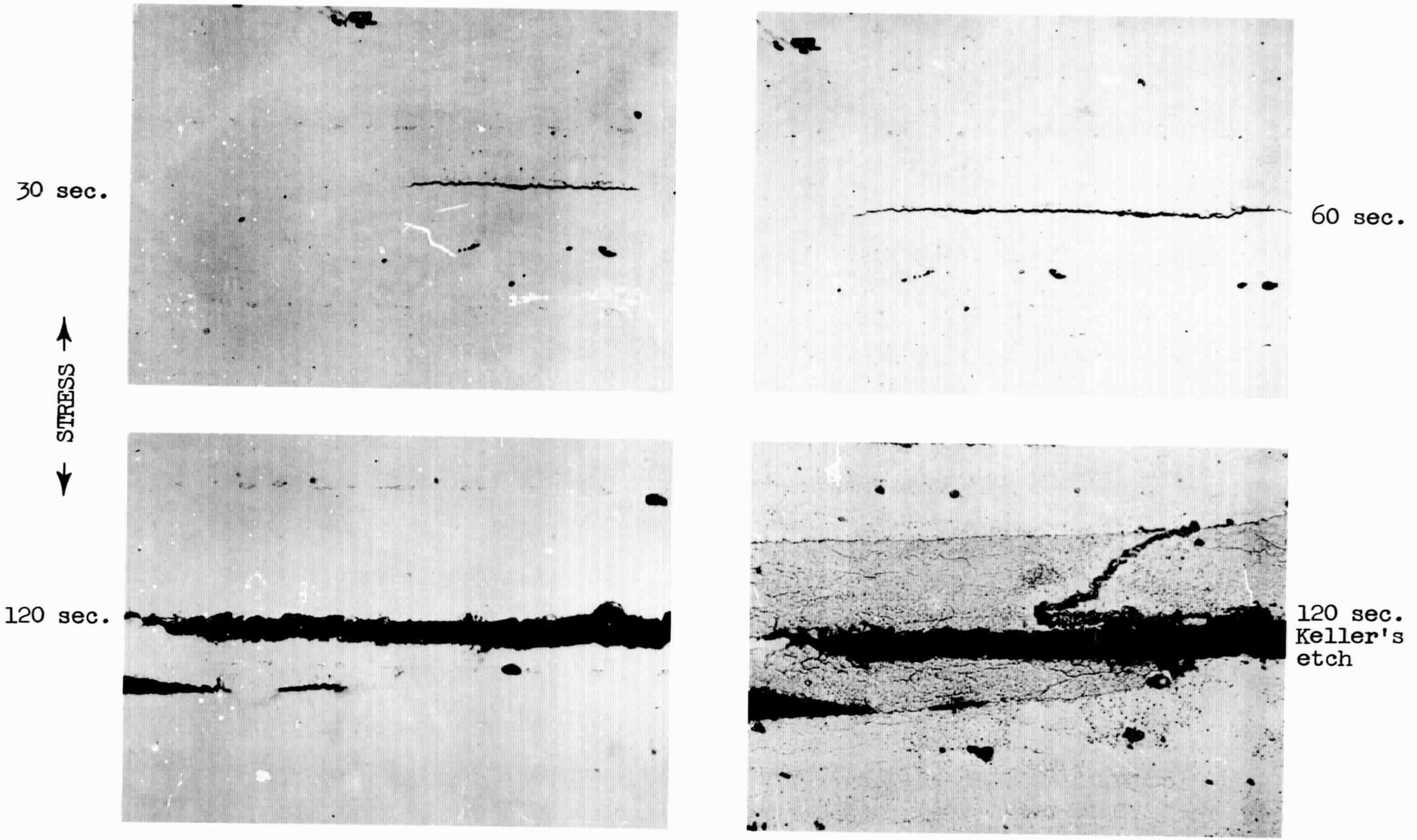

Crack development in 7075-T6 stressed short transversely to 75% YS and exposed in 4N NaCl + 0.5N KNO_3 solution at pH 0.4. (X500)

Figure 96

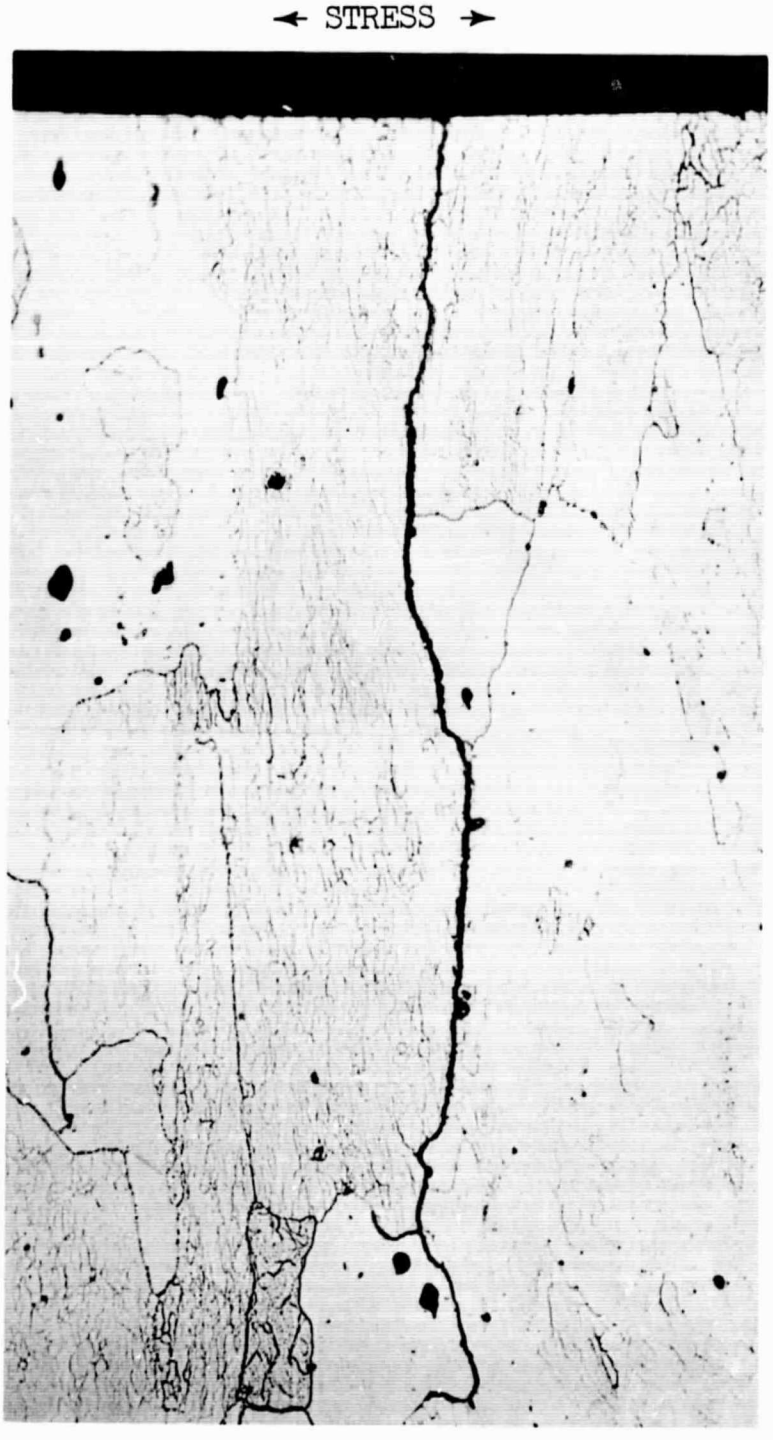

Cross section of specimen in Fig. 96 (X500)

Figure 97

166301-2

166334-35
166337
166791

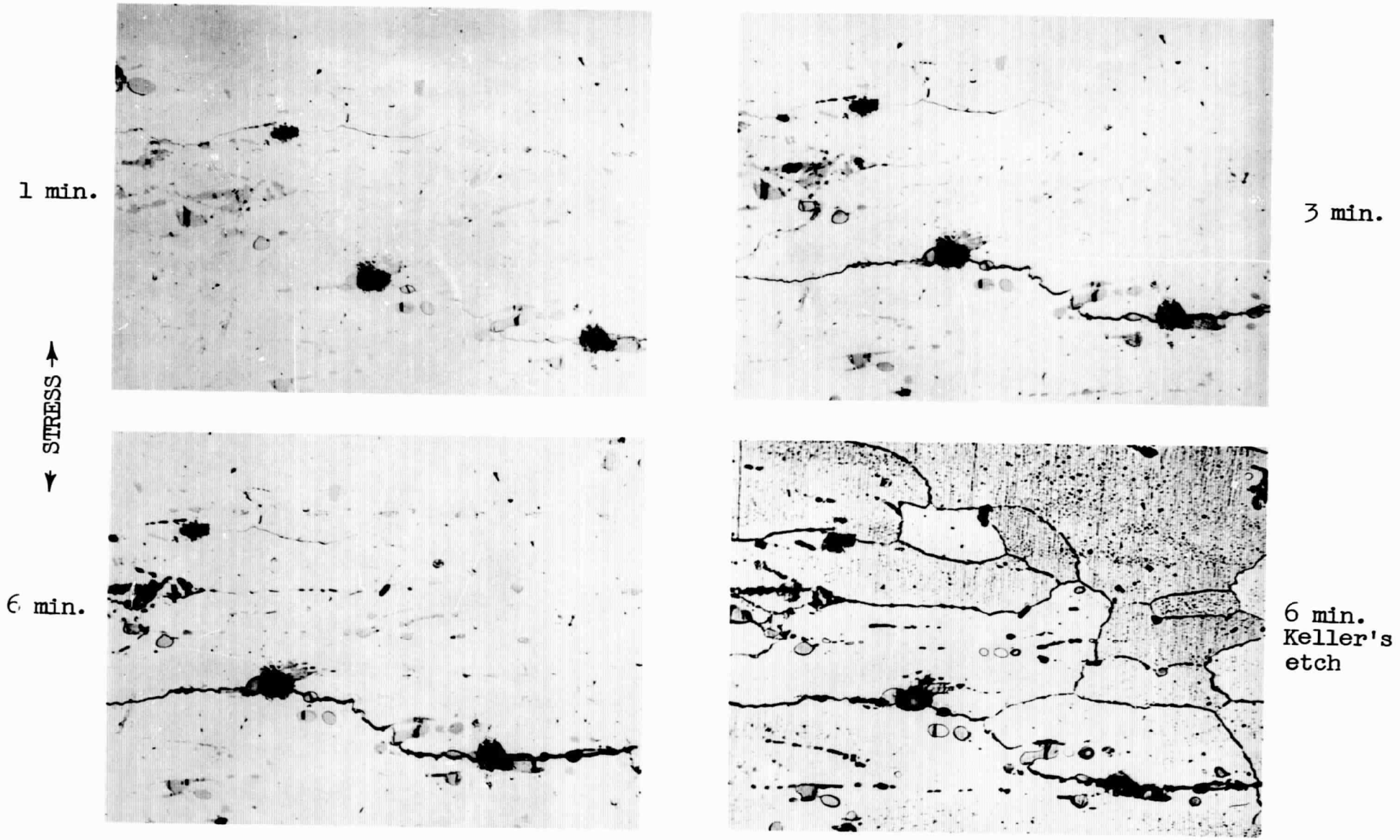

Crack initiation and development in 2219-T37 tuning-fork specimen stressed to 75% YS in short transverse direction and exposed to 4N NaCl + 0.5N KNO_3 solution at pH 0.4. (X500)

Figure 98

← STRESS →

Cross section of specimen seen in Fig. 98 (X500)

Figure 99

166792-93

7075-T6
3 hrs

2219-T37
30 min.

Unstressed corrosion in 0.5N
NaCl + 0.5N Na_2SO_4 solution at pH 2.
(X500)

Figure 100

166358-60
166790

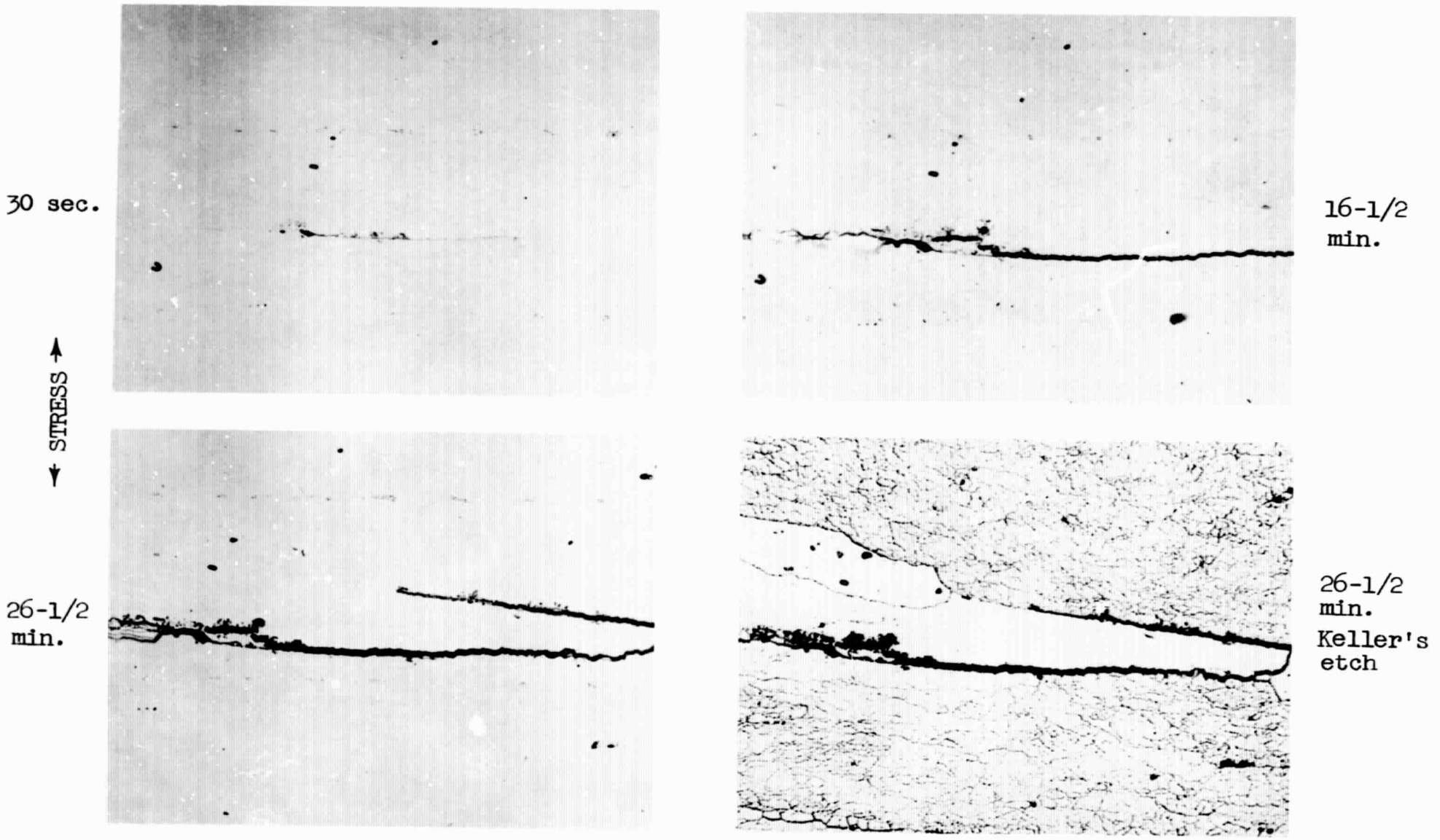

Crack initiation and development in 7075-T6 stressed short transversely to 75% YS and exposed to 0.5 NaCl + 0.5 Na_2SO_4 solution at pH2. (X500)

Figure 101

← STRESS →

Cross section of sample in Fig. 101 (X500)

Figure 102

166461-63
166793

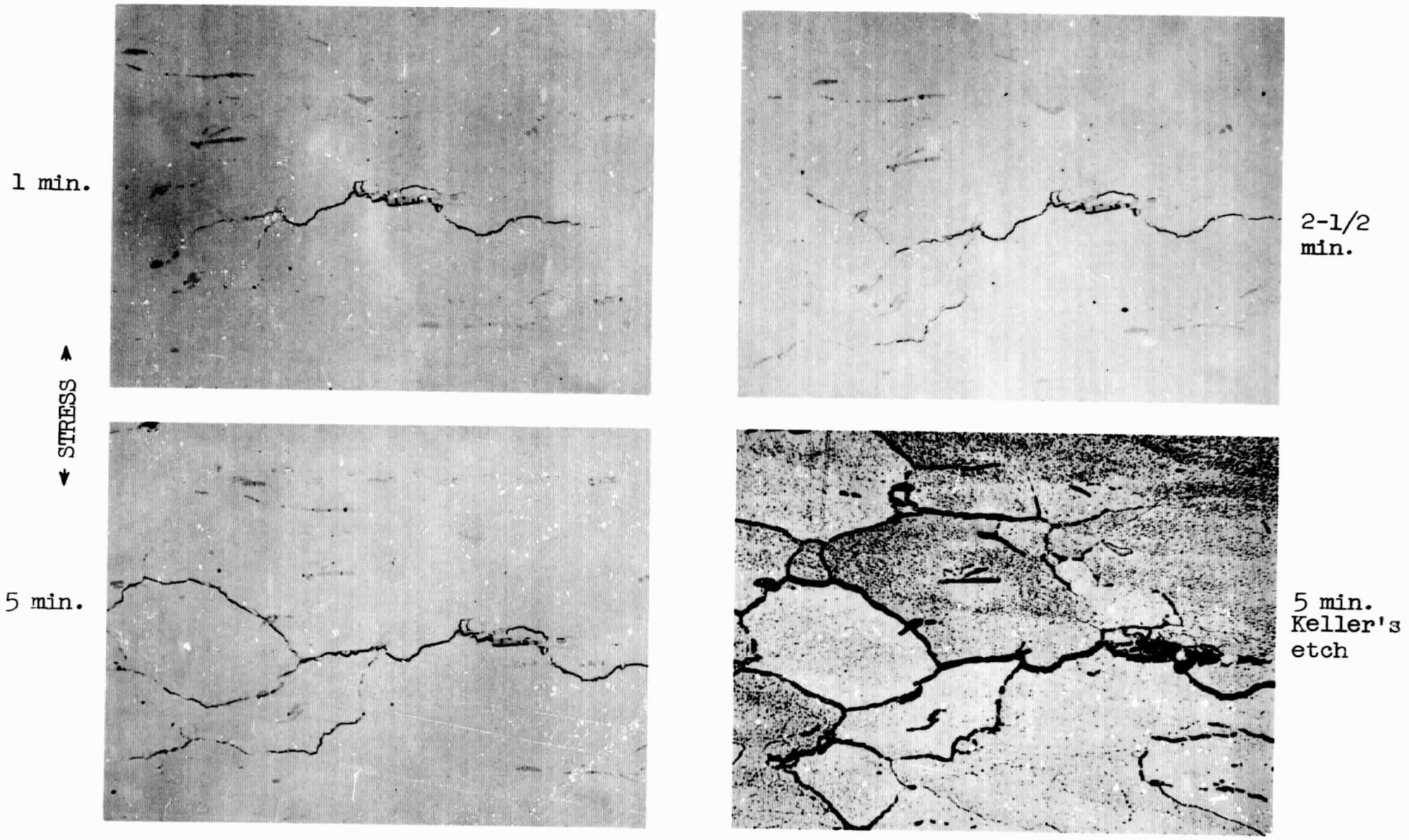

Crack initiation and development in stressed specimen (S.T. - 75% YS) of 2219-T37 exposed to 0.5N NaCl + 0.5N Na_2SO_4 at pH2. (X500)

Figure 103

167016-18

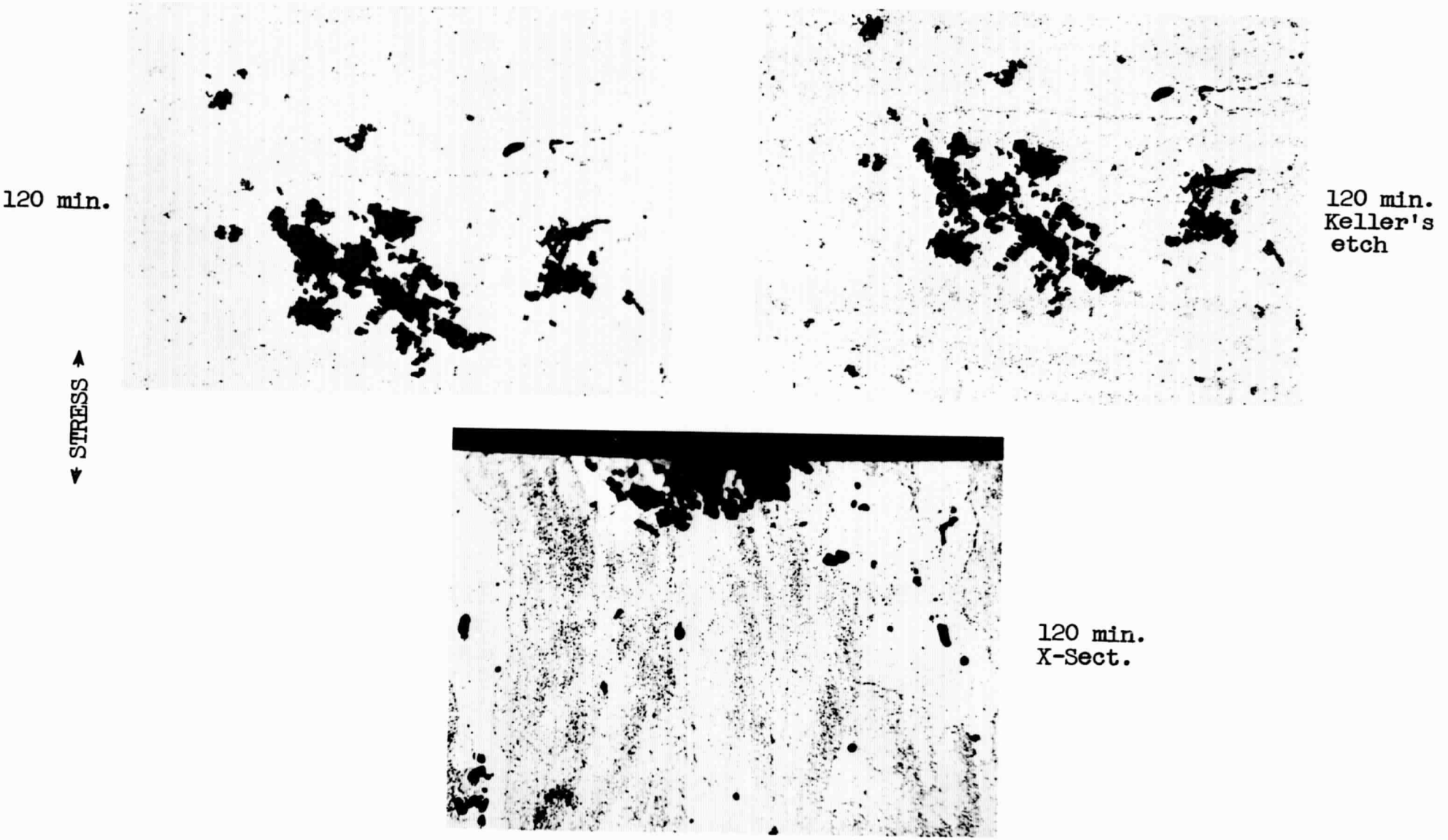

Tuning fork specimen of 7075-T73 stressed short transversely to 75% YS and exposed to 1N NaCl solution adjusted to pH2 with HCl. (X500)

Figure 104

167503
167505
167506
167507

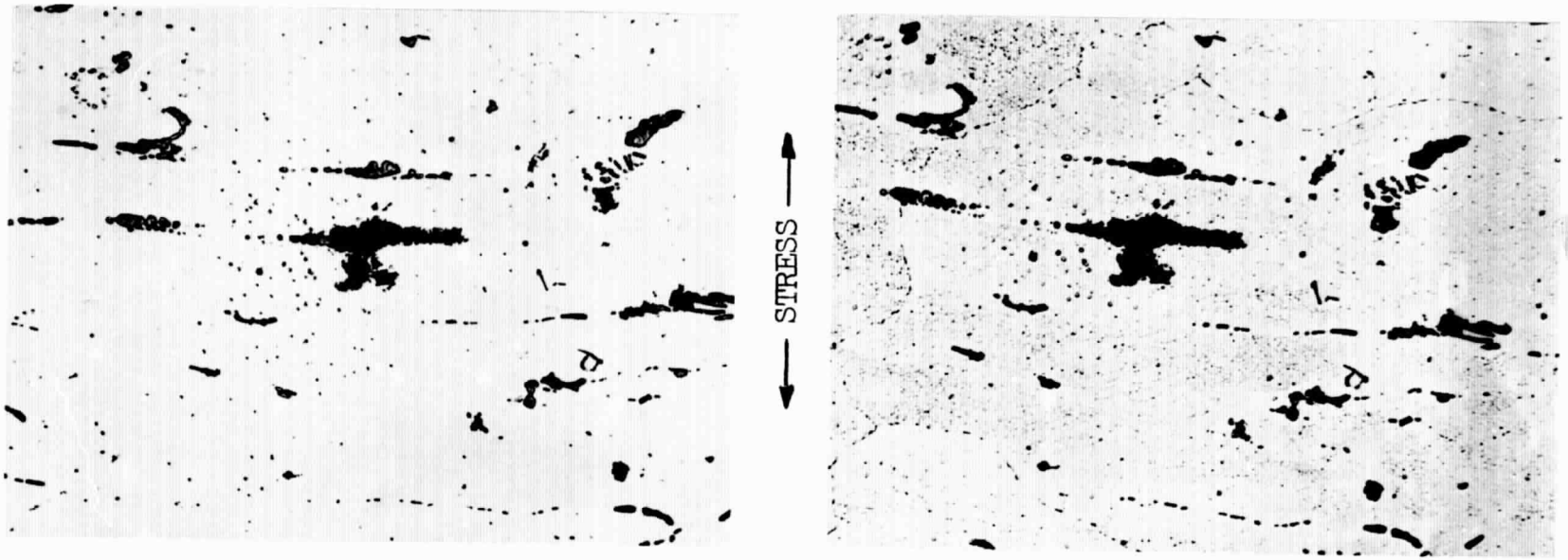

Tuning fork specimen of 2219-T87 stressed short transversely to 75% YS and exposed to 1N NaCl solution adjusted to pH2 with HCl (X500).

Figure 105

167498
167499
167500
167501

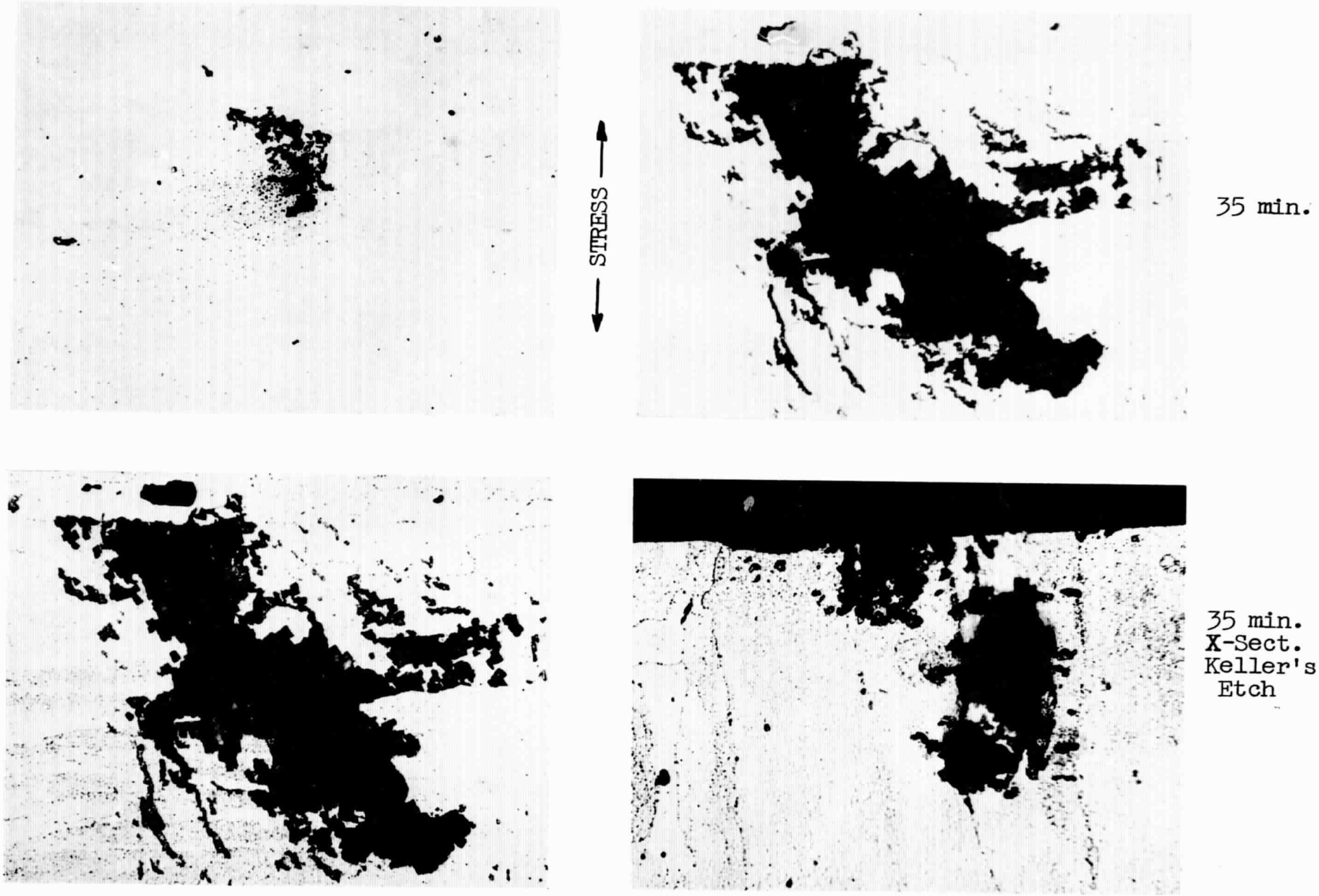

Pitting developed in 7075-T73 stressed short transversely to 75% YS and exposed to 1N NaCl solution adjusted to pH2 with H_2SO_4 (X500).

167519
167521
167523
167524

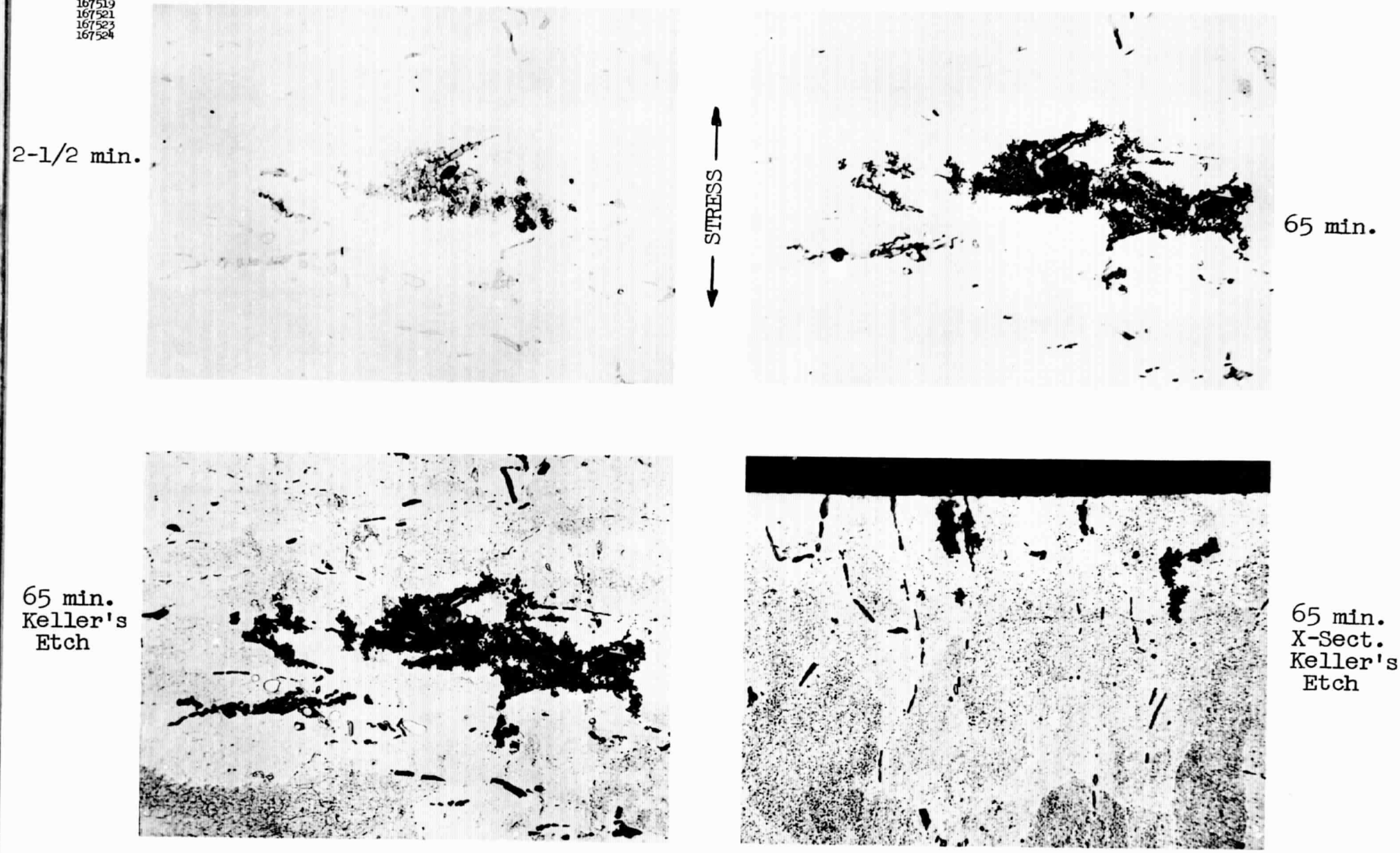

Pitting of 2219-T87 stressed short transversely to 75% YS and exposed to 1N NaCl adjusted to pH2 with H_2SO_4 (X500).

Figure 107

167511
167492
167493
167494

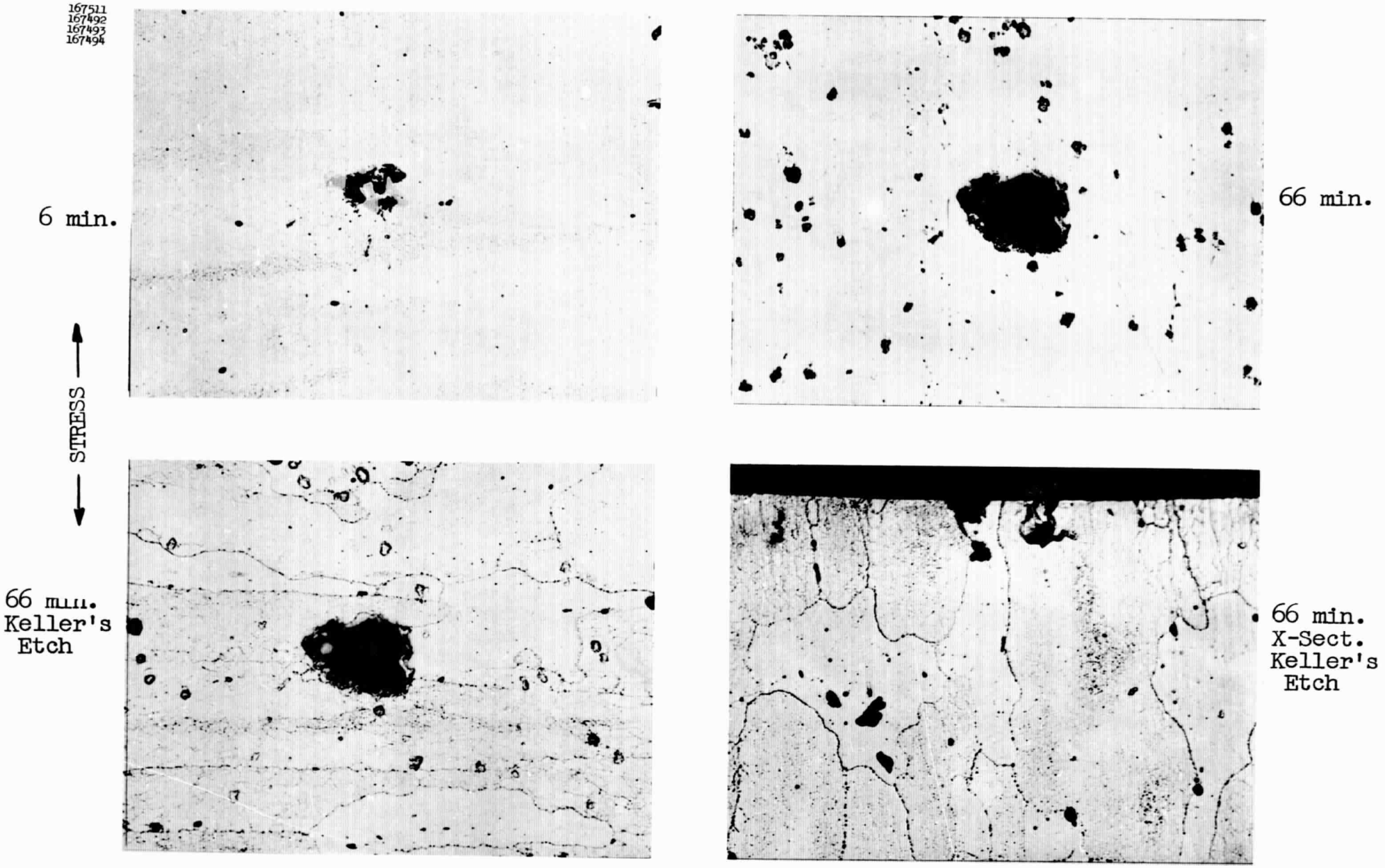

Pitting of 7075-T73 stressed short transversely to 75% YS and exposed to 1N KHF_2 at pH2 (X500).

Figure 108

167516
167517
167525

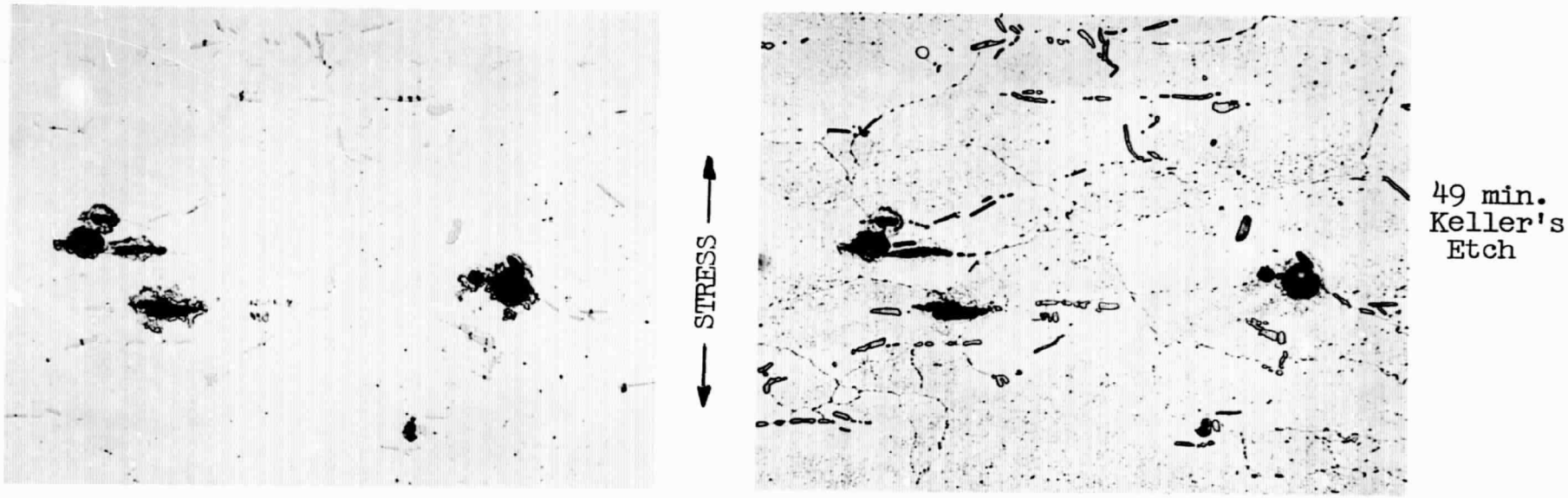

Attack of 2219-T87 stressed short transversely to 75% YS and exposed to 1N KHF_2 at pH2 (X500).

Figure 109

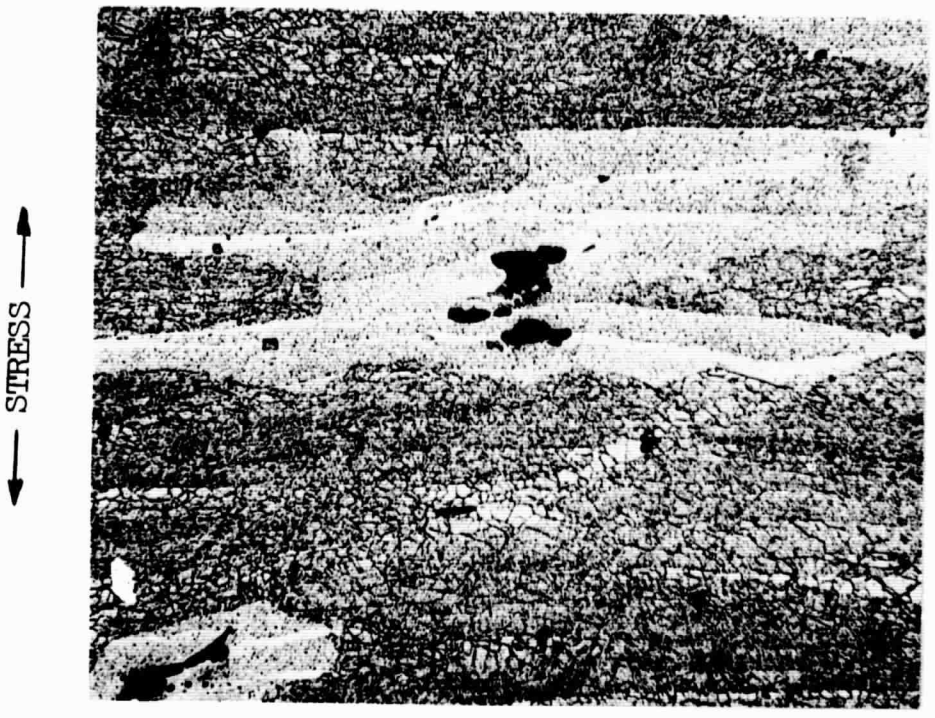

General attack of 7075-T73 stressed short transversely to 75% YS and exposed to 1N NaBr at pH2 for 65 minutes (X500).

Figure 110

167495
167496
167497
167510

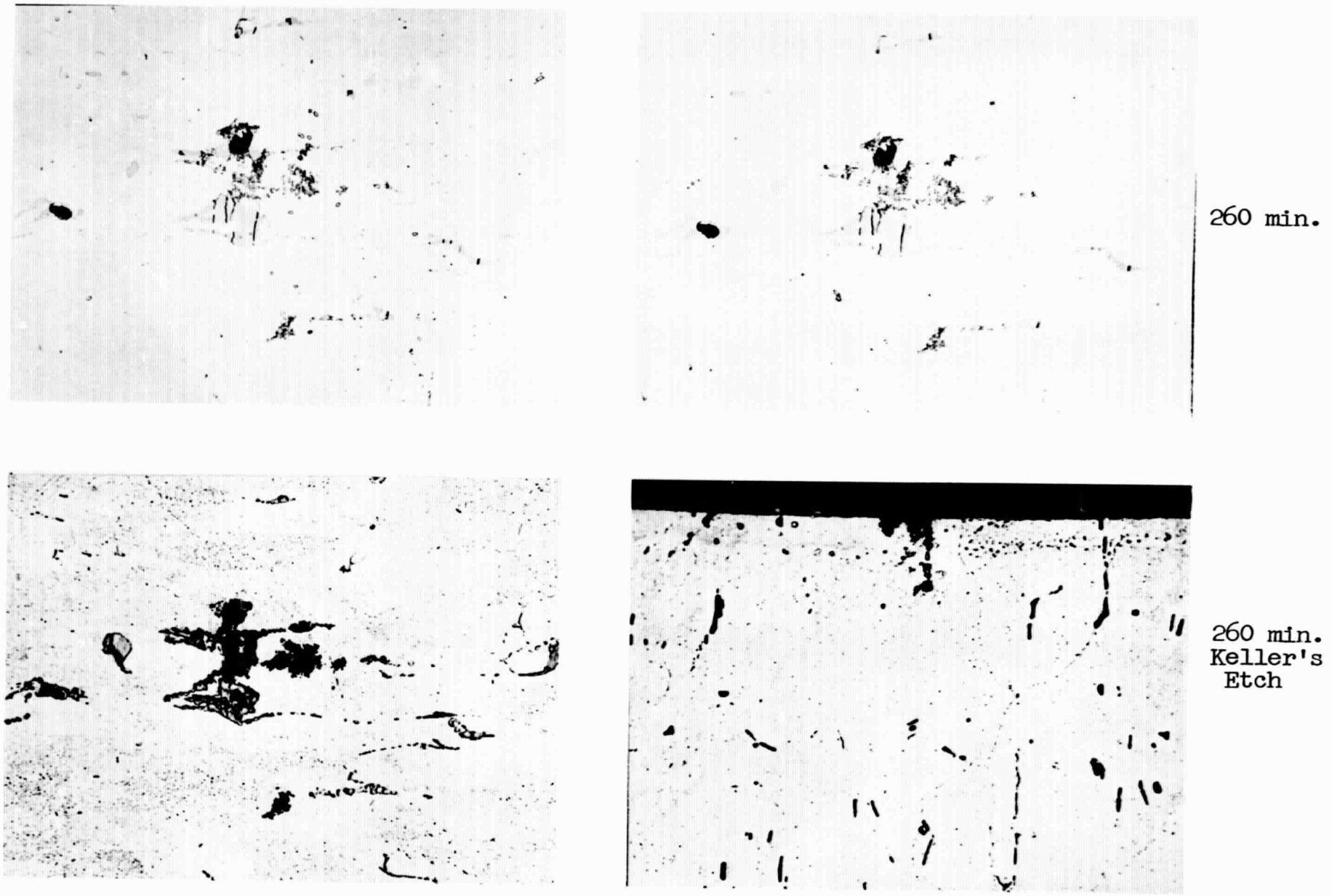

Pitting of 2219-T87 stressed short transversely to 75% YS and exposed to 1N NaCl adjusted to pH2 with CrO_3 (X500).

Figure 111